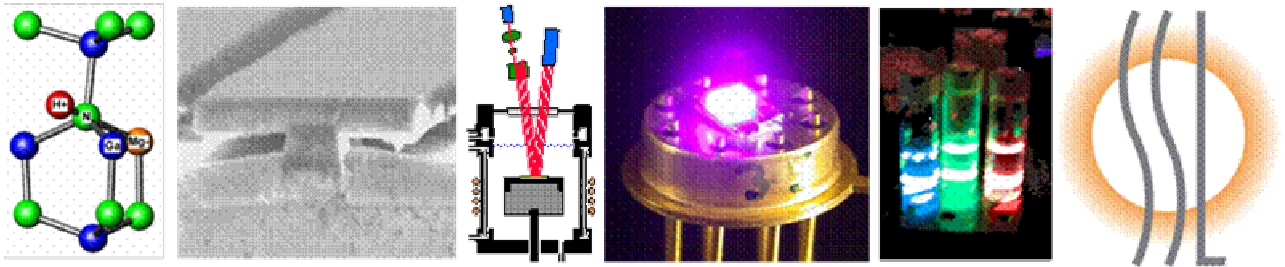


Final Report on Grand Challenge LDRD Project:



A Revolution in Lighting – Building the Science and Technology Base for Ultra-Efficient Solid-State Lighting

J. A. Simmons, J. Y. Tsao, S. R. Kurtz, T. M. Bauer, R. J. Kaplar, W. W. Chow, E. D. Jones,
K. E. Waldrup, S. R. Lee, A. J. Fischer, M. H. Crawford, K. W. Fullmer, and B. L. Abrams
Semiconductor Material and Device Sciences Department

R. M. Biefeld, D. D. Koleske, A. A. Allerman, J. J. Figiel, R. J. Creighton, M. E. Coltrin,
K. C. Cross, C. C. Mitchell, T. M. Kerley, G. T. Wang, and K. H. A. Bogart
Chemical Processing Science Department

C. H. Seager, J. M. Campbell, D. M. Follstaedt, M. P. Moran, and A. K. Norman
Radiation Solid Interactions Department

A. F. Wright, S. M. Myers, N. A. Missert, and R. G. Copeland
Nanostructure and Semiconductor Physics Department

J. M. Gee
Energy, Infrastructure, and Knowledge Systems Department

P. P. Provencio, J. P. Wilcoxon, and S. Woessner
Nanostructures and Advanced Materials Chemistry Department

G. R. Hadley
RF Microsystems Technologies Department

J. R. Wendt
Photonic Microsystem Technologies Department

R. J. Shul
Microdevice Technologies Department

C. I. H. Ashby
Microsensors Science and Technology Department

L. E. S. Rohwer
BEOL Advanced Packaging Department

D. R. Tallant and R. L. Simpson
Materials Characterization Department

H. K. Moffat
Multiphase Transport Processes Department

A. G. Salinger and R. P. Pawlowski
Computational Sciences Department

J. A. Emerson, S. G. Thoma, and P. J. Cole
Organic Materials Department

K. W. Boyack
Computational Biology Department

R. Elliot, M. L. Garcia, A. Salamone, M. Allen
Legal Intellectual Property Department

B. A. Burdick and N. M. Rahal
Licensing and IP Management Department

M. A. Monson and R. M. Gonzales
S&T Business Development Department

Sandia National Laboratories
P. O. Box 5800, Albuquerque, NM 87185

E. T. Southwell, A. E. Miksovic, A. O. Pinson, and M. J. Pinzon
Perspectives, Sedona, AZ

Abstract

This SAND report is the final report on Sandia's Grand Challenge LDRD Project 27328, "A Revolution in Lighting -- Building the Science and Technology Base for Ultra-Efficient Solid-State Lighting." This project, which for brevity we refer to as the SSL GCLDRD, is considered one of Sandia's most successful GCLDRDs. As a result, this report reviews not only technical highlights, but also the genesis of the idea for Solid-State Lighting (SSL), the initiation of the SSL GCLDRD, and the goals, scope, success metrics, and evolution of the SSL GCLDRD over the course of its life.

One way in which the SSL GCLDRD was different from other GCLDRDs was that it coincided with a larger effort by the SSL community – primarily industrial companies investing in SSL, but also universities, trade organizations, and other Department of Energy (DOE) national laboratories – to support a national initiative in SSL R&D. *Sandia was a major player in publicizing the tremendous energy savings potential of SSL, and in helping to develop, unify, and support community consensus for such an initiative.* Hence, our activities in this area, discussed in Chapter 6, were substantial: white papers; SSL technology workshops and roadmaps; support for the Optoelectronics Industry Development Association (OIDA), DOE and Senator Bingaman's office; extensive public relations and media activities; and a worldwide SSL community website.

Many science and technology advances and breakthroughs were also enabled under this GCLDRD, resulting in: 55 publications; 124 presentations; 10 book chapters and reports; 5 U.S. patent applications including 1 already issued; and 14 patent disclosures not yet applied for. Twenty-six invited talks were given, at prestigious venues such as the American Physical Society Meeting, the Materials Research Society Meeting, the AVS International Symposium, and the Electrochemical Society Meeting. This report contains a summary of these science and technology advances and breakthroughs, with Chapters 1-5 devoted to the five technical task areas: 1 Fundamental Materials Physics; 2 III-Nitride Growth Chemistry and Substrate Physics; 3 III-Nitride MOCVD Reactor Design and In-Situ Monitoring; 4 Advanced Light-Emitting Devices; and 5 Phosphors and Encapsulants. Chapter 7 (Appendix A) contains a listing of publications, presentations, and patents.

Finally, the SSL GCLDRD resulted in numerous actual and pending follow-on programs for Sandia, including multiple grants from DOE and the Defense Advanced Research Projects Agency (DARPA), and Cooperative Research and Development Agreements (CRADAs) with SSL companies. Many of these follow-on programs arose out of contacts developed through our External Advisory Committee (EAC). In this and other ways, the EAC played a very important role. Chapter 8 (Appendix B) contains the full (unedited) text of the EAC reviews that were held periodically during the course of the project.

TABLE OF CONTENTS

TABLE OF CONTENTS.....	6
0 PROJECT OVERVIEW.....	8
0.1 Genesis of the Solid-State Lighting Concept (JA Simmons)	8
0.2 Project Goals (JA Simmons)	8
0.3 Project Scope, Budget, Personnel, Success Metrics (JA Simmons, JM Gee)	9
0.4 Project Management and Evolution (JA Simmons, JM Gee)	12
1 TASK 1: FUNDAMENTAL MATERIALS PHYSICS.....	15
1.1 Hydrogen Behavior in Mg-doped GaN (AF Wright, SM Myers, CH Seager).....	15
1.2 The Role of Substitutional Carbon in GaN (CH Seager, AF Wright)	16
2 TASK 2: III-NITRIDE GROWTH CHEMISTRY AND SUBSTRATE PHYSICS	19
2.1 Cantilever Epitaxy (DM Follstaedt, CC Mitchell, NA Missert, DD Koleske, KA Bogart, AA Allerman, PP Provencio, KC Cross, MP Moran, AK Norman).....	19
2.2 Controlling GaN Thin Film Evolution (DD Koleske, AJ Fischer, ME Coltrin, AA Allerman, CC Mitchell, KC Cross, SR Kurtz, MJ Russell, JJ Figiel, KW Fullmer, WG Breiland).....	29
2.3 AlGaInN Deposition Chemistry (JR Creighton, GT Wang, ME Coltrin)	47
2.4 Mg doping Chemistry (GT Wang, JR Creighton)	50
3 TASK 3: III-NITRIDE MOCVD REACTOR DESIGN AND IN-SITU MONITORING	54
3.1 Reactor Modeling (HK Moffat, WG Breiland, JR Creighton, A Salinger).....	54
3.2 In-situ Measurement of Thin-film Stress during MOCVD (SR Lee, WG Breiland, DD Koleske).....	57
3.3 In-situ Temperature Measurement during MOCVD (JR Creighton, WG Breiland, CM Mitchell, KE Waldrip)	58
4 TASK 4: ADVANCED LIGHT-EMITTING DEVICES	63
4.1 Theory of Nitride Quantum Well Emission (WW Chow)	63
4.2 Near UV LEDs using Low Dislocation Density Cantilever Epitaxy (AJ Fischer, DD Koleske, AA Allerman, MH Crawford, KHA Bogart, CC Mitchell, and DM Follstaedt, KC Cross, KW Fullmer, JJ Figiel)	64
4.3 Flip Chip Device Packaging (KHA Bogart, AJ Fischer)	67
5 TASK 5: PHOSPHORS AND ENCAPSULANTS.....	71
5.1 Conventional Phosphors (DR Tallant, RL Simpson)	71
5.2 Semiconductor-Nanocluster-Based Phosphors (JP Wilcoxon, LS Rohwer, BL Abrams, SG Thoma).....	82
5.3 Quantum-Dot Phosphors and Characterization (LS Rohwer, BL Abrams, JE Martin).....	87
5.4 Encapsulants of Nanoparticles (SG Thoma, BL Abrams, LS Rohwer, A Sanchez, JP Wilcoxon, SM Woessner)	95

6	TASK 6: STRATEGIC PLANNING AND BUSINESS DEVELOPMENT	105
6.1	Support for the National Lighting Initiative (JA Simmons).....	105
6.2	Public Relations and Community Outreach (JA Simmons, JM Gee)	106
6.3	White Papers and Specialized Reports (JY Tsao, AE Miksovic, MA Monson, KW Boyack, N Rahal).....	108
6.4	U.S. SSL Roadmaps (JY Tsao, ED Jones).....	110
6.5	SSL Website (JY Tsao, AE Miksovic, DC Meister, AO Pinson, MJ Pinzon).....	111
6.6	Life after LDRD: SSL Follow-On Programs (JA Simmons, JM Gee)	116
7	APPENDIX A: PUBLICATIONS, PRESENTATIONS, PATENTS, ETC.....	122
7.1	Publications	122
7.2	Presentations	125
7.3	Book Chapters and Reviews	131
7.4	Reports and Websites	131
7.5	Patents Issued.....	132
7.6	Patent Applications.....	132
7.7	Patent Disclosures	132
8	APPENDIX B: EXTERNAL ADVISORY COMMITTEE AND REVIEWS	134
8.1	Members	134
8.2	February 2, 2001 Review (ET Southwell).....	135
8.3	November 2, 2001 Review (ET Southwell)	137
8.4	September 18-19, 2002 Review (ET Southwell).....	140
8.5	May 15-16, 2004 Review (ET Southwell).....	143
	DISTRIBUTION	148

0 PROJECT OVERVIEW

0.1 Genesis of the Solid-State Lighting Concept (JA Simmons)

While it is difficult to pinpoint exactly when the idea of using LEDs for general white light illumination first occurred, it is certainly the case that one of the earliest (if not the earliest) *written* documents in which this topic was taken seriously was a white paper jointly authored by Roland Haitz and Fred Kish from Agilent (a spin-off from Hewlett-Packard, and a leader in LED science and technology), and Jeff Tsao and Jeff Nelson from Sandia. This paper was first presented publicly on October 6, 1999 at an Optoelectronics Industry Development Association (OIDA) forum in Washington DC.

This now-famous white paper was the first to set forth a coherent vision of the possibility of achieving 200lm/W (approximately 50% energy efficient) solid-state lighting (SSL); estimated the global energy savings that would result from massive adoption of the technology; and called for a national R&D initiative in SSL at \$50M per year for 10 years. The paper provided an impetus for OIDA, Senator Bingaman's office, and interested industrial firms to push for a national initiative in SSL modeled after Sematech. Equally important, it provided to the Sandia team a pre-existing vision that was heavily drawn upon when the SSL GCLDRD proposal was written and its goals established.

Thus, from its outset, the SSL GCLDRD had a clearly articulated vision, with well-defined goals, that dovetailed with a growing interest in the national optoelectronics community. This enabled us to “hit the ground running,” and to attract substantial external interest in our activities. One result of this external interest was that we were able to create an External Advisory Committee (EAC) composed of top-notch industry, university, and government leaders. As we will see later, the EAC was of inestimable benefit to the project.

0.2 Project Goals (JA Simmons)

At the time the proposal was being written, OIDA was already planning a DOE-funded workshop to prepare a SSL technology roadmap, and was promoting a ten year, \$50M per year national initiative under DOE. OIDA had already asked Sandia to edit the Roadmap report. We were able to cite this groundswell of support for SSL, which clearly demonstrated opportunities for significant technology advance and clear national benefit even after the GCLDRD had been completed, in our written proposal.

0.2.1 Primary Project Goal

The SSL GCLDRD focused on underlying science and technology breakthroughs, rather than on the actual demonstration of high brightness LEDs. We chose this focus since, despite the efforts of a number of industrial companies, it was clear that if the SSL efficiency targets of 200lm/W being discussed at that time were to be reached, some revolutionary new technologies, based on science understanding, would likely to be necessary. Indeed, at a June 22, 2000 steering committee meeting hosted by the OIDA and including representatives from all of the major US LED manufacturers as well as Sandia and LBNL, it had been unanimously agreed that fundamental studies were critical for the revolutionary advancement of LEDs to the performance levels required by the applications holy grail of SSL technology – general white lighting.

Furthermore, LED industry representatives recognized at that meeting that this vital task was best carried out by national laboratories (with Sandia as the main contributor for inorganic-semiconductor-based solid-state lighting) as well as by universities. Such a focus was also well suited to the semi-academic culture and science focus existing in Centers 1100 and 1700, which would perform the majority of the work under the SSL

GCLDRD. Thus the project goal, succinctly stated in the SSL GCLDRD abstract, was “*to establish the fundamental science and technology base that... will be required in order for ... ultra-efficient solid state illumination to become a reality.*”

0.2.2 Secondary Project Goal

Although this statement provided a clear vision for the SSL GC, the project also had a secondary goal. Although energy efficiency is clearly a topic of importance for DOE and Sandia, Sandia’s primary mission as a National Nuclear Security Administration (NNSA) laboratory naturally leads to a stronger focus on national security-related projects. The principals in the establishment of the SSL GCLDRD were well aware that the primary enabling material for SSL, GaN-based compound semiconductors, also had numerous uses in national security applications. Thus a secondary goal of the SSL GCLDRD was to “*build the science and technology infrastructure needed for closely related work in areas of grave importance to national security. These areas include such III-V semiconductor technologies as compact UV lasers for nonproliferation applications, and high temperature, high power, high speed electronics for military use.*”

0.3 Project Scope, Budget, Personnel, Success Metrics (JA Simmons, JM Gee)

0.3.1 Scope

Initially, we identified several thrust areas for the SSL GCLDRD project. These were areas in which (1) a substantial advance could dramatically improve SSL, (2) the science content was substantial, and (3) we had some existing expertise. These thrust areas evolved considerably throughout the duration of the Solid State Lighting Grand Challenge. The changes occurred due to limitations in resources, reassessments of the likelihood of success as work proceeded, and recommendations from the external advisory committee.

For example, the original list of thrust areas included smart luminaires, which covered the design of lighting fixtures and optical designs which would take advantage of the unique properties of SSL technologies. No work in this thrust was intended for the first year. Ultimately, we ended up abandoning this thrust, since it was felt that industrial firms were already quite focused on this task and that it did not take advantage of Sandia’s strengths.

The thrust areas and the tasks within them eventually evolved by the end of the project into the following form:

Task 1: Fundamental Materials Physics

- A. Point and extended defects in GaN and its alloys
- B. Hydrogen diffusivity and magnesium acceptor activation
- C. Carbon as an Alternative P-type Dopant

Task 2: III-Nitride Growth Chemistry and Substrate Physics

- A. Novel substrate patterning for reduced dislocation densities
- B. Investigation of nucleation layer formation for minimizing dislocations
- C. Modeling and investigation of growth chemistry; search for parasitic reactions

Task 3: III-Nitride Growth Reactor Design and MOCVD In-Situ Monitoring

- A. Modeling and prototypes of novel reactor designs
- B. In-situ monitoring techniques for improved growth control

Task 4: Advanced Light-Emitting Device Structures

- A. Surface texturing and micro-emitter arrays for improved light extraction

- B. Photonic lattices for light extraction and cavity formation
- C. Demonstration of LED benchmarks

Task 5: Phosphors and Encapsulants

- A. Investigation of nanocrystals as flexible phosphor replacements
- B. Sub-wavelength conventional phosphors for reduced backscattering
- C. Development of UV-compatible encapsulants

Task 6: Strategic Planning and Business Development

- A. Business development planning and support
- B. Market intelligence reports and headline news updates
- C. SSL patent database
- D. Solid state lighting website

Sandia’s work in each of these thrust areas is reviewed in Chapters 1-6 of this report; note that the specific titles of the Sections in these Chapters differ slightly from those of the tasks in the above list, so as to describe more precisely the final technical foci of the tasks.

0.3.2 Budget

At the time the proposal was first submitted in July of 2000, it appeared likely that a National Lighting Initiative would start by the time the proposal moved into its second year. The SSL GCLDRD team anticipated that Sandia would benefit on the order of \$1M per year from this Initiative. As a result, the original funding request did not contain funding growth in the out years. The original request was:

Original Request: FY01: \$1.6M FY02: \$1.3M FY03: \$1.4M

Mission council awarded us with only \$1.0M at the outset. However, as we continued to demonstrate good progress, we received several funding plus-ups from Mission Council, through the LDRD office. Ultimately, the funding the SSL GCLDRD received from the LDRD office was:

Funding Received: FY01: \$1.3M FY02: \$2.3M FY03: \$3.3M

We note that, due to delays in the Grand Challenge LDRD process in FY01, we did not receive our initial funding until late in November of 2000.

0.3.3 Personnel

Personnel working on the SSL GCLDRD varied throughout the life of the project. This occurred partly due to normal personnel changes and job movement, and partly due to the growth in project funding. At one time or another, the following individuals contributed to the project:

Project Management:

Jerry Simmons, PM (1123), James Gee, PI (6200), Jeff Tsao (1123), Bob Biefeld (1126)

Fundamental Materials Physics:

Carl Seager (1111), Jonathan Campbell (1111), Alan Wright (1112), Sam Myers (1112) Steve Kurtz (1123), Tom Bauer (1123), Bob Kaplar (1123), Weng Chow (1123), Dan Koleske (1126), Andy Allerman (1126), Jeff Fiegel (1126)

III-Nitride Growth Chemistry and Substrate Physics:

Dave M. Follstaedt (1111), Mike P. Moran (1111), Adam K. Norman (1111), Nancy Missert (1112), Guild Copeland (1112), Paula Provencio (1122), Eric Jones (1123), Karen Waldrip (1123), Steve Lee (1123), Randy Creighton (1126), Mike Coltrin (1126), Karen Cross (1126), Andy Allerman (1126), Dan Koleske (1126), Jeff Fiegel (1126), Christine Mitchell (1126), Carol Ashby (1744)

III-Nitride Growth Reactor Design and MOCVD In-Situ Modeling:

Steve Lee (1123), George Wang (1126), Randy Creighton (1126), Tom Kerley (1126), Harry Moffat (9114), Andrew Salinger (9233), Roger Pawlowski (9233)

Advanced Light-Emitting Device Structures

Art Fischer (1123), Mary Crawford (1123), Kristine Fullmer (1123), Steve Kurtz (1123), Tom Bauer (1123), Bob Kaplar (1123), Andy Allerman (1126), Jeff Figiel (1126), Kate Bogart (1126), Ron Hadley (1742), Joel Wendt (1743), Randy Shul (1763)

Phosphors and Encapsulants:

Carl Seager (1111), Jonathan Campbell (1111), Jess Wicoxon (1122), Steve Woessner (1122), Billie Abrams (1123), Lauren Rohwer (1745), Dave Tallant (1822), Regina Simpson (1822), John Emerson (14172), Steve Thoma (14172), Phillip Cole (14172)

Strategic Planning and Business Development:

Jerry Simmons (1123), Jeff Tsao (1123), Bob Biefeld (1126), Rusty Elliot (1300), Marie Garcia (1300) Angelo Salamone (1300), Mark Allen (1300), Brent Burdick (1300), Nabeel Rahal (1304), Mary Monson (1314), Rene Gonzales (1314), James Gee (6200), Kevin W. Boyack (9212), Edwin T. Southwell (Perspectives), Ann E. Miksovic (Perspectives), Ariane O. Pinson (Perspectives), Marcia J. Pinzon (Perspectives)

0.3.4 Success Metrics

Early on, with the help of our market intelligence and technology intelligence consultant, Perspectives, Inc., we established a number of metrics for success for our project. These metrics were, not in order of priority:

1. External collaborations
2. Funds-in proposals and grants
3. Concrete ties to Sandia's national security mission
4. Contributions to progress in a national lighting initiative
5. External recognition and publicity for our project
6. Technical achievements as evidenced by publications and presentations, and by technical disclosures, patent applications, and granted patents

The team was highly focused on these metrics throughout the duration of the project and, we believe, was very successful in all metrics.

Metrics 1 and 2 are discussed in Section 6.6 "Life after LDRD: SSL Follow-On Programs."

Metric 3 is also discussed in Section 6.6 "Life after LDRD: SSL Follow-On Programs," particularly the Subsection on semiconductor UV optical sources (SUVOS). Here, we wish only to point out that there is synergy between the SSL project technical goals and three important areas of importance to Sandia's national security mission. The first area is high-power electronics GaN transistor work, since improved GaN substrates and buffers for SSL improves substrates and buffers used in these electronics applications as well. The second area in which internal customers have shown interest is in deep UV light emitters, which are useful for fluorescence-based detection of chemical and biological agents, and of nuclear materials. The third area is deep UV detectors based on GaN, which could be useful for the detection of missile plumes -- internal customers could be developed in this area as well.

Metric 4 is discussed in Section 6.1 "Support for the National Lighting Initiative" and in Section 6.3 "White Papers and Specialized Reports." Here, we wish only to point out that Sandia has been instrumental in catalyzing the national lighting initiative since its gestation in 1999.

Metric 5 is discussed in Section 6.2 "Public Relations and Community Outreach," and Section 6.5 "SSL Website."

Metric 6 is discussed in Chapters 1-5, and is summarized in the lists of publications, presentations, patents, etc. given in Chapter 7 (Appendix A).

0.4 Project Management and Evolution (JA Simmons, JM Gee)

0.4.1 External Advisory Committee

The SSL GCLDRD team began recruiting members of the External Advisory Committee almost immediately after approval of the project. One of the first individuals approached was Dr. George Craford, Chief Technology Officer of Lumileds. George Craford was one of the original pioneers of LED technology in the 1960s, and had spent his career at Monsanto and Hewlett-Packard doing LED R&D. Lumileds, a joint venture between Agilent (spun out from HP) and Philips Lighting, was one of the major SSL companies and has continued to grow and be very successful in the past few years. Thus Dr. Craford commands tremendous respect throughout the SSL community, and is truly an expert in the field. His position as Chair of our EAC helped us to recruit additional EAC members of exceptionally high quality. We are immensely thankful for Dr. Craford's skillful and objective leadership of the EAC.

The other members of the EAC were also extremely well qualified, and their recommendations on the conduct of our technical work were very valuable. In addition, they provided us with advice on connecting to other Federal government programs related to SSL, and to potential CRADA (cooperative research and development agreement) partners. Finally, we note that many members of our EAC were themselves from companies that eventually explored CRADAs with Sandia (including two that were signed), or were from Government agencies that were contemplating funding SSL-related programs. These individuals were able to view first-hand Sandia's capabilities at our review meetings, and to advise Sandia on how to best align with, and complement, industry and government-agency directions.

The membership of Sandia's Solid State Lighting External Advisory Committee is listed in Appendix B. A few of the EAC members were added after the first meeting — James Brodrick, John Carrano, John Zolper. In addition, Bob Karlicek, originally with GELCORE and present at the first meeting, subsequently left GELCORE and was no longer associated with the committee.

We note that, in the Fall of 2003, two of our EAC members, George Craford and Russell Dupuis, were awarded the National Medal of Technology for their work on LEDs, a source of tremendous satisfaction to us!

0.4.2 EAC Recommendations and GCLDRD Management Responses

The EAC listed above met 4 times during the course of the project: Feb. 2, 2001; Nov. 2, 2001; Sept. 18-19, 2002, and May 15-16, 2003. At typical meetings 80% of the members were present. The meetings opened with project manager (PM) Jerry Simmons giving a welcome address and overview, and then principal investigator (PI) James Gee giving a preview of technical accomplishments. There then followed a series of technical talks from leading members of the SSL team, spanning the scope of activities in the SSL GCLDRD. The meeting then typically closed with a presentation of a summary and a charge to the committee by PM Jerry Simmons. The committee would then engage in a closed-caucus session of 1-2 hours, with Ed Southwell of Perspectives present as a facilitator and note taker, in which the committee deliberated over its assessment of the SSL GCLDRD's technical progress, technical directions, developing contacts and publicity, etc. An oral report-out was then given by the committee to SSL GCLDRD's PM and PI, and a written version prepared, vetted, and sent out to Sandia in the next few days.

The EAC reports are collected in Appendix B of this SAND report. Here, we give a brief summary of the reports, and of the changes we adopted in response to their recommendations.

Feb. 2, 2001 Review

In addition to a strong endorsement of our goals, the importance of our project, and the level of expertise of our team, the primary points of this report were that:

- resources were insufficient for the goals we had set for ourselves
- a better integration of focus was needed amongst the proposed tasks
- work on strained layers for carrier confinement in phosphides should be dropped

In response, we reorganized our tasks across the thrust areas, and dropped the proposed work on strained phosphide materials. We also pressed, in our renewal proposal, for an increase in funding to \$2.3M in the second year. This push for increased funding was ultimately successful, not only in the second but also in the third year.

Nov. 2, 2001 Review

This report stated that we had made excellent progress since our first meeting, and roundly applauded the increase in funding we had obtained by that time. The committee then urged us to continue to strive towards benchmarking actual LEDs, and trying to produce a blue or near-UV LED comparable in brightness and power efficiency to those currently being produced commercially. In response, we continued to strive to produce LEDs of high brightness. However, we were having reactor problems -- severe difficulty in producing p-type doping in one of the reactors -- and were also sharing that reactor with a project aimed at producing GaN HEMTs (high electron mobility transistors) for defense-program (DP) applications.

In this meeting we also proposed the creation of a Solid State Lighting website by Sandia, on which would be placed the Market Intelligence reports that were being produced by Perspectives, Inc. The committee felt this was a great idea, and it was subsequently implemented.

Sept. 18, 2002 Review

We again received a very positive review, and in fact the report listed five areas in which they judged our work to be “outstanding successes,” including the role of hydrogen in GaN, cantilever epitaxy, unexpected reactor physics and new understanding of growth chemistry, “blazing of new territory in luminescent materials,” and the “public service” activities of the SSL Website and technical roadmapping support.

We had queried the EAC on suggestions for future funding in our transition to “Life after LDRD.” They told us that while substantial funding from the Next Generation Lighting Initiative might be targeted for our project, the prospects for decisive Congressional action looked unclear. Beyond this, they gave us a number of suggestions, such as discrete funding opportunities with DOE’s Office of Building Technologies (OBT), DOE’s Office of Basic Energy Sciences (BES), and DARPA. We felt that we were already pursuing these possibilities quite vigorously. The EAC also strongly recommended that we receive a fourth year of LDRD funding, to keep the team together until the NGLI started in earnest.

We were also tasked by the EAC with two challenges over the next six months that the EAC felt needed to be overcome. First, they asked that we demonstrate a reproducible, stable LED growth and fabrication process that could be used to benchmark our advances. (We had been suffering from irreproducible growth, and as mentioned earlier, particular difficulty in getting stable p-type doping.) Second, we were asked to demonstrate the viability and advantages of organometallic quantum dots as a phosphor replacement technology.

In response to the first challenge, we carefully considered the demands on our growth reactors, and decided that a drastic change was needed. At this stage, as mentioned, we had one commercial reactor that was producing good material, but two home-built reactors that had never displayed good reproducibility. The growth demands of visible and near UV LEDs, GaN HEMT transistor material for synthetic aperture radar applications, and by this time deep-UV high-aluminum content AlGaIn LEDs, were simply too much for our single commercial reactor to supply. At this stage we decided to launch an all-out effort to obtain the funds, via DP and BES, to purchase a second commercial reactor, so as to enable LED benchmarking.

In response to the second challenge, we shifted some resources into the nanocrystalline quantum dot thrust, hiring a postdoc to work in this area. We also made the determination that we would no longer support the work if a demonstration of >50% quantum efficiency was not obtained by the next EAC meeting, planned for the early summer.

May 15-16, 2003 Review

This was our last EAC meeting. We started the meeting with an explanation of our responses to their last report, including the fact that we had obtained funding for our second commercial reactor, and that the order had been placed. We also made a technical presentation on some dramatic progress in our work on nanocrystalline quantum dots as phosphors, demonstrating 65% quantum efficiency for a single color, and a novel synthesis technique yielding a distribution of quantum dots that produced white fluorescence. Finally, we told them that we expected that the LDRD office would put together a couple of one-year, follow-on LDRD projects to continue some SSL activity, but that we expected that these would total only 800K in FY04, down from 3,300K in FY03. (As it turned out, we received 1,200K in FY04 in the form of three one-year 400K LDRD projects.)

The EAC commended us on our achievements throughout the project, and stated that they felt we had created a “center of excellence” in solid state lighting, and that “the aggregate is world class.” They also stated that they were “very concerned” about the “extreme cutbacks in funding planned for this project in FY04.” The committee stated that unless FY04 funding ended up being substantially larger than 800K, they did not see the usefulness of their meeting again.

We closed the EAC with some pomp and circumstance. Each EAC member was presented with a letter, co-signed by Bob Eagan and Al Romig, thanking them for their service on the EAC. They were also all given a state-of-the-art miniature LED flashlight, using an extremely bright Lumileds Luxeon 1W LED. Finally, the EAC and the entire SSL team had a celebratory dinner at La Piazza restaurant the night of May 15, and each team member was presented with a Color Kinetics LightWasher nightlight as a token of appreciation for their work.

This final review, in which the EAC gives an overall assessment of the project, is included with the other EAC reviews in Chapter 8 (Appendix B).

1 TASK 1: FUNDAMENTAL MATERIALS PHYSICS

1.1 Hydrogen Behavior in Mg-doped GaN (AF Wright, SM Myers, CH Seager)

Mg-doped GaN grown using metal-organic chemical vapor deposition (MOCVD) is insulating in the as-grown state. The discovery¹ that the Mg acceptors can be activated by a post-growth, thermal anneal treatment was crucial for the development of GaN-based light-emitting diodes and laser diodes. Soon after this discovery, it was established that the passivation arises from H incorporated during growth.² A post-growth anneal then causes the H to migrate to a surface and leave the material, thereby activating the *p*-type doping. The nature of the passivating H state and the atomic processes involved in the migration and release of H were investigated as part of this LDRD. Results for the passivating state are described below and detailed in the noted references. Results for atomic processes involved in H release are briefly summarized below and the noted references provide details.

The passivated H state in as-grown MOCVD GaN:Mg has been the subject of considerable controversy. Early on, Götz *et al.*³ observed an infrared absorption peak at 3125 cm⁻¹ in passivated GaN:Mg. Based on the density-functional theory (DFT) results of Neugebauer and Van de Walle in zinc-blende GaN,⁴ they ascribed this peak to the N-H stretch mode of an Mg-N-H complex consisting of H at an anti-bonding site of a N neighbor of the Mg with the N-H bond oriented parallel to the Mg-N bond at an angle of 109° with respect to the wurtzite GaN *c* axis. Somewhat later, this identification was challenged by Clerjaud *et al.*⁵ whose infrared absorption measurements indicated the N-H bond angle is 130° with respect to the *c* axis. Following this experimental result, Limpijumng, Northrup, and Van de Walle⁶ used DFT to identify an unusual Mg-N-H configuration (denoted OA_{||}) with an N-H bond angle close to that given by Clerjaud *et al.*⁵ The energy of this OA_{||} configuration was 0.19 eV higher than for the previously identified configuration (denoted AB_⊥). However, Limpijumng *et al.*⁶ argued that vibrational contributions to the entropy of the OA_{||} configuration stabilized it with respect to the AB_⊥ configuration at temperatures above 627°C, and the H atom then becomes trapped in the OA_{||} configuration when the material is cooled following growth.

Upon examining the DFT and experimental results, two inconsistencies became apparent to us. First, a single infrared absorption peak is observed in H contaminated GaN:Mg regardless of whether spectra are obtained from as-grown material or material first annealed to remove grown-in H and then reloaded with H at temperatures well below those used for growth (600°C and 700°C).^{3,7} Furthermore, this peak reappears following a 200°C anneal of material previously activated via electron beam irradiation.⁸ Second, the analysis by Limpijumng *et al.*⁶ of H state populations neglected the H interstitial state and the configurational degeneracy of the AB_⊥ Mg-N-H configuration. When we took these considerations into account and refined the analysis of Limpijumng *et al.*,⁶ OA_{||} was found to be a minority H state at all temperatures. In an effort to clarify the identity of the passivated state, we performed our own DFT examination of Mg-N-H. The resulting energies of the six most stable configurations and the associated H vibration frequencies were utilized, along with corresponding results for interstitial H, to compute equilibrium H state populations in GaN:Mg as a function of temperature.⁹ Similar to our earlier analysis, the dominant H state at *T* > 550°C was found to be interstitial H, the dominant state at *T* < 550°C was AB_⊥ Mg-N-H, and the OA_{||} Mg-N-H population was found to be negligible at all temperatures. With regard to the infrared absorption data of Clerjaud *et al.*,⁵ Seager performed a reanalysis which revealed that this data was indeterminate with regard to the N-H bond angle.¹⁰ (Clerjaud *et al.* have agreed with this conclusion.)

Our investigations of atomic processes involved in H release have revealed that the rate determining step is formation of H₂ at the surface.^{7,12,13} This process is second order in the H surface coverage, which is generally

low due to the exceptional bulk stability of H in Mg-doped GaN.^{9,11,12} Further investigations have indicated that weaker, first order processes occur during anneals in both vacuum and N₂ or O₂,¹⁴ suggesting that N-H species leave the surface during vacuum and N₂ anneals, and O-H species leave the surface during O₂ anneals. Bulk H diffusion has been examined using experimental and theoretical techniques.^{15,16} Experiments indicate that the activation energy for H diffusion in the presence of strong trapping by Mg is 1.76 eV. DFT calculations yield a H diffusion activation energy of 1.0 eV and a binding energy of 0.6 eV to the Mg acceptor, with the sum being in good agreement with the measured value. The DFT calculations also indicate a pronounced anisotropy in H diffusion activation energies for motion along and transverse to the *c* axis.^{16,17} Additional DFT studies have examined the interaction of H with two types of native point defects in GaN: the Ga vacancy and the N interstitial.¹⁸

1. S. Nakamura, T. Mukai, M. Senoh, and N. Iwasa, *Jpn. J. Appl. Phys.* **31**, L139 Part 2 (1992).
2. S. Nakamura, N. Iwasa, M. Senoh, and T. Mukai, *Jpn. J. Appl. Phys.* **31**, 1258 part1 (1992).
3. W. Götz, N. M. Johnson, D. P. Bour, M. D. McCluskey, and E. E. Haller, *Appl. Phys. Lett.* **69**, 3725 (1996).
4. J. Neugebauer and C. G. Van de Walle, *Phys. Rev. Lett.* **75**, 4452 (1995).
5. B. Clerjoud, D. Côte, A. Lebkiri, C. Naud, J. M. Baranowski, K. Pakula, D. Wasik, and T. Suski, *Phys. Rev. B* **61**, 8238 (2000).
6. S. Limpijumnong, J. E. Northrup, and C. G. Van de Walle, *Phys. Rev. Lett.* **87**, 205505 (2001); *Phys. Rev. B* **68**, 075206 (2003).
7. S. M. Myers, A. F. Wright, G. A. Petersen, W. R. Wampler, C. H. Seager, M. H. Crawford, and J. Han, *J. Appl. Phys.* **89**, 3195 (2001).
8. S. M. Myers, C. H. Seager, A. F. Wright, and B. L. Vaandrager, *J. Appl. Phys.* **92**, 6630 (2002).
9. A. F. Wright and S. M. Myers, *J. Appl. Phys.* **94**, 4918 (2003).
10. C. H. Seager, *Phys. Rev. B* **67**, 037201 (2003).
11. S. M. Myers, A. F. Wright, G. A. Petersen, C. H. Seager, W. R. Wampler, M. H. Crawford, and J. Han, *J. Appl. Phys.* **88**, 4676 (2000).
12. W. R. Wampler and S. M. Myers, *J. Appl. Phys.* **94**, 5682 (2003).
13. S. M. Myers and C. H. Seager, *J. Appl. Phys.* **95**, 520 (2004).
14. S. M. Myers, B. L. Vaandrager, W. R. Wampler, C. H. Seager, *J. Appl. Phys.* **95**, 76 (2004).
15. C. H. Seager, S. M. Myers, A. F. Wright, D. D. Koleske, and A. A. Allerman, *J. Appl. Phys.* **92**, 7246 (2002).
16. A. F. Wright, C. H. Seager, S. M. Myers, D. D. Koleske, and A. A. Allerman, *J. Appl. Phys.* **94**, 2311 (2003).
17. S. M. Myers and A. F. Wright, *J. Appl. Phys.* **93**, 2608 (2003).
18. A. F. Wright, *J. Appl. Phys.* **90**, 1164 (2001); A. F. Wright, *J. Appl. Phys.* **90**, 6526 (2001).

1.2 The Role of Substitutional Carbon in GaN (CH Seager, AF Wright)

Despite a considerable amount of experimental effort, the role of C introduced as an impurity into GaN has been a matter of considerable controversy. A major impetus for this work has been the realization that Mg, presently the only viable *p*-type dopant in GaN, has numerous problems including a high thermal ionization energy (130-210 meV, depending on concentration) and the tendency to form defect structures which apparently compete with the substitutional configuration. The expectation is that C could, in principle, be an alternative *p*-type dopant in GaN when substituting on the nitrogen site (C_N); if confirmed, this could have a major impact on the performance of GaN-based LEDs. While some carbon is always present in GaN films grown from metal-

organic precursors, numerous attempts have been made to deliberately introduce this impurity as a dopant. Although SIMS measurements have confirmed that this can be accomplished, the reported electrical properties of deliberately doped films have varied widely, and it was generally recognized that film growth conditions play an important role in controlling the amount of C that is actually incorporated.

From photoluminescence (PL) measurements on undoped material, Fischer *et al.*¹ concluded that C_N is indeed an acceptor in GaN with an optical binding energy of 230 meV. However, efforts to produce *p*-type GaN:C have met with only limited success. Abernathy *et al.*^{2,3} measured a 300 K hole concentration of $3 \times 10^{17} \text{ cm}^{-3}$ in wurtzite GaN grown via metal-organic molecular beam epitaxy using a CCl_4 source. As *et al.*⁴ achieved a hole concentration of $6 \times 10^{17} \text{ cm}^{-3}$ recently in cubic GaN grown using plasma-assisted molecular beam epitaxy with an e-beam evaporation source. However, the hole concentration saturated and then decreased with increasing C flux, and these authors concluded that self-compensation was likely taking place.

To address these issues, we have, in cooperation with Lumileds, grown and characterized GaN samples doped with both Si (a donor) and varying amounts of carbon. These materials were grown by Metal-Organic-Chemical-Vapor Deposition (MOCVD) on sapphire substrates whose c-axis was normal to the top (growth) surface. GaN grown in this fashion has the wurtzite structure with its c-axis perpendicular to the plane of the substrate. Growth was accomplished in a vertical flow MOCVD reactor at $\sim 1050^\circ\text{C}$ at a rate of $\sim 8 \text{ \AA/s}$. The group III and group V precursors were trimethyl-gallium and ammonia, respectively, and the carrier gas was hydrogen. The V/III ratio at the reactor inlet was 3000 and the reactor chamber pressure was 700 torr except for growth of the Si doped layers. For these layers the growth pressure was varied between 700 and 78 torr to adjust the C concentration. After growth, wafers were characterized by X-ray diffraction and exhibited a symmetric and asymmetric rocking curve FWHM of 0.08° and 0.13° for the (0002) and (20-24) reflection, respectively. Si was incorporated in varying amounts with the addition of silane to the gas stream. Structures with two layers were grown by varying the silane gas flow. The lower layer, typically $1 \mu\text{m}$ thick, was heavily ($\sim 5 \times 10^{18} \text{ cm}^{-3}$) Si doped, while the upper layer had $\sim 50\times$ less Si and varying amounts of C. The heavily doped lower layer was used as a back contact for Schottky diode structures. Secondary Ion Mass Spectrometry (SIMS) was performed on all samples to determine thicknesses and compositional variations. Optical and electrical measurements were performed on these layers to characterize the net charge density (equal to the difference between the Si donor density plus any donors contributed by carbon minus the density of any acceptors due to carbon). Cathodoluminescence (CL) and photoluminescence (PL) were also measured to characterize any optical transitions caused by in-gap electronic levels.

In addition to our experimental studies, Density-Functional Theory⁵ (DFT) calculations were performed for substitutional carbon at a gallium site (C_{Ga}), a nitrogen site (C_N), and at various interstitial sites (C_i). Relaxed configurations were obtained as a function of charge state and formation energies were then computed for these structures. The calculations utilized a 72-atom supercell, ultrasoft pseudopotentials⁶, a plane-wave basis set⁷, and Monkhorst-Pack⁸ parameters {2,2,2} to sample the Brillouin zone. Ga 3d electrons were treated as valence electrons in the Ga pseudopotential.

The electrical measurements indicate that if carbon densities are less than those of the Si donor, one acceptor is introduced for every C atom. By contrast when the carbon density is larger than that of the Si donors, the number of acceptors introduced does not equal the carbon density. This implies that in samples where the silicon concentration exceeds that of carbon, carbon sits in the N substitutional site, acting as an acceptor and partially compensating the material. However when carbon densities exceed those for Si, GaN becomes semi-insulating due to carbon occupation of both N and Ga substitutional lattice sites, and a new luminescence peak appears at $\sim 3 \text{ eV}$. To explain these observations, we invoked the fact that the formation energies we calculated using DFT for carbon in both sites are strong functions of both the Fermi level and growth stoichiometry. The former dependence gives rise to self-compensation when $[C] > [Si]$ because the formation energy of the Ga substitutional configuration (the donor state) becomes equal to that of the N substitutional site, effectively pinning the Fermi level as it approaches mid-gap. Our results suggest that effective *p*-type doping of GaN can only be achieved under Ga-rich growth conditions; these conditions can only be achieved with MBE growth techniques. Recent studies⁹ of MBE-grown GaN by the Berkeley group have confirmed our work at low C concentrations. This same work has also shown that for C levels well above those used in our study ($> 10^{18} \text{ cm}^{-3}$)

other C sites are occupied (probably interstitial species), and p-type doping is not observed. Other important consequences of our study include the identification of a new 3.0 eV luminescence peak seen in the heavily C-doped samples with transitions between C acceptors and C donors, and the fact that we observed a strong link between the ubiquitous “yellow” luminescence in GaN and the presence of carbon.

1. S. Fischer, C. Wetzel, E. E. Haller, and B. K. Meyer, *Appl. Phys. Lett.* **67**, 1298 (1995).
2. C. R. Abernathy, J. D. MacKenzie, S. J. Pearton, and W. S. Hobson, *Appl. Phys. Lett.* **66**, 1969 (1995).
3. W. Geerts, J. D. Mackenzie, C. R. Abernathy, S. J. Pearton, and T. Schmiedel, *Solid State Electronics* **39**, 1289 (1996).
4. D. J. As and U. Köhler, *J. Phys. Condens. Mater.* **13**, 8923 (2001); U. Köhler, M. Lübbbers, J. Mimkes, and D. J. As, *Physica B* **308-310**, 126 (2001); *Phys. Stat. Solidi. A* **188**, 699 (2002).
5. W. Kohn and L. J. Sham, *Phys. Rev.* **140**, A1133 (1965); D. M. Ceperley and B. J. Alder, *Phys. Rev. Lett.* **45**, 566 (1980); J. P. Perdew and A. Zunger, *Phys. Rev. B* **23**, 5048 (1981).
6. U. Grossner, J. Furthmüller, and F. Bechstedt, *Phys. Rev. B* **58**, R1722 (1998).
7. G. Kresse and J. Hafner, *Phys. Rev. B* **47**, 558 (1993); **49**, 14251 (1994); G. Kresse and J. Furthmüller, *Comput. Mater. Sci.* **6**, 15 (1996); *Phys. Rev. B* **54**, 11169 (1996).
8. H. J. Monkhorst and J. D. Pack, *Phys. Rev. B* **13**, 5188 (1976).
9. R. Armitage et al., to be published.

2 TASK 2: III-NITRIDE GROWTH CHEMISTRY AND SUBSTRATE PHYSICS

2.1 Cantilever Epitaxy (DM Follstaedt, CC Mitchell, NA Missert, DD Koleske, KA Bogart, AA Allerman, PP Provencio, KC Cross, MP Moran, AK Norman)

2.1.1 Motivation for Investigation of Cantilever Epitaxy

Gallium nitride (GaN) is now widely studied by growing it heteroepitaxially on other hexagonal substrates, usually sapphire or silicon carbide (SiC). These substrates must be used because wafers of GaN are not available as in the case of more common semiconductors (eg., Si, GaAs). A layer grown at lower temperature (the “nucleation layer”) is used to initiate oriented growth on the substrate, followed by epitaxial growth on this layer at higher temperatures. However, there is a serious mismatch in the distance of atomic spacings of GaN with respect to those of sapphire (16%) and SiC (3.5%). Growth of GaN on planar sapphire substrates results in high densities of dislocation defects, 10^9 - $10^{10}/\text{cm}^2$, that thread vertically from the interface up through the GaN to device regions. These densities need to be drastically reduced because dislocations quench light emission from light-emitting devices. Removing vertical threading dislocations (VTDs) appears even more important for shorter-wavelength emitters, such as near-UV LEDs envisioned as one method to produce white lighting.

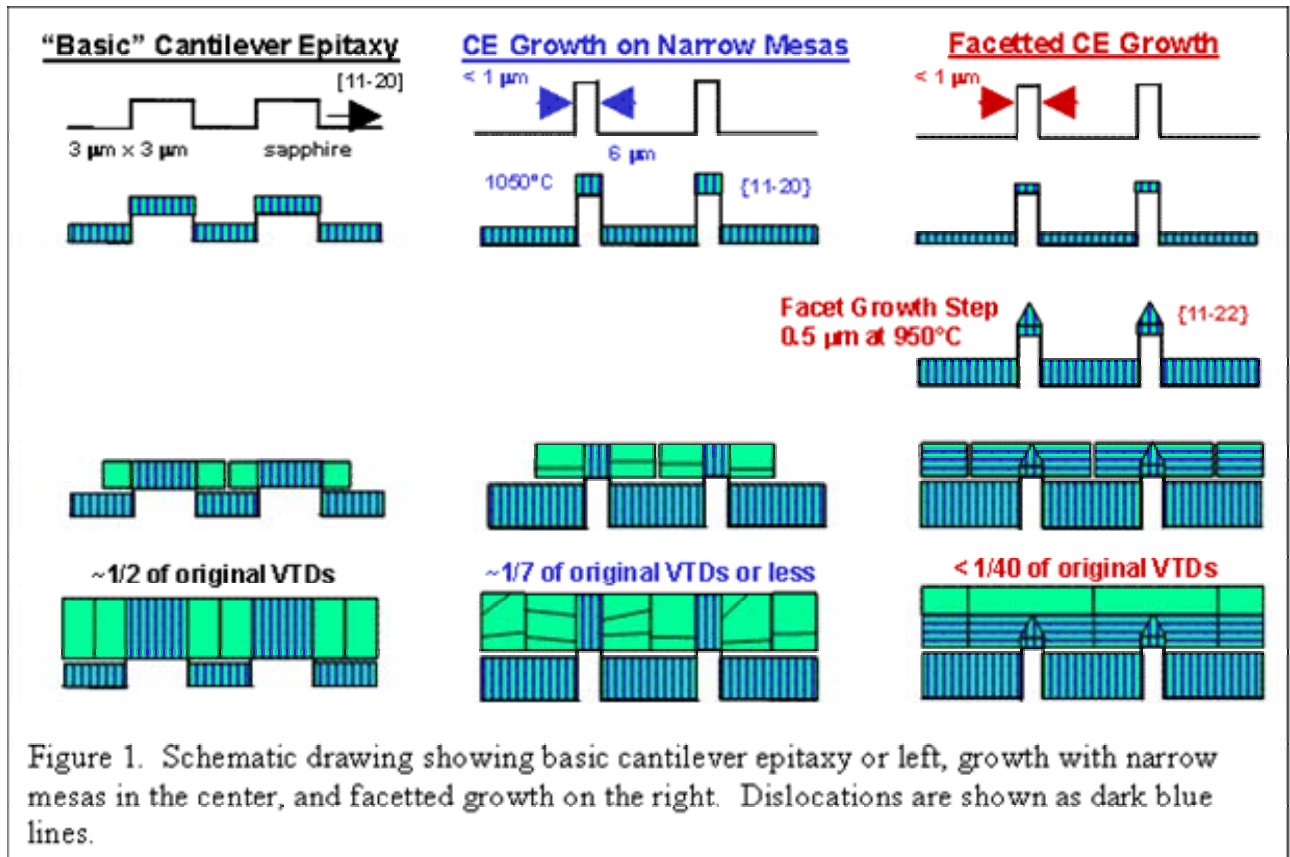


Figure 1. Schematic drawing showing basic cantilever epitaxy on left, growth with narrow mesas in the center, and facetted growth on the right. Dislocations are shown as dark blue lines.

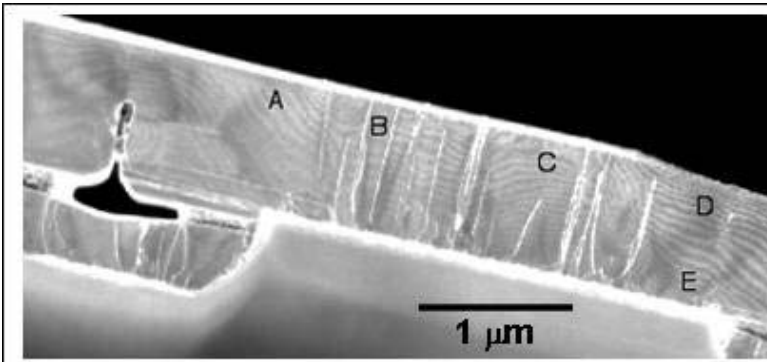


Figure 2. Cross-section TEM image of VTDs (white lines) in CE-GaN grown with 3 μm-wide trenches and mesas. VTDs within 0.5 μm of the mesa edge are seen often to turn to horizontal.

Cantilever Epitaxy (CE) was invented at Sandia just before the initiation of this Grand Challenge LDRD [1]. This prior work showed that greatly reduced dislocation densities were possible with this growth method. Growth by CE also offered a significant advantage over other methods to reduce dislocation densities: *CE can be accomplished with a single growth in the MOCVD reactor.* Sandia has now received a patent on this growth process [2]. However, the detailed growth techniques needed development, and characterization of defects over larger areas as needed for devices was required. Moreover, the benefits of using CE-GaN for light emission were yet to be demonstrated through growth of LEDs on

this material. Below we describe this growth method and summarize several technical achievements in the development of improved material, and we demonstrate that LEDs grown on CE-GaN have improved emission over those on conventional, planar-growth GaN.

2.1.2 Description of Cantilever Epitaxial Growth of GaN

The basic CE growth process is illustrated on the left side of Fig. 1. First, trenches are etched into the substrate leaving stripes of mesas with the original surface. Etching trenches into the very resistant sapphire (Al_2O_3) is accomplished by patterning with photoresist and etching with an inductively-coupled plasma using BCl_3 . Vertical growth of the overlayer is then initiated on the mesas; this material is epitaxial with the substrate but contains dislocation lines (shown as dark lines) that propagate vertically into the material. After some vertical growth, the conditions of the growth reactor are adjusted to produce lateral growth over the trenches; this lateral (“cantilever”) material is suspended from the mesas and does not contain VTDs because it is not in contact with the substrate. After adjacent cantilevers are grown together, the continuous solid is grown vertically to produce the desired thickness of the layer material. In the end, VTDs produced by contact with the substrate are confined to mesa areas, but the cantilever regions over trenches have very low dislocation densities. In the initial version of the method, the trench width and mesa width were comparable, giving total overall reductions of $\sim 1/2$. This approach could be adequate if devices are placed only within the dislocation-free cantilever regions, but achieving broader areas with low overall density requires reducing dislocations over mesa areas also.

2.1.3 Technical Achievements in Producing Cantilever Epitaxial GaN with Fewer Defects

A. Reducing Dislocation Density by Growth on Narrow Mesas and by Facetted Growth

An example of the VTDs in our early CE growths is shown in Fig. 2, where these dislocations are seen to emerge vertically from the mesa. Note that some VTDs

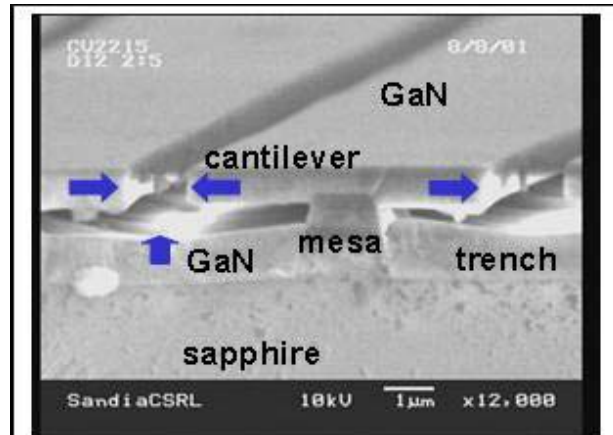


Figure 3. Cross-sectional SEM image with GaN cantilevers growing toward each other with GaN growing upward in the trenches.

within 0.5 μm of the mesa edge (eg., near positions A and E) turn to horizontal and do not thread to the top of the GaN layer, where devices would be formed. These observations lead to the concept that a mesa less than 1 μm wide might have many dislocations that turned to horizontal and few threading to the top. This process is indicated schematically in the middle column on Fig. 1. We also noted that in the literature [3], GaN that was initially faceted would result in VTDs turned to horizontal when followed by lateral growth. We therefore developed a sequence of growth steps to produce GaN grown on narrow mesas with facets, as indicated schematically on the right side of Fig. 1. These ideas formed the basis for a first (and successful!) attempt to improve on Cantilever Epitaxy and achieve further reductions in VTDs in this Grand Challenge LDRD.

Both schemes reduce VTD density at the top of the GaN, and if done correctly, the faceted turning is especially effective. Further, when narrow mesas are used, a greater fraction of area at the top of the GaN is over trenches and is relatively dislocation free, giving a lower overall VTD density. But wider cantilever spans require greater growth times, as does forming facets on GaN over the mesas also. The exact growth scheme must then be carefully timed so that lateral growth and coalescence of the cantilevers is completed before unwanted GaN growing vertically in the trenches encounters the cantilevers and introduces numerous additional dislocations. (This unwanted growth in trenches can be seen in the lower left of Fig. 2.) The close timing of these events is illustrated in Fig. 3, where growth was halted before adjacent cantilevers were joined. In this instance, the gap between the cantilever and GaN in the trench is well maintained. A significant processing accomplishment that allowed greater freedom in developing growth schemes was improving the patterning and etching of the trenches to obtain a trench depth of $\sim 3 \mu\text{m}$, allowing greater time for manipulating cantilever growth.

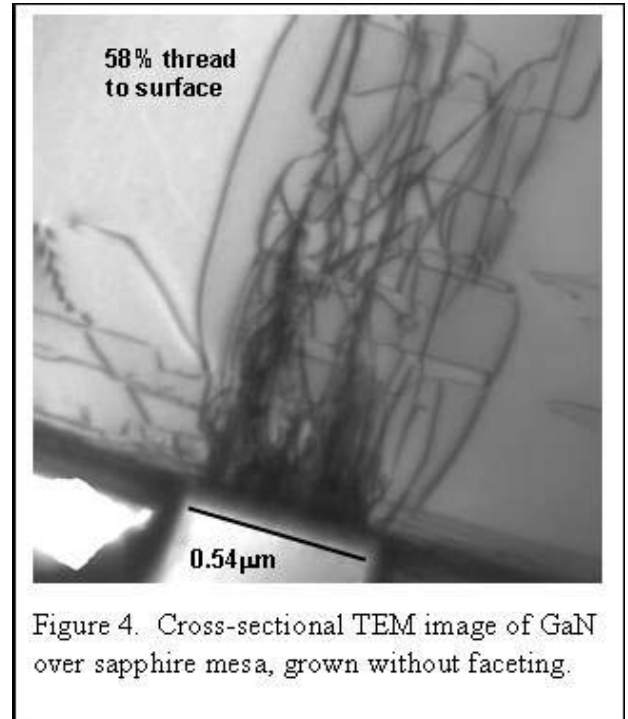


Figure 4. Cross-sectional TEM image of GaN over sapphire mesa, grown without faceting.

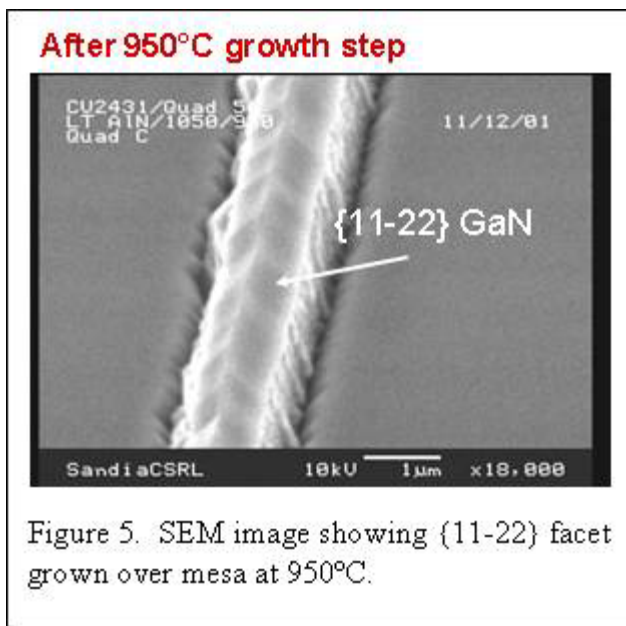


Figure 5. SEM image showing {11-22} facet grown over mesa at 950°C.

Figure 4 shows a cross-section TEM image of CE-GaN grown on a narrow mesa but without faceting. Many VTDs are seen to turn to horizontal, but many also remain vertical. The number remaining vertical varied between observations, but was usually in the range of 30 -70%. When a faceted growth step at 950°C of GaN over the mesa was included in the sequence (see Fig. 5), the fraction of VTDs remaining vertical was further reduced and depended on mesa width. In Fig. 6, the examples show (left) all VTDs turned to horizontal with none remaining vertical, and (right) a significant fraction remaining vertical. Also indicated on the images is the faceted shape expected for growth over the mesa to a height of 0.5 μm . The right figure shows that most remaining VTDs pass through the central mesa area, away from the {11-22} slanted facets that turn dislocations. We therefore interpreted the percentage of VTDs remaining vertical with a geometrical model using the fractional area of

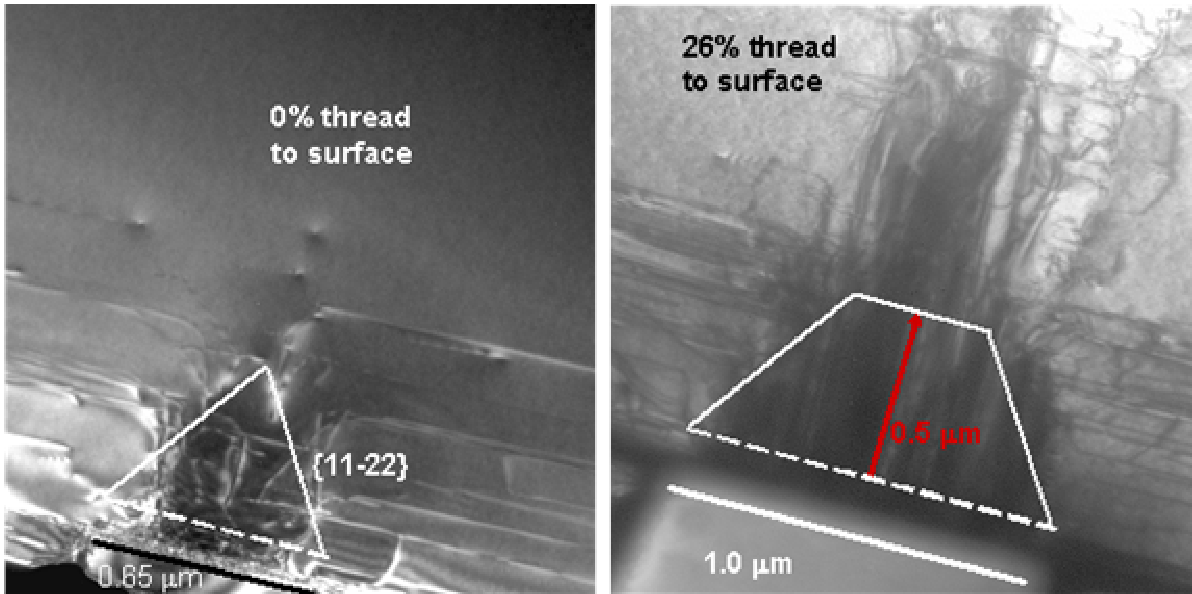


Figure 6. Cross-sectional TEM images of VTDs over mesas, grown with 950°C facet-forming step; expected facet shape is indicated. All VTDs are turned to horizontal over the narrow mesa (left), while VTDs remain vertical in the center of the wide mesa (right).

the mesa not covered by slanted facets, as in Fig. 7. The model correctly predicts the threshold in mesa width,

$\approx 0.6 \mu\text{m}$, below which no VTDs remain vertical. At greater mesa widths, the observed number falls below that predicted geometrically because both facet-based turning and turning due to narrow mesa width alone are operating together. This successful advance of CE growth methods was published in Applied Physics Letters [4].

In this investigation, nucleation of the nitride structure on the sapphire was done with an AlN nucleation layer, which in growth on planar sapphire (no CE) produces a VTD density of $\sim 2 \times 10^9/\text{cm}^2$. With the VTD turning methods just described, the VTD density at the top of the GaN layer was reduced to $3 - 8 \times 10^7/\text{cm}^2$, averaged across broad areas that included several mesas and coalescences. This represents a reduction in VTD density achieved with cantilever epitaxy of $\sim 1/40$ relative to planar growth.

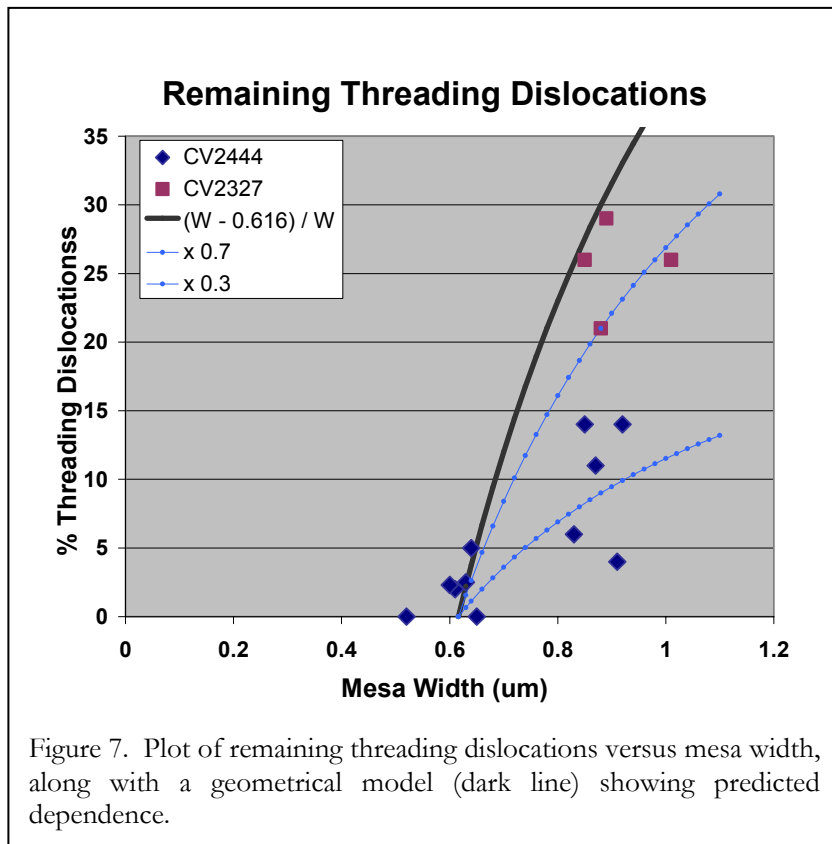


Figure 7. Plot of remaining threading dislocations versus mesa width, along with a geometrical model (dark line) showing predicted dependence.

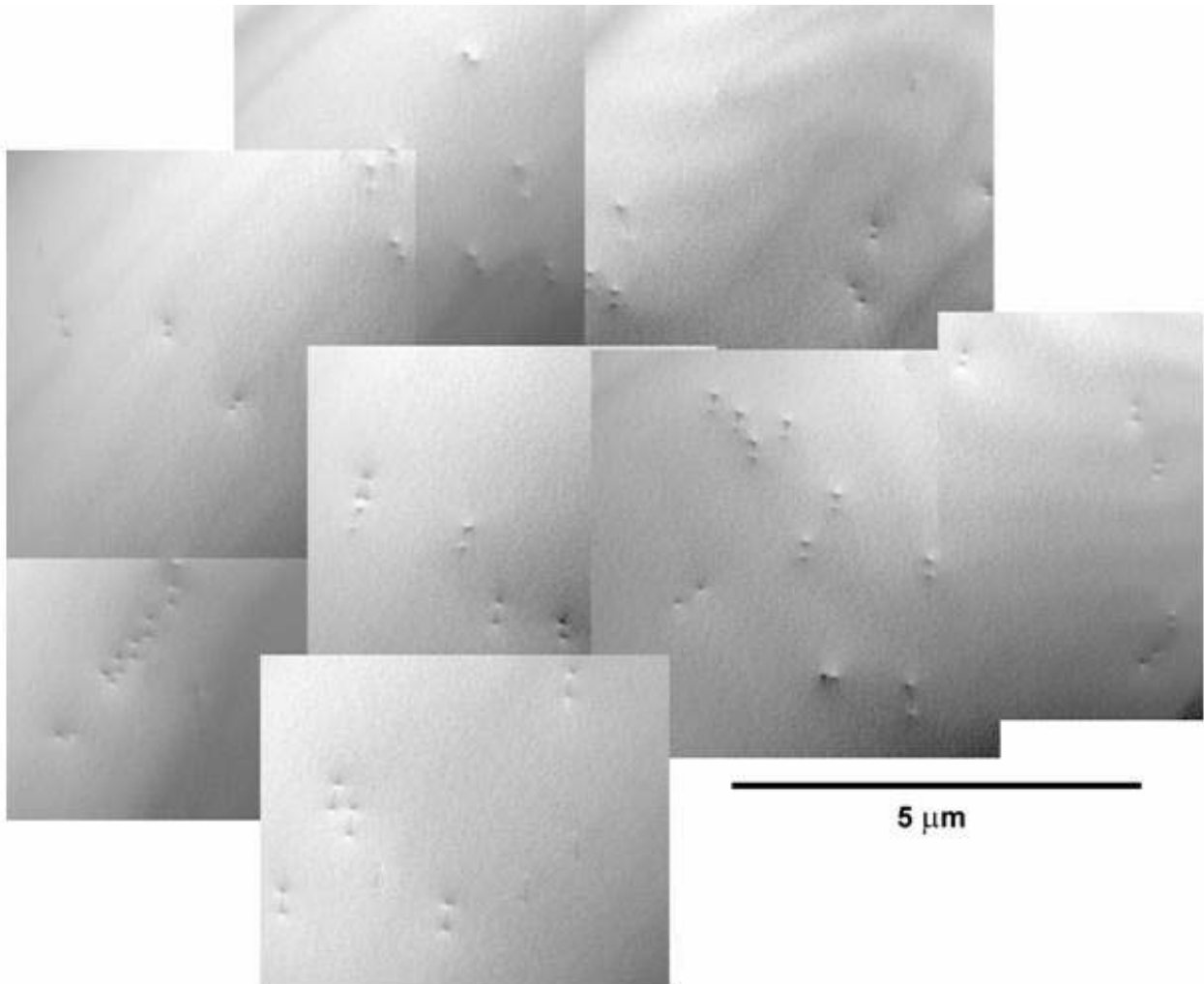


Figure 8. Plan-view transmission electron microscopy (TEM) image showing dislocations at the top surface of GaN, grown with facet-based dislocation turning during cantilever epitaxy. Most dislocations appear as two dots, in some cases with a thin line between them. The collage of images was put together to examine larger areas crossing multiple cantilevers. The dislocation density observed was $4.3 \times 10^7/\text{cm}^2$. In Ref. [7], we developed special contrast methods for TEM to insure that all dislocations were being detected and counted in such images.

B. Implement Inherently Low-VTD GaN Nucleation Layer

To reduce VTD densities further, we implemented a GaN nucleation layer to CE growth. This nucleation method was developed to reduce VTD density for planar growth on sapphire by delaying the transition from the nucleation layer with its faceted island morphology to the smooth, planar growth at high temperature [5]. In planar growth, this scheme produced a reduced dislocation density of $5 \times 10^8/\text{cm}^2$. When this method is used to nucleate GaN on mesas for CE growth that included faceting for VTD turning, a broad-area VTD density of $2\text{--}5 \times 10^7/\text{cm}^2$ was achieved for a reduction factor of $\sim 1/12$.

To assess VTD densities at the top of the GaN layer, we used a combination of AFM, scanning cathodoluminescence (CL), and plan-view TEM. A collage of plan-view TEM images is shown in Fig. 8, extending across several cantilever periods. To produce such broad-area TEM evaluations of VTD density,

special methods were developed for back-thinning the specimen through the sapphire substrate [6]. In cathodoluminescence, the VTDs reaching the surface appear as dark spots where the luminescence is quenched around the dislocations. With CL, even larger areas can be scanned readily using an SEM; this method gave the range of density noted immediately above using observations between several areas and specimens grown with the special GaN nucleation layer and the same CE growth details. The dark spots directly indicate why it is important to reduce VTDs: the dislocations are centers of non-radiative recombination of electrons and holes in GaN and in the active layer of LEDs that would be formed at the top surface.

C. Elimination of Dark-Block Defects

As we developed the CE growth methods described in A (narrow, faceted mesas) and B (GaN nucleation layer) above, our material apparently became more susceptible to a new type of structural defect. We labeled these “dark-block defects” for reasons that are apparent in the scanning cathodoluminescence image in Fig. 10: the defect appears as a dark, non-radiative rectangular block. Cross-section TEM showed that these are produced when misoriented cantilevers are grown together, which produces a crack between the cantilevers as seen in Fig. 11. Plan-view TEM showed dislocations bowing out along the crackline and radiating outward from voids at the ends of the crack. The typical dark-block defect microstructure is sketched in Fig. 12, and a plan-view TEM image with these features is shown in Fig. 13 [8]. Higher-magnification cathode-luminescence images like Fig. 10 (right) confirm that TEM is indeed examining the same defects by resolving individual dislocations bowing outward from the centerline. Because of their removing light emitted from their area, these defects clearly had to be eliminated.

Clues to the inherent cause of these defects were discovered through close examination of cantilever growths that were halted before coalescence. The SEM image in Fig. 14 shows that during cantilever growth, sections of material had developed that were tilted just as found with cross-section TEM. The perspective cross-section

SEM image in Fig. 15 shows the void at one end of the defect and the crack between coalesced cantilevers. It also shows that when the two tilted sections are grown together, the higher side overgrows the lower. This produces a surface relief that can be detected with optical microscopy and corresponds in shape and position with the dark, non-radiative areas seen with cathodoluminescence. All this information together indicated that the problem was with the initial growth of cantilevers and with the way they are grown together at coalescence.

We found that two modifications to our CE growths were able to eliminate dark-block defects [9]. First, the initial nucleation of GaN on the mesas needed to be fully dense. The SEM images of GaN nucleated on mesa tops and grown to the facet stage in Fig. 16 show a “worst case” produced with our earlier nucleation at 550°C, and the improvement to a fully developed, completed “gable” structure composed of two {11-22} crystal facets when the nucleation is done at 500°C instead. This well developed structure reduces the tilting of subsequently grown

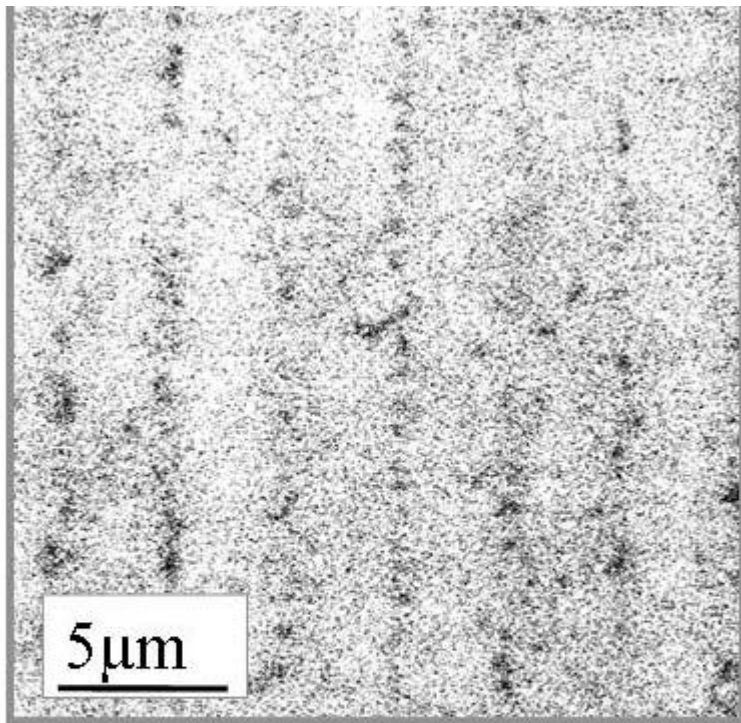


Figure 9. Scanning cathodoluminescence image showing VTDs (dark spots) at the surface of CE-GaN grown using the GaN nucleation layer [5] designed to reduce dislocation densities.

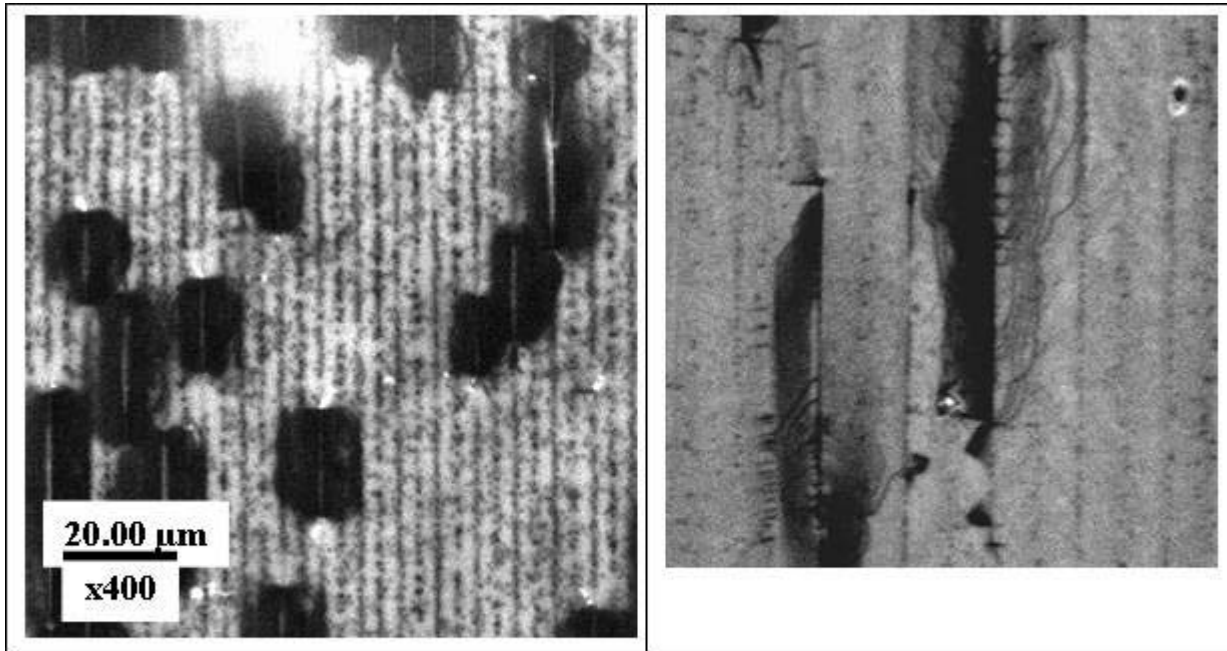


Figure 10. Scanning cathodoluminescence images showing dark-block defects that appear as non-radiative “blocks” (left), and at high magnification (right) are seen to show individual non-radiative dislocation lines bowing out from the centerline as found with TEM.

cantilever sections. Second, we found that when the cantilevers are grown together with reactor conditions producing $\{11-22\}$ facets at their edges, all dark-block defects could be eliminated. An example of such faceting at coalescence is shown in Fig. 17 where coalescence is almost completed. With these two modifications to our growth methods, non-radiative dark-block defects were eliminated.

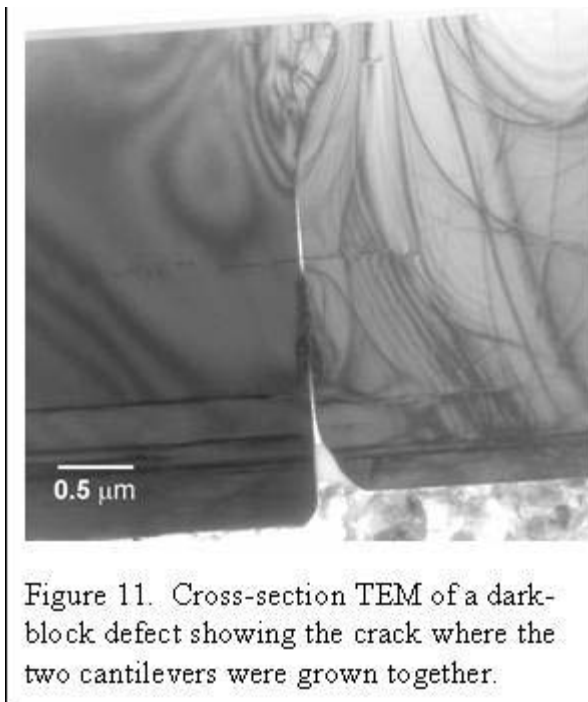


Figure 11. Cross-section TEM of a dark-block defect showing the crack where the two cantilevers were grown together.

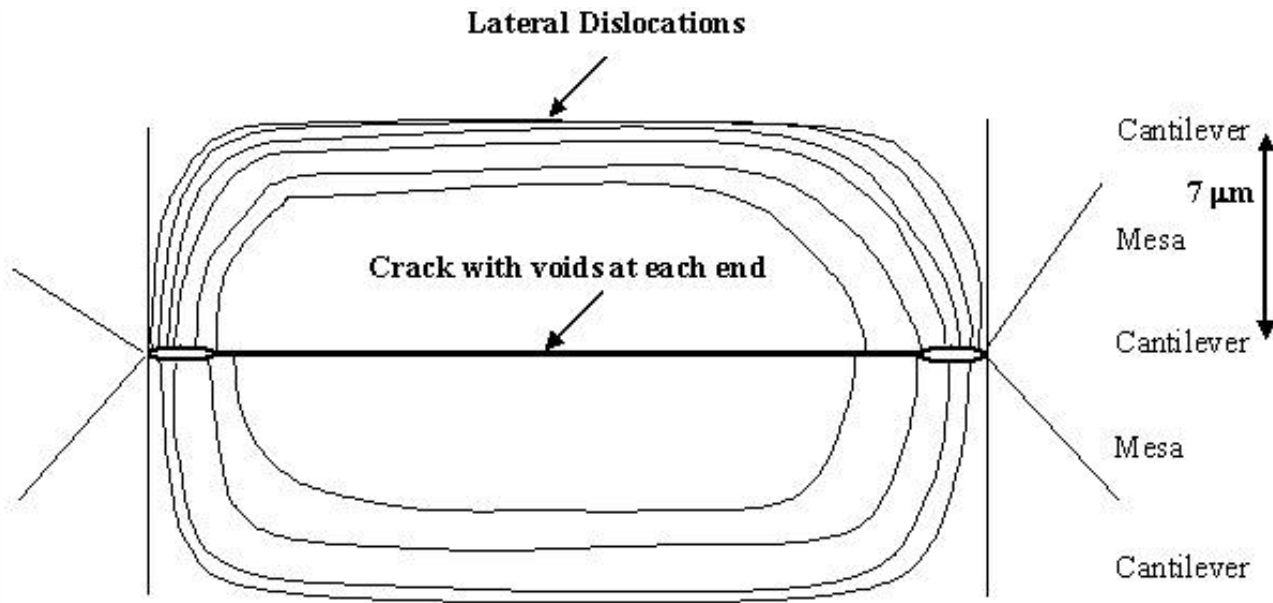


Figure 12. Schematic of microstructure of a dark-block defect as seen with plan-view TEM.

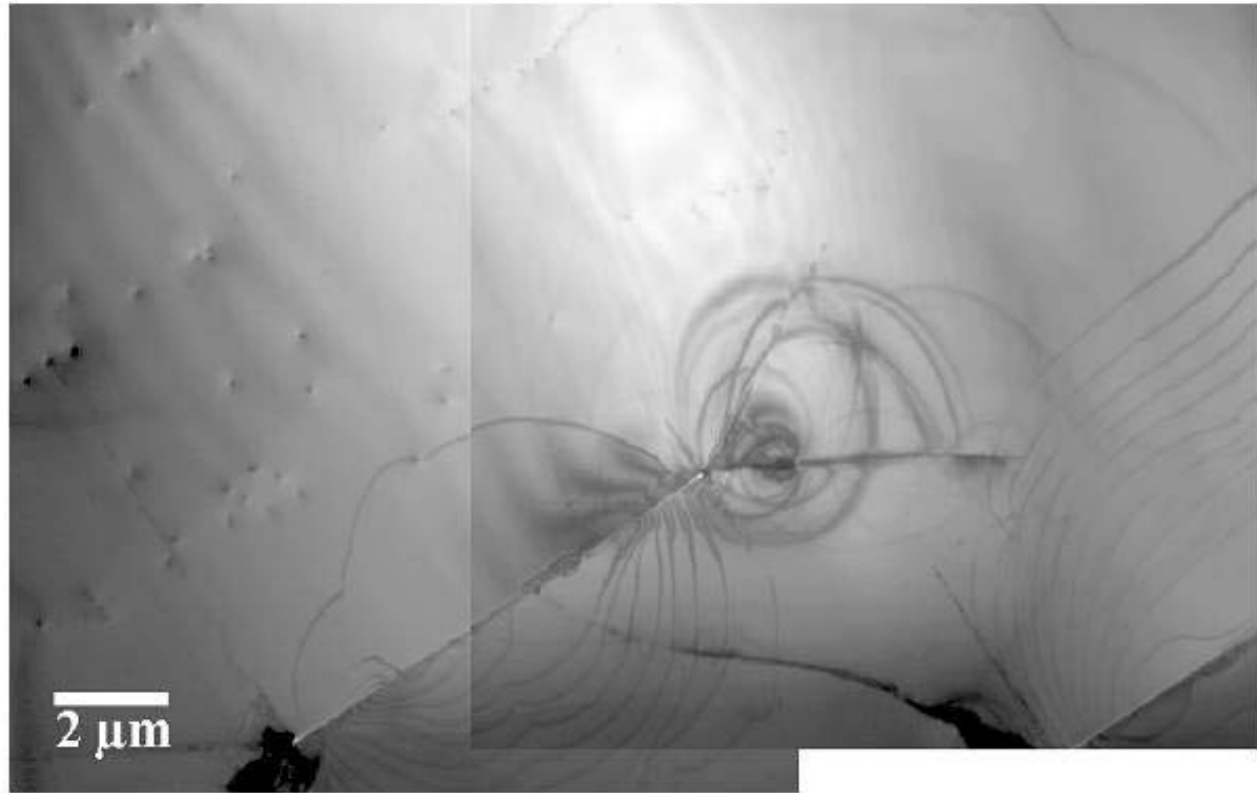


Figure 13. Plan-view TEM image showing a dark-block defect (lower and left of center) and part of a second defect at right. Note that the crack in the center appears as a line with a slightly broader void at each end. Dislocations bow outward from the centerline, and radiate in a “vee” shape from the end.

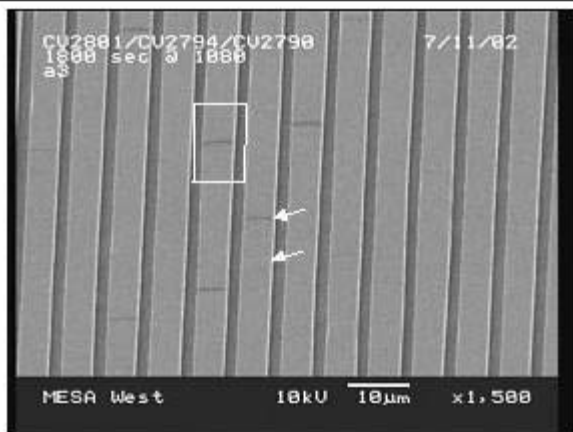


Figure 14. SEM image showing tilted sections of material formed along cantilevers during their growth.

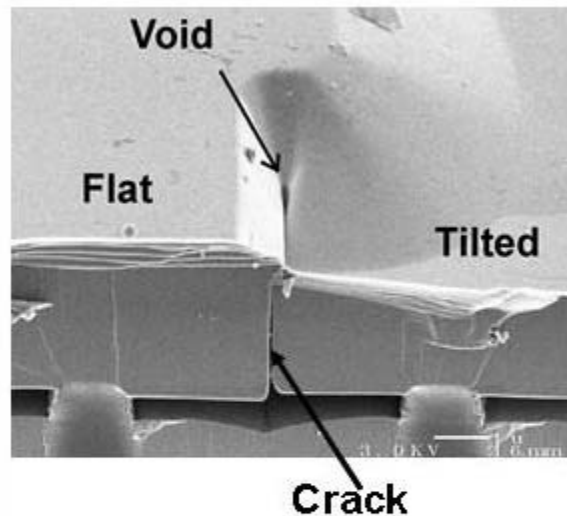


Figure 15. Perspective cross-section SEM image of one end of a dark-block defect, showing the crack between coalescing cantilevers, the void at the end, and overgrowth of the higher side.

D. Methods to Count Dislocations Accurately

TEM is generally accepted as the most accurate method to detect dislocations reliably, although it is limited to the small areas of the growth surface thinned for electron penetration. However, in the case of VTDs, discussions in the literature and with colleagues working with GaN suggested that screw dislocations, which have Burgers vector $\mathbf{b} = \mathbf{c}$ (where \mathbf{c} is the crystallographic unit displacement along the hexagonal axis) might go undetected. This was thought because the widely used criterion for TEM dislocation contrast, $\mathbf{g} \cdot \mathbf{b}$, is zero when imaging with diffraction vectors \mathbf{g} in the basal plane of the hexagonal crystal. With this criterion, the other

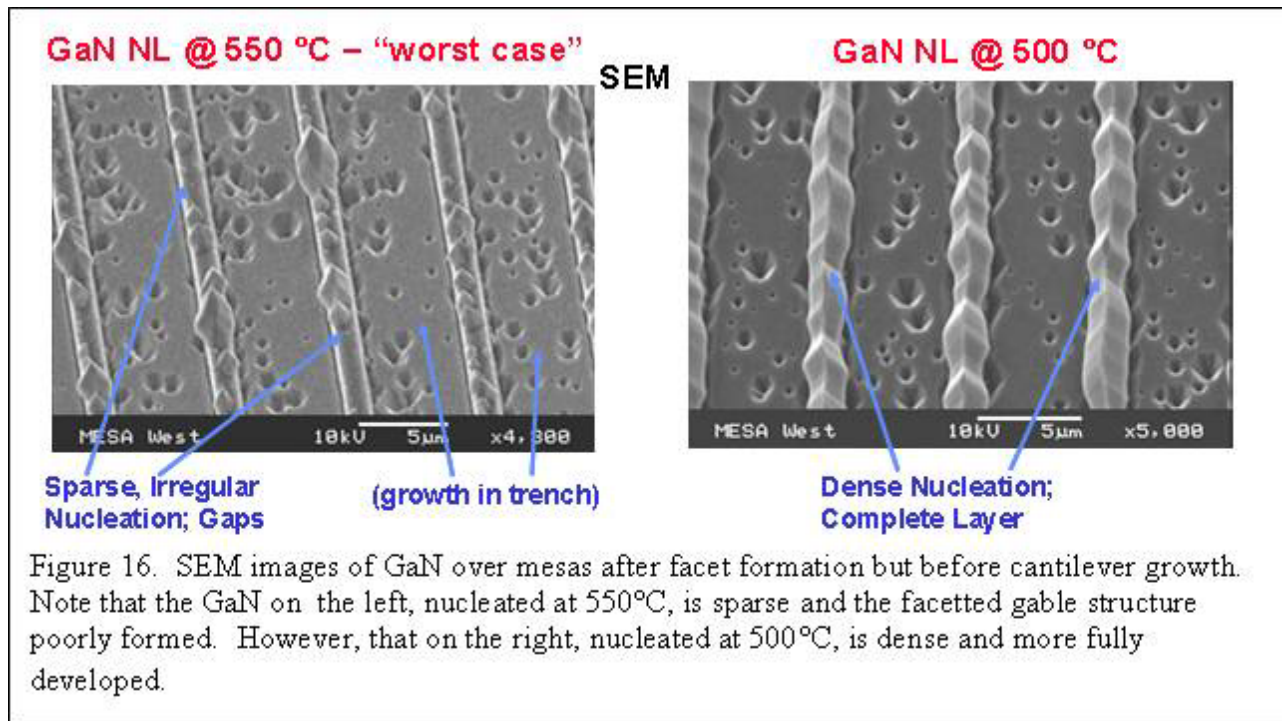


Figure 16. SEM images of GaN over mesas after facet formation but before cantilever growth. Note that the GaN on the left, nucleated at 550°C, is sparse and the faceted gable structure poorly formed. However, that on the right, nucleated at 500°C, is dense and more fully developed.

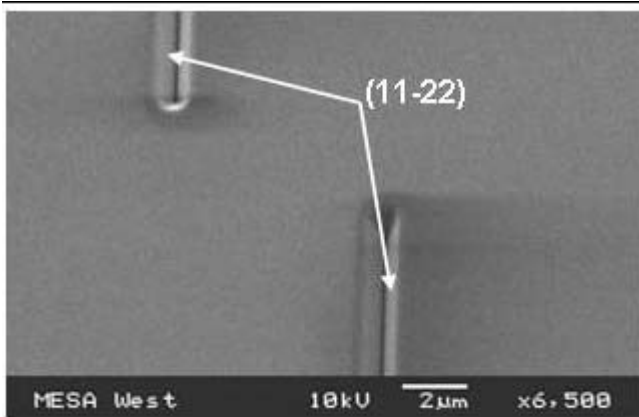


Figure 17. SEM image of coalescing cantilevers with (11-22) facets growing together.

We also developed methods to prepare TEM specimens with larger thin area for observation. These used special polishing wheels as discussed in Ref. [6]. These preparation methods produced the extended thin area for assessing dislocation densities seen in Fig. 8. We used the contrast identification method in Fig.18 to determine the percentages of the three VTD types in Fig. 8: screw: 22%, edge: 14%, mixed: 64%.

2.1.4 Cantilever Epitaxy: Summary and Implications for White Lighting

We have succeeded in developing cantilever epitaxial growth of GaN on sapphire substrates with dislocation densities as low as $2\text{-}5 \times 10^7/\text{cm}^2$, which is an order of magnitude or more lower than the densities with conventional planar growth. This CE-GaN meets the dislocation density specifications that the national roadmap for solid-state white lighting [11] calls for in 2007. Moreover, our density meets that required by an analysis considering how dislocations can limit the lifetime of devices [12]. It appears possible that further reductions are possible, and that CE-GaN can be produced at economically competitive prices. As shown in Sec. 5.2, near-UV LEDs grown on CE-GaN substrates show marked improvement in light output relative to similarly processed LEDs on planar GaN [10]. Thus cantilever epitaxy shows important potential as a substrate for the development of LEDs for solid-state white lighting.

2.1.5 References

1. C. I. H. Ashby, C. C. Mitchell, J. Han, N. A. Missert, P. P. Provencio, D. M. Follstaedt, G. M. Peake and L. Griego, *Appl. Phys. Lett.* 77, 3233 (2000).
2. Carol Iris Hill Ashby, David Martin Follstaedt, Christine C. Mitchell, and Jung Han, U.S. Patent No. 6,599,362 B2, Cantilever Epitaxial Process, issued July 29, 2003.

two dislocation types, edge with $\mathbf{b} = \mathbf{a}$ (\mathbf{a} is the crystallographic unit displacement in the basal plane) and mixed with $\mathbf{b} = \mathbf{a} + \mathbf{c}$, should be detected.

However, we demonstrated that a second contrast mechanism produced by strain relaxation around screw dislocation cores that intersect a free surface also operates. We identified an imaging method that allows all three dislocation types to be detected at once; moreover, it allows the type (screw, edge or mixed) of individual dislocations to be determined from their contrast. This identification of the three types is demonstrated in Fig. 18. In a rather dramatic reversal from the expected contrast, screw dislocations show strong contrast and are readily detected, whereas edge dislocations show weaker contrast and require careful imaging to detect. Our imaging methods and the demonstration of dislocation identification were published in Ref. [7]

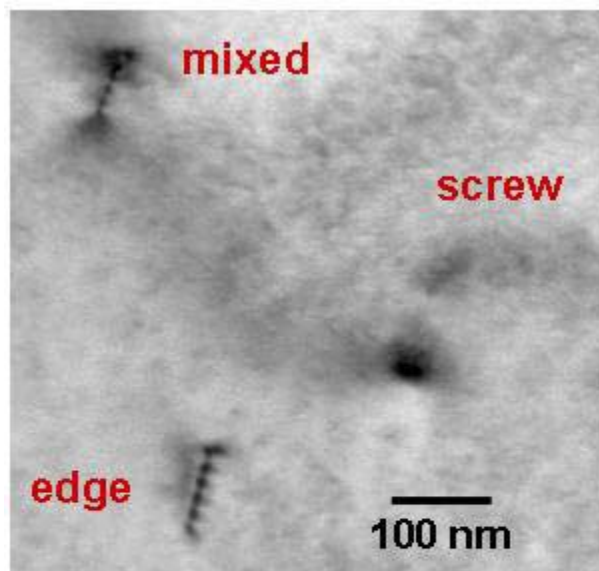


Figure 18. Image demonstrating that all three VTD types can be detected and identified in plan-view TEM [7].

3. A. Sakai, H. Sunakawa and A. Usui, Appl. Phys. Lett. 71, 2259 (1997); Appl. Phys. Lett. 76, 442 (2000).
4. D. M. Follstaedt, P. P. Provencio, N. A. Missert, C. C. Mitchell, D. D. Koleske, A. A. Allerman and C. I. H. Ashby, Appl. Phys. Lett. 81, 2758 (2002).
5. D. D. Koleske, A. J. Fischer, A. A. Allerman, C. C. Mitchell, S. R. Kurtz, J. J. Figiel, K. W. Fullmer and W. G. Breiland, Appl. Phys. Lett. 81, 1940 (2002).
6. M. P. Moran, A. K. Norman and D. M. Follstaedt, Microscopy and Microanalysis 9, Suppl. 2, 106 (2003).
7. D. M. Follstaedt, N. A. Missert, D. D. Koleske, C. C. Mitchell and K. C. Cross, Appl. Phys. Lett. 83, 4797 (2003).
8. P.P. Provencio, D.M. Follstaedt, N.A. Missert, D.D. Koleske, C.C. Mitchell, A.A. Allerman and C.I.H. Ashby, Mat. Res. Soc. Symp. Proc. 743, L3.15 (2003).
9. C. C. Mitchell, Defect Reduction in Gallium Nitride using Cantilever Epitaxy, Thesis, UNM Electrical Engineering Department, 4/4/03, Albuquerque, NM.
10. A. J. Fischer, D. D. Koleske, A. A. Allerman, M. H. Crawford, K. H. A. Bogart, C. C. Mitchell, D. M. Follstaedt, K. C. Cross, K. W. Fullmer and J. J. Figiel, Proceedings of the 204th Mtg. of the Electrochemical Society meeting, Florida, October 12-16, 2003.
11. "Light Emitting Diodes (LEDs) for General Illumination: An OIDA Technology Roadmap Update", ed. J. Y. Tsao (Optoelectronics Industry Development Association, 2002).
12. J. Y. Tsao, "Solid-State Lighting: Lamps, Chips and Materials for Tomorrow", to be published in IEEE Circuits and Devices, May, 2004.

2.2 Controlling GaN Thin Film Evolution (DD Koleske, AJ Fischer, ME Coltrin, AA Allerman, CC Mitchell, KC Cross, SR Kurtz, MJ Russell, JJ Figiel, KW Fullmer, WG Breiland)

2.2.1 Abstract

The utility of optical reflectance to measure and control GaN thin film evolution on sapphire is discussed. We show how optical reflectance can be used to quantitatively control the GaN nucleation layer (NL) thickness, measure GaN NL decomposition kinetics and NL roughening, and intentionally delay the transition from three-dimensional (3D) grain growth to two-dimensional (2D) coalescence of GaN films on sapphire. Factors that contribute to the measured optical reflectance signal, such as thickness changes and roughness attenuation, are used to quantify the GaN film evolution. Optical reflectance is also used in conjunction with atomic force microscopy to study the details of GaN NL evolution as it is heated from low to high temperature. Finally, based on the optical reflectance measurements of grain coalescence, the reduction in the dislocation density of GaN films on sapphire is demonstrated by intentionally delaying the 3D grain growth to 2D coalescence transition. Improvements in 380 nm light emitting diodes (LEDs) were also observed when the 3D to 2D coalescence transition was intentionally delayed.

2.2.2 Introduction: Need for Control Over GaN Epitaxy

GaN-based ultraviolet (UV) emitters are gaining interest as pump sources for developing white light emitting diodes (LEDs), and much research is currently focused on maximizing the efficiency of visible and UV GaN-emitters. As recently observed in UV LEDs, threading dislocations (TDs) may reduce light output to a greater degree than they do for blue GaN-based LEDs [1, 2]. The proposed reason for the greater influence of TD on UV light output is because the minority carriers are decreasingly localized in the In-rich quantum wells and increasingly trapped at TDs or other nonradiative recombination centers [3]. Ultimately, if TDs limit UV LED light output, then approaches that reduce the TD density such as lateral overgrowth [4-6], in-situ masking [7], facet control [8] or interlayers [9], will be necessary to reduce the TD density in GaN UV LEDs.

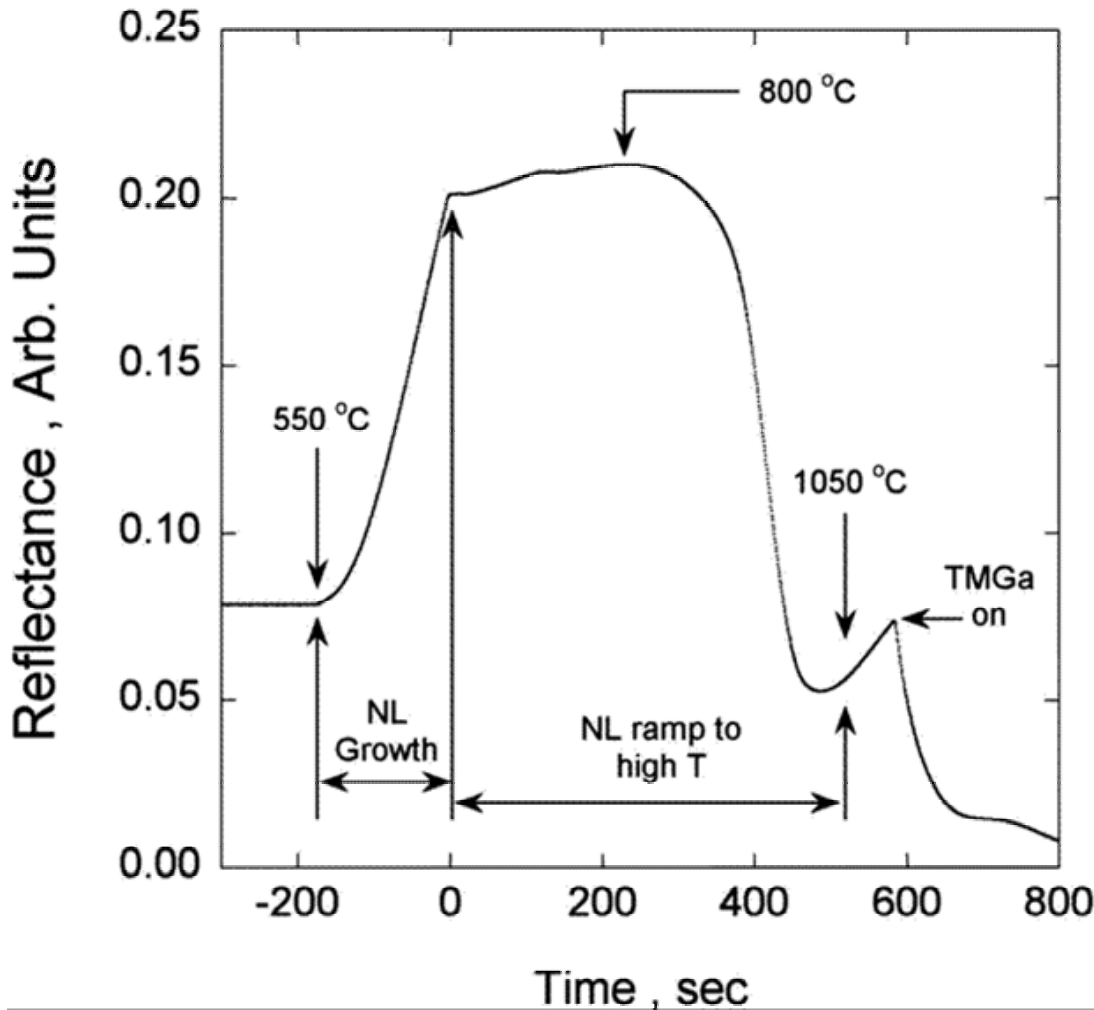


Fig. 1. Plot of the reflectance waveform measured at 550 nm vs. time for GaN nucleation layer growth and annealing. The reflectance signal is normalized to room temperature sapphire ($R_{\text{initial}} = 0.0773$ based on $n_i = 1.77$).

In addition to reducing dislocation density in UV LEDs, monitoring and controlling the group III-nitride MOCVD growth process is desired because of changes in the kinetic reaction rates, parasitic gas phase chemistry, and build up of wall deposits in the reactor. While several light-based in-situ diagnostics have been used to monitor MOCVD growth, normal-incidence optical reflectance has proved to be most useful for monitoring growth and determining growth rates [10]. During each growth run the optical reflectance provides a unique signature, however the interpretation of this unique signature is sometime difficult because the relative physical contributions to optical reflectance are not well understood.

No where is the lack of understanding more apparent than in understanding the details of GaN nucleation layer (NL) evolution on sapphire. Even after GaN NLs were first developed independently by Nakamura [11] and Wickenden et al. [12], few comprehensive studies have been conducted on how the NLs evolve after they are deposited at low temperature (ex. 550 °C) and annealed up to the high temperature (ex. 1050 °C) growth conditions. Typically, the NL growth conditions are empirically varied until optimal optical or electronic properties are achieved [11]. The NL evolution can be readily observed in the optical reflectance waveform [13] and the evolution can be dramatically changed by changing the decomposition kinetics that contribute to the NL evolution.

While the use of GaN NLs is universally practiced for achieving smooth low dislocation density (10^9 cm^{-2}) GaN films, the high temperature, T, growth factors have also been shown to influence the GaN dislocation density. The pressure, NH₃ flow, and growth T also influence the TD density [14] and lateral ordering [15]. Recently, Figge et al. have shown that lower V/III ratios (i.e. the NH₃ flux divided by the trimethylgallium flux) can be used to delay coalescence of GaN films grown at 150 Torr [16]. As suggested by Figge and coworkers, delaying the GaN islands from too quickly coalescing reduces the TD density [16]. Although the mechanism for the TD reduction was not demonstrated in Ref 16, both the 150 Torr (at low V/III) and 700 Torr (at high V/III) growth conditions favor the formation of hexagonal pyramids with (1101) facets, which bend TDs laterally as the grains coalesce [8]. In addition, the growth conditions at 150 and 700 Torr resulted in similar reflectance waveforms [16], suggesting a similar GaN microstructure can be achieved at both high and low growth pressure.

2.2.3 Experimental Conditions

For these studies GaN was grown on c-plane sapphire using metalorganic chemical vapor deposition (MOCVD) in a high-speed rotating disk reactor [17, 18]. Trimethylgallium (TMGa), trimethylaluminum (TMAI), trimethylindium (TMIIn), and ammonia (NH₃) were used in H₂ and N₂ carrier gases to grow, the GaN NLs, GaN high T layers, and LED structures. The films were doped n-type using 100 ppm silane (SiH₄) in He and p-type using biscyclopentadienylmagnesium (cp₂Mg).

Prior to the growth of the NLs the c-plane sapphire wafers were heated to 1080 °C in following H₂ for 10 min., heated in NH₃ for 2 min. at 750 °C. The NLs were grown at 540 °C and the high T GaN layers were grown at 1050 °C. The total reactor flow rate was maintained at 12 SLM by adding or removing H₂. The LED structures were grown on top of > 3 μm thick GaN films. The LED structure consisted of a 20 nm thick Si:AlGaIn layer (4%), a 4 nm thick InGaIn (4%) quantum well, a 10 nm thick Si:GaIn quantum barrier (repeated 5 times), a 10 nm Mg:GaIn layer, a 20 nm thick Mg:AlGaIn (10%) confinement layer, followed by a 250 nm thick Mg:GaIn layer was grown. The active region of the LED was grown at 200 Torr and the p-type doped layers at 140 Torr.

The T of the Mo and SiC coated susceptor was measured through a top quartz window using an emissivity correcting pyrometer at wavelengths of 550 and 900 nm. The T was also measured with a thermocouple placed 5 mm beneath the susceptor. Since sapphire is transparent at the measured wavelengths, the optical pyrometer reads the emission from the Mo plate under the sapphire wafer. The T reproducibility measured with both the pyrometer and thermocouple was to within 2 °C.

The optical reflectance unit is a near-normal probe using a tungsten-halogen lamp and a 10 nm bandwidth filter at 550 and 900 nm [10]. During data collection the initial reflectance voltage from the photodiode was normalized to the reflectance of sapphire at room temperature which is 0.0773, based on the value for the optical constant $n_i = 1.77$ [19, 20]. One large advantage of the reflectance design is that a tungsten halogen lamp is used which produces much more stable light intensity compared to other light sources [10]. In addition the susceptor and rotation shaft were precision machined to reduce wobble on the susceptor. As a result the reflectance could be typically measured to 5 decimal places, resulting in a large signal to noise ratio. The measured signal to noise ratio even at 1080 °C was measured during some growth runs greater than 2000.

2.2.4 Controlling Nucleation Layer Thickness

Early on, Nakamura reported on the influence of the NL thickness on the electronic properties of GaN films [11]. Other groups have also demonstrated the importance of NL thickness [21-23] for achieving high quality GaN films. Typically a constant NL growth rate is assumed so that a given NL thickness can be obtained in a fixed amount of time. While this approach gives specular GaN films on sapphire most of the time, non specular or rougher films can occur due to drift in GaN reactor conditions, especially after the reactor has been cleaned or if thick coatings develop over time on the reactor walls.

A typical reflectance waveform for the early stages of GaN growth on sapphire is shown in Fig. 1. The initial reflectance signal is assigned the value of 0.773 for sapphire. As the GaN NL grows the reflectance signal

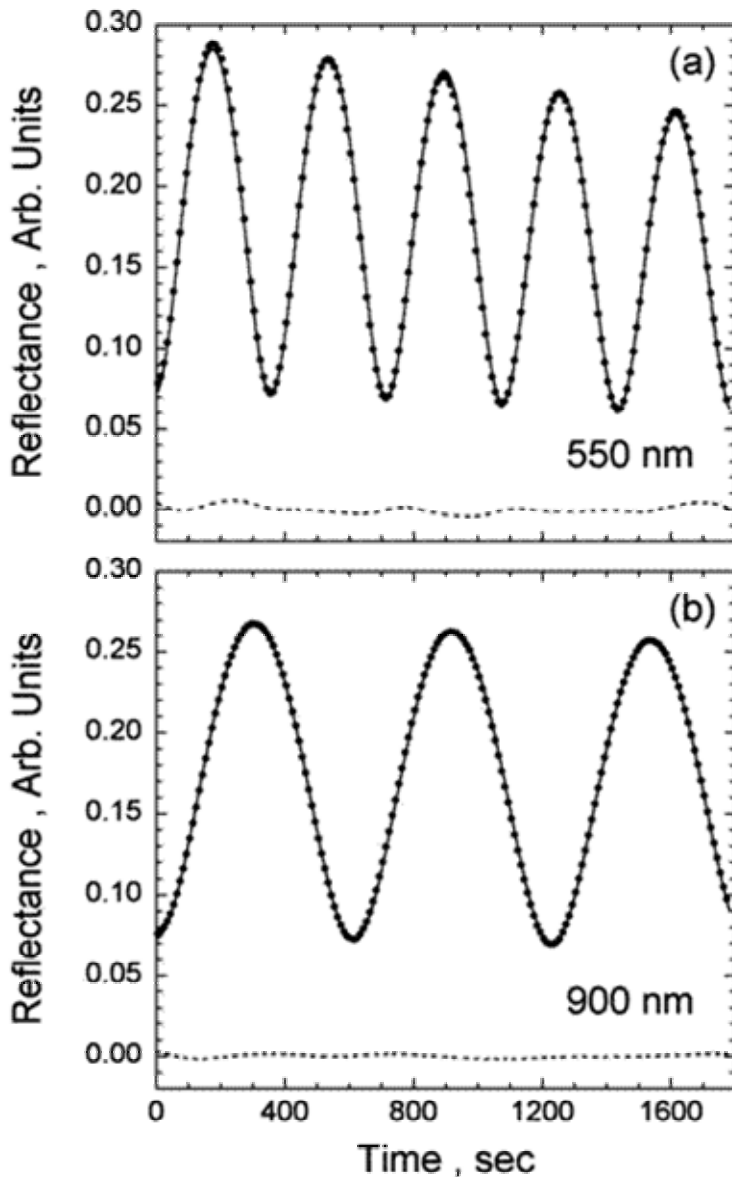


Fig. 2. The reflectance waveforms for thick GaN NL are plotted vs. time at wavelengths of (a) 550 nm and (b) 900 nm. The solid circles denote 10% of the measured reflectance signal and the solid lines are fits to the data using Eq. 4 from Appendix A. The dashed line is the difference between the experimental data and the theoretical fit. Growth rates of 0.319 nm/s and 0.305 nm/s were calculated from the 550 nm and 900 nm waveforms, respectively.

0.009 nm/s. Since the NL thickness increases linearly in time and the reflectance signal is measured linearly in time, a one-to-one mapping of the reflectance signal to the NL thickness can be achieved.

increases, until after about 3 min. a reflectance value of 0.200 is achieved. At this time the TMGa is shut off and the NL growth stops. After growth, the NL is ramped in T to 1050 °C in flowing NH₃ and H₂ and the reflectance signal first increases and then decreases. When the T reaches 1050 °C the reflectance signal reaches a minimum and the NL is annealed for 60 additional seconds before the TMGa is again turned on for continued growth of GaN. In this section we will discuss controlling the NL thickness, while in sections 4 and 5 the NL decomposition kinetics and changes in the NL morphology will be discussed, respectively.

While stopping at the reflectance value of 0.200 is arbitrary, it provides a well defined NL thickness as a starting point for the GaN film growth. By using reflectance the NL thickness can be controlled rather than relying on NL growth rate to be constant and timing the NL growth to achieve a particular thickness.

To calibrate the NL thickness optically, thick GaN NL were grown. In Fig. 2, the optical reflectance waveform for a thick NL is shown at both (a) 550 nm and (b) 900 nm. The solid circles denote 10% of the measured reflectance waveform values. The solid lines are fits based on Eq. 6 from Ref. 10 with the assumptions that the substrate and film are optically transparent and the NL roughness increases linearly with the film thickness. The waveform derivation includes a roughness term which accounts for the gradual decrease in the waveform amplitude as the NL thickness increases. The dotted lines in Fig. 2 are the calculated residuals between the measured waveform and the fit. From these fits growth rates of 0.319 nm/s is calculated for the 550 nm waveform and a growth rate of 0.305 nm/s is calculated for the 900 nm waveform for an average of $0.312 \pm$

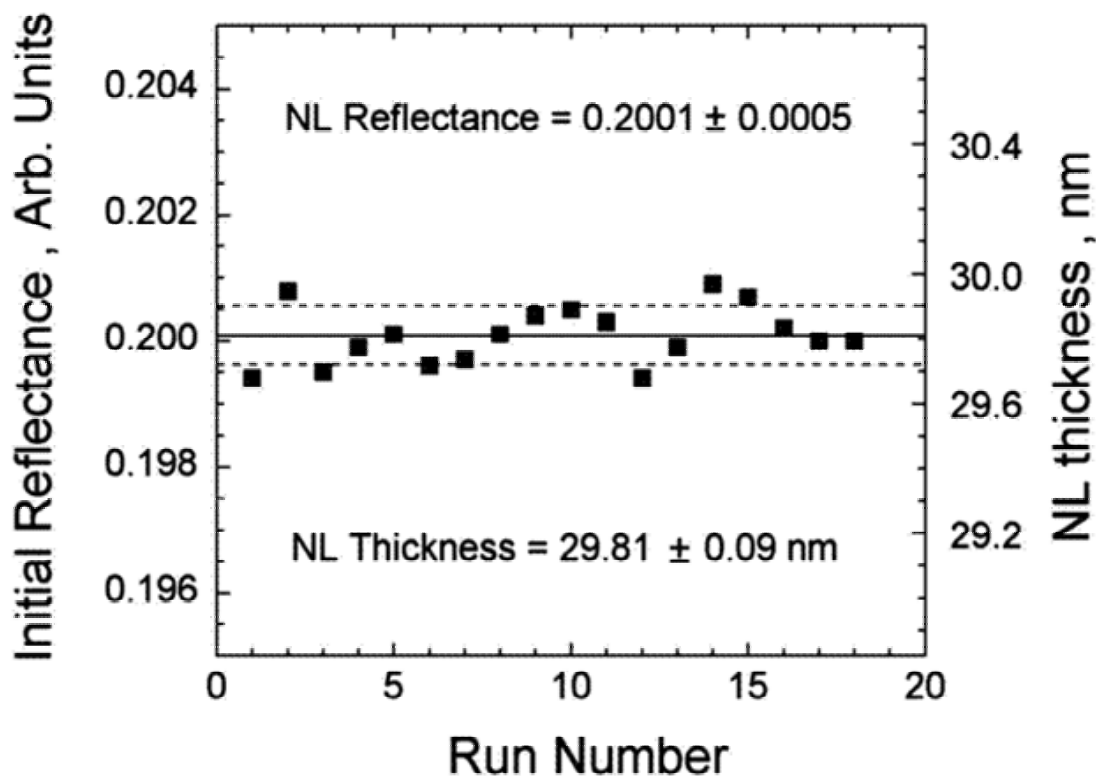


Fig. 3. Plot of the NL reflectance (left axis) and the NL thickness (right axis) vs. run number. For these growth runs a reflectance value of 0.2000 was targeted to shut off the TMGa to complete the NL growth. The NL thickness was calculated from the reflectance signal based on Fig. 6. For these 18 growth runs, an average NL reflectance of 0.2001 ± 0.0005 was achieved, which corresponded to a NL thickness of 29.81 ± 0.09 nm.

To test the use of reflectance to control NL thickness, 18 GaN NLs were grown. For each NLs shown in Fig. 3, the TMGa was shut off near a reflectance value of 0.195 to target a final reflectance value of 0.200. For the growth of these 18 NLs, the growth time had to be varied in order to reach the 0.200 reflectance level. As shown in Fig. 3, reflectance signals of 0.2001 ± 0.0005 were obtained. Using the NL growth rate obtained from Fig. 3, the reflectance signal corresponds to a NL thickness of 29.81 ± 0.09 nm. The solid line on Fig. 3 is the average of the NL thicknesses and the dashed lines are one standard deviation (0.09 nm) away from this average. The growth times for the NLs varied from 123 to 192 sec. with the average being 145.5 ± 13 sec. If a fixed NL growth time of 120 seconds was used instead of the reflectance a NL thickness of 25.4 ± 1.5 nm would have been achieved, which is 16 times larger deviation in the NL thickness compared to reflectance control.

2.2.5 GaN Nucleation Layer Decomposition Kinetics

After the growth of the low T GaN nucleation layer (NL), it is well known that the NL evolves during the T ramp from low (≈ 550 °C) to high (≈ 1050 °C) T before growth of the high T GaN layer. Because the annealed NL is a key determinant of the resultant defect densities in subsequently grown high-T GaN epilayers, it is important to understand the NL evolution and to ultimately develop methods to track and quantify the NL evolution. In this letter, we present systematic measurements of the NL decomposition kinetics over a range of pressures, gas mixtures, and temperatures. We show that in addition to coarsening [24, 25], the NL can undergo significant decomposition during the ramp from low to high T [13].

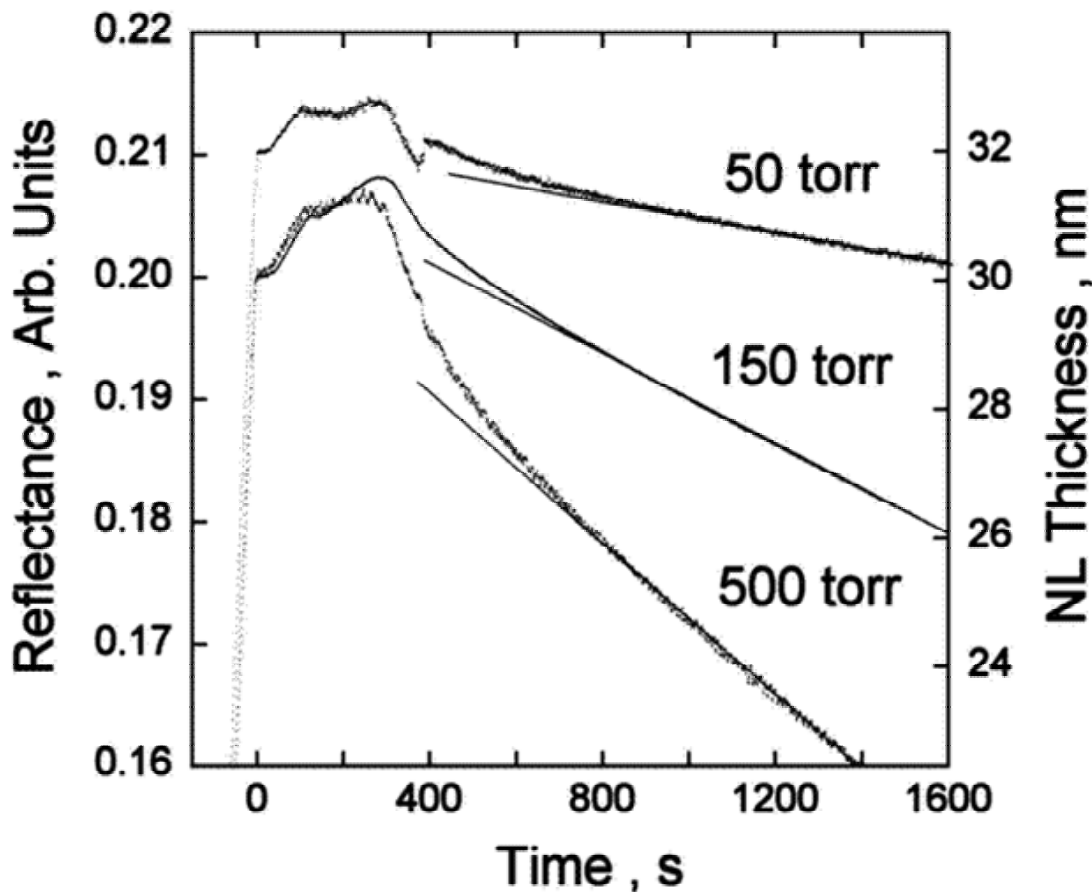


Fig. 4. Reflectance wave forms plotted vs time for three different pressures. Along the left axis the reflectance signal is plotted and along the right axis the nucleation layer thickness is plotted. At time zero the nucleation layer growth is completed and the final annealing conditions are established by 500 s. The solid lines are linear fits to the decrease in the nucleation layer thickness.

Atomic force microscope (AFM) images of as grown and annealed GaN NL at different T are shown in Fig. 4. In Fig. 4, an as grown NL is shown along with three subsequent NLs annealed to T of (b) 850 °C, (c) 960 °C, and (d) 1050 °C. Each AFM image in Fig. 4 is $3 \times 3 \mu\text{m}$ in width and 150 nm full scale in height. The measured root-mean-square roughness in Figs. 4(a) and 4(b) was 1 nm and increased to 5 nm in Fig. 4(c) and 16 nm in Fig. 4(d). Note that no significant restructuring of the NL occurs until the $T \geq 960$ °C. This is important for the decomposition measurements because it allows simple interpretation of decreases in the reflectance signal into decreases in the NL thickness.

To study NL decomposition, the GaN NL growth conditions were kept the same and only the GaN NL ramp and annealing conditions were varied. To obtain the NL decomposition rates for different annealing conditions, the GaN NLs were grown and the decomposition rate measured, followed by high T anneals without NH_3 to fully remove the NL and return the reflectance signal close to the initial sapphire value. This process of NL growth, decomposition, and desorption was repeated up to 10 times in a single experiment.

The reflectance waveforms for GaN NLs annealed at three different P are plotted in Fig. 5, along with the NL thickness that the waveform signal corresponds to. At time zero the 30 nm thick NL growth is complete. The NL is then ramped to 850 °C at a ramp rate of 70 °C/min. Next, the NL was ramped to 900 °C, and the pressure adjusted under 6 SLM NH_3 flow. Note that for times greater than 800 s, the GaN NL thickness decreases linearly in time, which then yields the NL decomposition rate. Note that the NL decomposition rate is

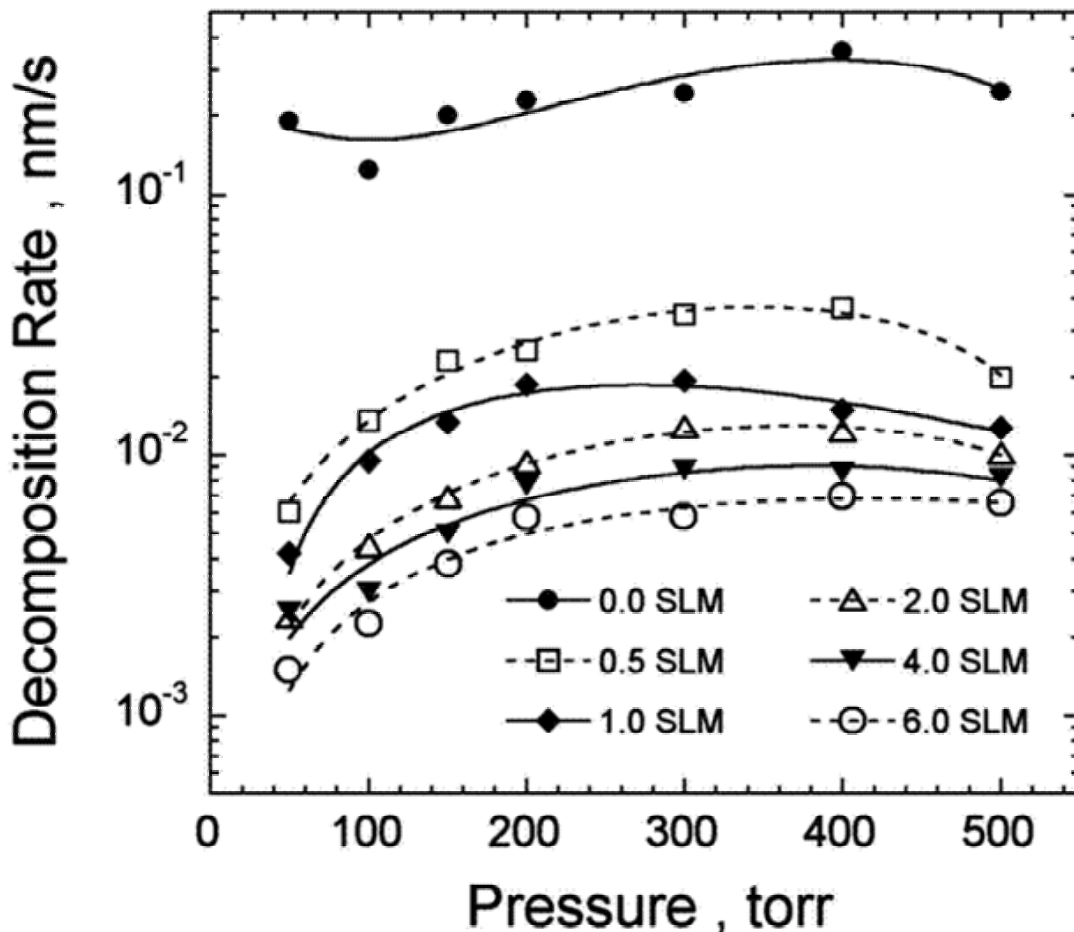


Fig. 5. Plot of the nucleation layer decomposition rate at 900 °C vs. pressure. The four sets of data correspond to NH₃ flow rates of 0.5 SLM (filled circles), 2.0 SLM (open squares), 4.0 SLM (solid diamonds), and 6.0 SLM (open triangles). The solid and dashed lines are fits to guide the eye.

largest at 500 Torr and decreases at 150 and at 50 Torr. Note that a straight line can be fit to the data for times > 800 s with the slope being the NL decomposition rate.

The GaN NL decomposition rates at 900 °C vs. pressure are shown in Fig. 5. Six data sets are shown using different flows of NH₃, ranging from 0.0 to 6.0 SLM. The solid and dashed lines are fits to the data to serve as guides for the eye. In general, the decomposition rate increases with increasing P up to 400 torr with a slight decrease at 500 torr for the lower NH₃ flows. Also, the decomposition rate decreases as the NH₃ flow increases, suggesting that the additional N from the NH₃ partially suppress decomposition. Note that a similar decomposition rate of 0.006 nm/s can be achieved using 0.5 SLM NH₃ at 50 torr, 4.0 SLM NH₃ at 200 torr, and 6.0 SLM NH₃ at 400 torr.

Although the decomposition rates vary as a function of NH₃ flow and P, a similar decomposition mechanism is likely responsible for these changes. This is shown in Fig. 6 where the GaN NL decomposition rates (filled symbols) are plotted vs. reciprocal T at P of 500, 150 and 50 torr. Independent fits for all three P resulted in an average activation energy, EA, of 2.71, 2.66, and 2.66 eV for P of 500, 150, and 50 torr, resulting in an average EA of 2.7 ± 0.2 eV over the T range 820 to 960 °C. In Fig. 4, the NL decomposition rates are fit using the EA of 2.7 eV, resulting in a different pre-exponential factor A₀ (i.e. intercept) for each P.

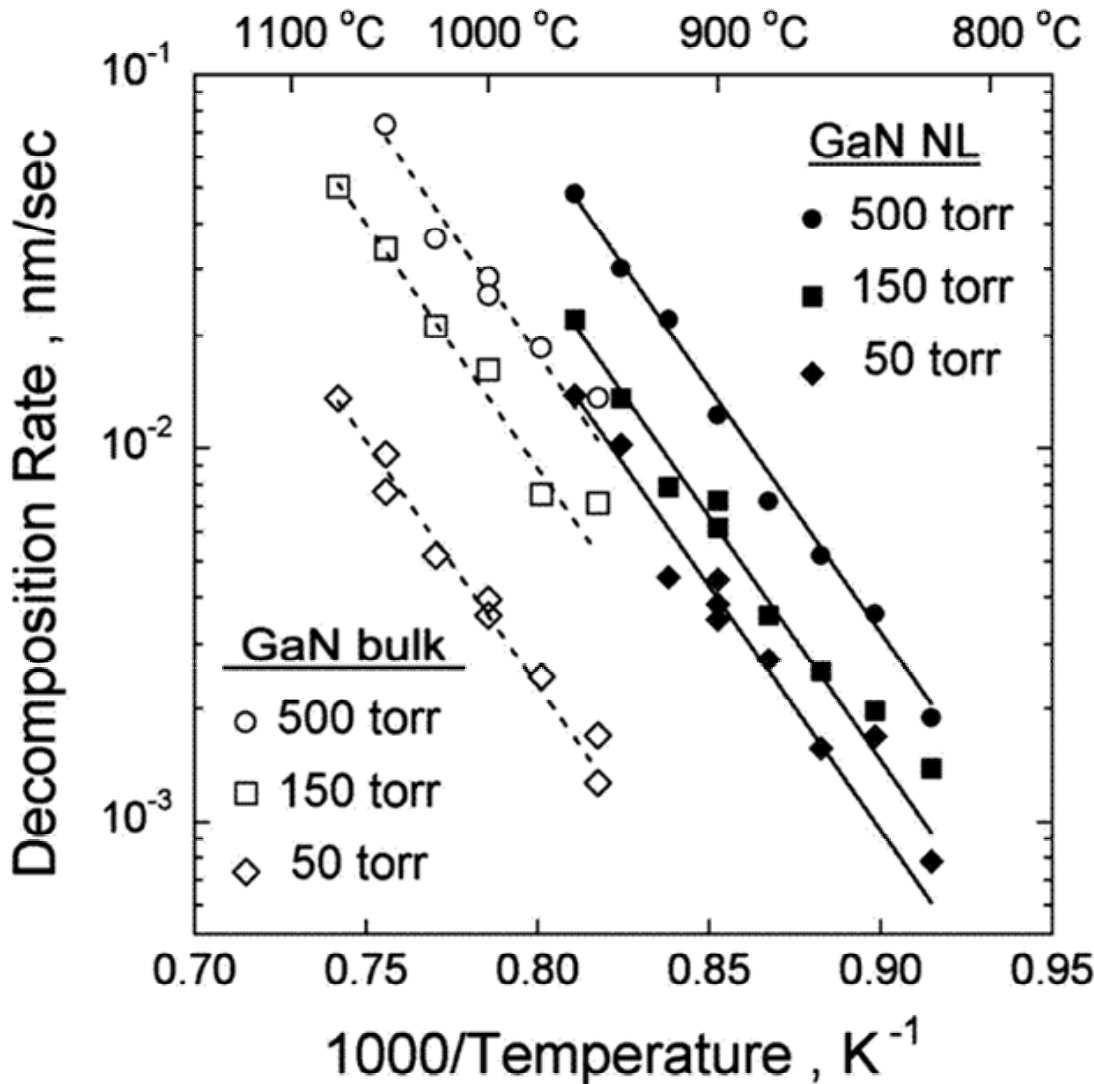


Fig. 6. Arrhenius plot of the GaN NL and bulk film decomposition rates vs. reciprocal temperature. The filled symbols denote decomposition rates for GaN NL at 500 (circles), 150 (squares), and 50 (diamonds) torr. The open symbols denote the decomposition rates of bulk GaN films grown at high temperature for the same pressures. The solid and dashed lines are exponential fits to the data using an activation energy of 2.7 eV. The temperatures corresponding the reciprocal temperature values are marked on the top x-axis.

Also plotted in Fig. 6 are the GaN decomposition rates (open symbols) for thick ($> 2 \mu\text{m}$) bulk high T GaN films for P of 500, 150, and 50 torr over the T range of 900 to 1075 °C. The average EA for decomposition on these bulk films was also 2.7 ± 0.2 eV, which is the same as the EA for NL decomposition.

Interpretation of the differences in A_0 for both NL and bulk film decomposition as the P changes is complicated by possible changes in the surface T as P is varied. However, comparison of the A_0 for NL and bulk film decomposition at constant P is valid since both films are annealed under the same conditions. From Fig. 6 it is apparent that the A_0 for NL decomposition was a factor 4 (500 torr) to 9 (50 torr) times larger than the A_0 for bulk GaN decomposition, suggesting an increase in the site density for the decomposition chemistry.

The EA measured for NL and bulk decomposition are very close to the EA of 2.7-2.8 eV measured for Ga desorption from GaN, GaAs, and liquid Ga surfaces [26]. This suggests a decomposition mechanism whereby H₂ and NH₃ add H to the GaN surface, leading to the formation of NH₃ and liquid Ga atoms. This is possible

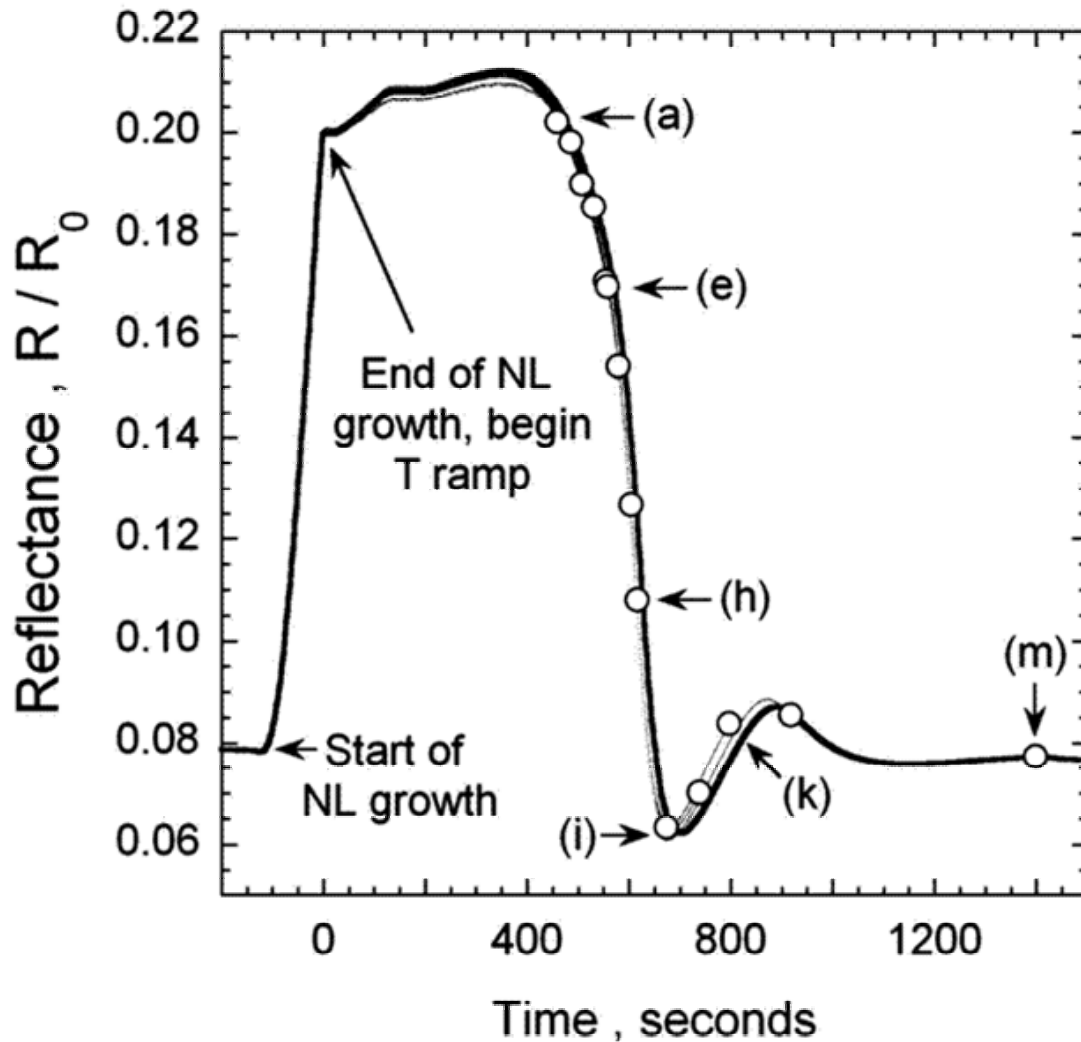


Fig 7. Plot of the reflectance waveform vs. time for the GaN nucleation layer (NL) growth and annealing is shown as the thick line. The NL is grown to a thickness of 30.0 ± 0.1 nm, after which the NL is ramped from 550 °C to 1050 °C. The open circles denote the points at which the annealing schedule was stopped and the T decreased to freeze in the NL structure. The thin lines are the individual reflectance waveforms for each of the 13 annealing runs. The letter symbols denote the various stopping points in T and time corresponding to the images shown in Fig. 4.

because of the increased T stability of N-H bonds compared to Ga-H bonds on the GaN surface [27]. Also the EA for NH₃ desorption is estimated from experiments to be 1.5-1.7 eV [26], suggesting that NH₃ formation and desorption is not rate limiting. The lower EA for NH₃ desorption and the measured EA of 2.7 eV implies that the rate-limiting step for GaN decomposition in H₂ and NH₃ is Ga desorption from the surface. Clearly, from the decomposition rates Ga atoms do leave the surface, however, some of the Ga atoms may also be reincorporated into the evolving NL.

2.2.6 GaN Nucleation Layer Evolution

In this section, the physical mechanisms involved in GaN NL evolution on sapphire before high T growth are examined. Evidence was presented in Section 4 that the NL decomposes during the ramp to high T [13] and that the Ga atoms from the decomposing NL initiate the formation of new, more stable GaN nuclei. This evidence is

derived from analysis of AFM images of a progression of annealed NLs, following the examples of experiments by Tong and Williams [28] and analysis by Herring [29].

The GaN NL films were grown on c-plane sapphire to a thickness of 30 nm as shown in Figs. 3 and 7. The annealing schedule consisted of a 50 °C per min. T ramp from 550 °C to 1050 °C then holding T at 1050 °C for a given length of time, followed by rapid cooling under NH₃ and N₂ flow to prevent further changes to the NL. A total of 13 NLs were grown to a thickness of 30 nm and heated to different points along the annealing schedule.

The reflectance waveform for the NL growth and annealing is shown in Fig. 7 by the thick solid line. Initially, the 550 nm reflectance signal, R, is normalized to room T sapphire ($R_0 = 0.773$). Note that the reflectance signal increases during these two ramps until near 375 sec. ($T \approx 850$ °C) the signal decreases. The points labeled (a) – (m) in Fig. 7 denote the times and positions along the reflectance curve at which the NL annealing schedule was interrupted for AFM study. Also shown in Fig. 7 are the individual reflectance waveforms from the 13 interrupted annealing experiments. Except for times near 600 to 900 s the reflectance waveforms reproduce each other and the waveform denoted by the solid line, suggesting good reproducibility in the optical and morphological character of the 13 NLs used for this study.

AFM images from the interrupted annealing experiments are shown in Fig. 8. For these interrupted NLs, three distinct regimes are observed and are arranged in Fig. 8 by the three rows of images in Fig. 8. In the first row the NLs are annealed to T of (a) 920 °C, (b) 940 °C, (c) 960 °C, and (d) 980 °C. For these annealed NLs, the σ_{RMS} is ≈ 3 nm, which is similar to the σ_{RMS} for as grown NLs. The lack of morphology changes as the NLs are annealed implies that the initial reflectance signal decrease shown in Fig. 7 is due to NL decomposition [13].

In the second row of Fig. 8, images (e) – (i) show the formation and growth of GaN nuclei on the NL. The nuclei form from the desorbed Ga atoms generated during the NL decomposition. These Ga atoms recombine with ambient NH₃ to form GaN on the NLs. For the NLs shown in the second row of Fig. 8 the annealing T and times are (e) 1000 °C, (f) 1020 °C, (g) 1040 °C, (h) 1050 °C, (i) 1050 °C + 1 min. The nuclei increase in size, reaching a maximum height and width in Fig 8(i) of 180 nm and 500 nm, respectively. After the GaN nuclei reach their maximum size, the nuclei decompose as shown by the images (j) – (m) in the third row of Fig. 8. As the nuclei decompose their size and height decrease in size.

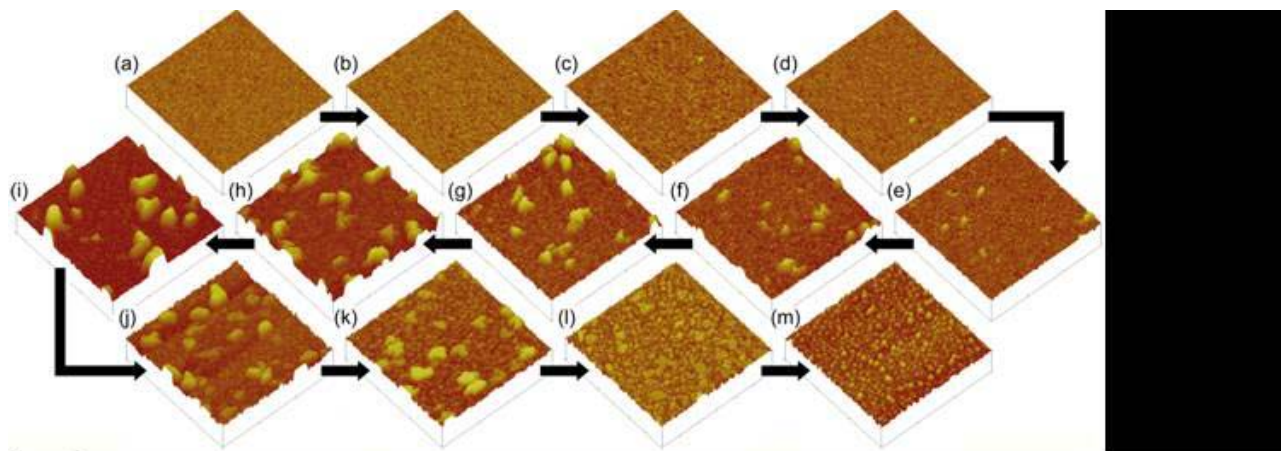


Fig. 8. Atomic force microscopy (AFM) images of the GaN nucleation layer morphology for different annealing temperatures and times. The points (a)-(m) correspond to annealing T and times of (a) 920 °C, (b) 940 °C, (c) 960 °C, (d) 980 °C, (e) 1000 °C, (f) 1020 °C, (g) 1040 °C, (h) 1050 °C, (i) 1050 °C + 1 min, (j) 1050 °C + 2 min, (k) 1050 °C + 3 min, (l) 1050 °C + 5 min, and (m) 1050 °C + 13 min. The arrows indicate the progression along the annealing schedule. The height scale is 200 nm and the scan size is 3 x 3 μ m. No change in the AFM morphology occurs on the first row as part of the annealing schedule is dominated by NL decomposition. The second row shows the birth and growth of the high T GaN nuclei and the third row shows the decomposition of the high T GaN nuclei.

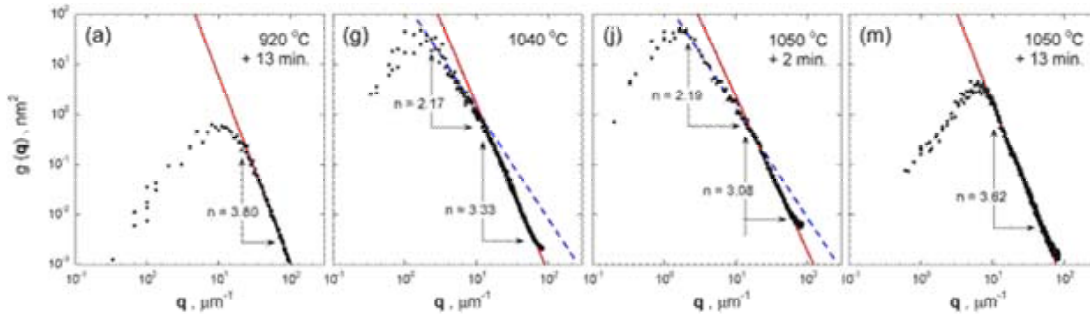


Fig. 9. Log-log plot of the power spectral density (PSD), $g(|q|)$, as a function of the reciprocal length, q , for AFM images (b), (g), (j), and (m) in Fig. 4. The lines denote linear fits at large q (short dashed line) or small q (long dashed line). A separate line at intermediate q (solid line) is given for (g) and (j).

From the previous NL decomposition study an activation energy, EA, of 2.7 eV was measured for all annealing conditions, suggesting the limiting step for NL decomposition is Ga desorption from the surface [13]. The previous work demonstrated that before the GaN nuclei are formed, the NL decomposes, losing mass (i.e. Ga atoms) to the gas phase. The GaN nuclei were assumed to grow from recondensation of the gas phase Ga atoms [13, 30], and here exceed the original height of the 30 nm by a factor of 6.

Further evidence of the GaN nuclei formation from a gas phase evaporation and recondensation mechanism can be attained through analysis of the AFM image height-height correlation function, $\langle |h(|q|, t)|^2 \rangle$, which is also denoted as the power spectral density (PSD) functions, $g(|q|, t)$. Following the analysis of Tong and Williams [28], the equation of motion for the surface height, h , evolution in reciprocal space, q , is given by,

$$\partial h(|q|, t) / \partial t \propto -cn|q|^n h(|q|, t) + \eta(|q|, t), \quad (1)$$

where, t is time, cn are constants, and η is the stochastic noise term that describes the random arrival of growth species to the surface. The exponents, n , range from 1 to 4 and are associated with smoothing mechanisms of the otherwise stochastically rough surface first calculated by Herring [29]. The solution to Eq. (1) is, $g(|q|, t)$, given by,

$$g(|q|, t) = \Omega (1 - \exp(-2cn|q|^n t)) / cn|q|^n, \quad (2)$$

where Ω is proportional to the growth flux [28]. At large q , (i.e. small length scales), the exponential is small and $g(|q|, t)$ is proportional to $\Omega / cn|q|^n$. The four smoothing mechanisms derived by Herring are $n = 1$ for plastic flow, $n = 2$ for evaporation and recondensation, $n = 3$ for bulk diffusion, and $n = 4$ for surface diffusion [29].

A plot of $g(|q|)$ vs. q is shown Fig. 9 for four different stages (Figs. 1(a), 1(g), 1(j), 1(m)) along the NL annealing schedule. For each annealing stage, $g(|q|)$ reaches a maximum at q_{max} , which corresponds to the maximum height-height difference. Note that as the NL is annealed, q_{max} changes from large q (smaller length scale) to smaller q (larger length scale) and then back to large q . The value of n was calculated from a power law fit of $g(|q|)$ vs. q for q larger than q_{max} to obtain the relevant smoothing mechanisms [29].

As shown in Fig. 9(a) at 920 °C, the power law fit of $g(|q|)$ vs. q gives an n of 3.8 at large q , consistent with the NL being smoothed by surface diffusion. In Fig. 9(g) at 1040 °C, two values of n are observed at large q (3.33) and intermediate q (2.17). The value of 3.33 at large q again suggests smoothing by surface diffusion, while the value of 2.17 at intermediate q suggests smoothing by evaporation and recondensation. Further along the annealing schedule at 1050 °C + 2 min. in Fig. 9(j), $n = 3.08$ at large q and $n = 2.19$ at intermediate q , similar to values observed in Fig. 9(g). Lastly, a NL annealed at 1050 °C + 13 min. is shown in Fig. 9(m) with a single slope of $n = 3.62$.

In Fig. 10, the smoothing exponents, n , are plotted vs. for each of the films shown in Fig. 8. Note that for films (a)-(d), the average value of n is 3.7 ± 0.1 as shown by the dashed red line and open circles in Fig. 2(a). As the GaN nuclei form in films (e)-(k), the value of n decreases to 2.3 ± 0.3 as shown by the blue solid line and

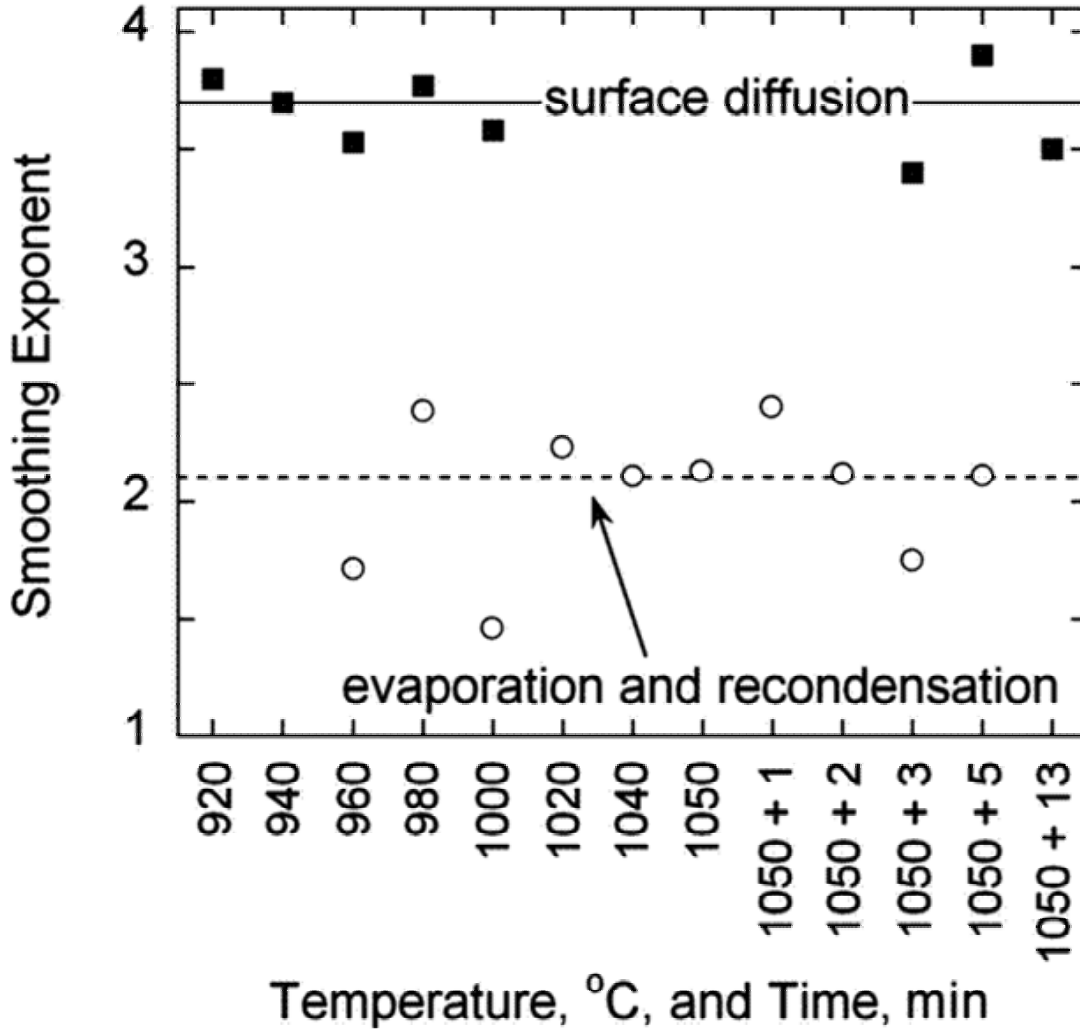


Fig. 10. Smoothing exponents from the $g(|q|)$ for the large and intermediate values of q for each AFM image in Fig. 4. An average value of $n = 3.7 \pm 0.2$ is obtained at large q and $n = 2.1 \pm 0.3$ for intermediate q . These values of n suggest surface diffusion ($n = 3.7 \pm 0.2$) and evaporation and recondensation ($n = 2.1 \pm 0.3$) smoothing mechanisms, respectively.

solid squares. For films (l) and (m) the value of n is again close to 3.7. This analysis indicates that the as grown NL is smoothed by surface diffusion ($n = 4$), even to the point when substantial decomposition of the NL occurs. Above 1000 °C, the GaN nuclei form and grow by an evaporation and recondensation mechanism ($n = 2$). Once the GaN nuclei reach a certain size and have decomposed, the surface morphology is again smoothed by surface diffusion ($n = 4$). The evaporation and recondensation mechanism is consistent with gas phase mass transport observed in selected area growth of GaN [31].

To determine the relative NL and nuclei decomposition rates, the NL and nuclei volume per unit area (i.e. thickness of the NL) must be compared as a function of time. This is difficult however, because the NL thickness (height) changes primarily during the T ramp, while the nuclei volume decreases at constant T. From previous work, we know that the decomposition follows Arrhenius kinetics, with a constant activation energy, EA, of 2.7 eV [13]. Therefore the height (or volume) as a function of time is,

$$dh(t)/dt = -A_0 \exp[-EA/kBT(t)] \equiv -A_0 f(t), (3)$$

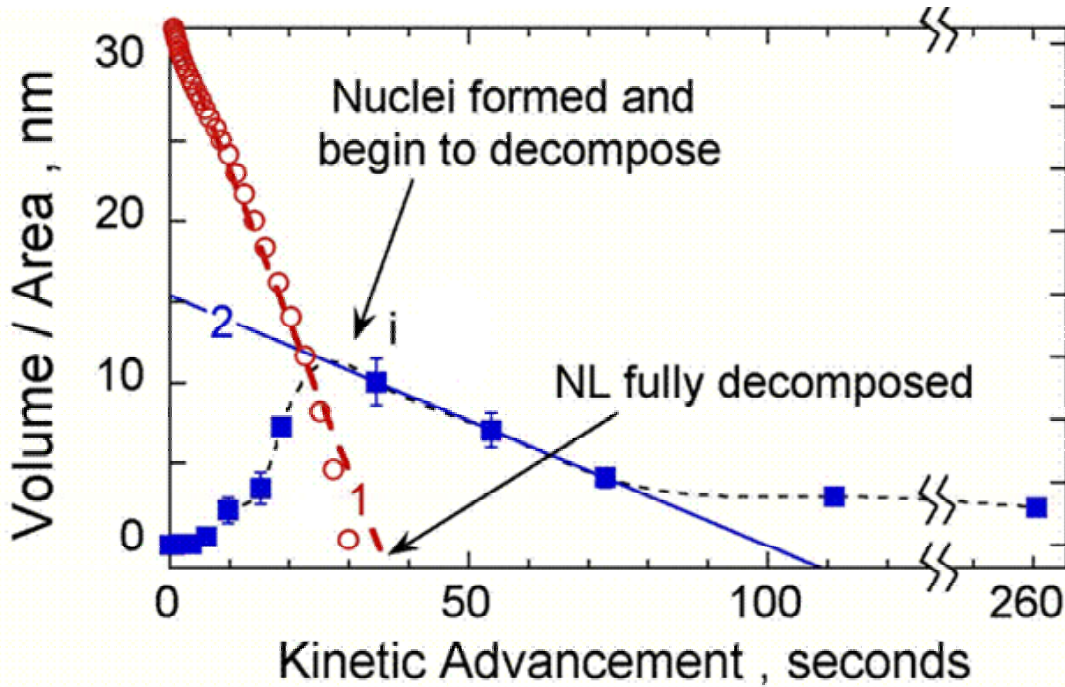


Fig. 11. Nucleation layer thickness (volume / area) measured using reflectance (red open circles) and the GaN nuclei volume per unit area (blue filled squares) vs. $F(t)$. Lines 1 and 2 are linear fits to the NL thickness and the GaN nuclei volume per unit area during the decomposition dominated steps. Note that the NL thickness is zero at the same time that the GaN nuclei volume is a maximum.

where k_B is the Boltzman constant. For simplification, a new function, $f(t) \equiv \exp[-EA/k_B T(t)]$ is defined, which allows the rescaling of time, t , to account for changes in the decomposition rate due to $T(t)$. Two regimes emerge, one where T is constant and the other when T is a function of t . At constant $T = T_C$, $f(t)$ is constant, and Eq. 3 can be integrated to yield, $h(t) = h(t_0) - A_0 f(T_C) t$, where $h(t_0)$ is the initial thickness of the NL. For the other case, $h(t) = A_0 \int_0^t f(t') dt' \equiv -A_0 F(t)$ and Eq. 3 must be solved knowing $T(t)$ and subtracted from $h(t_0)$. In other words, the instantaneous decomposition rate, i.e. $-A_0 f(t)$, must be integrated and subtracted from the initial height or thickness. Note that a plot of $h(t)$ vs. $F(t)$ will yield a straight line with a slope of $-A_0$, providing EA (2.7 eV in this case) does not change during the given kinetic process. We denote $F(t)$ as the kinetic advancement, since it allows rates at different T to be compared directly. Since $f(t)$ is unitless, $F(t)$ has the units of time.

To calculate the relative differences in A_0 from the NL and nuclei decomposition rates, the NL thickness and the nuclei volume per unit area (i.e. same units as thickness) are plotted by the kinetic advancement function, $F(t)$, in Fig. 11. Note that the maximum nuclei volume per unit area is 10.5 nm, (point i in Fig. 11), which means that 1/3 of the original Ga atoms from the as grown NL are transformed into GaN nuclei via the evaporation and recondensation mechanism. Linear fits for the NL thickness and nuclei volume per unit area decomposition are shown in Fig. 11 and are labeled 1 and 2, respectively. The slope (i.e. $-A_0$) of line 1 is 5.9 times larger than the slope of line 2, showing that A_0 is larger for the NL decomposition than for nuclei decomposition. This is consistent with previously measured decomposition rates of the NL, where A_0 for NL decomposition was shown to be 4 to 9 times larger than for bulk GaN decomposition [13]. The smaller A_0 measured for nuclei decomposition suggests that the nuclei are more stable than the NLs to decomposition, and structurally closer to bulk GaN [25, 32].

It is clear from Fig. 11 why the nuclei grow in size up to a certain point and then decompose. As long as the original NL is decomposing it provides a source of Ga atoms that can incorporate into the growing GaN nuclei.

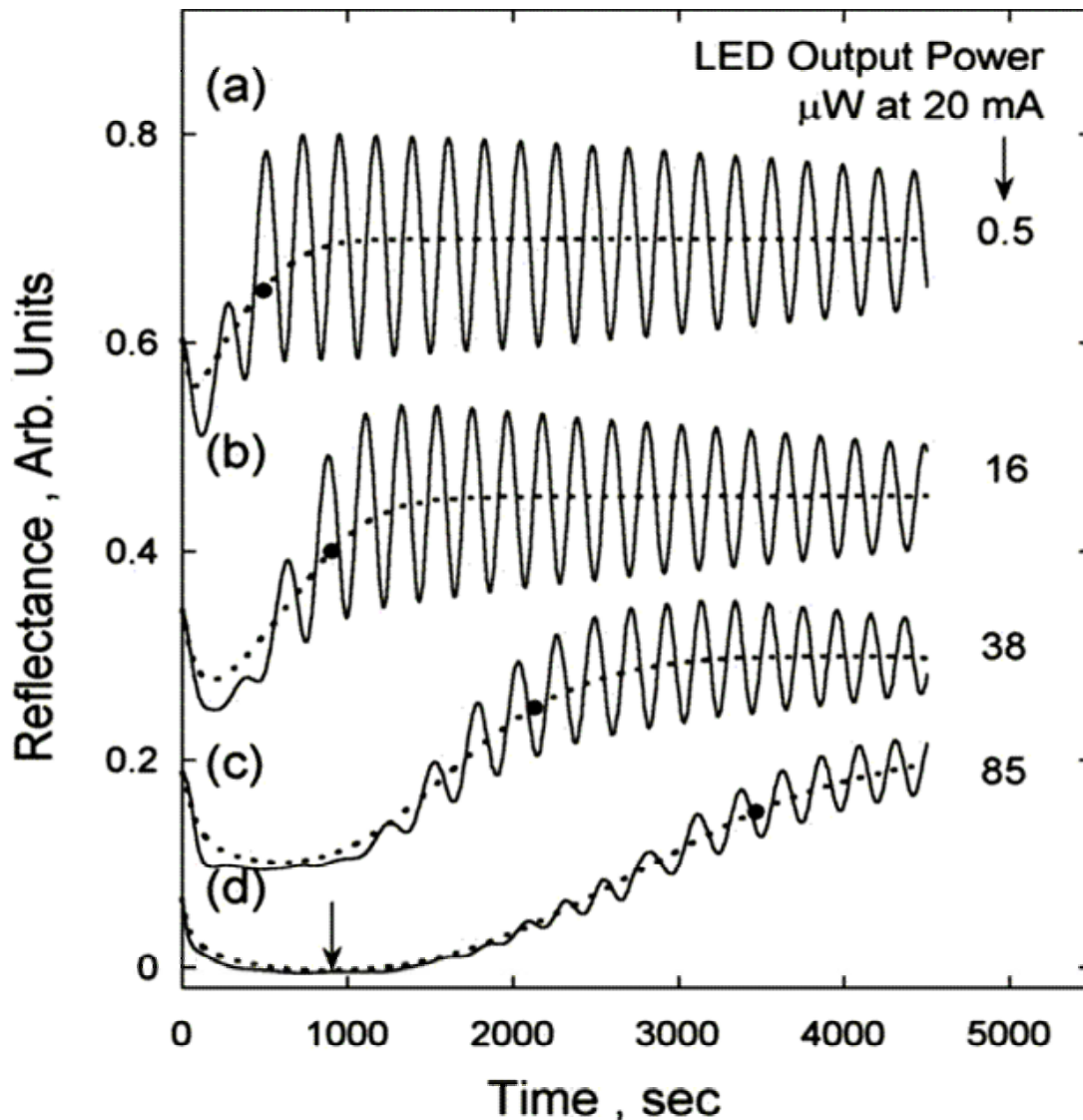
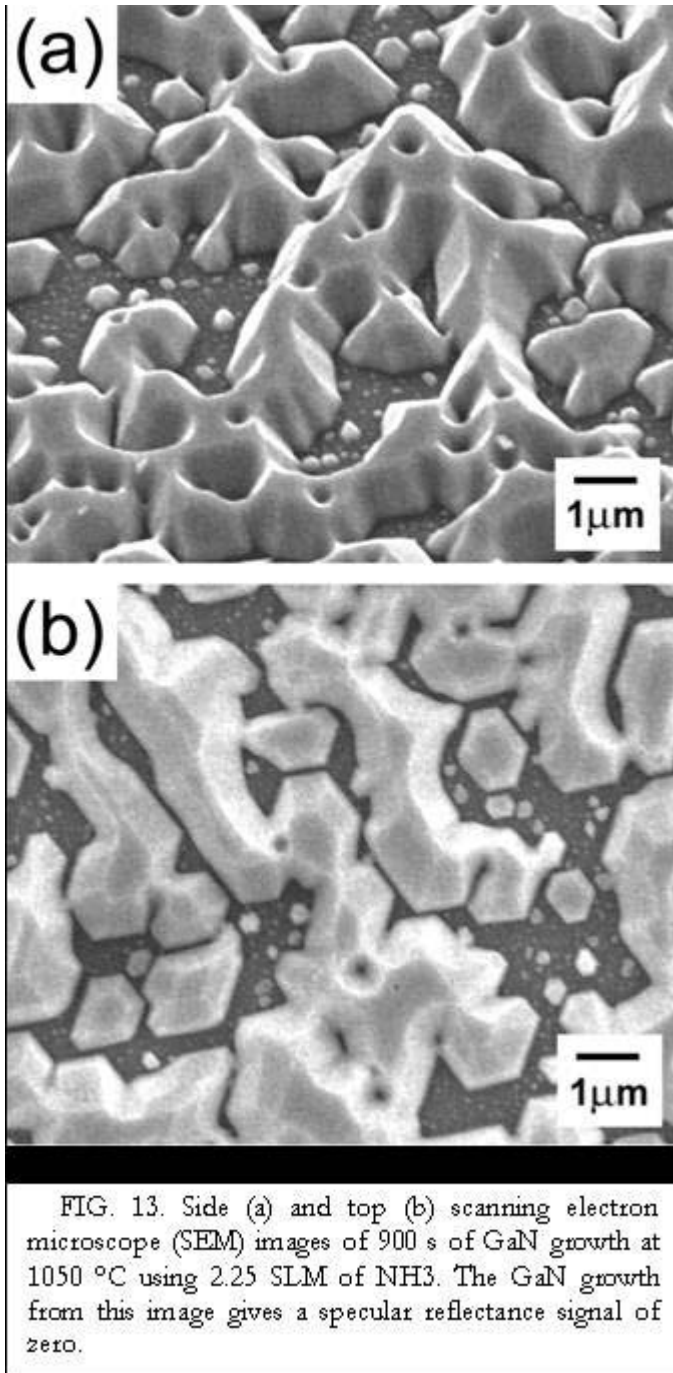


Fig. 12. A series of reflectance waveforms (solid lines) for GaN growth. The time zero is when the TMGa is turned on after annealing the GaN nucleation layer to 1050 °C. The dashed line is a smoothed fit through the reflectance signal. The reflectance signal at 0.15 (i.e. 75% of the level of bulk GaN) is shown as the solid circle for each smoothed reflectance waveform. The measured LED output power from a quick fabrication process is listed next to each reflectance trace.

However, once the NL has been depleted (fully decomposed) the GaN nuclei reach their maximum size and begin to decrease in size (decompose), leaving behind a morphology similar to the initial GaN NL.

2.2.7 Delaying GaN Coalescence for Improved UV LED Performance.

In this section, we demonstrate that the transition from three-dimensional (3D) grain to two-dimensional (2D) coalesced growth can be intentionally prolonged by reducing the NH₃ flow during the initial high T GaN growth. Using in-situ optical reflectance during growth, we show that the length of time spent prolonging the 3D to 2D transition is proportional to the increased light output of LEDs at 380 nm. We speculate that the increased light output is due to the reduced TD density and related influence of these TDs on nonradiative recombination [18].



large grains. Once coalescence begins, the smaller GaN grains are likely overgrown [33] and ultimately do not contribute to the overall TD density.

Two atomic force microscope images of fully coalesced GaN films without the LED structure are shown in Fig. 14. For these films, the same growth procedures for the LEDs shown in Figs. 12(a) and 12(d) were used. In Fig. 14(a), a pit density of $4 \times 10^9 \text{ cm}^{-2}$ is counted, while in Fig. 14(b) a pit density of $1.5 \times 10^8 \text{ cm}^{-2}$ is counted. These small pits are thought to signify dislocations with mixed screw and edge components where step edges meet [34] and pure edge components when they are located on a terrace. Although not a direct measure of the dislocation density, the pits shown in Fig. 14 place a lower limit on the actual dislocation density. Using planview

The reflectance waveforms (solid lines) of four LED structures are shown vs. time in Fig. 12. The reflectance signals in Fig. 12 have been normalized to the room T reflectance of sapphire (0.0773) and the top three reflectance signals (a-c) have been shifted vertically along the y-axis. As the GaN growth is commenced on the annealed NL, the reflectance signal decreases to zero due to roughening of the GaN film. As the GaN film grows, the reflectance signal increases, oscillating around a mean reflectance value of 0.20, which is the reflectance value for bulk GaN at 1050 °C.

Note that the time needed to recover to the reflectance value of 0.20 increases from Fig. 12(a) to 12(d). For the films in Figs. 12(a) and 12(b), an NH₃ flow of 6.0 SLM was used for both the NL ramp to high T as well as the high T GaN growth step. By lowering the NH₃ flow during the NL ramp to high T and initial high T growth, a longer recovery time is required for complete coalescence and smoothing of the GaN film. This is shown in Figs. 12(c) and 12(d), where NH₃ flows of 4.0 and 2.25 SLM were used for both the NL high T anneal as well as the first 15 min. of the high T growth. The short dashed line is a smoothed fit to the reflectance signal and is used in quantifying the reflectance recovery time. The reflectance recovery time is defined here as the length of time to reach a reflectance signal of 0.15, which is 75% of the reflectance signal for smooth GaN (0.20). The filled solid circles in Fig. 12 denote the reflectance signal of 0.15 on each of the reflectance waveforms.

Figure 13 shows the GaN film morphology for films with zero specular reflectance. The same NH₃ flows were used as the films shown in Fig. 12(d), but growth was quenched in T and N₂ after 900 s. The film in Fig. 13 is composed of hexagonally shaped grains, which are slightly coalesced. The GaN grains are roughly 1 μm in size and appear to have a trapezoidal shape. Note that smaller GaN grains are formed between the

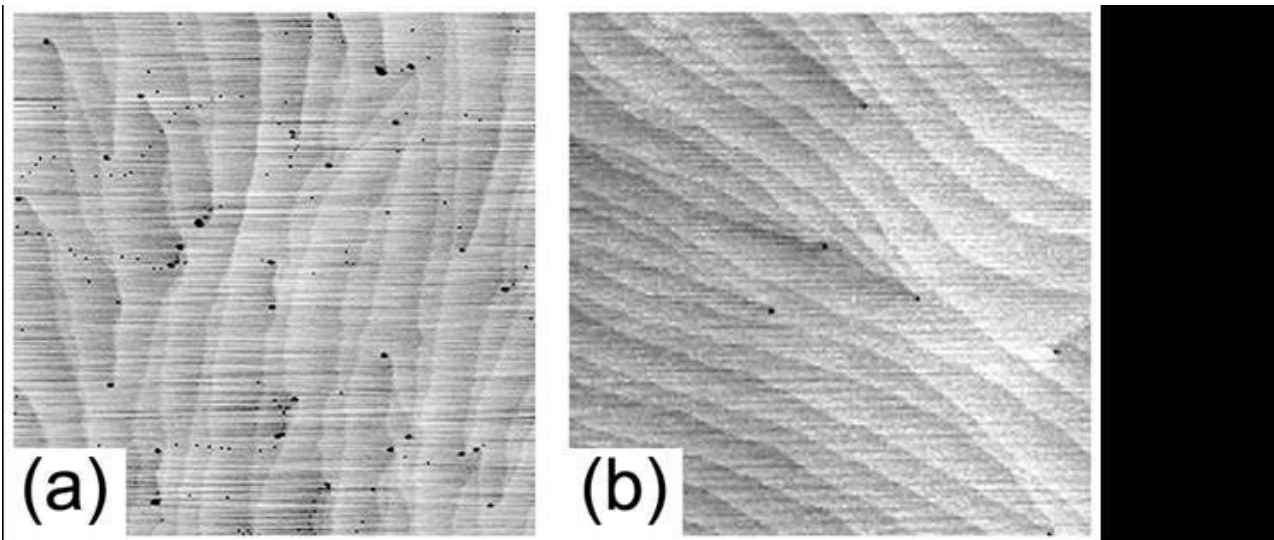


FIG. 14. Atomic force microscope images of Si doped GaN films grown using similar growth conditions as the LED structures shown (a) in Fig. 1(a) and (b) in Fig. 1(d). The size of both images is $2 \times 2 \mu\text{m}$. In Fig. 3(a) a total of 160 pits are observed, while in Fig. 3(b) a total of 6 pits are observed. This puts a lower limit on the dislocation density of $4 \times 10^9 \text{ cm}^{-2}$ in (a) and $1.5 \times 10^8 \text{ cm}^{-2}$ in (b).

TEM the dislocation density of $4.6\text{--}6.1 \times 10^8/\text{cm}^2$ was measured for the film shown in Fig. 14(b) [35], while from an examination of the XRD (0004) and (1012) linewidths a dislocation density estimate of $7.6 \times 10^8 \text{ cm}^{-2}$.

The LED output powers at 20 mA made using a quick fabrication process are also listed in Fig. 12 next to each reflectance waveform. The quick fabrication process, which results in bottom emitting LEDs, uses only two photoresist (PR) steps and two metal depositions. A Pd/Au ($50 \text{ \AA} / 2000 \text{ \AA}$) p-contact is first deposited. The first PR step defines the p-contact and wet chemical etching is used to remove the unwanted Pd and Au. The first PR step is then reused for the reactive ion etching of the mesa. A second PR step and metal deposition yields a Ti/Al ($200 \text{ \AA} / 2000 \text{ \AA}$) n-contact that completes the LED. The contacts are then annealed at 500 C for 30 seconds in N_2 ambient. This process is a compromise between high output power and rapid processing. These quick LEDs are tested at the wafer level using a probe station with a wavelength-calibrated Si detector. For comparison, many wafers were also processed using a more conventional process with a transparent contact and a thick p-contact pad. The devices with a transparent contact were mounted on TO-headers and measured using a calibrated integrating sphere with an attached Si detector. The LED that is shown in Fig. 12(d), which yielded $\sim 85 \mu\text{W}$ at 20 mA with the quick process, exhibited 1.3 mW of output power at 20 mA when fabricated with a transparent contact and measured using an integrating sphere.

In Fig. 15, the LED output power is plotted vs. the recovery time to reach 75% of the full GaN reflectance signal. The LED output power for the quick process at 20 mA (filled circles) is plotted along the left y-axis and at 100 mA (open squares) is plotted along the right y-axis. The solid and dashed lines are linear fits to the data. From Fig. 15 it is clear that as the reflectance recovery time increases, the light output increases.

The LED output power for the reflectance waveforms in Fig. 1(a)-(d) are labeled (a)-(d) in Fig. 15. Ideally, for a linear power dependence the output power at 100 mA should be 5 times the output power at 20 mA. However, for many of the LEDs with a short reflectance recovery time, the output power at 100 mA is > 5 times the output power at 20 mA and these LEDs show a super-linear LED light-current output. This is especially true of the LED (b) in Fig. 15, where the output power at 100 mA is 11.1x the output power at 20 mA. However, for LED (d) in Fig. 14, the output power at 100 mA is 5.1x the output power at 20 mA, indicating a linear light-current output. Also note that the linear fits for 20 mA (solid line) and 100 mA (dashed line) approach each other as the recovery delay increases, further indicating a more linear light-current output. As shown in Fig. 15, the change from a super-linear to linear light-current output is likely due to the decreased TD density, limiting the number of nonradiative recombination centers in the LEDs with longer reflectance recoveries.

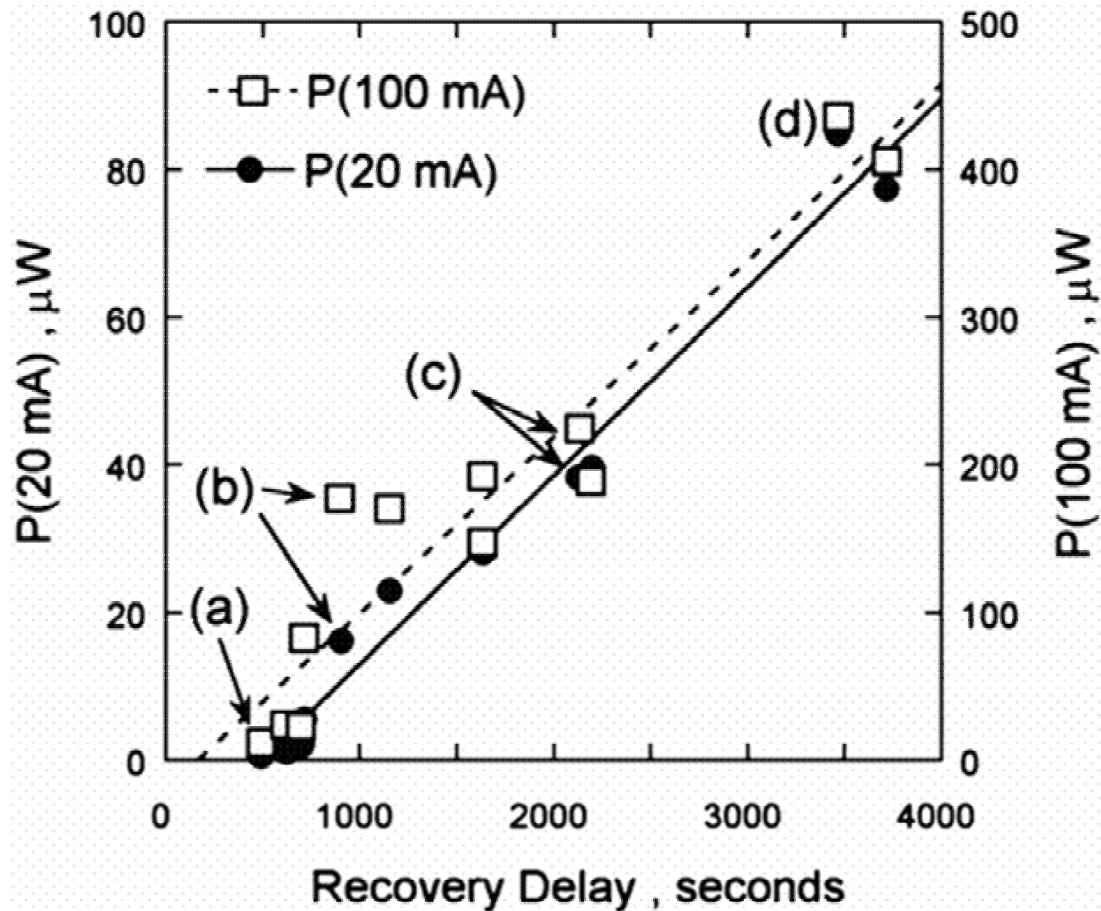


FIG. 15. Plot of the LED output power at 20 mA (left axis) and 100 mA (right axis) vs. the recovery delay. The LED output powers from the reflectance waveforms (a)-(d) in Fig. 1 are labeled (a)-(d). The solid and dashed lines are linear fits to the output power at 20 mA and 100 mA, respectively.

While lower NH₃ flow early in the growth increases the LED output power, it is not apparent to what degree the recovery should be delayed. Clearly, if the recovery is too rapid, the GaN will contain a larger number of dislocations. Conversely, if the recovery is too long, the GaN film will be rough and possibly discontinuous. In addition, the NL growth and T ramp also influences the recovery time. Further study of the relationship between the GaN growth conditions, the reflectance recovery time, and LED output power is currently underway.

2.2.8 Summary and Conclusions

One of the goals of the work presented here is to obtain the physical reasons behind the reflectance changes observed during GaN growth. We are currently using this information to fit the reflectance waveforms during the NL evolution, with the ultimate aim of measuring and controlling the GaN NL grain density and subsequent GaN evolution.

From this work we have been able to develop a method to accurately control the GaN NL thickness. To fit the entire low T grown NL reflectance waveform, a modified version of the virtual interface model [10] was derived which includes a roughening term that attenuates the reflectance signal. This model will also work on high T GaN layers that undergo roughening. NL thickness control has been demonstrated to better than 0.1 nm for a 30 nm thick NL, which is 1 part in 300.

Using optical reflectance, the decomposition kinetics for GaN NLs has been measured for the first time. The GaN NL decomposition rates increase with increasing P, increasing T, and decreasing NH₃ flow. The same

activation energy of 2.7 eV was measured for GaN NL and bulk GaN film decomposition. The pre-exponential factor, A_0 , at constant pressure was larger for the GaN NL decomposition compared to bulk GaN decomposition. The measured EA for GaN NL and bulk decomposition is similar to the measured EA for Ga desorption from GaN surfaces, suggesting that Ga desorption is the rate limiting step for GaN decomposition in the mixed NH_3/H_2 flows used for GaN MOCVD.

Optical reflectance along with AFM images was used to measure the NL evolution as it was heated to the high T growth conditions. The GaN NL evolution is initiated by NL decomposition kinetics. After some decomposition of the original NL, Ga atoms liberated during the decomposition are incorporated into growing GaN nuclei, which emerge atop the NL near 1000 °C. These nuclei grow in size, until the original NL is fully decomposed, after which the nuclei decompose and reduce in size. While the morphology of the NL is smoothed by surface diffusion, the GaN nuclei are smoothed by an evaporation and recondensation mechanism as shown by the analysis of the AFM height-height correlation functions. Initiating high T GaN growth on a NL with maximum roughness should produce dislocation bending near the GaN sapphire interface leading to GaN films with reduced dislocation densities [18]. Further work is underway to determine the extent to which the GaN nucleation density can be controlled through the choice of growth conditions.

Finally, a correlation has been shown between the reflectance recovery time as monitored by reflectance and UV LED output power. By delaying the reflectance recovery time through the use of low NH_3 flow at the initial stages of high T growth, UV LEDs with higher output power were fabricated. These UV LEDs show a near linear light-current output dependence a lower TD density, suggesting a reduction of nonradiative recombination in these LEDs.

2.2.9 Acknowledgements

We thank J. R. Creighton, J. Tsao, K. H. A. Bogart, and R. M. Biefeld for helpful advice and T. M. Kerley for technical assistance. Sandia is a multiprogram laboratory operated by Sandia Corporation, a Lockheed Martin Company, for the United States Department of Energy under Contract DE-AC04-94AL85000.

2.2.10 References

1. S. D. Lester, F. A. Ponce, M. G. Craford, et al., *Appl. Phys. Lett.* 66, 1249 (1995).
2. T. Wang, T. Shirahama, H. B. Sun, et al., *Appl. Phys. Lett.* 75, 2220 (2000).
3. S. F. Chichibu, H. Marchand, M. S. Minsky, et al., *Appl. Phys. Lett.* 74, 1460 (1999).
4. O.-H. Nam, M. D. Bremser, T. S. Zheleva, et al., *Appl. Phys. Lett.* 71, 2638 (1994).
5. T. Gehrke, K. J. Linthicum, D. B. Thomson, et al., *MRS Internet J. Nitride Semicond. Res.* 4S1, G3.2 (2000). 4S1, G3.2 (2000).
6. C. I. H. Ashby, C. C. Mitchell, J. Han, et al., *Appl. Phys. Lett.* 77, 3233 (2000).
7. S. Sakai, T. Wang, Y. Morishima, et al., *J. Cryst. Growth* 221, 334 (2000).
8. K. Hiramatsu, K. Nishiyama, M. Onishi, et al., *J. Cryst. Growth* 221, 316 (2000).
9. M. Iwaya, T. Takeuchi, S. Yamaguchi, et al., *Jpn. J. Appl. Phys.* 37, L316 (1998).
10. W. G. Breiland and K. P. Killeen, *J. Appl. Phys.* 78, 6726 (1995).
11. S. Nakamura, *Jpn. J. Appl. Phys.* 30, L1705 (1991).
12. D. K. Wickenden, T. J. Kistenmacher, W. A. Bryden, et al., *Mat. Res. Soc. Symp. Proc.* 221, 167 (1991).
13. D. D. Koleske, M. E. Coltrin, A. A. Allerman, et al., *Appl. Phys. Lett.* 82, 1170 (2003).
14. A. E. Wickenden, D. D. Koleske, R. L. Henry, et al., *J. Electron. Mat.* 29, 21 (2000).
15. P. Fini, X. Wu, E. J. Tarsa, et al., *Jpn. J. Appl. Phys.* 37 Part 1, 4460 (1998).
16. S. Figge, T. Bottcher, S. Einfeldt, et al., *J. Cryst. Growth* 221, 262 (2000).
17. J. Han, T.-B. Ng, R. M. Biefeld, et al., *Appl. Phys. Lett.* 71, 3114 (1997).
18. D. D. Koleske, A. J. Fischer, A. A. Allerman, et al., *Appl. Phys. Lett.* 81, 1940 (2002).
19. E. S. Zouboulis and M. Grimsditch, *J. Appl. Phys.* 70, 772 (1991).

20. L. Liu and J. H. Edgar, *Mat. Sci. Eng. R* 37, 61 (2002).
21. J. N. Kuznia, M. A. Khan, D. T. Olson, et al., *J. Appl. Phys.* 73, 4700 (1993).
22. K. Doverspike, L. B. Rowland, D. K. Gaskill, et al., *Inst. Phys. Conf. Ser.* 141, 101 (1995).
23. S. D. Hersee, J. Ramer, K. Zheng, et al., *J. Electron. Mat.* 24, 1519 (1995).
24. S. Keller, D. Kapolnek, B. P. Keller, et al., *Jpn J. Appl. Phys., Part 2* 35, L285 (1996).
25. X. H. Wu, D. Kapolnek, E. J. Tarsa, et al., *Appl. Phys. Lett.* 68, 1371 (1996).
26. D. D. Koleske, A. E. Wickenden, R. L. Henry, et al., *Journal of Crystal Growth* 223, 466 (2001).
27. S. W. King, E. P. Carlson, R. J. Therrien, et al., *J. Appl. Phys.* 86, 5584 (1999).
28. W. M. Tong and R. S. Williams, *Ann. Rev. Phys. Chem.* 45, 401 (1994).
29. C. Herring, *J. Appl. Phys.* 21, 301 (1950).
30. K. Lorenz, M. Gonsalves, W. Kim, et al., *Appl. Phys. Lett.* 77, 3391 (2000).
31. C. C. Mitchell, M. E. Coltrin, and J. Han, *J. Cryst. Growth* 222, 144 (2001).
32. A. Munkholm, C. Thompson, C. M. Foster, et al., *Appl. Phys. Lett.* 72, 2972 (1998).
33. V. Narayanan, K. Lorenz, W. Kim, et al., *Philo. Mag. A* 82, 885 (2002).
34. E. J. Tarsa, B. Heying, X. H. Wu, et al., *J. Appl. Phys.* 82, 5472 (1997).
35. D. M. Follstaedt, N. A. Missert, D. D. Koleske, et al., *Appl. Phys. Lett.* 83, 4797 (2003).

2.3 AlGaInN Deposition Chemistry (JR Creighton, GT Wang, ME Coltrin)

2.3.1 Background

The AlGaInN MOCVD process is complicated by parasitic gas-phase chemical reactions that diminish the group-III deposition efficiency and make it difficult to control alloy composition. The parasitic reactions may also induce a strong temperature dependence on the growth rate and incorporation efficiency under conditions that would otherwise be in the mass transport limit and relatively easy to control. Many chemical mechanisms have been proposed, usually initiated by the formation of adducts between the group-III metalorganic and ammonia, but a complete understanding of the critical reaction pathways has not yet been synthesized. The experimental approaches include methods of investigating chemical reactions from room temperature to the

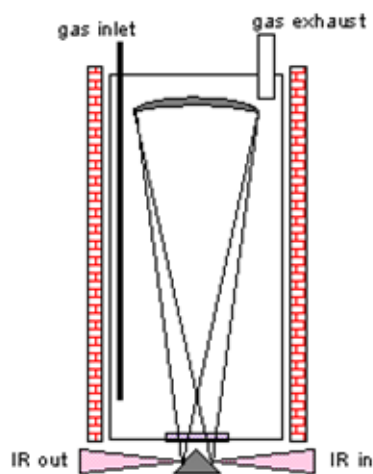


Figure 1. Schematic of 300° FTIR cell

deposition temperature. For example, using laser-light scattering we have directly observed the formation of gas-phase nanoparticles during AlGaIn MOCVD. By measuring their size and density we determined that the degree of mass loss into AlN particles was sufficient to account for the diminution in growth rate. In order to examine direct precursor reactions, we chose to use FTIR as the diagnostic, and built a cell capable of performing in-situ measurements up to 300°C (limited by O-ring), see Figure 1.

2.3.2 TMAI + NH₃

An AlN MOCVD mechanism including parasitic chemistry was proposed by Mihopoulos et al. (JCG, 1998) that successfully reproduced many of the observations in the literature available at that time. A key reaction in the proposed mechanism is a concerted methane elimination step from the TMAI:NH₃ adduct, i.e. $\text{TMAI:NH}_3 \rightarrow \text{DMAI-NH}_2 + \text{CH}_4$.

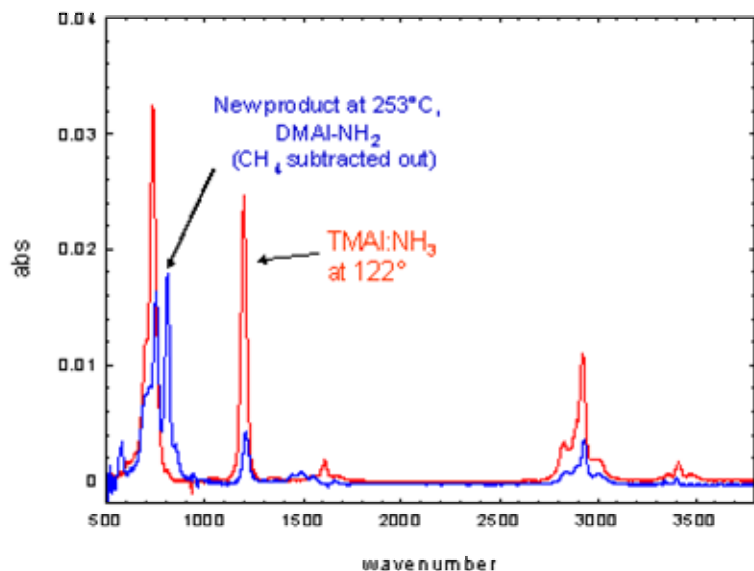


Figure 2. Gas-phase IR of TMAI:NH₃ and DMAI-NH₂

Our preliminary kinetic analysis of the adduct dissociation reaction yields an activation energy of 25 ± 2 kcal/mole, in good agreement with the DFT value (Mihopoulos) of 27 kcal/mole. The agreement between our measured rate constant and the theoretical estimate is surprisingly good (within a factor of two) and is probably fortuitous.

No further reaction could be detected at the maximum cell temperature of 300°C. Some other reaction(s) involving the DMAI-NH₂ intermediate that lead to particle nucleation must occur between 300°C and typical MOCVD temperatures. Based on a host of other observations we suspect that these reactions are similar in nature, involving concerted CH₄ elimination. Other observations that support this idea are the lack of a strong H₂/N₂ carrier gas dependence (supports a non-radical pathway), and the relatively low apparent activation energy (~25-30 kcal/mole) for the particle light scattering signal.

2.3.3 TMGa + NH₃

The reactions of TMGa + NH₃ are often thought to follow a similar pathway as the TMAI + NH₃ reactions. Some literature reports that the methane elimination reaction is very rapid and occurs readily below 200°C. It may therefore be surprising to some that we found no evidence of methane formation up to 300°C. The IR spectrum of the TMGa:NH₃ adduct at 24°C is displayed (blue curve) in Figure 3 (NH₃ IR removed for clarity). The IR spectrum for this adduct has been reported in the literature (e.g. Edgar) and our results are in agreement. But unlike the TMAI:NH₃ adduct, heating the TMGa:NH₃ adduct to ~200°C does not lead to methane elimination. Instead, the TMGa:NH₃ adduct simply dissociates back into the original reactants, TMGa + NH₃. The red curve in Fig. 3 is identical to the IR spectrum of TMGa. Heating further to 300°C causes no additional reactions to occur.

The lack of a facile CH₄ elimination reaction, coupled with a host of other observations we have made, lead us to believe that the particle nucleation mechanism for GaN is quite different from the AlN mechanism. The GaN mechanism most likely involves gas-phase homolysis of TMGa, followed by radical condensation reactions. Other information supporting this idea are the H₂/N₂ carrier gas dependence observed for GaN particle formation, and the high apparent activation energy for the particle light scattering signal. The fact that the GaN deposition rate begins to fall in the 900-950°C range also supports a high activation energy process (e.g. 60 kcal/mole).

Mihopoulos used quantum mechanical calculations (DFT) to estimate the rate constant for this step. Similar reactions are thought to occur for TMGa and TMIIn. The literature regarding adduct formation and subsequent reactions of the metalorganics is incomplete, and often contradictory. Our results demonstrate that the TMAI:NH₃ adduct is formed, as expected, and it begins to eliminate methane near 120°C (see Fig. 2). These results are at 100 Torr total pressure, and a residence time of 2.5 seconds. The CH₄ and NH₃ components have been removed from Figure 2 for clarity.

This is the first gas-phase IR spectrum reported for TMAI:NH₃ and DMAI-NH₂. Almost exactly one mole of methane is produced per mole of adduct consumed, and the reaction is complete by 250°C.

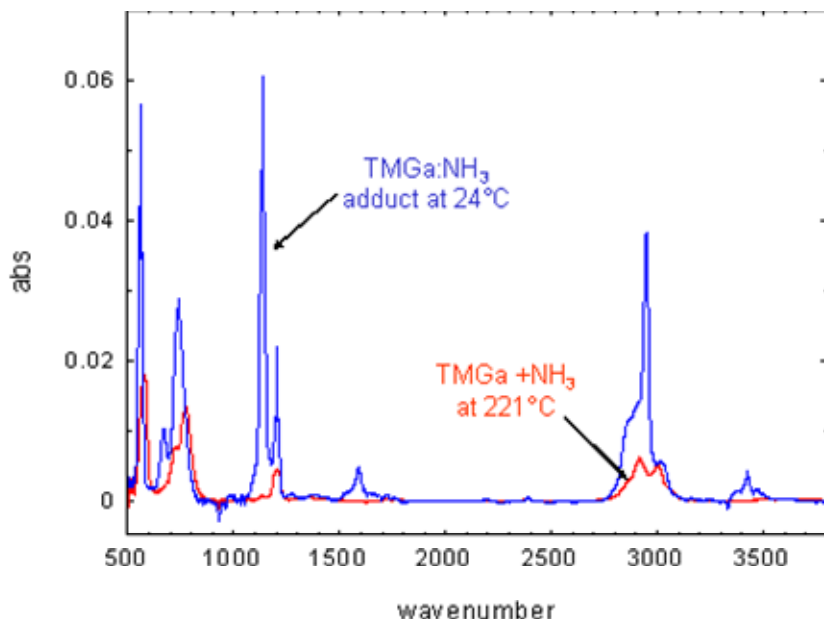


Figure 3. TMGa + NH₃ at 24°C (blue) and 221°C (red)

2.3.4 TMIn + NH₃

Much less is known about TMIn + NH₃ interactions [In fact, Allendorf (Chem. Mater. 2000) has called into question the reliability of much of the literature regarding homogeneous pyrolysis of TMIn]. Our results demonstrate that TMIn behaves much like TMGa up to about 275°C. The IR spectra for TMIn + NH₃ at 24°C (blue curve) and 200°C (red curve) are shown in Figure 4. Based on similarities with the TMAI:NH₃ and TMGa:NH₃ spectra we assign the blue curve in Fig. 4 to the TMIn:NH₃ adduct. This is likely the first recorded IR spectrum of the gas-phase TMIn:NH₃ adduct. Upon heating, the adduct dissociates back into

TMIn + NH₃, so by 200°C the spectrum (red curve) is essentially pure TMIn. No methane was observed up to 275°C. At 300°C (maximum cell temperature) a small amount of CH₄ was observed for TMIn + H₂ mixtures. The amount of CH₄ detected corresponds to about 8% TMIn decomposition. The first order rate constant for this reaction was 0.05 sec⁻¹, which is in good agreement with the TMIn pyrolysis literature. Adding NH₃ did not accelerate methane production, in fact, it may have suppressed it. Therefore it appears that the TMIn pyrolysis we observed did not involve NH₃. The uncertainty is whether we are seeing the onset of homogeneous or heterogeneous TMIn pyrolysis (the issue raised by Allendorf).

It is harder to generalize the TMIn results, in part because we do not have as many ancillary observations to draw upon. We hope to examine particle formation during InN MOCVD in the near future, and this should greatly aid our understanding. The lack of an irreversible reaction with NH₃ below 275°C, taken together with the H₂/N₂ carrier gas dependence observed for In incorporation during InGaN MOCVD, lead us to propose that the InN parasitic mechanism is similar to the GaN mechanism. It is probably initiated by TMIn pyrolysis, followed by radical condensation reactions (nucleation). The lower In-C bond energy (relative to Ga-C) leads to TMIn pyrolysis at lower temperatures, and may be a dominant reason why InGaN must be grown at lower temperatures (e.g. 750-800°C).

2.3.5 Summary

Of the three metalorganics studied (TMAI, TMGa, TMIn), only TMAI exhibits clear evidence of an irreversible reaction with NH₃ at temperatures up to 300°C. The DMAI-NH₂ product formed is probably an important intermediate in the pathway leading to nucleation, but more reaction steps must exist before particle nucleation occurs. After reviewing the entire body of evidence we believe the AlN mechanism involves concerted reactions (non-radical) with relatively low activation energies (< 30 kcal/mole).

There is no irreversible reaction between TMGa and NH₃ for temperatures up to 300°C and at the concentrations studied (which are close to MOCVD conditions). From the entire body of evidence we believe the GaN parasitic mechanism involves radical chemistry, i.e. TMGa pyrolysis followed by condensation reactions.

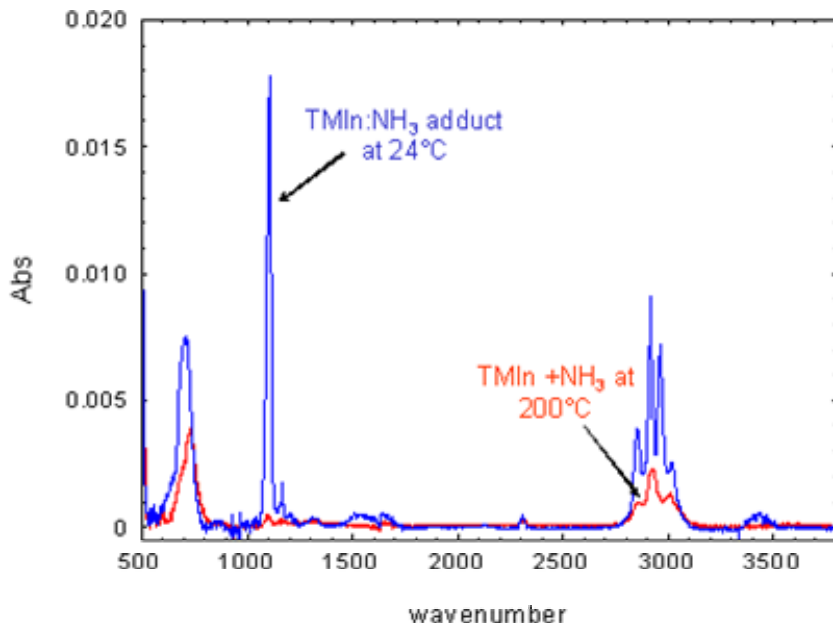


Figure 4. TMIn + NH₃ at 24°C (blue) and 200 °C (red). NH₃ has been subtracted out for clarity

There is no irreversible reaction between TMIn and NH₃ for temperatures up to 275°C. The small amount of TMIn decomposition detected at 300°C is probably due to TMIn pyrolysis and is not due to a reaction with NH₃. From the entire body of evidence we believe the InN parasitic mechanism also involves radical chemistry, i.e. TMIn pyrolysis followed by condensation reactions. The parasitic reactions occur at lower temperatures due to the lower thermal stability of TMIn.

Looking ahead to the complete mechanism required to explain

AlGaInN MOCVD, a critical component we have not discussed is the particle growth mechanism (distinct from particle nucleation). For example, particle growth kinetics must be included in order to capture the non-linear residence time dependence observed for GaN.

2.4 Mg doping Chemistry (GT Wang, JR Creighton)

2.4.1 Background

Magnesium serves as the dominant p-type dopant for GaN and its alloys, and is typically delivered during MOCVD film growth via the organometallic precursor magnesocene (MgCp₂). Unfortunately, to date controlled incorporation of Mg into III-nitride films via MOCVD has not been without problems. The result often is unpredictable Mg concentration profiles that may greatly vary after the reactor has been perturbed (e.g. from changing substrates) or even from run-to-run, as has been observed in our research RDR GaN systems. Even in reactors in which the Mg doping process is largely reproducible, the Mg profile in the grown films is marked by long transients corresponding to the turn-on and turn off of the doping process. This issue, sometimes referred to as a Mg “memory effect,” is problematic since sharp doping profiles are required for optimal device performance.

We have examined the interaction between MgCp₂ and NH₃ at typical III-nitride reactor inlet conditions in order to improve our understanding of Mg incorporation issues. This work represents the first in-depth investigation of the reaction between MgCp₂ and NH₃, and was performed using a joint experimental and theoretical approach. Our results demonstrate that complexation reactions between MgCp₂ and NH₃ are very likely responsible for the Mg doping “memory effects” and erratic incorporation problems.

2.4.2 Theoretical Results

Magnesium is associated with a positive charge in MgCp₂ due to a large Mg-Cp charge separation resulting from the low electronegativity of Mg. The electron deficiency of the Mg center in MgCp₂ suggests that it may be susceptible to nucleophilic attack by NH₃ to form a Lewis acid-base complex, NH₃:MgCp₂, which we will refer

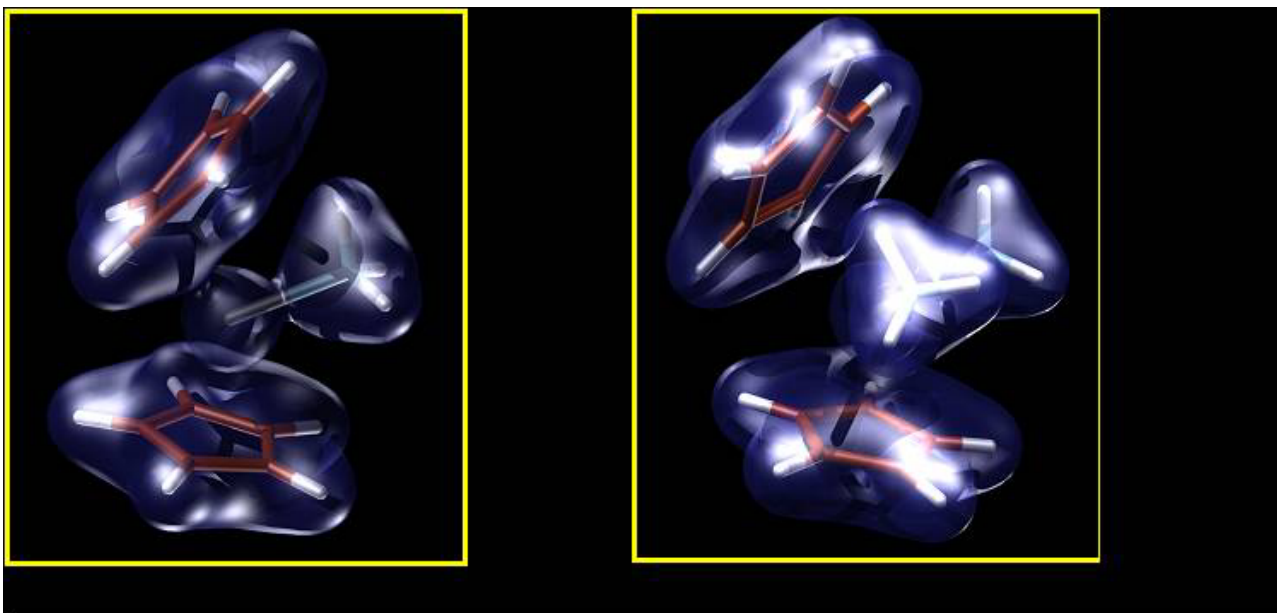


Figure 5. Optimized geometries (with electron density plot in blue) of the complexes formed between MgCp_2 and NH_3 : (a) $\text{NH}_3:\text{MgCp}_2$; (b) $2\text{NH}_3:\text{MgCp}_2$.

to as a “1:1 adduct.” However, the proclivity of Mg to attain tetracoordination in most organometallic compounds has led us to also consider the possibility of a “2:1 adduct,” $2\text{NH}_3:\text{MgCp}_2$, formed via the nucleophilic attack of the “1:1” $\text{NH}_3:\text{MgCp}_2$ complex by a second NH_3 molecule.

We have performed first principles quantum chemistry calculations using the *Gaussian 98* code in order to probe the energetics of these two possible reactions. Specifically, we employed density functional theory (DFT) calculations using the B3LYP hybrid functional. Equilibrium structures for both the 1:1 and 2:1 adducts were successfully located via geometry optimizations using a 6-31G(d) basis set, and are shown in Figures 5a and 5b, respectively.

The single-point energies of the optimized 1:1 adduct and 2:1 adduct were calculated using a higher-level 6-311+G(3df,2p) basis set. For the 1:1 adduct, the calculated energy relative to the reactants is -5.4 kcal/mol, indicating that formation of the 1:1 adduct is energetically favorable. A transition state search was also conducted in order to determine whether a barrier exists for the 1:1 complexation reaction. A transition state structure was successfully located, which normal mode analysis indicates is associated with the bending of linear MgCp_2 upon attack of NH_3 . However, the relative energy of the transition state compared to the reactants was found only to be 1.0 kcal/mol, indicating that formation of the 1:1 adduct is likely to be facile at room temperature.

For the 2:1 adduct, shown in Figure 1b, the calculated energy relative to the reactants is -13.2 kcal/mol. This result indicates that formation of the 2:1 adduct is energetically favorable relative to both the reactants as well as the 1:1 adduct. Interestingly, nucleophilic attack of $\text{NH}_3:\text{MgCp}_2$ by the 2nd NH_3 molecule results in

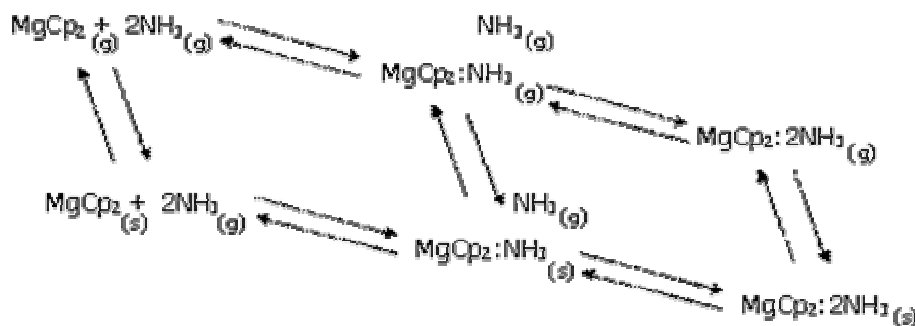


Figure 6. Equilibrium relation for the interaction between magnesocene and ammonia.

a greater incremental stabilization energy (7.8 kcal/mol) than the initial attack of MgCp_2 by the 1st NH_3 molecule (5.4 kcal/mol). This result may reflect a preference for tetracoordination over three-fold coordination of the Mg atom. We were able to locate a barrierless pathway for the formation of the 2:1 adduct from the 1:1 adduct, indicating that its formation should be facile.

From the theoretical results, we can propose an equilibrium relation for the interaction of MgCp_2 and NH_3 in the gas and condensed (i.e., on reactor walls) phases, which is shown in Figure 6.

In the next sections, we describe our efforts to further examine this interaction using in situ Fourier transform infrared (FTIR) spectroscopy and quartz crystal microbalance (QCM) studies.

2.4.3 Experimental Results

We have found that mixing MgCp_2 and NH_3 under typical MOCVD flow conditions at room temperature results in the buildup of a condensable film visible to the naked eye, which can be seen on the KCl window in the infrared cell in Figure 7.

Introducing MgCp_2 (via a H_2 carrier gas) or NH_3 separately into the IR cell does not result in any film buildup. In order to identify the composition of the film at various growth conditions, we have performed FTIR spectroscopy experiments. In our setup, an infrared beam is passed through the IR cell pictured in Figure 7 to probe the growth of any condensable adducts of MgCp_2 and NH_3 on the internal KCl window.

We have spectroscopically isolated and identified two similar but distinct condensable products at room temperature—one formed at low pressures and one formed at high pressures. The IR spectra of the condensed adducts at 20 torr and 500 torr (all flow rates held constant) are shown in Figure 8. Both spectra show features indicative of MgCp_2 and NH_3 components, consistent with their assignment as adducts of MgCp_2 and NH_3 . Because NH_3 is present in great excess over MgCp_2 , increasing the pressure will increase the NH_3 concentration and shift the equilibrium given in Figure 6 towards the 2:1 adduct. We therefore assign the low pressure product as the 1:1 adduct ($\text{NH}_3:\text{MgCp}_2$) and the high pressure product as the 2:1 adduct ($2\text{NH}_3:\text{MgCp}_2$).

We find via IR spectroscopy that this assignment is entirely consistent with the observed film growth behavior when MgCp_2 and NH_3 interact, which is described here. When the total pressure in the cell is increased from 20 torr to 500 torr, the low pressure (1:1) adduct (Figure 5a) converts to the high pressure (2:1) adduct (Figure 5b). If the MgCp_2 flow is then removed but the NH_3 is left on at 500 torr, growth of the high pressure adduct stops and the film is maintained at a steady state thickness. However, if the NH_3 flow into the cell is stopped (but the pressure is maintained at 500 torr), the high pressure adduct quickly converts (on the order of a minute) to an adduct which can be identified via its IR signature as the same that is formed at low pressure (the 1:1 adduct). This is followed by gradual and complete disappearance of the film as long as the NH_3 flow remains off. If the NH_3 flow is turned back on before the film has completely disappeared, conversion back to the

energetically favorable high pressure (2:1) adduct is observed. Thus, the 1:1 and 2:1 adducts can be converted from one to another by controlling the NH_3 concentration and their formation is completely reversible at room temperature. The observed growth behavior can be explained by the equilibrium model proposed in Figure 2. Additionally, DFT IR frequency calculations of the 1:1 and 2:1 adducts we performed were found to be good fits with the low pressure

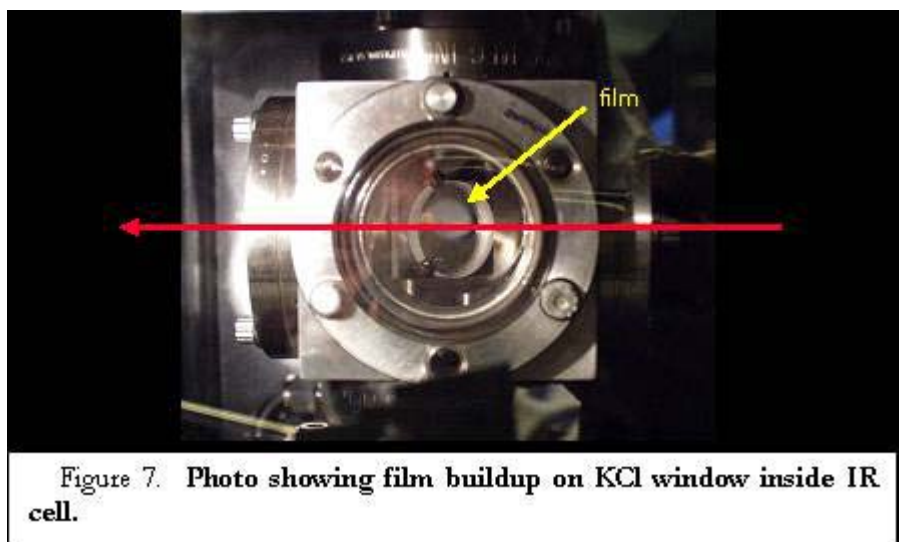


Figure 7. Photo showing film buildup on KCl window inside IR cell.

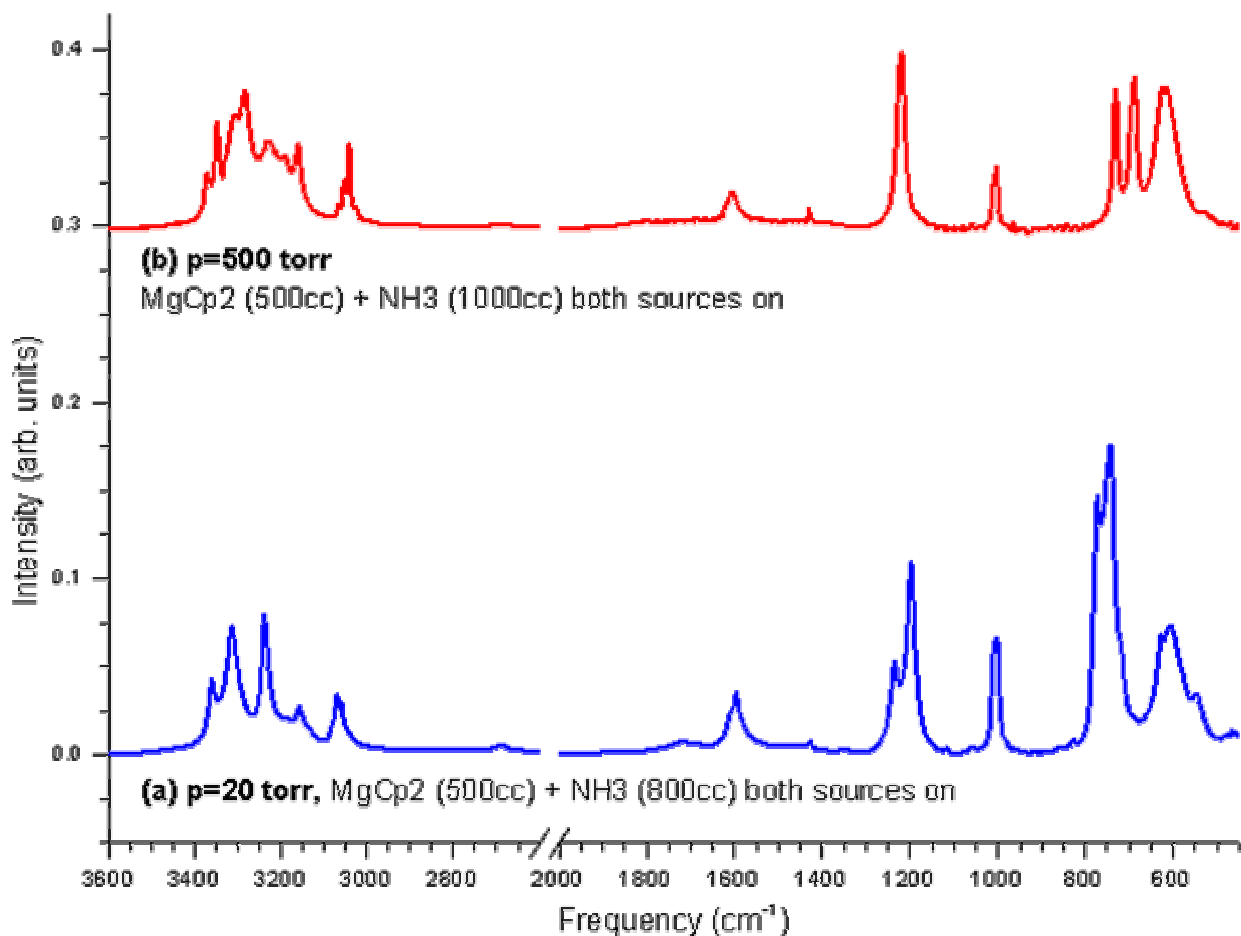


Figure 8. FTIR spectra of the condensable adducts of MgCp₂ and NH₃ at (a) 20 torr and (b) 500 torr.

and high pressure adducts, and lend further support to our assignments.

We have also begun quartz crystal microbalance (QCM) studies, which allow for the real-time monitoring of film growth and film loss in a temperature controlled environment. The purpose of these experiments is to identify reactor inlet conditions at which condensation of the complexes of MgCp₂ and NH₃ does and does not occur.

2.4.4 Summary

Based on FTIR spectroscopy experiments and DFT quantum chemistry calculations, we have isolated and identified the room-temperature products of magnesocene and ammonia as Lewis acid-base complexes. These complexes can exist as either NH₃:MgCp₂ or 2NH₃:MgCp₂, with both adducts being condensable at room temperature. We believe the formation of these complexes can explain to a large degree the Mg doping issues observed during MOCVD growth of p-type GaN and other III-nitrides. An improved quantitative understanding of adduct condensation should allow for reactor design modifications and determination of film growth conditions that reduce or eliminate the Mg incorporation problem.

3 TASK 3: III-NITRIDE MOCVD REACTOR DESIGN AND IN-SITU MONITORING

3.1 Reactor Modeling (HK Moffat, WG Breiland, JR Creighton, A Salinger)

3.1.1 Background

This subtask has focused on creating new reactor designs with the aid of computational fluid dynamics coupled to chemistry/particulate growth and transport analysis that reduce sensitivity to operating conditions, improve uniformity, and improve optical access for process sensors. Compared to other III-V CVD systems, the AlGaN MOCVD suffers from extreme sensitivity to temperature, gas-phase precursor concentrations, and reactor residence time due to parasitic chemical processes. Reactor conditions that have produced the best material quality for nitride growth systems have favored higher temperatures and pressures than typically used previously, where there is very little experience. Therefore, numerical calculations become helpful to elucidate the transport phenomena in new reactor designs.

Legacy numerical modeling tools (MPSalsa) that couple fluid flow, temperature distribution, and homogeneous and heterogeneous chemical reactions in reasonably complex reactor geometries were employed in the numerical modeling. Sandia's optimization tool, Dakota, was also used to quantify reactor designs.

3.1.2 Reactor Design Evolution

At the start of the numerical modeling work, run conditions were optimized for the "Sparky" reactor, which was located in Building 893. This work is presented in the first enclosed Sandia Memo [1]. As the program progressed, work became focused on a new reactor design [2] that could potentially reduce sensitivity to operating conditions, improve uniformity, and improve optical access for process sensors.

The new reactor geometry used baffled injectors and exhaust to provide constant velocity injection of the reactants into the reactor. This design avoids the use of screens that are currently used in reactors to provide "uniform" injection of reactants, and which involve numerous engineering challenges not the least of which is a large amount of surface area at an elevated temperature. The reactor design also affords unfettered optical access to the top of the wafer, important for the implementation of in situ diagnostics. The design assumed premixed gases, the viability of which was proven through chemistry studies that demonstrated that the parasitic reactions associated with the nitride system weren't active in cold sections of the reactor.

Run conditions and geometry were optimized by MPSalsa/Dakota. Optimization calculations pointed to a significantly different geometry than the one initially conceptually envisioned. Two general principles appeared to hold.

The throat at the top of reactor needed to be enlarged from the original design. Essentially a constriction was envisioned to be necessary to orient the flow onto the substrate and reduce the total volume of free heated space about the susceptor. Numerical calculations, an example of which is displayed in Figure 1, demonstrated this was not the case. Instead, the best uniformity was achieved when the radial inlet was pushed back almost to the side of the can, and the gas flow was allowed to spill over the side and onto the top of the boundary layer created from the spinning disk. These results were pressure dependent. Various mechanisms created problems at both the high and low ends of the pressure ranges studied. Also, at the high end of the pressure spectrum, natural convection caused multiple steady state solutions to appear in the parameter space under some conditions. This caused major difficulties with the optimization software. Generally, the new reactor design doesn't work for higher pressures. At the low end of the pressure ranges, the flow bypassed the middle of the susceptor for

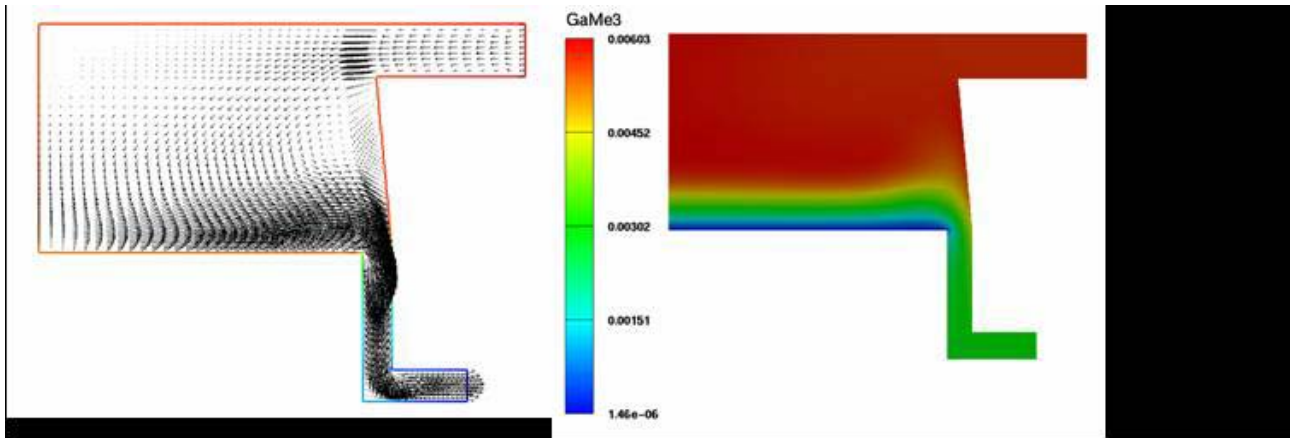


Figure 1: Optimal geometry has a large neck and a correspondingly large susceptor. On the left are arrow plots of the v_y and v_x fluid flow in the optimal geometry (v_θ not shown). On the right is a color contour plot of the group III source, trimethylgallium, exhibiting a uniform distribution of the group III at the top of the boundary layer over the disk.

nonconstricted inlet region cases. Thus, large neck design may only be acceptable for a range of pressures around 100 torr to 230 torr. Other pressure regimes may require either different reactor geometries or larger flow velocities.

An additional design principle was that the susceptor on which the single wafer sits should be significantly larger than the wafer itself. Boundary edge effects were pushed beyond where they could influence the deposition uniformity. Enhancing temperature uniformity over the wafer, though not addressed in the numerical study, because it was assumed a priori, should be enhanced by the larger susceptor size.

In contrast to the pressure, there is a wide range of spin rates for which there are optimal growth rate solutions were obtained. The inlet mass flow rate was loosely correlated with the spin rate, as expected.

Based on the performance of the reactor in the numerical studies, a Technical Announcement was made and then a patent application was pursued on the design of the reactor [4]. An experimental prototype is also envisioned, funding permitted.

In general, 2D color contour plots, where the optimization parameter was displayed in color, as a function of two reactor parameters, were found to be more enlightening than the actual optimization calculation itself. They provided a better understanding of the mechanisms involved, and of the extent of the size of the parameter region which provides acceptable results. Considering the uncertainties in the chemistry mechanism, the size of the parameter region was determined to be the more important effect than an actual minimization in the objective function.

Under the SSL program, we developed the necessary amount of infrastructure in order to conduct optimization calculations of deformed-mesh CVD deposition systems, while trying to reuse as much of Sandia's legacy code capabilities as possible. The idea was to develop the needed infrastructure first with the simplistic model chemistries and perhaps inaccurate reactor boundary conditions. Then, work on the model fidelity at a later date, when the nitride chemistry modeling task came up with preliminary models and the soot modeling infrastructure was in place. The reactor geometry was based on a 2D axisymmetric flow of NH_3 , TMG , H_2 , with a simple sticking coefficient reaction at the surface assuming idealized boundary conditions consisting of uniform substrate temperatures and perfectly cooled side walls. A significant accomplishment of the SSL program was to make the actual reactor geometry a parameter of the optimization calculation. This was accomplished within MPSalsa by breaking the geometry of the mesh up into regions. The size and positioning of the regions are parameterized by the geometry parameters that are also optimization parameters. Each finite elements which makes up the mesh is assigned to a single region. The region itself is parameterized utilizing an isoparametric mapping technique that can calculate each finite element node's position as a function of the region's geometry. This treatment allowed for a smooth change in the mesh positioning as a function of the geometry optimization

parameters. MPSalsa's new mesh movement capability was integrated into Sandia's finite element package, Exodus, by using Exodus' displacement field capability. Additional Exodus nodal variables called displacement fields are carried along within Exodus to track the change in MPSalsa's mesh locations. Note, displacement fields are not added to MPSalsa's solution vector. However, whenever a solution is written out to an Exodus file or read in from an Exodus file during restarts or initialization operations, the Exodus displacement field is used to calculate the mesh locations of MPSalsa's grid. Displacement fields are also recognized by visualization software such as Mustafa or Blot, so that the deformed geometries may be accurately visualized.

Initially, the objective function used in the analysis was based on growth uniformity, only. In order to simplify the analysis, the basic function of merit was kept constant in all of the analyses. Another aspect of the problem that may be adequately captured by reactor models is a measure of the efficiency of reactant utilization. For example, this may be couched in terms of the cost in chemicals to grow a 1 micron film on a 50 cm substrate. This cost metric was formalized but not added to the objective function in these studies.

Procedures for optimization of large scale calculations were also demonstrated. Salinger et al. [3] demonstrated the capability to do similar CVD growth-rate uniformity optimization problems using 3D MPSalsa calculations on massively parallel machines. Their work also compared black-box optimization schemes (i.e., Dakota) against invasive optimization schemes (using MOOCHO) that couple the nonlinear solution scheme to the optimization procedure itself. Significant speedups, important for this class of problems, were obtained for the later approach.

Under this task, fluid instabilities were also investigated both theoretically and experimentally. Theoretically, fluid instabilities are found in systems where multiple solutions exist in the fluid dynamics. The instabilities were experimentally sought using laser-deflection spectroscopy ("mirage" effect) and using shadowgraph of an expanded laser beam over the growth surface. Fluctuations in the signals were consistent with the predicted instabilities. Commercial reactors are evolving towards pressure regimes where fluid instabilities are not as prevalent, so this task is now considered complete. However, the importance of this issue is addressed in the numerical modeling of the reactors. Stability boundaries for the onset of buoyant natural convective flow have been followed with MPSalsa [1], and this effect greatly influences reactor design.

3.1.3 Conclusions and Future Work

The enclosed memo [2] showed that, once the reactor dimensions were optimized, there was a wide range of reactor operating conditions where the proposed reactor operated satisfactorily. The confidence intervals over which the reactor performed satisfactorily spanned a wide range of spin rates, net velocities, and pressures. Perhaps, the parameter that was limited the most in these studies was the pressure. Adequate results were only obtained at bounded pressure regimes. Failures were obtained at both the low (< 100 torr) and high (> 230 torr) pressures.

The confidence intervals obtained with the simple sticking coefficient chemistry should only be considered as an upper bound to those obtained with a more detailed chemistry mechanism. That the reactor would produce uniform depositions under group-III mass transport limited conditions, the result of the chemistry mechanism used to date, is probably a prerequisite condition to a proper design. However, as pointed out in the growth chemistry chapter of this report, a significant portion of the group III species is transformed into particles via a homogeneous kinetics mechanism at the edge of the hot zone of the reactor. Relatively more Aluminum than Gallium is lost to the particulate phase, as well, leading to a very challenging problem in predicting both the average composition of a layer and the variation of the compositional uniformity as a function of the radius. Large radial variations in group III compositions would prevent a reactor from being used in production; it's a show stopper. Thus, without the inclusion of a particle generation chemistry that could model the loss of the group III component into these studies, the results presented here are only of academic interest, as they don't account for this most significant design issue.

The focus thus has shifted towards incorporating particle transport and reaction models into the current generation of CVD modeling codes. A large effort initially aimed at modeling soot generation in fires is underway to develop a sectional modeling capability. The plan is to revisit these optimization studies once

particle sectional models are installed into SPIN and MPSALSA, and particle chemistry mechanisms are developed for the nitride CVD growth systems.

3.1.4 References

1. H. K. Moffat "Setup of Optimization Problem for GaN CVD Reactors," Sandia Labs Memo, Sandia National Laboratories, Albuquerque, NM, March 28, 2001.
2. H. K. Moffat, "Simulations of the Proposed Spillway Reactor: Viability Studies," Sandia Memo, Sandia National Laboratories, Albuquerque, NM, August 14, 2002.
3. A. G. Salinger, R. P. Pawlowski, J. N. Shadid, "Computational Analysis and Optimization of a Chemical Vapor Deposition Reactor with Large-Scale Computing," Industrial and Engineering Chemistry Research (in press 2003).
4. Patent Application filed for "Rotating Disk Chemical Vapor Deposition Apparatus", W. G. B. Breiland, H. K. Moffat, Technical Disclosure, SD7056/S-98,621.
5. B. Van Bloemen Waanders, K. R. Long, P. T. Boggs, "Large scale non-linear programming for PDE constrained optimization," Technical Report, Sandia National Laboratories, Albuquerque, NM 87185, SAND2002-0396 (2002).

3.2 In-situ Measurement of Thin-film Stress during MOCVD (SR Lee, WG Breiland, DD Koleske)

3.2.1 Background

A central activity of our program is to measure the real-time stress evolution that occurs during thin-film growth by MOCVD. Stress is measured using a multi-beam optical stress sensor (MOSS) that is coupled to our MOCVD reactor. In FY99, we first demonstrated a prototype MOSS/MOCVD system as proof of principle; this prototype system was completely rebuilt in FY01/FY02 to fully achieve routine and reliable real-time measurements of thin-film stress during heteroepitaxy. Upgrades include installation of a higher resolution digital CCD camera, a 27-mW fiber-couple diode laser, and new control software, as well as redesign of the MOCVD reactor's optical access. To test and further improve the new system, real-time wafer curvature measurements were made during the growth of more than 100 samples. Preliminary stress-evolution data were obtained for growth of a wide variety of III-nitride heterostructures including: (1) GaN on sapphire, (2) AlGaIn on GaN/sapphire, (3) AlN on SiC, and (4) GaN on AlN/SiC. Since few systems exist worldwide that can probe the real-time stress evolution during heteroepitaxy, the improved MOSS/MOCVD facility is an important distinguishing strength of our program.

3.2.2 Optical diffraction modeling of laser-deflectometry measurements of thin-film stress

The MOSS technique measures wafer curvature (and hence, the thin-film stress) by precisely measuring the deflection of parallel laser beams reflected from the film-substrate surface. A fundamental assumption of the technique is that optical reflection of each laser beam is specular such that only stress-induced wafer curvature can modify the laser-beam deflection. We have discovered that significant deviations from specularity may occur if the thickness of the film is nonuniform, as is often the case during the growth of real films. Variations in the optical pathlength inside the nonuniform film create phase-shifts that interfere to steer the reflected beam. This steering produces additional beam deflections that vary with film thickness in a manner unrelated to the film's stress.

We have developed a Fresnel-Kirchhoff diffraction model of laser-beam steering by nonuniform films that allows accurate interpretation of our wafer-curvature measurements of stress. The model shows that beam-steering effects vary strongly with film nonuniformity, film thickness, wavelength dispersion, laser-beam spot

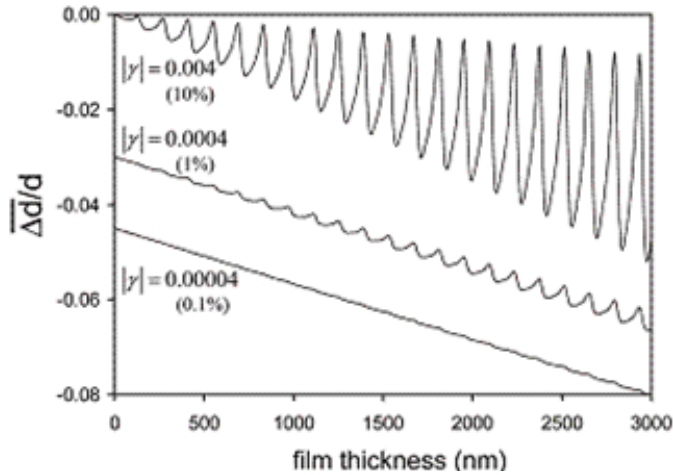


Figure 1. Optical diffraction theory simulations of the relative change in laser-beam spot spacing, $\Delta d/d$, versus GaN film thickness. Gamma indicates the film-thickness gradient (e.g., $\gamma=0.004$ indicates a thickness change of 10% from the center to the edge of a 50-mm-diameter wafer). The lower simulations are vertically offset from the origin for clarity.

size, and refractive index. Figure 1 shows model simulations of stressed GaN films (0.2 GPa) grown on sapphire; three film-thickness nonuniformities are shown: 0.1%, 1%, and 10%. The average slope of each curve is due to film stress, while the oscillatory features are beam-steering artifacts produced by the film-thickness nonuniformities. The 1% curve at the center in Figure 1 is typical of MOCVD heteroepitaxy conducted in a research setting; artificial oscillations are clearly visible but are not dominant. We conclude that increased care is warranted when extracting stress data from wafer-curvature measurements, because the laser-beam deflection is due to both film stress and film-thickness nonuniformity. These diffraction-model results underpin sound interpretation of stress-evolution data collected using laser deflectometry (accepted for publication in *Journal of Applied Physics*).

3.3 In-situ Temperature Measurement during MOCVD (JR Creighton, WG Breiland, CM Mitchell, KE Waldrip)

3.3.1 Background

Surface temperature measurement during AlGaInN MOCVD is particularly difficult because the epilayers and substrates (e.g. sapphire) are transparent at the wavelengths normally used for pyrometry (typically near-IR). We have proposed two alternative pyrometer approaches to deal with the transparency problem. One approach is to measure radiation in the mid-IR (MIR), where the sapphire wafer is opaque. The second approach is to work near 400 nm where the GaN epilayers are opaque at the high temperatures encountered during deposition. Various methods of emissivity-correction (EC) can be applied to improve the utility and accuracy of the pyrometers. The MIR and 400 nm pyrometers each have certain advantages and disadvantages, which we will discuss, in the following sections.

3.3.2 MIR Pyrometer

At wavelengths > 7 microns sapphire is opaque at room temperature, and the absorption shifts to shorter wavelengths as the temperature is increased. Other factors must be considered, however, such as IR absorption by the reactant gases (see Fig. 1).

We have identified the optimum detection wavelength of 7.5 microns and built a non-emissivity-correcting (non-EC) pyrometer centered at this wavelength using a bandpass filter. The first prototype uses a thermopile detector, which has good sensitivity but currently suffers from temperature drift problems. The calibration curve for the MIR pyrometer is shown in Figure 2. The data is well represented by the Planck equation using an effective wavelength of 7.56 microns.

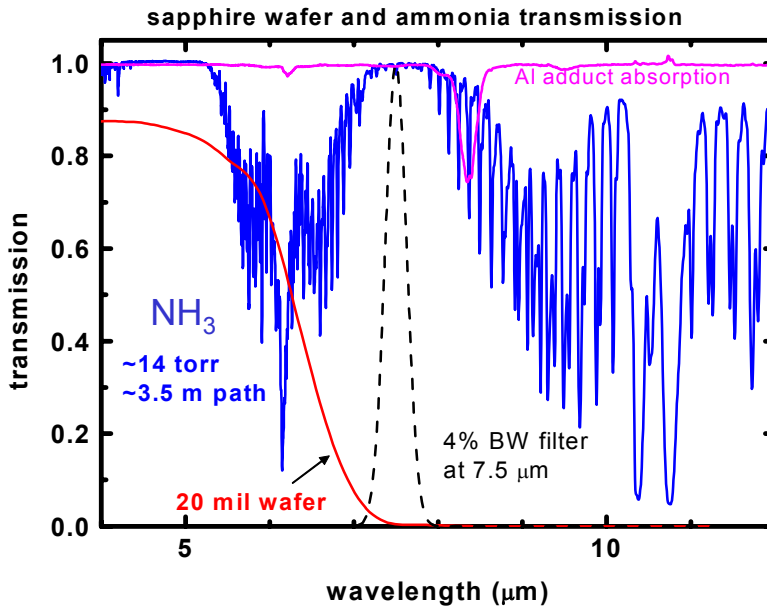


Figure 1. IR transmission of sapphire and reactive gases

Note that the response becomes nearly linear above 600°C (the Rayleigh-Jeans limit). This points to the major disadvantage of MIR pyrometry; small changes in sample emissivity lead to relatively large temperature errors. An emissivity change of only 0.01 will cause the apparent temperature to change by ~ 10°C at typical deposition temperatures.

A non-ECP may have some utility as a pregrowth sapphire-wafer temperature monitor. For instance, we have found that the bare sapphire wafer temperature changes significantly as the reactor pressure is varied, even though the temperature controller is maintaining a constant temperature on the wafer holder. For a wafer holder temperature of 1080°C, as the reactor pressure is raised from 50 to 200 Torr the wafer temperature

increases by ~50°C, apparently from the improved thermal contact with the holder. Any pyrometer detecting visible or NIR light would simply look through the wafer and not see this effect.

Once deposition is initiated some type of emissivity correction is absolutely necessary for the MIR pyrometer. Concerns that our standard EC technique might not provide the needed level of accuracy led Breiland to propose two new methods. Some progress was made towards developing the “Reference Oven” approach, but we first decided to test the non-ECP version on our research reactor. Results of the non-EC MIR pyrometer during a long GaN on sapphire run are shown in Figure 3. Note the severe apparent temperature oscillations (initial amplitude ~80°C) and the -85°C offset in the “average” temperature (relative to the 415 nm pyrometer). The severe oscillations and offset are both due to the large sensitivity to emissivity changes of the MIR pyrometer. So as expected, an emissivity-correction method must be used once thin film deposition begins. Incidentally, a “post-mortem” adjustment of the apparent “average” MIR temperature using the estimated GaN optical constants at 7.5 microns yields a corrected temperature of

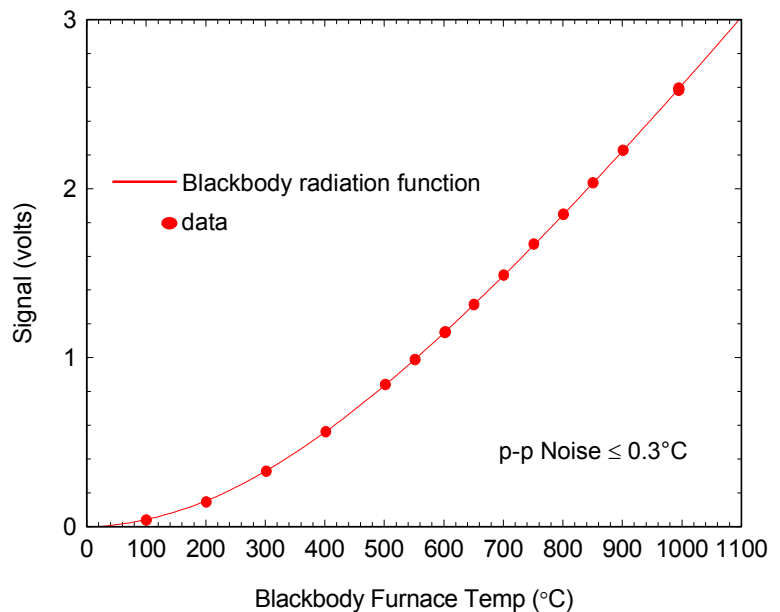


Figure 2. Response curve of MIR pyrometer

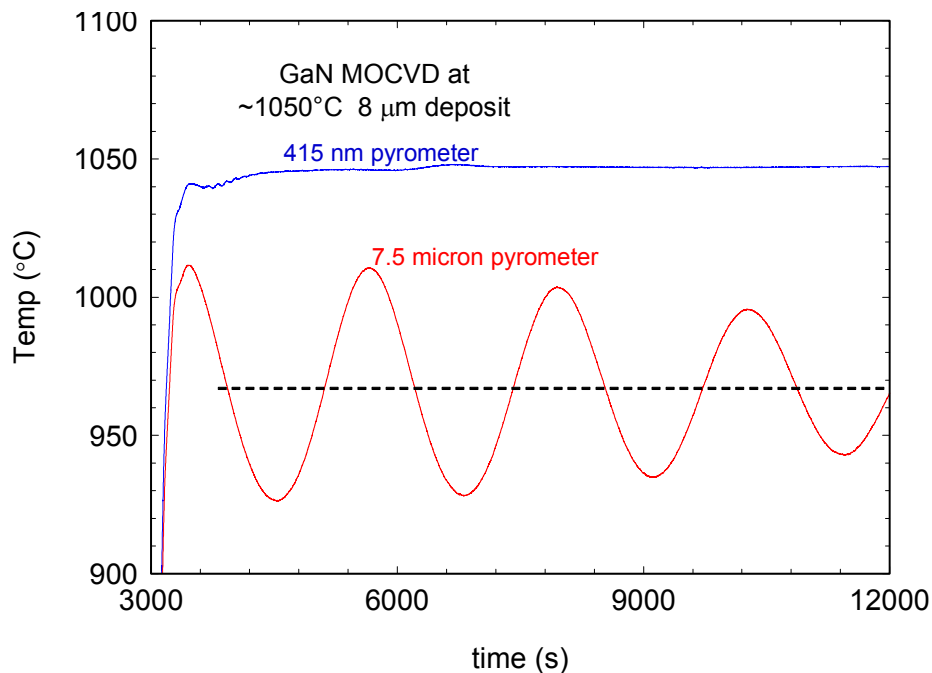


Figure 3. MIR and 415 nm pyrometer during GaN/sapphire MOCVD

these short wavelengths. Fortunately, the bandgap of GaN shifts from the UV into the visible (420-440 nm) as the temperature is raised to near 1000°C. The literature regarding the high temperature optical constants for GaN is rather sparse (most is extrapolated from lower temperatures), so there is some uncertainty as to the minimum wavelength required to achieve opacity. A major advantage of working in this wavelength range is the exponential response with temperature (Wien limit), which significantly reduces the sensitivity to emissivity changes.

Sandia had previously developed a pyrometer (non-EC) with an effective wavelength of 415 nm (top curve, Fig. 3), and the results showed that opacity is achieved for a GaN thickness of ~0.5 microns at typical growth temperatures (1000-1050°C). This first version uses a GaP photodiode, and very good S/N is achieved above 1000°C. The lower useful temperature limit is in the 850-900°C range, which is due to noise and drift in the analog electronics.

Because InGaN is typically grown in the 750-800°C range, we examined methods of extending the violet pyrometer to lower temperatures. “Back-of-the-envelope” calculations showed that we should expect 10^3 - 10^5 photons/sec for InGaN conditions, so we decided to use a photon-counting photomultiplier tube (PMT) as the detector. Due to the shift in GaN

1063°C, much closer to the expected value.

Given the uncertainties in developing a new EC method for the MIR, we decided to focus our recent efforts on improving the 400-nm method. We plan to reexamine the MIR options next year.

3.3.3 UV-Violet (400nm) Pyrometer

The other pyrometer approach is at the opposite side of the spectrum, near the bandgap of GaN. The difficulty here is the small amount of thermal emission that occurs at

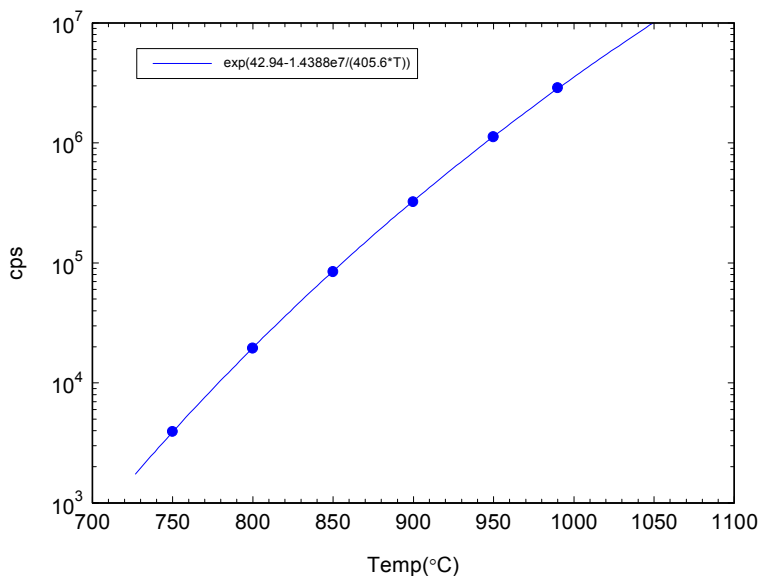


Figure 4. Calibration curve of PMT-based violet pyrometer

bandgap we were also concerned that we might have to shorten the wavelength somewhat. The calibration curve for the first prototype is shown in Figure 4. From the filter set chosen and measured, we expected the effective wavelength to be 405 ± 2 nm, and the best fit (solid line) uses $\lambda = 405.6$ nm.

After some initial tests we also decided to add emissivity correction to this pyrometer, using the basic approach used by Breiland. Some aspects of the hardware and software are different for the PMT-based pyrometer, but the basic idea is the same. An external and chopped beam of light is

reflected off the surface where the emission is also being collected. The data collection software separates the AC component (reflectance) from the DC component (thermal emission). If the sample is opaque and specular, then the emissivity (ϵ) = $1 - R$, which is then applied to compute the corrected temperature. The success of this approach depends on a number of factors; the most obvious is the quality of the reflectance data. The first measurement from this new system is shown in Figure 5.

The damped oscillations during the GaN growth demonstrate that the film is absorbing at this wavelength

and temperature, as expected. The red line in Fig. 5 is the ADVISOR fit, which is near perfect using the optical constants; $n = 2.628$ and $k = 0.1896$, and a growth rate of 2.982 microns/hr.

Results using ECP during our second run are shown in Figure 6. The ECP temperature (red) is compared to the non-ECP temperature (blue). During AlN deposition the non-ECP temperature rises about 2°C, while the ECP temperature falls about 2°C. During GaN deposition the non-ECP temperature exhibits damped oscillations with initial amplitude of 6-7°C. The ECP exhibits

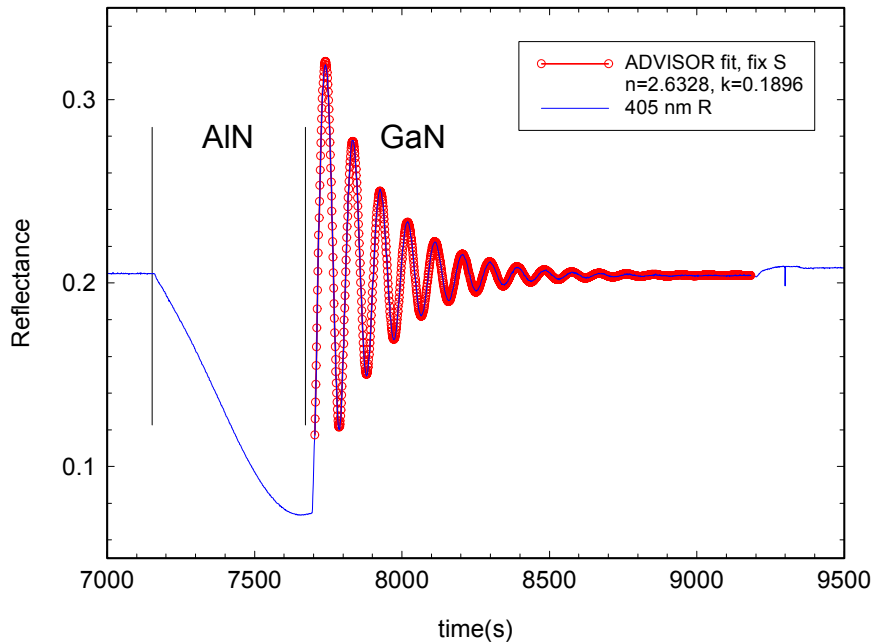


Figure 5. Reflectance measured during GaN/AlN MOCVD at 992°C

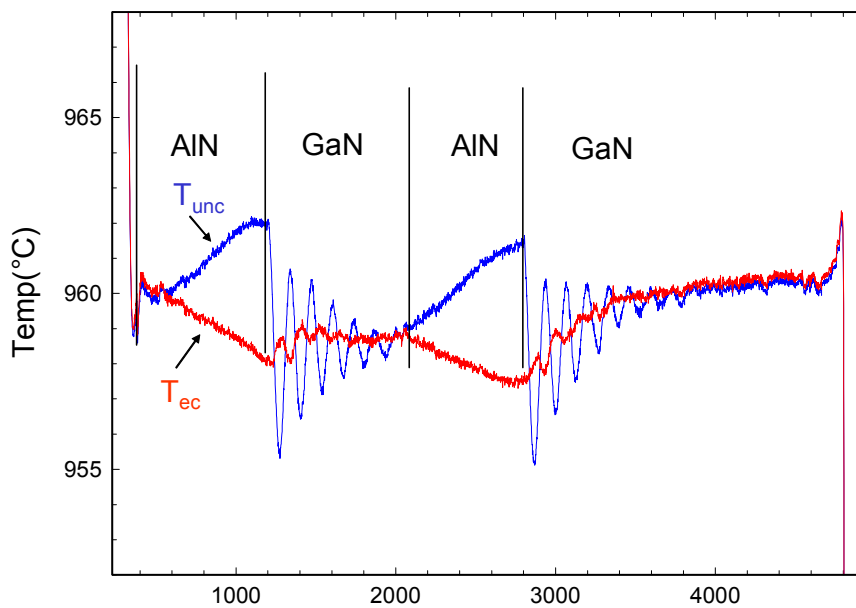


Figure 6. 405 nm ECP for GaN/AlN MOCVD at 960°C

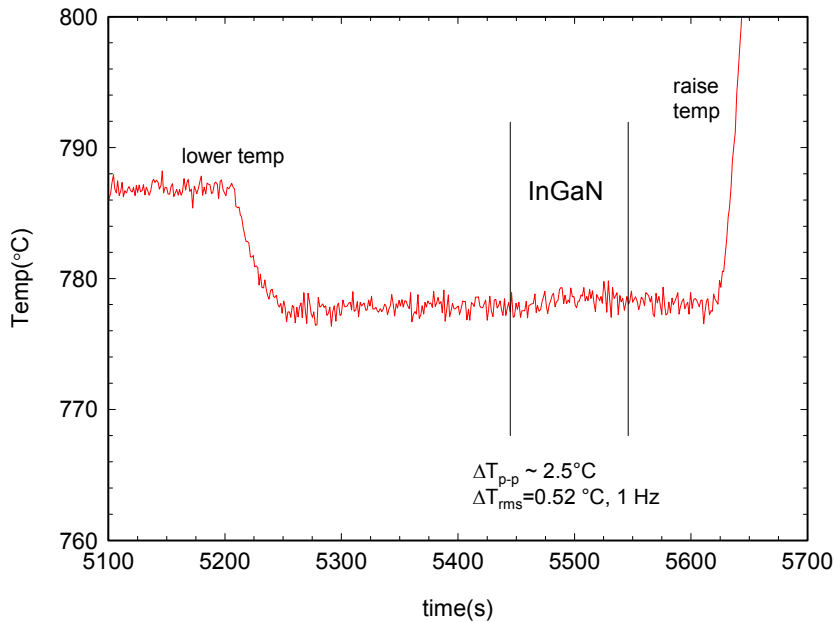


Figure 7. 405 nm ECP during InGaN at 778°C

termed “over-compensation”. There are hardware methods of minimizing the artifacts, and software methods for accounting for errors, which we will address in the near future.

The other major test of the PMT-based pyrometer is temperature measurement in the 750-800°C range during InGaN deposition. Results during our second run for InGaN/GaN at 778°C are shown in Figure 7, taken with a 1 Hz integration time. At this temperature the peak-to-peak noise is ~2.5°C, corresponding to a rms noise of 0.52°C. This noise level may be acceptable, but improvements would be welcome. This is pure intrinsic shot noise, so the only method of improving Signal/Noise is to integrate longer, or increase the signal level. Longer integration times are probably acceptable for some applications, but there is always an upper limit. We believe we can recover some signal (maybe X 2) through improved filters and optics, and if we decide we can work at longer wavelengths (e.g. 415 nm) we can recover another X 2-3.

In this example, the emissivity change is very small (~0.01) when the thin InGaN layer is deposited on GaN, so the ECP value is virtually identical to the non-ECP temperature (not shown). More complex structures may demonstrate the need for emissivity correction during InGaN MOCVD.

3.3.4 Summary

The initial tests of the 405 nm ECP with PMT detector look very promising, but more work is needed to test and refine the instrument. One problem we didn’t discuss is the possible non-linearity in the PMT response at the high-count rates encountered above 1000°C. The stray light issue, which is probably the main source of error during ECP, needs further examination. It is possible the stray light problem is much worse in a radiatively heated reactor (the Sandia research reactor is inductively heated) and could limit the utility of 400 nm pyrometry.

small oscillations of about 1°C of opposite phase. Our first run (not shown) exhibited somewhat larger ECP oscillations (about 2°C) and we are not sure which result is more typical.

The ECP results are a definite improvement over the non-ECP results, but the small residual oscillations seen in the data are almost certainly not true temperature oscillations. Previous extensive testing at Sandia (Breiland) on AlGaAs layers demonstrated that a number of artifacts can arise that lead to imperfect emissivity correction. These artifacts almost always lead to small temperature oscillations of opposite phase (compared to the non-ECP), an effect Breiland

4 TASK 4: ADVANCED LIGHT-EMITTING DEVICES

4.1 Theory of Nitride Quantum Well Emission (WW Chow)

4.1.1 Theory

Group-III nitrides differ from conventional III-V compounds in two important aspects. Many-body Coulomb effects are significantly stronger and there is likelihood of strong internal electric fields in quantum well structures. Owing to these differences, it is necessary to modify the usual calculation of optical properties.

To account for the effects of the internal electric field and its screening due to the resulting electron-hole spatial separation, we use an iterative solution of the $\mathbf{k}\cdot\mathbf{p}$ Hamiltonian and Poisson equation to determine the quantum-well or quantum-dot bandstructure. The solutions contain the effects of the quantum confinement, the built-in electric field and the mixing between hole states.

The result of the bandstructure calculation is used in the semiconductor Bloch equations to provide a systematic treatment of many-body effects. Solutions of the semiconductor Bloch equations may be obtained at various levels of approximation. The Padé approximation was used in the early III-N gain calculations, and it brought attention to the large bandgap renormalization and Coulomb (excitonic) enhancement effects on optical properties. We have improved on the Padé approach by including the next higher order of correlations in the Coulomb interaction. A result is a microscopic description of collision effects at the level of quantum kinetic equations, which eliminates the dephasing rate as a free parameter, thus greatly improving predictive power.

The solution of the semiconductor Bloch equations gives the polarization of the active medium, which we use in Maxwell's equations to obtain the complex susceptibility. An energy balance argument is used to determine the spontaneous emission. The detailed treatment of Coulomb correlations afforded by the present theory is found to be crucial to agreement between theory and experiment.

4.1.2 Internal field effects on optical nonlinearities and spontaneous emission lifetime

Using the above theory, calculations of the absorption/gain and luminescence spectra are performed for different GaInN/GaN quantum well configurations. We find that narrow wells (width < 2nm), exhibit the usual excitation dependent bleaching of the exciton resonance without shifting spectral position. On the other hand, a significant blue shift of the exciton peak is obtained for wide quantum wells (width > 3nm). This blue shift, which is also present in the excitation dependent luminescence spectra, is attributed to the interplay between the screening of piezoelectric and spontaneous polarization fields and the density dependence of many-body effects. The calculations give quantitative predictions of the spontaneous electron-hole-pair lifetime for different quantum-well widths.

4.1.3 Internal field effects on refractive index and optical mode properties.

Our investigations also uncover a strong dependence of the real part of the optical susceptibility on quantum-confinement geometry, because of the interplay of quantum-confined Stark effect and many-body interaction. As a result, we expect filamentation (self-focusing) and consequently emission beam quality in nitride-based nanostructures to be significantly affected by device design, especially under high current conditions. For example, increasing facet reflectivities in a plane-facet cavity enhanced LED tends to exacerbate the filamentation problem. A negative-branch unstable cavity is found to mitigate filament effects, enabling single lateral lobe operation at high excitation in large emitting area geometries.

4.1.4 Quantum dots for long wavelength emission

A high indium concentration is necessary for long (green to yellow) wavelength operation. Because of the resulting high strain, spontaneous quantum dot formation is likely. We investigated the optical properties of long-wavelength quantum dot emitters, in particular, those of $\text{In}_{0.5}\text{Ga}_{0.7}\text{N}$ quantum dots embedded in a 2nm thick GaN quantum well. A truncated cone is used to approximate the quantum-dot shape.

The bandstructure calculation is more complicated than the quantum-well case because the simultaneously solution of Schrodinger and Poisson equations now has to be performed for all three dimensions. Additionally, the many-body physics is more involved, because both dot-dot and dot-well Coulomb couplings have to be considered

A result relevant to device efficiency is the difference in influence of the quantum-confined Stark effect between quantum wells and quantum dots. The quantum-dot calculations predict appreciable sensitivity of excitation dependence in the emission spectrum to quantum-dot geometry. Compared to quantum well structures, the quantum-confined Stark effect is more important in quantum-dot optical properties. This is because appreciably lower carrier densities are necessary for the onset of optical emission. In a nitride quantum well, emission occurs at carrier densities that are sufficiently high to partially screen the built-in electric field. In contrast, emission in a nitride quantum dot is achieved at much lower carrier density, so that the built-in electric field remains largely unscreened.

4.1.5 High aluminum and quaternary active regions for short wavelength emission

For short (uv) wavelength applications, we investigated spontaneous emission in AlGa_N and AlInGa_N wurtzite quantum wells. As with InGa_N/Ga_N structures, the combined effects of strain, internal electric field, and many-body Coulomb interactions lead to a significant dependence of optical properties on quantum well configuration. However, we notice one important difference, involving the mitigating of internal electric field effects for certain hole state alignment. Specifically, we identified an abrupt increase of spontaneous emission rate due to the change from heavy-hole to crystal-field-split-hole ground state.

Based on the above result, a disclosure was filed. It describes a bandstructure engineering solution for circumventing piezoelectric field and spontaneous polarization effects. The solution is based on the significant difference between the z-direction effective hole masses for the heavy-hole and crystal-field-split-hole bands. Using an AlN-like band alignment (i.e., with a ch ground-state) increases quantum-confinement energy, so that the quantum-well hole ground state lie above the triangular part of the valence confinement potential, thus resulting in good electron and hole wavefunction overlap. An AlN-like band alignment is achievable with sufficiently high Al concentration in AlGa_N. There is a drastic increase in spontaneous emission rate at the transition between Ga_N-like and AlN-like band alignments. This increase in spontaneous emission rate translates to decrease sensitivity to nonradiative carrier losses.

The above effect is not limited to AlGa_N quantum-well structures. Similar behavior can be found in quantum wells of the quaternary compounds, AlGaIn_N, which leads to a broader wavelength range over which the scheme applies.

4.2 Near UV LEDs using Low Dislocation Density Cantilever Epitaxy (AJ Fischer, DD Koleske, AA Allerman, MH Crawford, KHA Bogart, CC Mitchell, and DM Follstaedt, KC Cross, KW Fullmer, JJ Figiel)

4.2.1 Introduction

One main technological barrier to demonstrating high efficiency nitride LEDs is the large lattice mismatch between Ga_N and sapphire (16%) which results in vertical threading dislocation (VTD) densities of 10^9 to 10^{10}

VTDs/cm², with the very best samples exhibiting $\sim 5 \times 10^8$ VTDs/cm² [1]. Threading dislocations are known to be non-radiative recombination centers [2], and therefore can reduce the internal quantum efficiency of nitride-based emitters. Thus, eliminating threading dislocations may be a vital step towards improving the internal quantum efficiency of nitride LEDs. Furthermore, for many high photon flux applications, such as automobile headlights, nitride-based LEDs will likely be run at very high current densities where VTDs may negatively impact device lifetimes. For these reasons, it is desirable to reduce the density of threading dislocation in nitride LEDs.

4.2.2 Cantilever Epitaxy

Although many advanced growth techniques have effectively reduced threading dislocations, we have developed a lateral overgrowth technique called cantilever epitaxy (CE) [3], which has many inherent advantages for use in high efficiency LEDs. The details of this growth process and the resulting low dislocation density GaN films are presented in Section 3.1. Using cantilever epitaxy, it is possible to significantly reduce dislocations over both the post and wing regions. Since this technique has the potential for dislocation reduction over very large regions, CE is particularly well suited for large area devices such as LEDs. Another important benefit of CE is that dislocation reduction and an LED device structure can be produced in the same growth run starting from an etched sapphire wafer, whereas other dislocation reduction methods require multiple-growth processing. For large areas, we have achieved dislocation densities as low as $2\text{-}3 \times 10^7$ VTDs/cm². With further refinements in sapphire substrate etching and CE growth, it should be possible to achieve even lower dislocation densities.

4.2.3 Devices and Characterization

As a part of this grand challenge LDRD program, InGaN multiple quantum well LEDs were grown on substrates made by cantilever epitaxy. Beginning with an etched sapphire wafer, a fully coalesced GaN film was

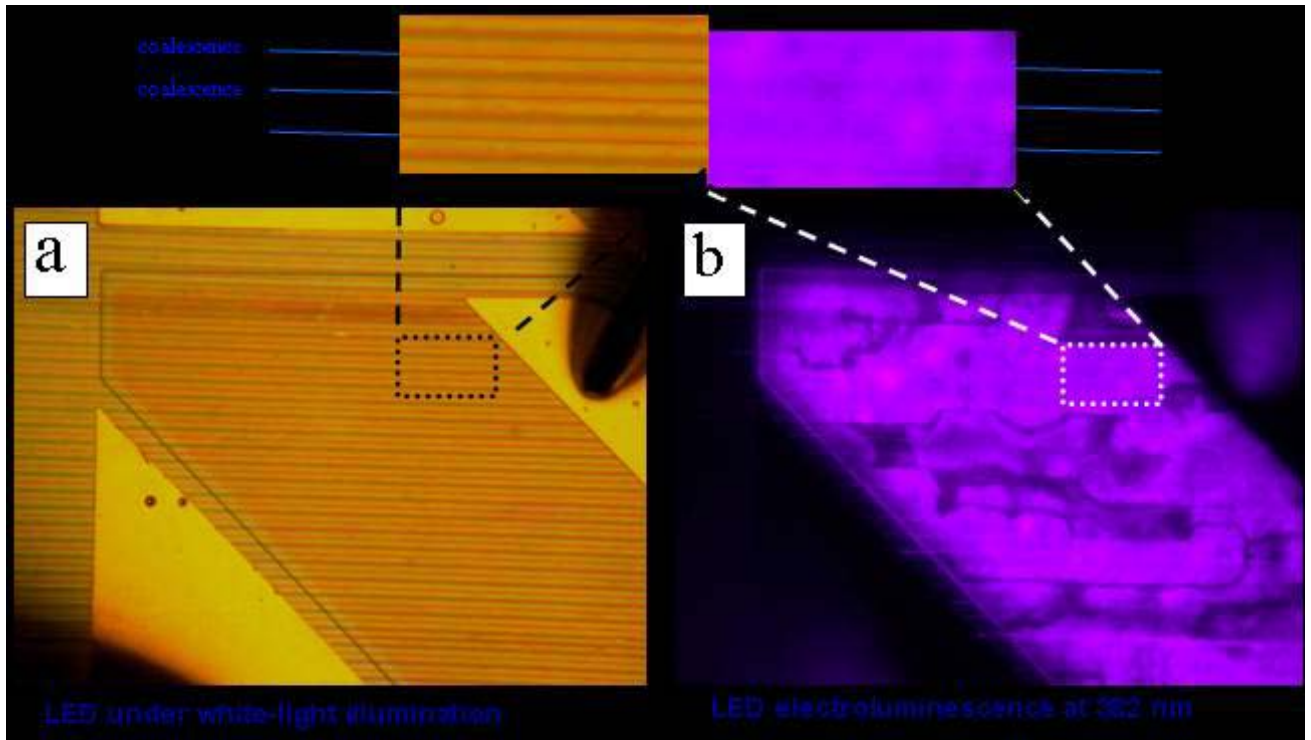


Figure A1. Optical microscope images of (a) an InGaN MQW LED under white light illumination and (b) the electroluminescence (EL) pattern for the same LED. The inset shows a region where the EL intensity is uniform across several wing and post regions.

grown followed by a 2 – 3 micron n-type current spreading layer. An LED active region was then grown consisting of five 40Å In_{0.04}Ga_{0.96}N quantum wells with 100Å GaN barriers followed by a 200Å p-type Al_{0.15}Ga_{0.85}N layer which was used for electron confinement. Finally, a 2500Å layer of p-type GaN was grown and the structure was capped with a 200Å P++ contact layer. LEDs were fabricated using standard lithographic techniques for patterning. Inductively coupled plasma reactive ion beam etching (ICP-RIE) was used to expose the n-type layer and a Ti/Al/Ni/Au contact was deposited by electron beam evaporation to form an n-type metal contact. The p-type contact consisted of a thin semitransparent Ni/Au contact with a thick Au bond pad to allow for wire bonding. The p-contact was annealed in an oxygen ambient at 500C for 10 minutes to promote transparency of the Ni/Au contact.

Wafer level testing of LEDs showed interesting electroluminescence (EL) patterns which are a result of the cantilever growth process. An optical microscope image of an LED under white light illumination is shown in Fig. A1(a) while an electroluminescence image from the same LED emitting at 382 nm is shown in Fig. A1(b). For large regions (> 200 μm²), the LED intensity is uniform over multiple wing and post regions. Since threading dislocations are known to be non-radiative recombination centers in GaN [2], the uniform electroluminescence pattern suggests that the wing and coalescence regions have comparable dislocation densities. This is consistent with the cross-sectional TEM images shown in Section 3.1 which show that dislocations can be effectively turned over the post region yielding large areas of low dislocation density material.

Other features in the EL image appear like dark rectangles lying along the stripe direction. Investigation using several microscopies shows that these “dark-block defects” form cantilever material with tilt along the stripe direction [4]. The coalescence with the adjacent cantilever is then defected, with a crack along their intersection and lateral dislocations bowing outward from the crack. The dislocations are again non-radiative centers and reduce the light output. Recent work has shown that these can be eliminated by reducing the causes of tilting and improving the coalescence [5], as discussed in Section 3.1. With this improvement in lateral uniformity, we expect that wafer scale dislocation reduction will be possible using cantilever epitaxy, thus making this a valuable growth technique for nitride LEDs.

For comparison, identical LED structures were also grown on planar sapphire wafers where the same processing steps were used to fabricate the LEDs. The LEDs were grown in the same time frame of the MOCVD reactor only several runs apart in order to minimize variations in the LED epitaxial material. Both planar LEDs and CE-LEDs were diced into small die, mounted on TO-headers, and wire bonded such that the unencapsulated LEDs could be placed in an integrating sphere for maximum light collection. The EL image (not shown) of the LED grown on planar material showed a uniform luminescence pattern with only small fluctuations in intensity with a 1 – 2 micron length scale which is presumably due to In alloy fluctuations. A comparison of the LED intensity from a CE-LED

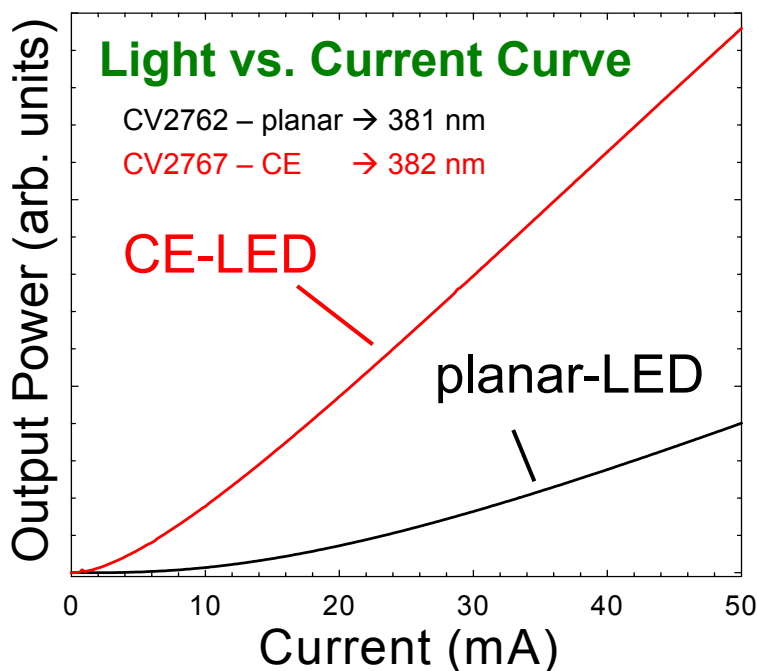


Figure A2. Light vs. current curve for an LED grown using cantilever epitaxy (CE) shown together with a curve for an identical LED grown on planar sapphire. The CE-LED shows a 3.7 times increase in output power at 50 mA (103 A/cm²).

and a planar LED is shown in Fig. A2. The CE-LED shows a 6.6 times improvement in output power at 20 mA (41 A/cm²) and a 3.7 times improvement at 50 mA (103 A/cm²). We have reduced the density of threading dislocations using CE and observe an improvement in both the light output and the linearity of our light vs. current curve. We believe that the nonlinearity of the light vs. current curve for the planar LED is due to the effect of non-radiative recombination centers. At lower current densities a larger fraction of carriers are efficiently captured by non-radiative recombination centers, while at higher carrier densities the non-radiative recombination channels begin to saturate and more carriers are able to recombine radiatively generating near UV photons. Thus, using CE we have fewer threading dislocations and hence fewer non-radiative centers and we observe an improved output power as well as improved linearity of the light vs. current curve. Although the improvement in output power will clearly depend on the quality of the starting planar material, an increase in output power of several times is typical when comparing planar and CE LEDs.

4.2.4 Summary

In summary, we have grown near UV InGaN multiple quantum well LEDs using CE with dislocation densities of $2 - 3 \times 10^7$ VTDs/cm² and compared them to LEDs grown on planar sapphire substrates. Electroluminescence images of LEDs grown using CE can show uniform patterns of luminescence intensity over regions as large as 200 μm^2 . CE-LEDs emitting at 382 nm showed a 3.7 times improvement in output power for room temperature operation at 50 mA (103 A/cm²). With improvements in lateral uniformity, we expect that wafer scale dislocation reduction will be possible using cantilever epitaxy making this a promising technique for improving the efficiency nitride-based LEDs.

4.2.5 References

[1] D.D. Koleske, A.J. Fischer, A.A. Allerman, C.C. Mitchell, S.R. Kurtz, J.J. Figiel, K.W. Fullmer and W.G. Brieland, Appl. Phys. Lett. 81, 1940 (2002).

[2] D. Cherns, et al., Appl. Phys. Lett. 78, 2691 (2001).

[3] C.I.H. Ashby, C.C. Willan, J. Han, N.A. Missert, P.P. Provencio, D.M. Follstaedt, G.M. Peake, and L. Griego, Appl. Phys. Lett. 77, 3233 (2000).

[4] P.P. Provencio, D.M. Follstaedt, N.A. Missert, D.D. Koleske, C.C. Mitchell, A.A. Allerman and C.I.H. Ashby, Mat. Res. Soc. Symp. Proc. 743, paper L3.15, p.115 (2003).

[5] C.C. Mitchell, D.D. Koleske, A.A. Allerman and N.A. Missert, private communication, 2003.

4.3 Flip Chip Device Packaging (KHA Bogart, AJ Fischer)

Top-emitting LEDs suffer from reduced light extraction due to blockage and absorption of the light by opaque metal contacts and bond pads located on the top surface of the p-type/active region mesa. By inverting the emission geometry to a bottom emitter, light extraction through the transparent sapphire substrate can be enhanced by 1.6X (J. J. Wierer, et al, Apl. Phys. Lett. 78 3379 (2001). Use of highly reflective metals or an optical reflector (e.g. a distributed Bragg reflector) on the LED surfaces can enhance light extraction in the inverted flip chip

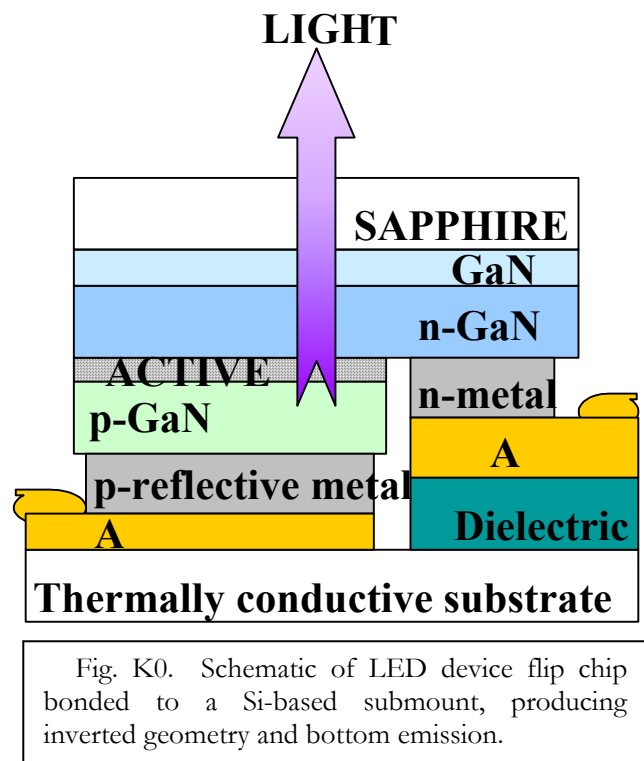
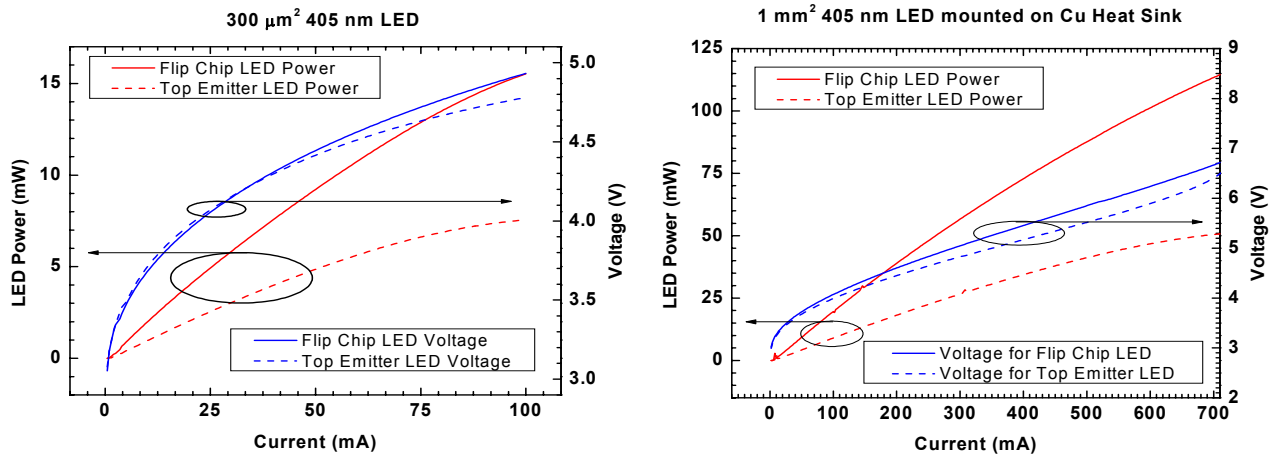


Fig. K0. Schematic of LED device flip chip bonded to a Si-based submount, producing inverted geometry and bottom emission.



Left (Fig. K1): Plot of LED output power and operating voltage as a function of drive current comparing performance of a top-emitting and flip chip bonded 405 nm 300 μm^2 LEDs. Right (Fig. K2): Plot of LED output power and operating voltage as a function of drive current comparing performance of a top-emitting and flip chip bonded 405 nm 1mm² LEDs.

geometry by reflecting light through the transparent sapphire substrate (Fig. K0). A metal contact that covers the entire p-type mesa also increases current spreading allowing operation at higher current densities. By physically bonding the inverted LED to a flip chip submount with a high thermal conductivity (Fig. K0), improvements in thermal conduction away from the LED are possible, decreasing LED operating temperatures. In this geometry, placement of wirebonds off the LED structure is facilitated, reducing blockage of LED emission.

The goals of the flip chip project were to increase light extraction efficiency and improve device performance through decreased operating voltages, increased thermal management, and increase optical output power. As part of the objectives of this Grand Challenge LDRD, we demonstrated light emission from 380-460 nm LEDs devices of various die sizes fabricated here at Sandia. We flip chip bonded these LEDs with reflective contacts using both Si- and SiC-based submounts. We performed L-I-V measurements on flip chip bonded LEDs, with comparisons to standard top-emitting LEDs, in order to compare operating voltage, output power, and thermal performance.

Our standard flip chip submounts were Si wafers with patterned Si₃N₄ and metallized with gold (Fig. K0). The Si₃N₄ performs a dual role of dielectric between p- and n-type contacts and GaN and matching the mesa height when the LED is inverted. The LEDs have Au as the upper-most metal in both the p- and n-type metal contacts. We used a Research Devices M8 Flip Chip Aligner-Bonder with microprocessor-controlled visible optics, dual sensors for die and submount, video overlay of process images, and positional and planarity alignments. We performed a thermal-compression bond, with gold as the bonding metal of choice. Issues we had to overcome successfully flip chip bond LEDs included modification of the vacuum port sizes to accommodate small (~1mm²) device die, optimize submount-device geometries for wirebonding, poor adhesion of metal pads used for wirebonding, loss of LED die during dicing, and initially, low device yields for flip chip bonded LEDs. Another related issue was designing a submount and header package that would increase thermal conduction away from the device during operation of a flip chip bonded LED. Solutions to these issues included custom-made flip chip bonder chuck pedestals to reduce vacuum port size. A new mask design incorporated increased bond pad length for wirebonding. Use of Ti metal and/or ion milling increased metal adhesion on the submounts. Diaphragm-vacuum bonding of LED to Si substrates was incorporated into the process to reduce die loss during dicing.

We performed design of experiments (DOE) studies of bonding parameters to optimize flip chip bonding. The optimal bonding parameters deduced were 9000 g of pressure, 300°C bonding temperature, and 15 minutes

of bonding time. With the optimized flip chip bonding parameters we obtained significant increases in our yields for successfully bonded devices. For example, we obtained commercial wafers with LED structures designed to emit at 405 nm. We fabricated the LED devices here at Sandia. We then flip chip bonded these devices to the Si-based submounts. We defined good flip chip bonded LED performance as achieving good optical power for this commercial LED with little to no increase in operating voltage (<0.5 V) after flip chip bonding. In this case, the bond yield was 88.6% with low operating voltages (4.09 ± 0.26 V). We were able to extend this technology to deep UV LEDs, in which the high % Al AlGaIn LED structure (295 nm) were grown and LED devices were fabricated here at Sandia. For example, one study looked at 14 LED die and our process gave a 77.1% yield with a small increase in operating voltage.

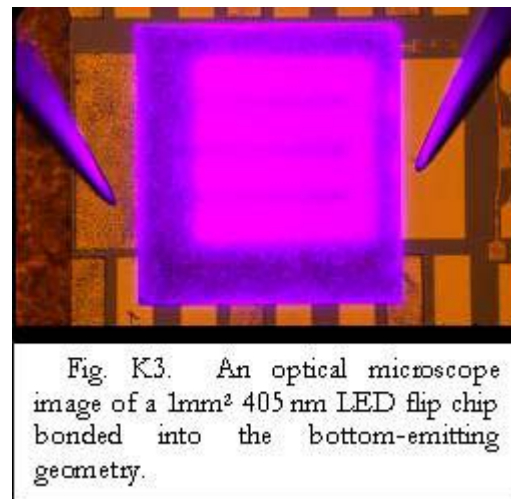


Fig. K3. An optical microscope image of a 1mm^2 405 nm LED flip chip bonded into the bottom-emitting geometry.

We investigated reflective p-type contacts to 380-450 nm LEDs with a combined goal of low operating voltages (low contact resistance) and good reflection in this wavelength range in order to increase light extraction through reduced optical absorption. Metals with good Ohmic contact behavior to p-type GaN include Ni, Pt, Pd, Ag, and Au. For n-type GaN, good Ohmic contact metals include Ti and Al. Al has the highest reflectivity (R) between 380 and 460 nm ($>90\%$), but is a poor p-contact metal. Ag has the next highest R over 380-460 nm (0.80-0.88%), but has very poor adhesion to GaN-based materials. We used a thin film (25Å) of Pd (R = 60-65%) as an adhesion layer with several metal stacks. The four contact designs included 100Å Pd/2000Å Au (control 1), 25Å Pd/2000Å Ag/3000Å Au, 25Å Pd/2000Å Al/3000 Å Au, and semi-transparent NiO-Au with Au p-pad (control 2) contacts. As expected, the NiO-Au gave the lowest operating voltages (4.1 ± 0.1 V). We determined that the Pd/Ag/Au and Pd/Au contacts gave the next lowest operating voltages (4.3 ± 0.08 V), followed by the Pd/Al/Au contact (5.6 ± 0.2 V, 30% higher) for LEDs operating at 20 mA. The data shown in Table K1 are for several voltage measurements made (average and standard deviation) on several devices on each wafer.

Metal Stack	Pd/Al/Au	Pd/Ag/Au	Pd/Au	transp-NiO/Au
Voltage (V) @20 mA	5.57 ± 0.017	4.29 ± 0.07	4.28 ± 0.078	4.05 ± 0.11

Table K1. Comparison of operating voltages for several p-type metal contacts on commercial 405 nm LEDs operating at 20 mA.

To determine if we had achieved increased light extraction with our flip chip bonding, we compared top-emitter and flip-chip geometry LEDs at 405 nm, mounted on a TO header and measured in an integrating sphere. The LED design for these devices used interdigitated contacts to enhance current spreading. The p-contact metal used here was Pd/Au. At 100 mA drive current, the top-emitting LED had an output power of 7.9 mW at 4.78 V. The flip-chip bonded LEDs had an average output power of 15.4 ± 0.12 mW at 4.90 ± 0.04 V. We found that light power for the flip chip LED increased by 2.1X (105%) at 100 mA, with a slight (~ 0.2 V) increase in operating voltage (Fig. K1). We observed no thermal roll-over at the higher drive currents, indicating that the flip chip submount made a reasonably good heat sink.

Similar data for other drive currents are given below in Table K2.

Current (mA)	Power (mW) Top Emit	Voltage (V) Top Emit	Power (mW) Flip Chip	Voltage (V) Flip Chip
20	2.18 ± 0.11	3.99 ± 0.06	3.95 ± 0.04	3.96 ± 0.02
50	5.05 ± 0.24	4.39 ± 0.08	9.11 ± 0.07	4.42 ± 0.02
100	7.86 ± 0.31	4.78 ± 0.12	15.4 ± 0.12	4.90 ± 0.04

Table K2. Comparison of output powers and operating voltages for top-emitting and flip-chip bonded 405 nm LEDs.

We also investigated the performance of large LED die structures. In Fig. K2, top-emitting and flip-chip bonded 1mm² 405 nm LEDs are compared. In this case, the LEDs were mounted onto a Cu block heat sink to further reduce thermal degradation during operation. The light output was also measured in an integrating sphere. At 700 mA drive current, the top-emitting LED had an output power of 50.5 mW at 6.41 V. The flip-chip bonded LED had an output power of 113 mW at 6.67 V. This is a 2.2X (124%) increase in extracted light power with an acceptable increase (0.33 V) in operating voltage. We also observed no thermal rollover despite the high drive currents, indicating that the flip chip bonded LED/ Cu block package reduced thermal degradation at higher drive currents. An optical image of this LED is shown below in Fig. K3.

We also investigated use of highly reflective metals for bonding contacts on the flip chip submount. In this case we used a 460 nm commercial LED fabricated here at Sandia. The p-metal contacts were transparent NiO-Au with a Au p-pad flip chip bonded onto a Si-based submount using Ag metal for the thermal compression bond. We measured a significant increase in light output power for the flip chip bonded LED, ~2X over the top-emitting LED.

Similar light extraction enhancement was measured for 390 nm LEDs grown and fabricated here at Sandia. The LEDs used the NiO-Au transparent contact and Au p-pad. The flip chip submount used the Ag metal as a highly reflective bonding metal. The top-emitter had 2.8 mW output power and the flip chip bonded LED had 5.6 mW output power for a 100 mA drive current, resulting in a 2.0X increase in light extraction. A photograph of the flip chip bonded LED on a TO header is shown in Fig. K5. The LED emission scatters well from the unpolished sapphire epitaxial substrate, causing the whole LED die to light up in the photograph.



We also fabricated SiC-based submounts in order to exploit the superior thermal conductivity of SiC over Si. Our initial experiments did not show a significant improvement in thermal rollover at higher operating currents between the two submounts. These data suggested that other components of the overall LED package, such as the epoxy used to glue the flip chip submount to the TO header or the TO header itself, may be limiting effective heat sinking during operation.

In summary, we demonstrated increased light emission from flip chip bonded LEDs with reflective contacts. We optimized flip chip bonding parameters obtaining yields of 77-86% for flip chip bonded LED die with good device performance. We also showed a >2X increase in light output power through improve light extraction for flip chip bonded LEDs over conventional top-emitting geometries for square devices with dimensions ranging from 300 μm to 1000 μm.

5 TASK 5: PHOSPHORS AND ENCAPSULANTS

5.1 Conventional Phosphors (DR Tallant, RL Simpson)

Phosphors are used as color converters, to achieve “white” output and the desired color rendering, in some types of solid state lighting (SSL) devices. These devices utilize blue light-emitting diodes (LEDs) with a single yellow-emitting phosphor or with a combination of green- and red-emitting phosphors. An alternative design is to use a near-ultraviolet (UV)-emitting LED with a combination of blue-, green- and red-emitting phosphors. Most devices thus far fabricated have used conventionally synthesized phosphors, which have crystalline sizes in the multi-micrometer range. These phosphors are prepared by fusing mixed reagents and milling and annealing the fusion product. However, conventionally synthesized phosphors have a number of shortcomings. In order to achieve a high quantum efficiency (photons emitted divided by photons absorbed), the concentration, in the phosphor matrix, of the chemical species that converts and emits absorbed LED photons (the activator) is restricted to relatively low values. At activator concentrations above the optimum, interactions between activators in excited states compete in the energy conversion mechanisms and degrade the phosphor’s quantum efficiency [1]. At the (low) activator concentrations that provide optimum quantum efficiency, phosphors suitable for SSL devices absorb near-UV and blue wavelengths inefficiently. Consequently, it is necessary to use relatively thick coatings of phosphors over the LEDs in SSL devices. Thick phosphor coatings are more difficult to fabricate and degrade the emission of the SSL device by reflective scattering.

In this portion of the SSL Grand Challenge, we sought to improve the efficiency of color conversion in SSL devices using conventional phosphors. We surveyed phosphor materials to identify alternatives to commonly used phosphors. We sought to enhance activator concentrations while maintaining high quantum efficiencies. And we sought to synthesize phosphors with conventional formulations but with reduced scattering. In conjunction with these efforts we developed a relatively simple method of measuring the quantum efficiencies of phosphors in powder form. A parallel effort, reported in a separate chapter, investigated phosphors based on quantum dot technology.

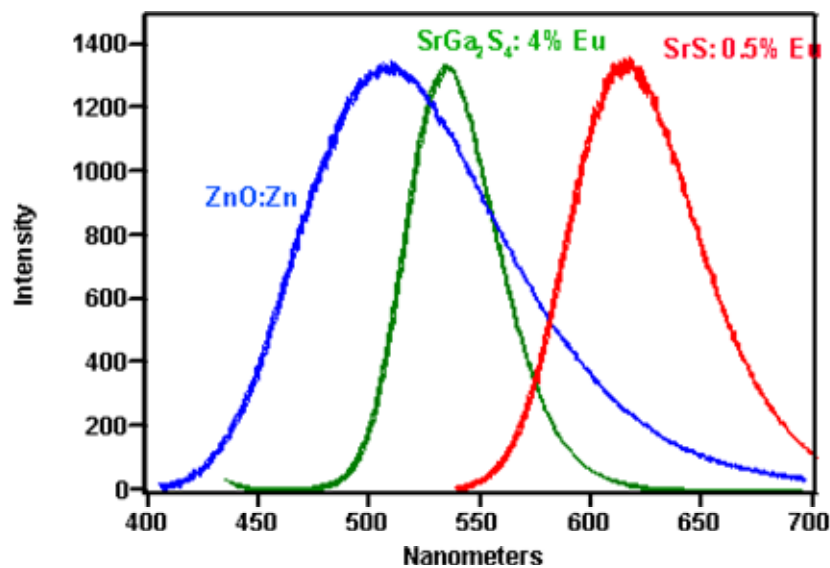


Figure 1. PL spectra of ZnO and strontium thiogallate and strontium sulfide phosphors

We collaborated with LumiLeds Lighting in this effort. They provided a number of phosphors, synthesized by a third party, that served as state-of-the-art standards. We refer to these as the “LumiLeds phosphors.” In addition, we contracted with Superior MicroPowders (SMP, since acquired by Cabot Corporation) to synthesize phosphors by a novel technique.

5.1.1 Survey of Phosphors

This survey was not meant to be exhaustive, but we surveyed a fairly extensive set of phosphor formulations collected as part of previous research projects in display technology. These phosphors had not been examined for their ability to

be excited by near UV to blue excitation. LumiLeds SSL devices use phosphors excitable by blue-emitting LEDs. They seek to capitalize on their rapidly developing blue LED technology and the relatively low nonradiative energy losses associated with a Stokes shift from blue excitation to green and red emission. We sought to identify not only other blue-excited phosphors but also near-UV-excited phosphors with high enough emission efficiency to compensate for increased nonradiative energy losses due to the greater Stokes shift between near UV (LED) excitation and visible emission.

Figure 1 shows photoluminescence (PL) spectra from three phosphors already in use in SSL devices. The intensities of the spectra have been normalized. The blue-green emitting zinc oxide, whose PL can be excited by near UV photons, is used in small (green) displays in, e.g., the automotive industry. The green-emitting thiogallate (SrGa₂S₄:4%Eu) and the red-emitting strontium sulfide (SrS:0.5 Eu) are used, with blue LED excitation, in LumiLeds SSL devices.

(Excitation: Violet - 380 nm Blue - 450 nm)
LumiLEDs Thiogallate @ 450 nm = 1.00

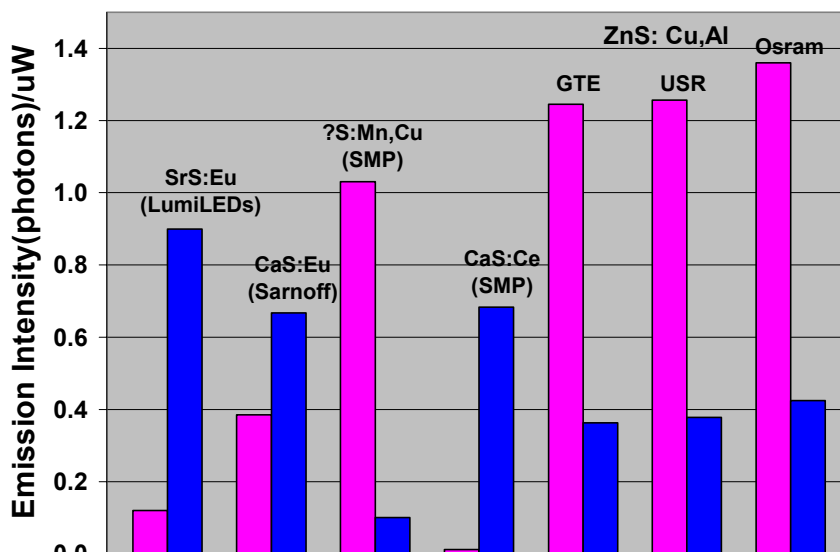


Figure 2. Integrated PL intensities from surveyed phosphors with blue and near UV excitation

Figure 2 shows integrated PL intensities from the most promising of the phosphors surveyed, some suitable for blue excitation and some suitable for near UV excitation.

The phosphors are from various manufacturers, as labeled in the figure. We have normalized the intensities relative to that obtained from the strontium thiogallate:europium phosphor powder provided by LumiLeds, as excited with 450 nm radiation. The phosphor labeled “?S:Mn,Cu” was determined to be a zinc sulfide formulation. Sulfide phosphors dominate the subset of promising phosphors. The zinc sulfide based phosphors show good potential for use with near UV LEDs, Calcium sulfide based phosphors may be viable alternatives for use with blue excitation.

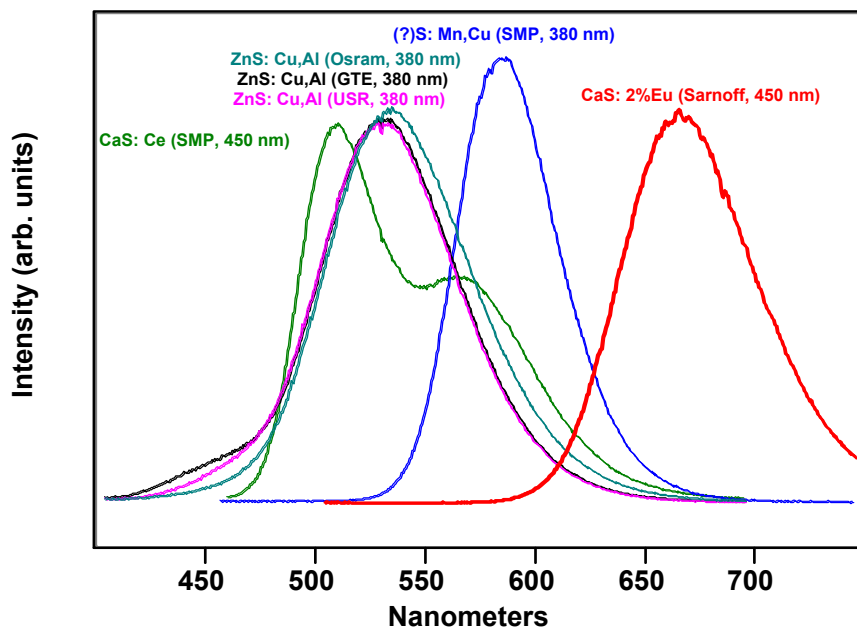


Figure 3. Normalized PL emission curves from surveyed phosphors with excitation wavelengths included in the labeling

(Excitation: Violet - 380 nm Blue - 450 nm)

LumiLEDs Thiogallate @ 450 nm = 1.00

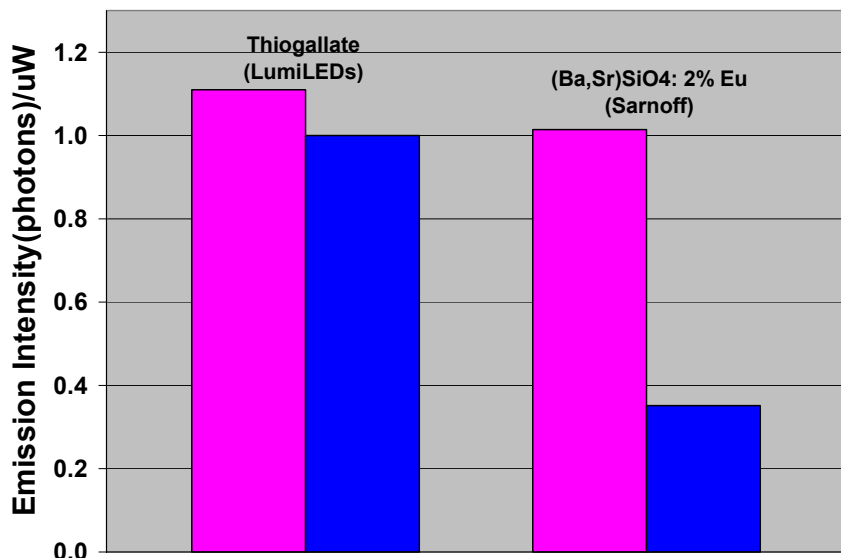


Figure 4. Integrated PL intensities for LumiLEDs thiogallate and a silicate-based phosphor

Figure 3 shows PL emission curves for the phosphors whose intensities are displayed in Figure 2. The PL from these phosphors ranges across much the visible region. Combinations of these and other phosphors may provide good white emission and good color rendering.

While sulfide based phosphors dominate the selection of those in use (LumiLEDs) and those showing potential (Figures 2-3) for use in SSL devices, the presence of sulfide has disadvantages. Oxygen-containing environments tend to oxidize sulfides, especially at elevated temperatures as occur in SSL devices. Oxidation degrades the PL properties of sulfide-based phosphors. Also, sulfur released from these phosphors tends to be corrosive, possibly attacking semiconductor materials used in

LEDs. For this reason oxide-based phosphors are potentially useful in SSL devices as more chemically robust and less a potential source of corrosive materials. We identified a phosphor based on an oxide of silicon that has potential for use in SSL devices incorporating near UV LEDs. Its integrated intensities are shown in Figure 4, and its PL profile is shown in Figure 5.

5.1.2 Reducing Excited Activator Interactions by Novel Synthesis Techniques

As noted above, activator concentrations in phosphors are generally limited to relatively low values because, at higher concentrations, with activators in close proximity, interactions between them degrade the phosphor's quantum efficiency. Conventional methods of phosphor synthesis begin with reagents, including the activator, in neat form. The reagents are mixed, fused, milled and annealed. Dispersion of the activator uniformly throughout the phosphor matrix may not occur, and any remaining aggregated activators are more likely to interact with each other. In contrast, a synthesis technique that

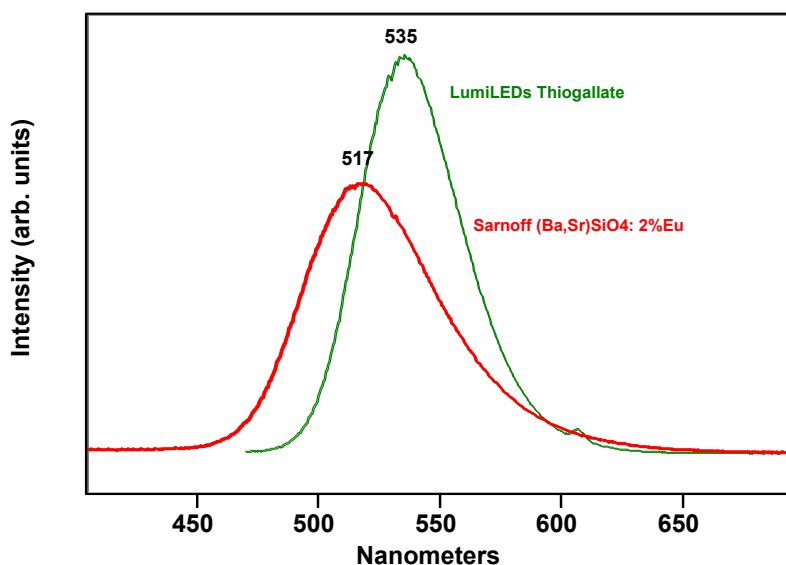
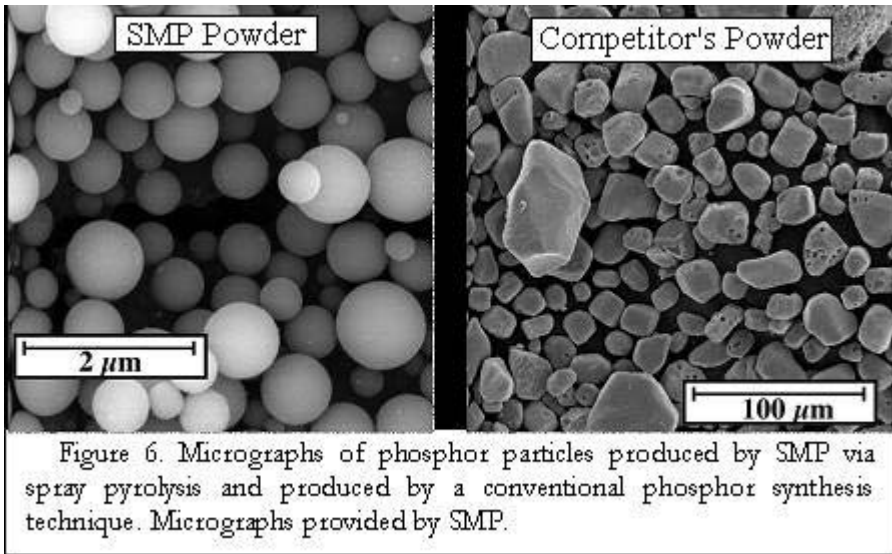


Figure 5. PL profiles for (Ba,Sr)SiO4: 2%Eu and LumiLEDs thiogallate with 380 nm excitation



begins with reagents initially dispersed at the atomic level should minimize activator aggregation in the final phosphor product. SMP specializes in spray pyrolysis, a synthesis technique that utilizes reagents dissolved and premixed in a solvent. The reagent solution is aspirated and flowed through a series of heated chambers that first, evaporate the solvent and pyrolyze any organic constituents, leaving microspheres of mixed phosphor precursors, and second, fuse the precursors into the final phosphor product.

Figure 6 shows micrographs of phosphor particles produced by spray pyrolysis (SMP) and conventional techniques. Synthesis by spray pyrolysis not only results in particles of uniform shape but also allows control of the particle size distribution, which can be used to optimize the phosphor packing efficiency.

Figure 7 shows integrated intensities, obtained with both near UV and blue excitation, of the green-emitting (Figure 1) thiogallate phosphor, using samples provided by LumiLeds (as part of this project) and by the Sarnoff Corporation and SMP (legacy materials from an earlier project). The LumiLeds and Sarnoff phosphors were synthesized by conventional techniques. The SMP phosphors were synthesized by spray pyrolysis. The LumiLeds thiogallate contains about 4 atomic % europium (Eu) activator and was optimized for blue excitation, whereas the phosphors from Sarnoff and SMP were not.

(Excitation: Violet - 380 nm Blue - 450 nm)

LumiLEDs Thiogallate @ 450 nm = 1.00

For the conventionally synthesized phosphors (LumiLeds and Sarnoff) the PL intensity is maximized at 4% activator and has decreased significantly at 8% activator (shown for the Sarnoff-supplied phosphor samples) as a result of increased interactions between activators. Because the quantum-efficiency-degrading interactions are between activators in excited states, the degradation is more pronounced with near UV excitation, because enhanced absorption efficiency in the near UV produces a higher concentration of excited

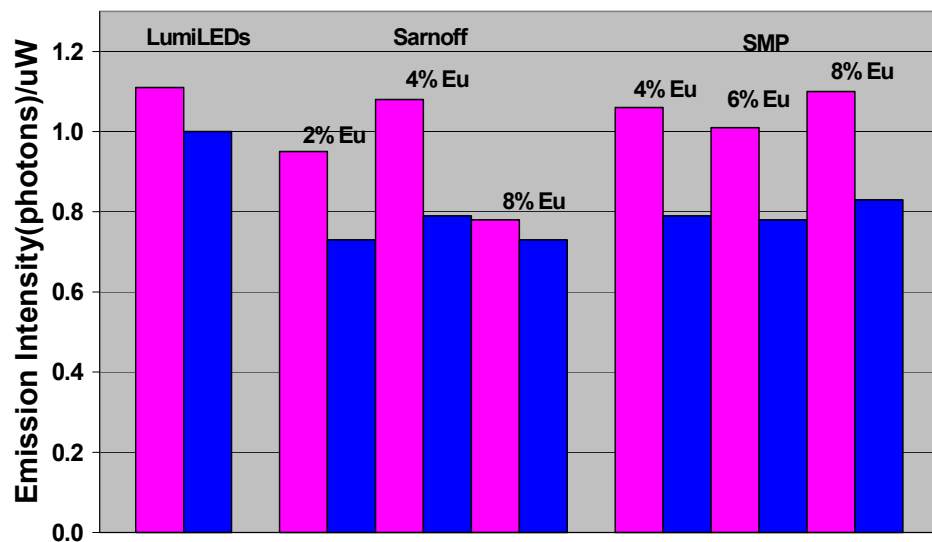


Figure 7. Integrated PL intensities for strontium thiogallate phosphors (SrGa₂S₄:Eu) synthesized by conventional methods (LumiLEDs, Sarnoff) and by spray pyrolysis (SMP). Concentrations are in atomic % Eu activator.

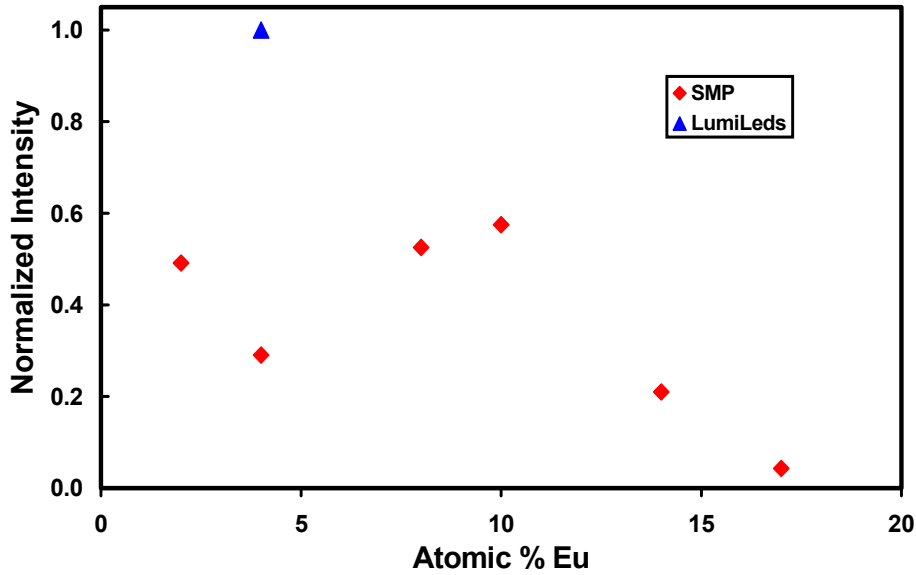


Figure 8. Integrated PL intensities of thiogallate:Eu phosphor samples with 380 nm excitation

spray pyrolysis to minimize activator aggregation, we contracted with SMP to synthesize thiogallate phosphors with activator concentrations up to 17 atomic %. As they proceeded to synthesize the phosphors, SMP found that, in their current facilities, sulfidation operations associated with phosphor synthesis tended to poison other operations. So, they produced Eu-doped phosphor microspheres, in oxide precursor form, by spray pyrolysis and sub-contracted with another firm to convert the gallium oxide precursors to thiogallates. Unfortunately, the sub-contracting meant that SMP lost control of critical phosphor optimization steps. We think that sulfidation may not have been complete. As a result, the batch of phosphors produced by SMP under this contract achieved about 60% of the PL emission efficiency attained in the SMP samples (Figure 7) synthesized during an earlier project. Also, the PL emission efficiencies for these phosphor samples tended to be less reproducible than earlier samples.

The integrated PL intensities for the thiogallate phosphors synthesized by spray pyrolysis for this project are shown in Figure 8 (380 nm excitation) and Figure 9 (450 nm excitation). Although their PL intensities are reduced compared to that of the LumiLeds thiogallate, the PL intensities of these phosphor samples do not exhibit the progressive decrease in PL intensity, associated with activator interactions until the Eu activator concentration exceeds 10 atomic %. For conventionally synthesized thiogallate:europium

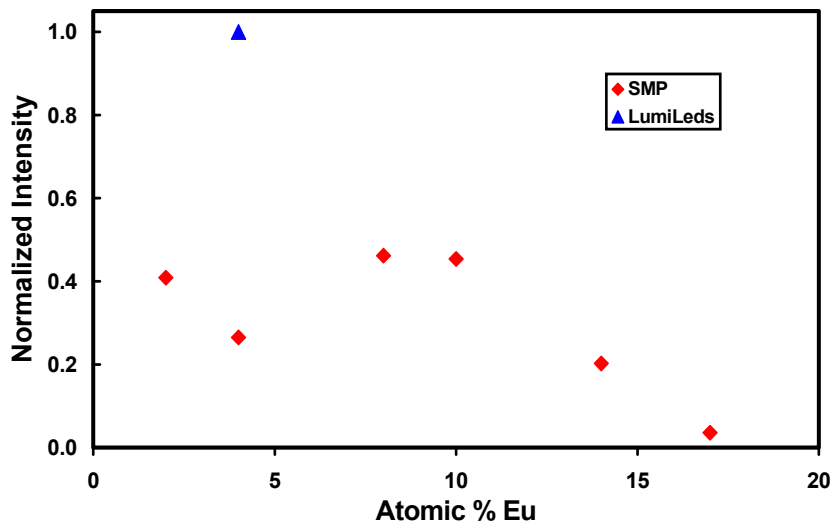


Figure 9. Integrated PL intensities of thiogallate:Eu phosphor samples with 450 nm excitation

states.

Two aspects of the performance of the spray-pyrolysis-synthesized SMP phosphors (Figure 7) are noteworthy. First, the spray pyrolysis technique produced phosphors about as efficient in PL intensity as the LumiLeds phosphor when excited by a near UV wavelength. Second, the PL intensity of the SMP phosphors is not degraded at 6% and 8% activator concentrations, indicating that the spray pyrolysis synthesis technique minimized aggregation of activators.

In order to further investigate the potential for

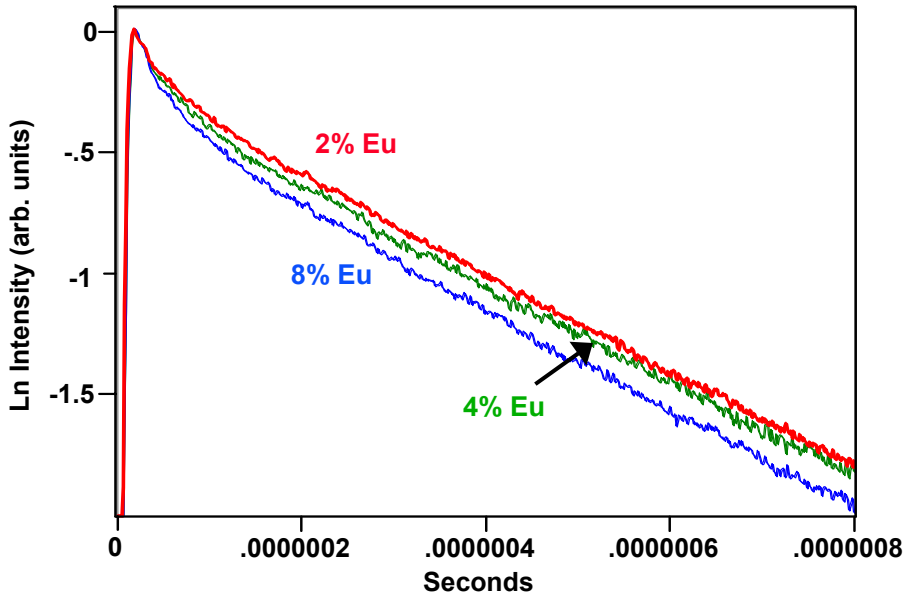


Figure 10. Persistence profiles, plotted logarithmically, of the Sarnoff thiogallates after excitation with pulsed, 232 nm excitation (initial intensities were normalized for comparison)

phosphors, the progressive decrease in PL intensity begins as the activator concentration exceeds about 4 atomic %. See Figure 7. This difference, we believe, is due to minimized activator aggregation in the spray-pyrolysis-synthesized phosphors.

Although these plots of PL intensities appear to show the effects of decreased activator interactions as a result of reduced activator aggregation, we were concerned that the PL intensity versus activator concentration plots merely reflect decreased overall phosphor emission efficiency. Another diagnostic of activator interactions is the persistence profile of a phosphor. PL persistence

refers to the progressive decrease with time of the PL intensity as the population of excited states of a phosphor is depleted by radiative and nonradiative events. In persistence experiments we excite the phosphor using a pulse of laser light and record the (decreasing) PL intensity as a function of time. The persistence profile of an excited, isolated activator is exponential with time and is linear in the logarithm of the intensity. Interactions (nonradiative) between activators both increase the rate of decrease of the intensity of the PL persistence and cause its logarithm to become nonlinear [1]. Thus, the persistence profiles (plotted logarithmically in Figure 10) of the thiogallate phosphors from Sarnoff (whose integrated intensities are plotted in Figure 7) show nonlinearity even at 2 atomic % activator, and the persistence intensity decreases more rapidly and becomes more nonlinear as the activator concentration increases. The overall decrease in the integrated PL intensity of the Sarnoff phosphors at 8 atomic % Eu activator (Figure 7) occurs because any increase in intensity related to increased activator concentration

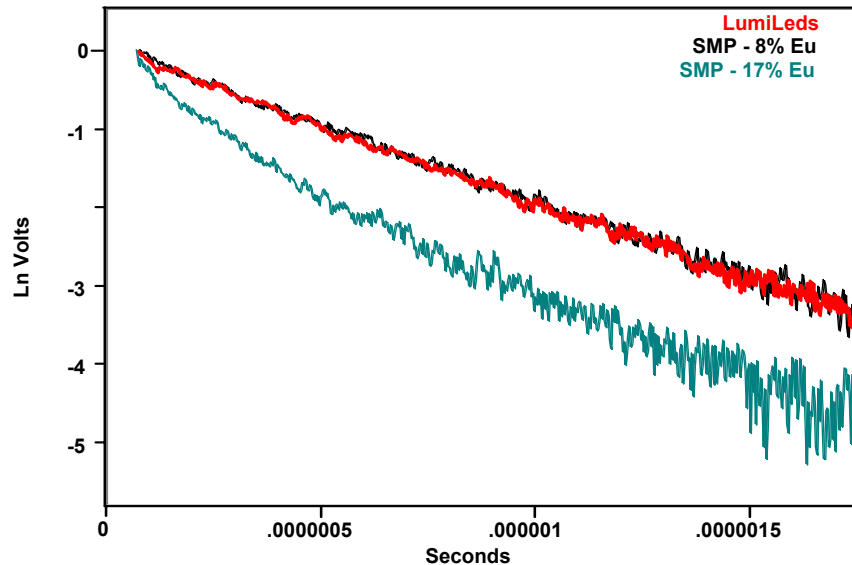


Figure 11. Persistence profiles, plotted logarithmically, of the SMP thiogallates after excitation with pulsed, 450 nm excitation (initial intensities were normalized for comparison)

is more than compensated by the effects of interactions between activators.

Persistence plots of selected spray-pyrolysis-synthesized SMP thiogallate phosphors are shown in Figure 11, along with that of the LumiLeds thiogallate (~4 atomic % Eu activator). The (logarithmic) persistence profiles of the (4% Eu) LumiLeds thiogallate is linear, and those of the SMP thiogallates (whose integrated intensities are plotted in Figures 8 and 9) are linear up to 8 atomic % Eu activator. The persistence of the SMP phosphor with 10 atomic % activator (not shown) is only slightly nonlinear, but the nonlinearity increases significantly for the persistence of the SMP phosphors with activator concentrations of 14 atomic % (not shown) and 17 atomic % (Figure 11). We have only the one (~4 atomic % Eu activator) LumiLeds phosphor, but we expect its persistence to follow the pattern of the Sarnoff phosphors (Figure 10), with increasing nonlinearity as the activator concentration increases above 4 atomic %.

The linearity of the persistence plot for the SMP phosphors up to at least 8 atomic % activator is further evidence that synthesis techniques like spray pyrolysis reduce the effects of activator interactions by minimizing their aggregation. We believe that synthesis techniques that minimize activator aggregation have the potential to produce phosphors with high quantum efficiencies at activator concentrations significantly enhanced over what are now commonly in use.

5.1.3 Enhancing SSL Device Emission Intensity by Reducing Phosphor Scattering

As noted in the introductory paragraphs, reflective scattering by phosphor particles significantly reduces the light output of SSL devices. One way to reduce this scatter is to reduce the size of the phosphor particles from multi-micrometer dimensions (Rayleigh scattering) to dimensions significantly less than the wavelengths of visible light (Mie scattering, occurring with particles less than 100 nanometers to a few hundred nanometers in dimension). We attempted to have SMP synthesize phosphor powders with multi-nanometer scale dimensions. We planned to do this with a blue-excited, oxide-based phosphor ($Y_3Al_5O_{12}$ with Ce^{3+} activator, a.k.a. YAG:Ce). However, SMP was acquired by Cabot Corporation before the contract was completed, and the phosphor aspect of SMP's operations was de-emphasized by their new managers. Nevertheless, we believe that synthesis of multi-nanometer-scale phosphor particles by spray pyrolysis is an approach that should be further investigated.

5.1.4 Development of a Technique for Measuring Quantum Efficiencies of Phosphor Powders

The measurement of quantum efficiency (photons emitted divided by photons absorbed) appears to be relatively simple but in fact has required extremely careful measurements using dedicated, specialized, and highly calibrated spectrometric instrumentation. Measuring the quantum efficiency of powders, whose spectroscopy involves a combination of absorption, emission and Rayleigh scattering, is especially challenging. We sought to develop a relatively straightforward technique

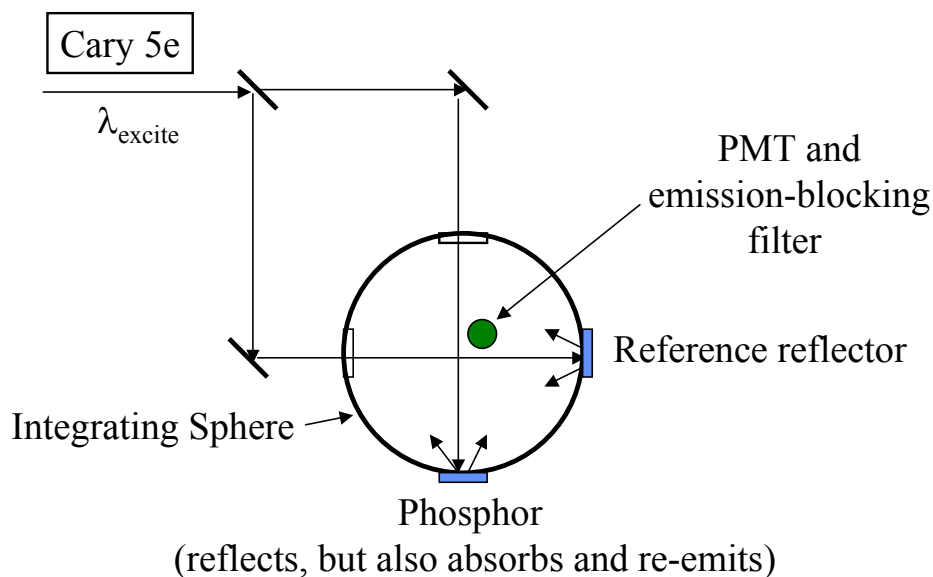


Figure 12. Diagram of apparatus for measuring the quantum efficiency of phosphor powders

for measuring quantum efficiencies using a commercially available spectrometer with minimal modification.

The approach we chose is to use a commercial UV-VIS-NIR spectrometer (Cary 5E) equipped with an integrating sphere (a sphere covered internally with a highly reflective coating). The phosphor is placed in a holder in an aluminum well with adjustable thickness and covered with a silica window. The depth of the well is adjusted so that the phosphor powder is “optically thick,” i.e. transmits only a negligible amount of incident light. The instrumental arrangement is shown in Figure 12.

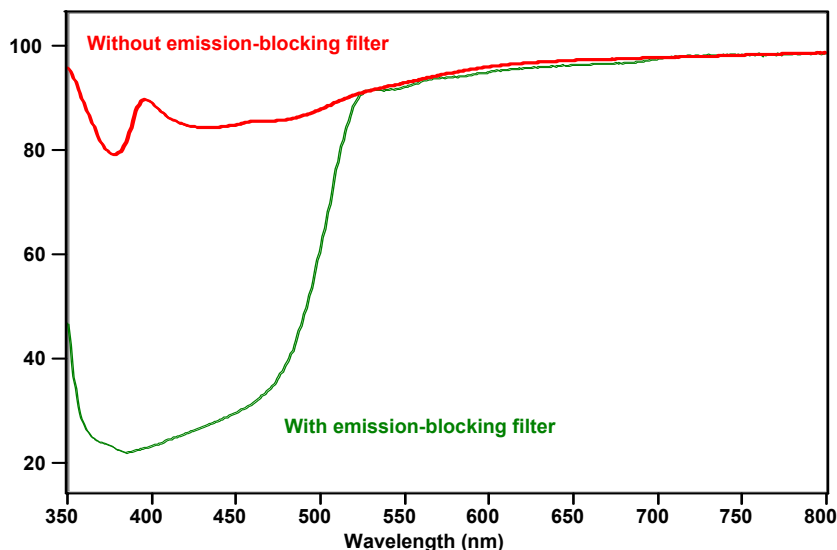


Figure 13. UV-Vis absorption spectra of the LumiLeds thiogallate:Eu phosphor both with and without the PL-blocking filter.

The phosphor powder in its holder is placed in one port of the integrating sphere and a reference reflector is placed in another port. A beam of monochromatic light is directed alternately to the phosphor and the reference reflector through two additional ports by the spectrometer. The wavelength of this light is scanned to produce a spectrum. A photomultiplier tube (PMT), mounted at yet another port, detects the light scattered throughout the integrating sphere. The advantage of the integrating sphere is that it provides collection of light emitted in all directions from the face of the phosphor, independent of its scattering characteristics. In the arrangement just described, the both the photons Rayleigh scattered by the phosphor (at the wavelength of the incident light) and those absorbed and re-emitted as PL are collected by the integrating sphere and detected by the PMT. If we place filter that blocks PL emission but not Rayleigh scattered incident light over the PMT, then only the Rayleigh scattered light will be transmitted to and detected by the PMT. Spectra of the LumiLeds thiogallate:Eu phosphor obtained both with and without the PL-blocking filter over the PMT are shown in Figure 13.

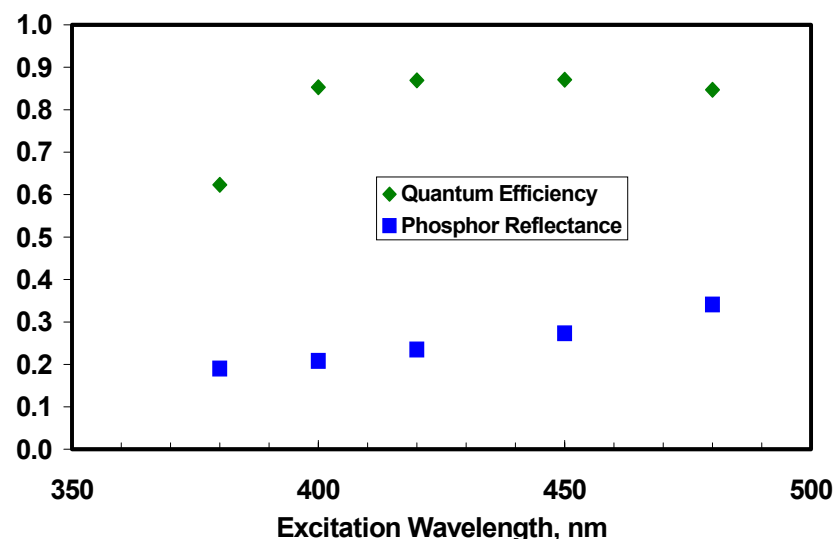


Figure 14. Quantum efficiencies and reflectances for the LumiLeds thiogallate:Eu phosphor calculated from the transmission curves in Figure 13.

With the PL-blocking filter in place, there is a dip in the reflectance (labeled as “%T”) curve (Figure 13) below 500 nm that is due to absorption by the Eu activator without compensation by photons re-emitted as PL. When the PL photons are allowed to reach the PMT, this dip in reflectance is largely

eliminated. Using these two curves, it is possible to calculate, at each wavelength for which there is a data point, both the quantum efficiency of the phosphor and its reflectance. The derivation of the equations for this calculation has been added to this chapter as an appendix. Results of this calculation for selected wavelengths are shown in Figure 14. The calculation could be automated so as provide quantum efficiencies and reflectances for each wavelength in the reflectance spectra.

LumiLeds personnel report that their thiogallate:Eu has a quantum efficiency of 0.90 to 0.95 at an excitation wavelength of 450 nm, which is consistent with the quantum efficiency shown in Figure 14. While the SSL Grand Challenge ended before we were able to test any other phosphor, we believe that this technique is applicable generally to near-UV- or blue-excited, visible-emitting phosphors.

5.1.5 References

1. D. R. Tallant, C. H. Seager and R. L. Simpson, J. Appl. Phys. 91(7), (2002), 4053-4064.

5.1.6 Appendix - Derivation of Equations Used in the Quantum Efficiency Measurement with Varian/Cary 5E UV-Vis-NIR Spectrometer/Lab Sphere Integrating Sphere (IS) and Short-Pass Filter

Introduction

Perform quantum efficiency (QE) determination on a phosphor powder using the Cary 5E spectrometer, integrating sphere (IS) and short-pass filter. The short-pass filter (or filters for different sets of phosphors) will be designed to pass the excitation wavelength (350 – 450 nm) and essentially completely absorb the phosphor’s photoluminescence. The filter will be placed over the (PMT) detector in the IS. We will calculate the QE at each excitation wavelength (the wavelength setting of the Cary) by comparing the Cary instrument response with and without the short-pass filter in place. In the Cary the excitation wavelength is alternately directed to the sample and the reference reflector positions in the IS, but the same PMT in the IS detects the response of both the sample and reference materials. We assume that the persistence of the sample decays quickly enough that negligible photoluminescence persists when the reference reflector is being irradiated.

Other Required Data

We will also need, to complete the calculation of the QE (λ = wavelength):

$I_{PN}(\lambda)$ = the photoluminescence intensity spectrum of the phosphor, corrected for the response of the instrument used to record it and normalized so that $\int_{\lambda} I_{PN}(\lambda) d\lambda = 1$ (effectively makes $I_{PN}(\lambda)$ unit less);

$CD(\lambda)$ = wavelength dependent response of the IS (collection efficiency)/PMT detector (responsivity) combination, measured in a “single beam” mode using known input powers (measured) of the Cary source at the IS and a reference reflector of known reflectance;

$T_F(\lambda)$ = transmittance spectrum of the short-pass filter, (measured in “single beam” mode) in place over the PMT detector (to assure that the filter effectively absorbs all the photoluminescence in the geometry of the IS); and

$R_R(\lambda)$ = reflectance spectrum of the reference reflector (Spectralon – available in the instrument manuals)

Other definitions

$R_P(\lambda)$ = reflectance of the phosphor powder sample at wavelength, λ

λ_{PL} = photoluminescence wavelength

λ_E = wavelength output by the Cary source (excitation wavelength)

$I_S(\lambda_E)$ = intensity of the Cary source at the IS (assumed to be the same at the sample and reference positions)

$I_P(\lambda_{PL}, \lambda_E)$ = photoluminescence intensity of the phosphor at λ_{PL} for a given excitation wavelength, λ_E

$S_P(\lambda_E)$ = signal from the IS/PMT when the Cary beam irradiates the phosphor

$S_R(\lambda_E)$ = signal from the IS/PMT when the Cary beam irradiates the reference reflector

$WF(\lambda_E)$ = Output signal of the Cary with the short-pass filter ($S_P(\lambda_E)/S_R(\lambda_E)$).

$WOF(\lambda_E)$ = Output signal of the Cary without the short-pass filter ($S_P(\lambda_E)/S_R(\lambda_E)$).

Definition of quantum efficiency

Assuming that the phosphor sample is optically thick (i.e., transmittance = 0 and reflectance + absorbance = 1, or absorbance = 1 - reflectance), the quantum efficiency (QE) of the phosphor at the excitation wavelength (λ_E) is

$$QE(\lambda_E) = \int_{\lambda} I_P(\lambda_{PL}, \lambda_E) \cdot d\lambda_{PL} / (I_S(\lambda_E) \cdot (1 - R_P(\lambda_E))) = \text{photons emitted/photons absorbed.} \quad (1)$$

At any excitation wavelength the photoluminescence intensity from the phosphor, $I_P(\lambda_{PL}, \lambda_E)$, is the phosphor's normalized photoluminescence intensity, $I_{PN}(\lambda_{PL})$, multiplied by a constant $K(\lambda_E)$, i.e.,

$$I_P(\lambda_{PL}, \lambda_E) = K(\lambda_E) \cdot I_{PN}(\lambda_{PL}); \quad (2)$$

($K(\lambda_E)$ takes the intensity units), assuming that $I_{PN}(\lambda_{PL})$ does not vary with excitation wavelength.

Therefore, substituting equation (2) into equation (1)

$$QE(\lambda_E) = \int_{\lambda} K(\lambda_E) \cdot I_{PN}(\lambda_{PL}) \cdot d\lambda_{PL} / (I_S(\lambda_E) \cdot (1 - R_P(\lambda_E))), \quad (3)$$

and, since $K(\lambda_E)$ is a constant for any λ_E , and since, by definition, $\int_{\lambda} I_{PN}(\lambda) d\lambda = 1$ (See "Other Required Data, p.1),

$$QE(\lambda_E) = K(\lambda_E) \cdot \int_{\lambda} I_{PN}(\lambda_{PL}) \cdot d\lambda_{PL} / (I_S(\lambda_E) \cdot (1 - R_P(\lambda_E))) = K(\lambda_E) / (I_S(\lambda_E) \cdot (1 - R_P(\lambda_E)))$$

and

$$K(\lambda_E) = QE(\lambda_E) \cdot I_S(\lambda_E) \cdot (1 - R_P(\lambda_E)). \quad (4)$$

Reflectance Spectrum without the Short-Pass Filter over the PMT

Measure the (double beam) output signal of the Cary with the phosphor powder in the sample position and the reference reflector in the reference position. Without the short-pass filter over the PMT, the phosphor's photoluminescence adds to its signal when the excitation beam irradiates it (here assuming negligible self-absorption).

$$S_P(\lambda_E) = I_S(\lambda_E) \cdot R_P(\lambda_E) \cdot CD(\lambda_E) + \int_{\lambda} I_P(\lambda_{PL}, \lambda_E) \cdot CD(\lambda_{PL}) \cdot d\lambda_{PL} \quad (5)$$

in which the first term is from the reflectance of the phosphor, and the second term is the integrated photoluminescence of the phosphor due to excitation at λ_E .

From (2),

$$S_P(\lambda_E) = I_S(\lambda_E) \cdot R_P(\lambda_E) \cdot CD(\lambda_E) + K(\lambda_E) \cdot \int_{\lambda} I_{PN}(\lambda_{PL}) \cdot CD(\lambda_{PL}) \cdot d\lambda_{PL} \quad (6)$$

and from (4),

$$S_P(\lambda_E) = I_S(\lambda_E) \cdot R_P(\lambda_E) \cdot CD(\lambda_E) + QE(\lambda_E) \cdot I_S(\lambda_E) \cdot (1 - R_P(\lambda_E)) \cdot \int_{\lambda} I_{PN}(\lambda_{PL}) \cdot CD(\lambda_{PL}) \cdot d\lambda_{PL} \quad (7)$$

$$S_R(\lambda_E) = I_S(\lambda_E) \cdot R_R(\lambda_E) \cdot CD(\lambda_E) \quad (8)$$

and, for the Cary signal without the short-pass filter over the PMT,

$$\begin{aligned}
WOF(\lambda_E) &= S_P(\lambda_E) / S_R(\lambda_E) = [I_S(\lambda_E) \cdot R_P(\lambda_E) \cdot CD(\lambda_E) + \\
&QE(\lambda_E) \cdot I_S(\lambda_E) \cdot (1 - R_P(\lambda_E)) \cdot \int_{\lambda} I_{PN}(\lambda_{PL}) \cdot CD(\lambda_{PL}) \cdot d\lambda_{PL}] / \\
&I_S(\lambda_E) \cdot R_R(\lambda_E) \cdot CD(\lambda_E)
\end{aligned}$$

and

$$\begin{aligned}
WOF(\lambda_E) &= R_P(\lambda_E) / R_R(\lambda_E) + \\
&[(QE(\lambda_E) \cdot (1 - R_P(\lambda_E))) / (R_R(\lambda_E) \cdot CD(\lambda_E))] \cdot \int_{\lambda} I_{PN}(\lambda_{PL}) \cdot CD(\lambda_{PL}) \cdot d\lambda_{PL}
\end{aligned}$$

Define a symbol for the integral over the phosphor luminescence

$$INTWOF = \int_{\lambda} I_{PN}(\lambda_{PL}) \cdot CD(\lambda_{PL}) \cdot d\lambda_{PL}$$

INTWOF can be calculated in GRAMS/AI display software and is constant for a given phosphor and instrument setup (instrument response function).

Then,

$$WOF(\lambda_E) = \frac{R_P(\lambda_E)}{R_R(\lambda_E)} + \frac{QE(\lambda_E) \cdot (1 - R_P(\lambda_E)) \cdot INTWOF}{R_R(\lambda_E) \cdot CD(\lambda_E)} \quad (9)$$

Reflectance Spectrum with the Short-Pass Filter over the PMT

Measure the (double beam) output signal of the Cary with the phosphor powder in the sample position, the reference reflector in the reference position and the short-pass filter over the PMT. The equation for the Cary output signal will be the same as for the case without the short pass filter, (7) and (8), except that the filter transmission, $TF(\lambda)$, appears in the terms of the expressions.

$$\begin{aligned}
S_P(\lambda_E) &= I_S(\lambda_E) \cdot R_P(\lambda_E) \cdot T_F(\lambda_E) \cdot CD(\lambda_E) + \\
&QE(\lambda_E) \cdot I_S(\lambda_E) \cdot (1 - R_P(\lambda_E)) \cdot \int_{\lambda} I_{PN}(\lambda_{PL}) \cdot T_F(\lambda_{PL}) \cdot CD(\lambda_{PL}) \cdot d\lambda_{PL}
\end{aligned}$$

and

$$S_R(\lambda_E) = I_S(\lambda_E) \cdot R_R(\lambda_E) \cdot T_F(\lambda_E) \cdot CD(\lambda_E)$$

Then,

$$\begin{aligned}
WF(\lambda_E) &= S_P(\lambda_E) / S_R(\lambda_E) = \\
&\left[\begin{aligned} &I_S(\lambda_E) \cdot R_P(\lambda_E) \cdot T_F(\lambda_E) \cdot CD(\lambda_E) + \\ &QE(\lambda_E) \cdot I_S(\lambda_E) \cdot (1 - R_P(\lambda_E)) \cdot \int_{\lambda} I_{PN}(\lambda_{PL}) \cdot T_F(\lambda_{PL}) \cdot CD(\lambda_{PL}) \cdot d\lambda_{PL} \end{aligned} \right] / \\
&I_S(\lambda_E) \cdot R_R(\lambda_E) \cdot T_F(\lambda_E) \cdot CD(\lambda_E)
\end{aligned}$$

and

$$\begin{aligned}
WF(\lambda_E) &= R_P(\lambda_E) / R_R(\lambda_E) + \\
&\{[QE(\lambda_E) \cdot (1 - R_P(\lambda_E))] / [R_R(\lambda_E) \cdot T_F(\lambda_E) \cdot CD(\lambda_E)]\} \cdot \int_{\lambda} I_{PN}(\lambda_{PL}) \cdot T_F(\lambda_{PL}) \cdot CD(\lambda_{PL}) \cdot d\lambda_{PL}
\end{aligned}$$

Define a symbol for the integral over the phosphor luminescence, as attenuated by the short-pass filter.

$$INTWF = \int_{\lambda} I_{PN}(\lambda_{PL}) \cdot T_F(\lambda_{PL}) \cdot CD(\lambda_{PL}) \cdot d\lambda_{PL}$$

INTWF can be calculated in GRAMS/AI display software and is a constant for a given phosphor, short-pass filter and instrument setup (instrument response function).

Then,

$$WF(\lambda_E) = \frac{R_P(\lambda_E)}{R_R(\lambda_E)} + \frac{QE(\lambda_E) \cdot (1 - R_P(\lambda_E)) \cdot INTWF}{R_R(\lambda_E) \cdot T_F(\lambda_E) \cdot CD(\lambda_E)} \quad (10)$$

Calculation of $QE(\lambda_E)$ and $R_P(\lambda_E)$

Equations (9) and (10) are two, independent equations in two unknowns - $QE(\lambda_E)$ and $R_P(\lambda_E)$. The other parameters in the two equations, $WF(\lambda_E)$, $WOF(\lambda_E)$, $INTWF$, $INTWOF$, $R_R(\lambda_E)$, $CD(\lambda_E)$ and $T_F(\lambda_E)$, are measured values, values from tables or values calculated from known or measured values. Simultaneous solution of (9) and (10), with constraints that $QE(\lambda_E) \leq 1$ and $R_P(\lambda_E) \leq 1$ yields the internal quantum efficiency and reflectance of the phosphor as a function of excitation wavelength.

5.2 Semiconductor-Nanocluster-Based Phosphors (JP Wilcoxon, LS Rohwer, BL Abrams, SG Thoma)

5.2.1 Motivation-

Creating a broadband (i.e. white) emission source based upon solid state LEDs may be achieved by appropriate mixing of red, green, and blue LEDs in a single device, but at a considerable fabrication cost. So the majority of white light emitting LEDs are based upon a blue LED which excites a single conventional phosphor which emits in the yellow region of the optical spectrum. However, the directional nature of the blue diode pump and the diffuse nature of the phosphor output produces a mixed light output which has a distinctly bluish hue in its center. Additionally, conventional phosphors consist of large particles which backscatter a significant portion of the exciting light into the absorbing LED substrate, reducing efficiency. A further difficulty which has been identified is that the most common, halophosphate based white light phosphors do not absorb light in the 380-420 nm regime available from NUV LEDs.

It has been suggested that phosphors based upon semiconductor nanoclusters might ameliorate many of the drawbacks associated with conventional phosphors. For example, scattering of the excitation light from nanosize particles is negligible, so full light extraction from a device of suitable geometry should be possible. Furthermore, the absorption edge of a semiconductor nanoparticle is determined not only by material type, but by physical dimension of the particle in the regime of strong quantum confinement. For many type of semiconductor nanocrystals, (e.g. CdS, CdSe, Si, Ge), this absorption onset can be selected to be ~380-420 nm, for ~2 nm particles providing strong absorption of the NUV excitation light.

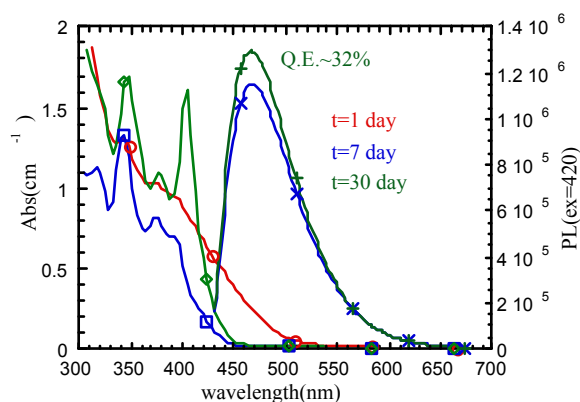


Figure 1. CdSe nanocrystals in pyridine with a size of ~1.9 nm undergo annealing at room T and develop multiple sharp absorbance features and strong blue luminescence.

5.2.2 Results and Discussion: Synthetic and Optical Studies of II-VI Semiconductor Nanocrystals

Historically, semiconductor quantum dots were produced by relatively high T (~300 °C) decomposition of expensive and toxic metal-organic precursors.[1] The highest luminescent quantum yields have been achieved with CdSe onto which other materials such as CdS or ZnS have been deposited. However, because of the large lattice mismatch and high radius of curvature of small nanoparticles, viewing such deposition as a core/shell material with a wider bandgap on the surface is incorrect. In fact, TEMs of such particles show irregular deposits or islands of ZnS on the seed particles.

It has been recognized that the expensive and dangerous nature of published organometallic II-VI nanocrystal synthesis probably prevents its widespread application in many technologies such as phosphors and photovoltaics.[2] The presence of non-volatile organics on the surface of nanocrystals has been demonstrated to degrade the electronic properties of solid state materials based upon quantum dots, so we developed new approaches to their synthesis[3]

We have demonstrated ambient T growth of semiconductor nanocrystals in volatile coordinating solvents like acetonitrile, pyridine, and tetrahydrofuran using simple salt precursors for both group II and group VI elements. If the growth of the nanocrystals can be made sufficiently slow, as occurs in inverse micelles, or if the crystals consist of only a few dozen formula units annealing of defects may occur at room T over a period of a few weeks. This produces nanocrystals with sharp absorbance features and strong luminescence as shown in figure 1.[4] Note that initially, (t=1 day), no PL can be observed from the material.. Dynamic light scattering measurements of apparent cluster size reveal this is partially due to incomplete dispersion of the clusters in the pyridine.

Figure 1 shows that nanocrystals develop good optical characteristics slowly at room T, however, mild elevations in temperature (T~60 °C) or use of sonication can accelerate the annealing process to 1-2 days. The state of dispersion of the nanocrystals can be measured with light scattering and correlates with the emergence of sharp absorbance features and strong blue PL. We used dynamic light scattering to measure the rate of diffusion and thus the hydrodynamic size of the cluster and discovered that association of the clusters is responsible for significant quenching of the PL at high cluster concentrations.

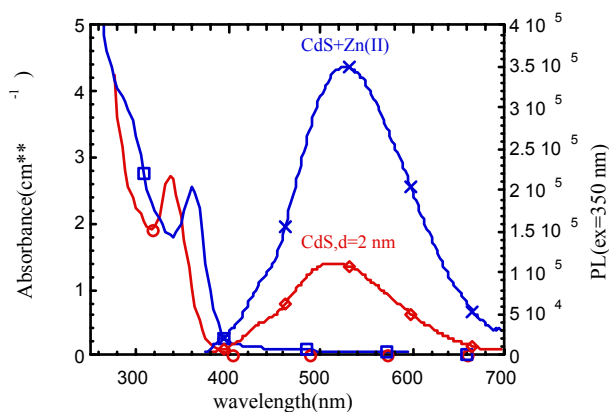


Figure 3. The absorbance and PL of a parent sample of D~2 nm CdS in octane stabilized by an anionic surfactant, AOT is compared to a daughter sample with Zn(II) deposited onto the surface.

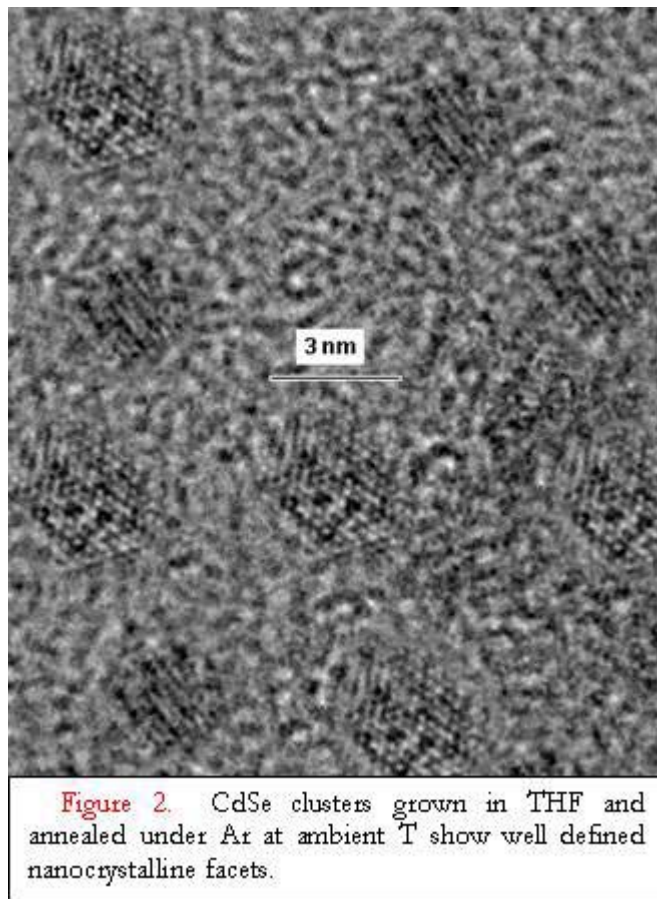


Figure 2. CdSe clusters grown in THF and annealed under Ar at ambient T show well defined nanocrystalline facets.

In this room T metathesis method the rate of growth of the nanocrystal is strongly influenced by the chemical nature of the coordinating solvent and the strength of the bond between the reactants. To help eliminate the cluster association problem noted above we have used better solvents such as pyridine or tetrahydrofuran to allow the use of higher concentrations of clusters required for complete light absorption of the excitation. A HRTEM of such clusters showing their nanocrystalline nature is shown in figure 2.

5.2.3 Results and Discussion: Interface Effects on the Optical Properties of Semiconductor Nanocrystals

The possibility of full color tuning by simple chemical changes at the interface of small dots has significant practical advantages in technical applications such as nanophosphors embedded in various solid matrices.^[5] As an example consider green emitting D~2 nm CdS dots synthesized with excess sulfur on their surfaces onto which we have desposited a 1:1 atomic ratio of zinc (surface) to cadmium (core). We observe shifts in both the first exciton position and large, 3-5x increases in emission.(see figure 3)

The strength of the photoluminescence (PL) increases ~3.5 times due to the presence of Zn(II) on the surface. The large energy shift between absorbance and PL indicates carrier recombination in these small clusters is nearly completely from interface states. In essence the quantum dot behaves like an organic dye molecule where small changes in the environment (solvent changes) has drastic effects on both

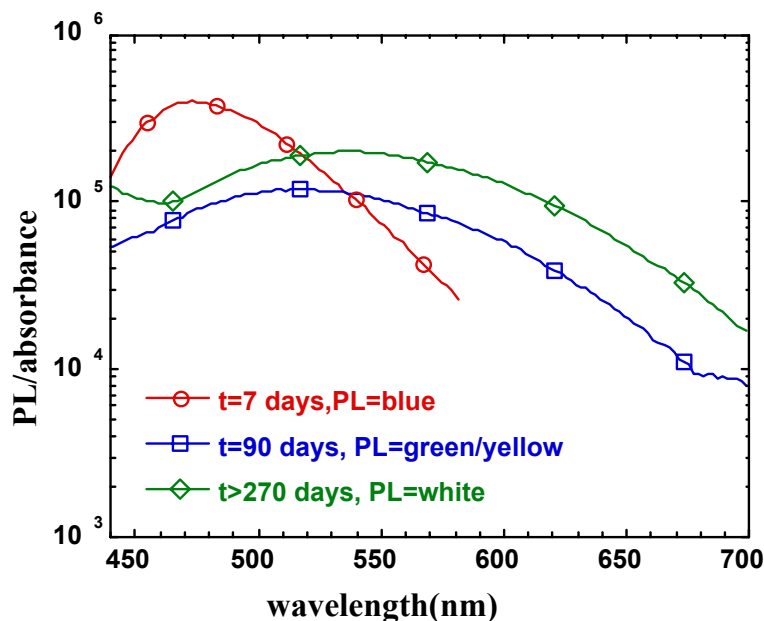


Figure 4. The photoluminescence (PL) normalized by the fraction of light absorbed at the excitation wavelength (370 nm) is shown as a function of sample age for a thiol passivated sample of 2 nm size CdS. The parent sample with blue PL is also shown.

color and emission intensity. Unlike larger dots, the separation between absorbance and emission simplifies their application as phosphors excited by a single GaN source since absorbance of the emitted energy of a dot of one color by another is negligible.

We investigated the effects of stoichiometry and interface systematically with a range of metal ions and organic ligands using nanocrystals sufficiently small (1-3 nm) that the light emission comes entirely from surface states. The competing non-radiative thermal relaxation can be very low due to the absence of internal defects which can easily diffuse the 1 or 2 lattice constants to the cluster surface at ambient temperature. Annealing in a coordinating solvent can be used to passivate the uncoordinated bonds at the surface.

Surface changes due to the addition of suitable organic surfactants to the cluster surface were also observed to favorably affect the PL intensity and width with age. For example, CdS nanocrystals 9 months to 3 years old are much more luminescent than when originally synthesized, provided they are stored in solvents containing suitable passivating agents like alkyl thiols or amines. An example

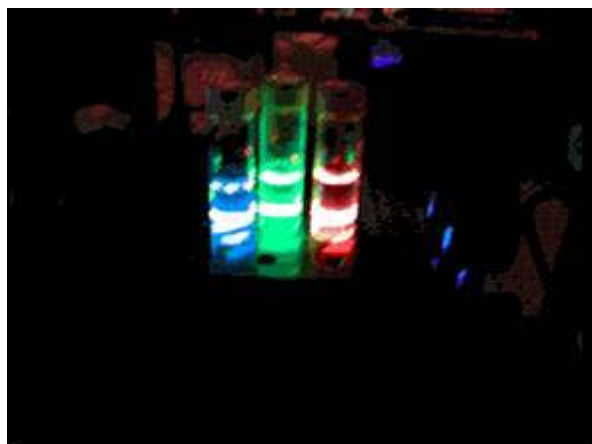


Figure 5. Three samples of D~2.5 nm CdS clusters whose surfaces have been chemically altered by addition of hole (Cd(II), blue color) or electron (S(II), orange/red color) traps are excited by a single source laser beam at $\lambda=365$ nm, and show emission in the blue, green, and red region. Note: the cluster size has not changed, only the surface is altered.

of the effect of such aging on the PL is shown in [figure 4](#), where a parent sample originally showing blue emission near 470 nm red shifts and broadens with age after addition of an alkyl thiol.

The change in electronic properties for a single size semiconductor cluster due to surface chemistry or morphology may be large. In our work we have discovered, for example, that D~2.5 nm CdS which, without surface modification emits in the yellow/green region, can be color tuned by addition of either electron traps like cationic (e.g. Cd(II)) or hole traps (S(II)). The overall ratio of II:VI atoms can be used to shift the output color, with very minor changes in the absorbance onset. As an example we have been able to observe blue, green, and orange/red output for a single CdS sample in an identical solvent as by adjusting the interface as shown in [figure 5](#).

When clusters are concentrated without agglomeration into a polymeric film, further changes of the spectral

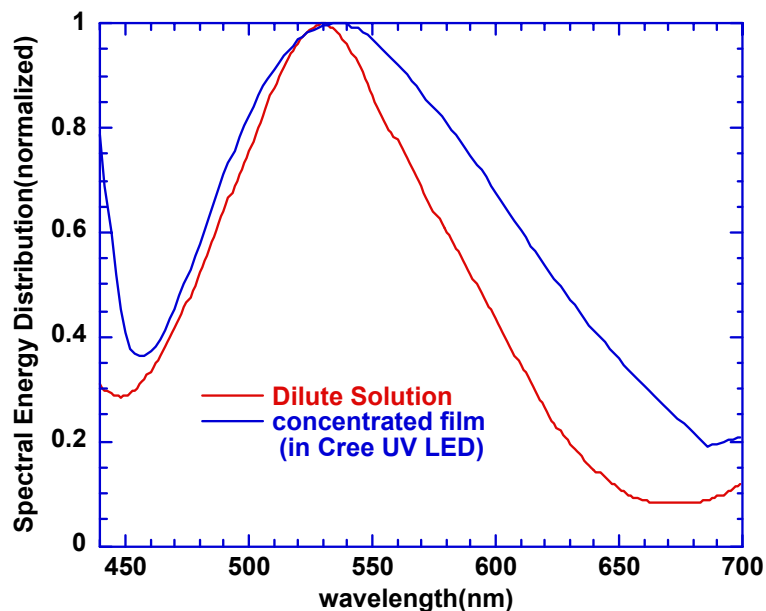


Figure 6. A broadly emitting dilute solution of CdS/alkyl thiol stabilized nanocrystals is allowed to dry into a concentrated film. The normalized spectral energy distribution is shown for both samples.

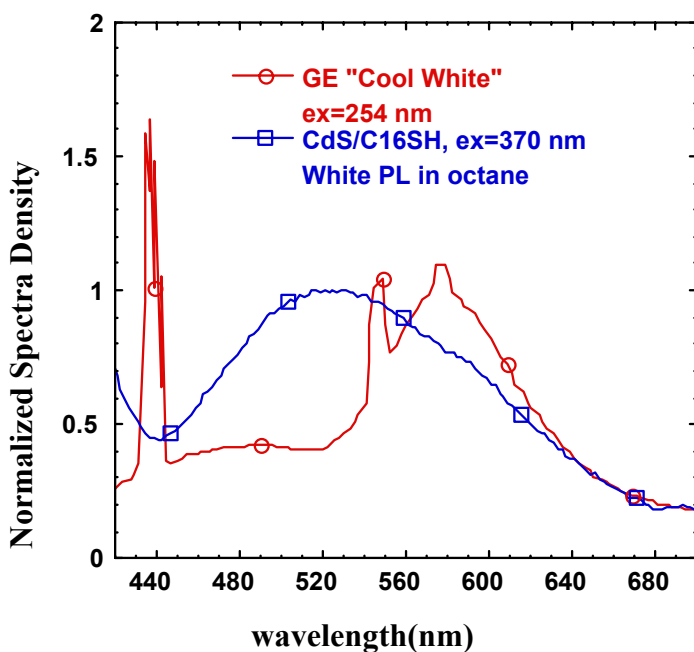


Figure 7. The spectral energy distribution of a GE cool white phosphor excited at 254 nm is compared to that of a dilute solution of CdS nanocrystals in octane excited at 370 nm.

energy distribution occur. For example, we observe a broadening and red shift of the peak emission energy as shown in [figure 6](#). This unexpected aging property was exploited to create broad, white emission from a single size nanocrystal.

The embedding medium used in the film formation process of [figure 6](#) was the same surfactant used to synthesize the nanoclusters in order to minimize cluster agglomeration and changes in the spectral energy distribution. We have noted in many cases, however, significant color shifts upon encapsulation of the nanoclusters in incompatible surfactants or polymers. These color changes are more obvious to the eye in the case of clusters with narrower emission energies (e.g. blue shifting to green).

How does the broad, emission from our embedded clusters excited by a commercial Cree LED compare to that of conventional white phosphors used in fluorescent lighting? [Figure 7](#) shows a normalized spectral energy distribution for both cases. Our nanophosphor produces larger amounts of

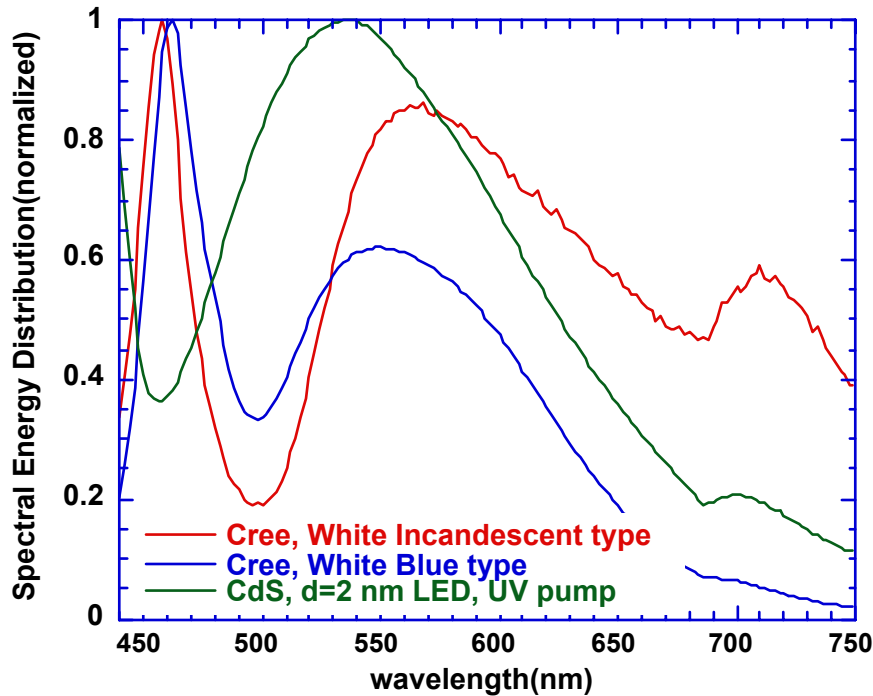


Figure 8. The spectral energy distribution of a commercial Cree™ white incandescent type and blue/white LED is compared to a nanocluster-based white emitting LED.

blue-green components than the GE halophosphor, whose peak emission energy lies to the red of our material. Note that this commercial phosphor cannot be used for NUV excitation since it has no absorption above ~300 nm.

Finally, in figure 8 we show the spectral energy distribution for two commercial white emitting LEDs whose excitation is provided by a blue emitting source at 460 nm. This is compared to a device made by us by deposition of a white emitting CdS/AOT film onto an invisible LED excitation source (excitation = 400 nm). The broadband visible emission from the commercial LEDs comes from the mixing of the directional blue excitation with the yellow diffuse emission from the phosphor used. In the case of the “incandescent” type LED considerably more deep

red energy is emitted. The nanocluster based device has a reduced bluish tint compared to either of the commercial, LEDs.

5.2.4 Conclusions

Using chemically induced changes in the interface structure of very small, $D < 2$ nm, clusters of CdS, we demonstrated the ability to independently control the absorption onset determined by the cluster size and the emission energy. The cluster absorption onset was adjusted to be around 420-440 nm, so that the clusters were transparent to the emitted PL. This allows large optical densities to be used to ensure complete absorbance of the excitation source.

It was discovered that chemical changes in the cluster surface led to a broad spectral energy distribution with sample age giving rise to white PL from a single size nanocluster. This simplifies the production of diffuse, white illuminating sources, eliminating the mixing of discrete colored phosphors. Our approach has similar characteristics to that employed in conventional lamp phosphors, but these new materials can be excited by NUV sources.

5.2.5 Future Directions

The effect of the cluster interface has been recognized in group IV nanoclusters like Si and Ge, where several groups, including ours, have reported H-passivated dots in the 1-2 nm range with luminescence in the blue (Si) or green (Ge) regions.[6,7] Si quantum dots with a diamond lattice core in the size range of 1-2 nm of Si passivated by an oxide luminesce in the red-yellow region.[8] Experimentally, Wolkin et al recently demonstrated that H-terminated nanocrystals which initially emitted in the blue around 3.0 eV, shifted their PL output to the red-yellow region near 2.0 eV when oxidized.[9] This difference in behavior has now been modeled in terms of

the influence of the interface.[10,11] For example, calculations indicate that shifts in the energy gap of ~ 1.1 nm in H-terminated Si clusters could occur due to deposition of heteroatoms such as F (1.8 eV) or S (3.4 eV).[11]

Though both pure Si and Ge nanoclusters have too low fluorescent yields to be viable candidates as nanophosphors, if the principles already demonstrated of resonant energy transfer from Si nanocrystals to rare earths like Tm(III) can be exploited, then new types of inexpensive, non-toxic nanophosphors like Si with Sb (blue/green) and/or Mn (orange) surface deposits would be very attractive for LED devices.[12] We intend to explore these issues experimentally with our very small H-terminated Si and Ge dots.

5.2.6 References

- [1] C.B. Murray, D.J. Norris, M.G. Bawendi, "Synthesis and Characterization of Nearly Monodisperse CdE (E=S,Se,Te) Semiconductor Nanocrystallites", *J. Am. Chem. Soc.*, **115**, 8706-8715, 1993.
- [2] Z. Peng and X. Peng., "Formation of High-Quality, CdTe, CdSe, and CdS Nanocrystals Using CdO as Precursor", *J. Amer. Chem.Soc.*, **123**, 183-184, 2001.
- [3] B.A. Ridley, B. Nivi, Joseph, M. Jacobson, "All-Inorganic Field Effect Transistors Fabricated by Printing", *Science*, **286**, 746, 1999.
- [4] J.P. Wilcoxon and P.P. Provencio, "Optical properties of II-VI semiconductor nanoclusters for use as phosphors", Proceedings of the SPIE on conference on "Optical Properties of Nanocrystals", Seattle, WA. July 7-11, 2002.
- [5] K.K. Nanda, F. Einar Krus, and H. Rissan, "Energy Levels in Embedded Semiconductor Nanoparticles and Nanowires", *Nano Lett.* **1(11)**, 605-611, 2001.
- [6] J.P. Wilcoxon, G.A. Samara, and P. Provencio, "Synthesis and Optical Properties of Colloidal Germanium Nanocrystals", *Phys. Rev. E*, **64**, 35417-1, 2001.
- [7] J.P. Wilcoxon, G.A. Samara, and P.N. Provencio, "Optical and Electronic Properties of Si Nanoclusters Synthesized in Inverse Micelles", *Phys. Rev B*, **60**, 2704, 1999.
- [8] K.A. Littau, P.J. Szajowski, A. J. Muller, A.R. Kortan, L.E. Brus, "A luminescent Silicon Nanocrystal Colloid via a High-Temperature Aerosol Reaction", *J. Phys. Chem.*, **97**, 1224, 1993.
- [9] M.V. Wolkin, J. Jorne, P.M. Fauchet, G. Allan, C. Delerue, *Phys. Rev. Lett.* **82**, 197, 1999.
- [10] Z. Zhou, L. Brus, R. Friesner, "Electronic Structure and Luminescence of 1.1- and 1.4 nm Silicon Nanocrystals: Oxide Shell versus Hydrogen Passivation", *Nano Letters*, in Press, 2003.
- [11] A Puzder, A.J. Williamson, J. C. Grossman, G. Galli, "Surface Chemistry of Silicon Nanoclusters", *Phys. Rev. Lett.*, **88**, 1-4, 2002.
- [12] K. Watanabe, H. Tamaoka, M. Fujii, and S. Hayashi, "Excitation of Tm³⁺ by resonant energy transfer from Si nanocrystals", *J. Appl. Phys.*, **92**, 4001, 2002.

5.3 Quantum-Dot Phosphors and Characterization (LS Rohwer, BL Abrams, JE Martin)

5.3.1 Introduction

The use of inorganic, solid state semiconductor light-emitting diodes (LEDs) to produce white light for illumination is known as solid state lighting (SSL). The wavelength conversion approach to SSL utilizes LEDs that emit near-UV or blue light in combination with phosphors that absorb the excitation light and convert it to visible light. Most phosphors for lighting (e.g., trivalent rare-earth doped oxides and halophosphates) were developed years ago for absorption of the rare-gas/mercury discharge lines (primarily at 254 and 365 nm) for application in fluorescent lamps. White emission from phosphors in fluorescent lamps is obtained by blending three distinct phosphor compositions emitting red, green, and blue light. White LEDs are made using a hybrid approach of blue LED plus yellow-emitting phosphor (e.g., YAG:Ce³⁺); blue LED plus a blend of green

(SrGa₂S₄:Eu²⁺) and red (SrS:Eu²⁺) phosphors [1]; or near-UV LED plus a blend of yellow (Sr₂P₂O₇:Eu²⁺,Mn²⁺) and blue-green (Sr₄Al₁₄O₂₅:Eu²⁺) phosphors [2]. For use in SSL, phosphors must have strong absorption in the near-UV to blue range, high quantum efficiency (>50%), and thermal stability. II-VI semiconductor nanocrystals, or quantum dots, (D~1-10 nm) are being investigated as alternatives to conventional, micron-sized phosphors for white light generation.

Quantum dots (QDs) have the advantage of emitting a range of visible photoluminescence as a result of their size and surface chemistry, strong absorption in the wavelength range of interest (380-460 nm), and low scattering. For use in SSL, QDs must be incorporated into encapsulating polymers without a loss of luminescence. Since QDs are mostly synthesized in solvent media, the transfer to polymeric media is often challenging as a result of changes in the chemical binding of the stabilizing organics on the QD surface, QD agglomeration, and chemical incompatibility between the QDs and the polymer. The concentration of QDs must be sufficiently high to eliminate leakage of the LED excitation light through the encapsulant. The Quantum Dots Task in the GCLDRD developed a unique Sandia strength that includes expertise spanning the synthesis, characterization, and encapsulation of QDs. A great deal of progress was made in understanding the issues relevant to the utilization of QDs in SSL. Key characterization accomplishments include the following:

- Developed a measurement system and mathematical procedure for determining the absolute quantum efficiency (QE) and quantum yield (QY) of QDs (in solvent and encapsulants) and other luminescent materials (laser dyes, conventional powder phosphors).
- Encapsulated QDs in epoxy and maintained their solution phase QE.
- Fabricated blue and white QD-LEDs with promising luminous efficiencies (5.5 and 3.5 lm/W, respectively).
- Samples were provided to us by J. Wilcoxon, who
- Identified the importance of surface chemistry on QD emission.
- Synthesized white-emitting QDs without blending.

5.3.2 Quantum Efficiency Measurements

In this program, quantum efficiency (QE) was used as a selection criterion for semiconductor QDs for potential use as phosphors in solid state lighting applications. Knowledge of the QE was used to provide crucial feedback in the development of new synthesis techniques for the variety of luminescent materials being studied. The technique described herein is unique in that it can be applied effectively to laser dyes, powder phosphors, and quantum dots in solvent or polymer encapsulants, all of which we are interested in characterizing.

A measurement system and mathematical procedure were developed for determining the absolute quantum efficiency (QE) and quantum yield (QY) of luminescent materials. This technique, based on absorption of diffuse light within an integrating sphere, was applied to fluorescent laser dyes, quantum dots dispersed in solvent or in polymer encapsulants, and conventional phosphor powders. The system was tested for excitation in the near-UV region, but can be applied to higher energy excitation (UV), as well as lower energy excitation in the visible to near-IR, with the appropriate photodetectors and optical filters. The system was tested on both liquid and solid samples such as Coumarin 500 (CM500) dye in methanol and ethyl acetate; CdS quantum dots in tetrahydrofuran and epoxy; and a variety of powder phosphors. The QY of quinine sulfate dihydrate solution (5x10⁻³M in 0.1N H₂SO₄), a NIST fluorescence standard, was found to be in good agreement with the NIST value under 390 nm excitation. The accuracy of this measurement technique holds for samples with absorption cross sections greater than 6 mm².

There is a need for a simple and accurate method to determine the quantum efficiency of both liquid and solid luminescent materials regardless of concentration. Such a method should account for a variety of sources of error. Principal among these is accounting for scattered light and non-specularly reflected light from powder phosphors. Ideally, such a technique should require minimal sample preparation. The technique developed in this GCLDRD satisfies these criteria and also fully accounts for the spectral energy distribution of the emitted light, detector responsivity, and lamp power fluctuations. This method enables accurate measurements when as

little as 1% of the incident light is absorbed. With this technique we are able to reproduce the established quantum yield for the fluorescence standard quinine sulfate dihydrate to good accuracy and precision.

System Description

Our experimental technique is based on exciting a luminescent sample with diffuse light within an integrating sphere. A 75 W Xe lamp (Oriel* 6251) and 1/8 m monochromator (Oriel 77250) is used to excite the samples throughout the near-UV region (360-400 nm). The grating is 1200 line/mm, and the monochromator bandpass is 2 nm. A diagram of the system is shown in Figure 1. The excitation light from the monochromator is focused by a 50 mm focal length lens.

The focused beam enters a diffuser that is mounted on the entrance port of a 4 in. diameter integrating sphere (Labsphere⁺, IS040-SF/IG). The sphere has four ports, all located around its equator: (1) excitation beam entrance port; (2) excitation light detection port; (3) emitted light detection port; and (4) sample entrance port. The diffuser is a 1.55mm thick, 6.5mm diameter Teflon disk mounted onto the end of a quartz NMR tube, and inserted into the excitation beam entrance port. A NIST-traceable silicon photodetector (Newport* 818-UV) is mounted on each of the two integrating sphere detection ports, located perpendicular to the beam and sample entrance ports. The optical power meter corrects for the detector response using a multiplier. With the appropriate bandpass filters in place, the optical power of the excitation and emission light can be measured simultaneously by the two photodetectors and recorded by two optical power meters (Newport 1830C). The photodetector used to measure the incident excitation light and the absorbed light was labeled Detector A. The photodetector used to measure the emitted light was labeled Detector B. Detector A uses a filter (Newport UG-11) that transmits near-UV light of wavelengths less than 400 nm. Detector B uses a filter (Newport GG400) that transmits visible light of wavelengths greater than 410 nm.

All samples, both solids and liquids, characterized in this system were placed in quartz or Pyrex NMR tubes, and inserted into the sphere through the sample entrance port. The tubes were inserted into the sphere at an angle slightly below horizontal. The end of the tube protruded approximately one inch into the sphere, and the angle and insertion depth were kept constant. The portion of the tube outside or near the sphere sample entrance port cannot have any residual sample coating the walls. The sample residue absorbs the incident excitation light, but its emitted light would tend to exit the port, reducing the measured QE.

The photoluminescence spectral energy distribution of the samples is measured using a SPEX Fluorolog II[♥] which contains a Hamamatsu R298 S20 type single-photon counting photomultiplier tube. The raw photocurrent spectra are corrected to account for the spectral responsivity of the PMT.

System Calibration

The relationship between the emitted light power measured at the Detector B port and the total emitted light power will generally depend on the excitation wavelength, due to the wavelength dependence of the integrating sphere surface coating reflectance, and the wavelength dependence of the detector filter. The sphere efficiency factor takes into account both of these effects, and must be determined for all wavelengths. The sphere efficiency factor, $E(\lambda)$, is the ratio of the power measured at Detector B and the incident light intensity. This ratio was determined at all relevant wavelengths in 10 nm increments from 350-390 nm, 5 nm increments from 390-425 nm, where the pass filters have a rapidly changing attenuation, and 25 nm increments from 425-700 nm. The power of the incident light is called P_{beam} . The stray light, or background signal, is measured by blocking the excitation beam and recording the power meter readings. The background signal is then subtracted from subsequent power measurements.

* Oriel Corporation, Stratford, CT 06497

+ Labsphere, North Sutton, NH 03260

* Newport Corporation, Irvine, CA 92606

♥ SPEX Industries, Inc., Edison, NJ 08820

Absorbed Light Measurements

To determine the amount of excitation light absorbed by the sample, P_{abs} , the excitation light power was measured with and without the sample in place. P_{abs} is given by

$$P_{abs} = P_{beam} \left[\frac{\bar{P}_{ex}^o - P_{ex}^b - \bar{P}_{ex}^s}{\bar{P}_{ex}^o} \right]. \quad (1)$$

Here \bar{P}_{ex}^o is the signal-averaged excitation light power measured by detector A without the sample inserted into the sphere, \bar{P}_{ex}^s is the signal-averaged excitation light power measured by detector A with the sample inserted, P_{ex}^b is the background signal. Solvents were chosen to be non-absorbing at the excitation wavelength. The signal-averaged data is the average of a series of data points collected in 0.5 second increments over a 15 second timeframe.

Emitted light measurements

To determine the emitted light power, P_{em} , the signal-averaged power measured by detector B is recorded with (\bar{P}_{em}^s) and without (\bar{P}_{em}^o) the sample inserted into the sphere. The background signal (P_{em}^b) is also recorded. For these measurements, power meter B is set to the peak wavelength of the sample emission, although this latter selection is really arbitrary, as discussed below.

These power measurements are only directly interpretable for single wavelength emissions. Because the samples of interest are broad band emitters, two wavelength-dependent factors must be taken into account: the sphere efficiency factor (with filter in place) and the detector responsivity.

Assume the detector B power meter is set to some arbitrary wavelength, which we call λ_0 , and that a source that emits at some wavelength λ is placed inside the sphere. The measured power, $P(\lambda_0, \lambda)$, is related to the true power, $P(\lambda) \equiv P(\lambda, \lambda)$, by

$$P(\lambda) = P(\lambda_0, \lambda) \frac{M(\lambda)}{M(\lambda_0)} \frac{1}{E(\lambda)} \quad (2)$$

where $M(\lambda)$ is the detector power meter multiplier, which is proportional to the inverse detector responsivity, and $E(\lambda)$ is the sphere efficiency factor. (The detector multiplier is easily measured in a relative sense by illuminating the detector with light of a given wavelength, and taking readings at various power meter wavelength settings.) A measurement from a broad band source gives the measured integrated power

$$P_{meas}(\lambda_0) = \int P(\lambda_0, \lambda) d\lambda = \int \frac{M(\lambda_0)}{M(\lambda)} E(\lambda) P(\lambda) d\lambda. \quad (3)$$

The correct light power is given by $P_{corr} = S(\lambda_0) \cdot P_{meas}(\lambda_0)$, where S is a ratio of two integrals over the relative spectral energy distribution of the light emission $cP(\lambda)$,

$$S(\lambda_0) = \int cP(\lambda) d\lambda \bigg/ \int \frac{M(\lambda_0)}{M(\lambda)} E(\lambda) cP(\lambda) d\lambda. \quad (4)$$

$P(\lambda)d\lambda$ is the light power in the wavelength interval $\lambda, \lambda+d\lambda$. Note that $S(\lambda_0)$ is independent of the unknown constant c . To compute these integrals, the relative spectral energy distribution and the sphere efficiency data can be interpolated over the wavelength range of interest using a cubic spline function.

To determine correctly the emitted light intensity, it must be recognized that detector B senses light from three sources: the emission, excitation light leaking through the filter, and stray room light. The stray light from the room is not affected by the sample, but the excitation light intensity in the sphere diminishes when the sample is introduced. Because of this, the correct value of P_{em} is given by

$$P_{em} = S(\lambda_0) \cdot \left[(\bar{P}_{em}^s - P_{em}^b) - [(\bar{P}_{em}^o - P_{em}^b) \left(\frac{\bar{P}_{ex}^s - P_{ex}^b}{\bar{P}_{ex}^o - P_{ex}^b} \right)] \right] \quad (5)$$

The final quantum efficiency is simply

$$QE = \frac{P_{em}}{P_{abs}} \quad (6)$$

The quantum yield can also be computed from the relative spectral energy distribution $cP(\lambda)$, with the result

$$QY = \left(\frac{QE}{\lambda_{ex}} \right) \left(\frac{\int P(\lambda) d\lambda}{\int \lambda^{-1} P(\lambda) d\lambda} \right) \quad (7)$$

where λ_{ex} is the excitation wavelength in nanometers.

The factor that limits the sensitivity of this technique is the noise in the excitation light measurements. This noise is $\sim 0.1\%$, so a reasonable lower sample absorption limit would be $\sim 0.6\%$, which corresponds to a sample cross section of 6 mm^2 , corresponding, for example, to $50 \text{ }\mu\text{l}$ of $3 \times 10^{-6} \text{ M}$ CM500, which is only 39 nanograms of dye. In all cases, the emission noise was negligible compared to the excitation noise. As observed experimentally, the position of the sample in the integrating sphere does not appreciably affect the measured QE, though it can affect both the light absorption and emission.

The quantum efficiency was measured for CM500 laser dye at different concentrations in methanol and ethyl acetate; CdS quantum dots in tetrahydrofuran (THF), octane, and polymer encapsulants; conventional phosphors (BaMgAl₁₀O₁₇:Eu, ZnS:Cu,Al, ZnO:Zn); and quinine sulfate dihydrate standard. This variety of samples was selected to demonstrate the versatility of this technique.

Coumarin 500: A series of Coumarin 500 (CM500) dye solutions with different concentrations (10^{-5} M to 10^{-3} M in methanol; $3 \times 10^{-6} \text{ M}$ to 10^{-3} M in ethyl acetate) were measured. The sample volumes were $\sim 45 \text{ }\mu\text{l}$. The QE was found to be nearly independent of the CM500 concentration over this concentration range, as shown in Table I. As described in reference 4, at concentrations $> 1 \times 10^{-3} \text{ M}$, the QE of fluorescent dyes decreases due to a self-quenching mechanism which obeys the Stern-Volmer law over a limited concentration range. Self-quenching results when there is overlap of the absorption and emission spectra, indicating coupling between excited and unexcited solute molecules. Calculations of QE of higher concentration solutions must be corrected for reabsorption effects.

The QY of CM500 was shown to depend on the solvent in studies by Nad and Pal [5]. The QY of CM500 at a concentration of $\sim 1 \times 10^{-5} \text{ M}$ in methanol, was measured to be 46% under 392 nm excitation, 61% in ethyl acetate under 382 nm excitation, and 76% in hexane under 360 nm excitation [5]. It should be noted that the Stokes shift also changes with solvent since the absorption and emission peaks change incommensurately. In our system, the QYs of CM500 (10^{-5} M) in methanol and ethyl acetate were measured to be 58% and 68%, respectively, under 390 nm excitation.

Quantum dots: The QE and QY were measured for CdS and CdSe quantum dots in THF or octane, and in epoxy. These values are listed in Tables I and II. Under 390 nm excitation, the QE/QY was measured to be 60%/74% for blue-emitting CdS ($D \sim 2 \text{ nm}$) and 17%/22% for white-emitting CdS in THF. The QE/QY of CdSe in THF was measured to be 54%/71%.

For use as solid state light sources, phosphors and quantum dots must be incorporated into encapsulants such as epoxy and silicone. The QE/QY of blue-emitting CdS quantum dots in epoxy was measured to be 57%/71%, as shown in Table II. The high QE/QY in the epoxy indicates good dispersion and stability of the QDs.

Phosphor powders: The QE and QY of the phosphor powders were compared with literature values, which are often reported under 254 and 365 nm excitation. The QY of BAM:Eu has been reported to be 91% [6] and 88% [7] under 254 nm excitation, 93% under 365 nm excitation [8], and 72% under 394 nm excitation [8]. (In

these papers these QY values are referred to as QE values). The QY of ZnS:Cu,Al under 365 nm excitation is reported to be 89% and 80% under 394 nm excitation [8]. Nanoparticles of ZnO:Zn are reported to have QE values of 20% and 12% under 280 nm excitation [9], the QE increasing with decreasing particle size.

Conventional phosphor samples pressed into pellets with organic binders often were found to have lower QEs than when polymerized in silicone films or left in loose powder form. The binders, polystyrene and polyethylene oxide, absorb some of the excitation and emitted light. Even a slight increase in binder absorption will reduce the QE because strong multiple scattering of the emitted light gives a long optical path length. Because the silicone is non-absorbing, the QE of BAM:Eu in silicone (75%) is in good agreement with BAM:Eu in loose powder form (79%). The QE of BAM:Eu pellets containing polystyrene binder was found to be 56%. The QEs of ZnS:Cu,Al samples were measured to be 56% and 46% for loose powders and pellets (using PEO binder), respectively. Measurements of ZnS in the two-part silicone were not reproducible since sulfur compounds are poisons for the Pt catalyst. To make QE measurements of sulfide-based phosphors in silicone, an optically clear, Pt-free formulation is required.

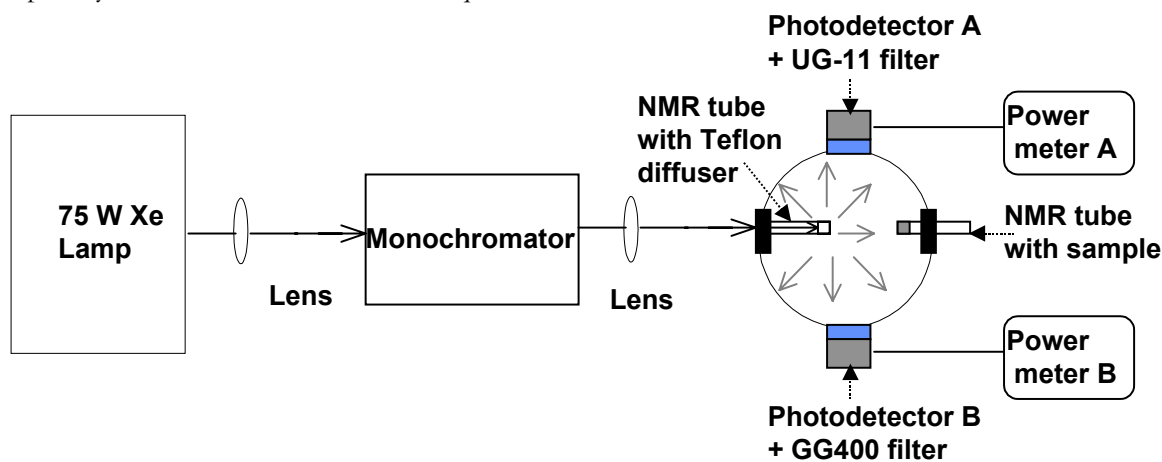


Figure 1. Schematic diagram of the diffuse light system developed for measuring quantum efficiency of liquid and solid samples.

Table I. Quantum efficiency and quantum yield of a series of liquid luminescent samples tested in this system. Excitation wavelength = 390 nm.

Sample	QE (%)	QY (%)
Quinine sulfate dihydrate in 1 N H ₂ SO ₄	45	55
CM500 (10 ⁻³ M in methanol)	38	50
CM500 (10 ⁻⁴ M in methanol)	42	56
CM500 (10 ⁻⁵ M in methanol)	44	58
CM500 (10 ⁻³ M in ethyl acetate)	51	64
CM500 (10 ⁻⁴ M in ethyl acetate)	58	72
CM500 (10 ⁻⁵ M in ethyl acetate)	55	68
CM500 (3x10 ⁻⁶ M in ethyl acetate)	49	61
CdS in THF $\lambda_{em} = 467$ nm	60	74
CdS in octane $\lambda_{em} = 550$ nm (appears white)	17	22
CdSe in THF $\lambda_{em} = 500$ nm	54	71

Table II. Quantum efficiency and quantum yield of a series of solid luminescent samples tested in this system. Excitation wavelength = 390 nm.

Sample	QE (%)	QY (%)
CdS in epoxy $\lambda_{em} = 467$ nm	57	71
BaMgAl ₁₀ O ₁₇ :Eu (BAM:Eu) powder	79	93
BAM:Eu in silicone	75	89
BAM:Eu in polystyrene	56	67
ZnS:Cu,Al powder	56	78
ZnS:Cu,Al in polyethylene oxide	46	64
ZnO:Zn in polyethylene oxide	12	15

5.3.3 Luminous Efficiency Measurements

The optical power and emission spectra of the QD-LEDs were measured using the same type of integrating sphere used in the aforementioned QE system. In a typical experiment, a QD-LED is inserted into the sphere entrance port. The two ports used in the measurements are: (1) sample entrance port, and (2) emitted light detection port. The remaining two ports are covered. A NIST-traceable silicon photodetector (Newport 818-UV) is mounted on the detection port of the integrating sphere, which is located perpendicular to the sample entrance port. A baffle is located inside the sphere at a 45° angle to both the sample and detection ports. The baffle prevents the emission from reaching the detector directly. The QD-LEDs were powered with 73 mW (20 mA/3.67 V) using a Keithley[♦] 236 current/voltage source with the compliance voltage set to 10 V. The dome of the LED was placed into the integrating sphere through a 0.25” diameter aperture mounted onto the sphere entrance port. Power measurements were made with a Newport 1830C optical power meter. Emission spectra of the LEDs were collected using an Oriel spectroradiometer with sighting optics. The emitted light was coupled into an optical fiber bundle leading to the spectroradiometer and dispersed by a 400 line/mm grating and imaged onto a 1024 element linear silicon photodiode array.

To measure the luminous efficiency in lumens per watt (lm/W), the calculation of lumens is given by

$$Lm = \frac{683 \int Ph(\lambda)cP(\lambda)d\lambda}{\int cP(\lambda)d\lambda} \times P_{corr} \quad (8)$$

where $Ph(\lambda)$ is the spectral response of the human eye as a function of wavelength (photopic curve), and $P_{corr} = S(\lambda_0) \cdot P_{meas}(\lambda_0)$, as defined in the quantum efficiency section. Knowing the amount of power used to drive the LED in Watts, the luminous efficiency can be calculated.

Two QD-LEDs were fabricated; one blue-emitting, and the other white-emitting. Monodisperse CdS (D~2 nm) QDs were used for both devices. The CdS surface chemistry was varied by J. Wilcoxon to achieve the different emission colors. Both of the devices were fabricated by milling a cavity in the dome of an encapsulated 400 nm LED chip, and backfilling the dome with the solution of QDs. For the white QD-LED, the solvent was evaporated, leaving behind CdS QDs in their stabilizing surfactant. The blue QD-LED contained some solvent (tetrahydrofuran). The near-UV LED chips were provided by Cree, Inc. The luminous efficiencies of these preliminary devices were 5.5 and 3.5 lm/W, for the blue and white LEDs, respectively. For comparison, QD-LEDs based on electroluminescence (EL), have a luminous efficiency of ~1 lm/W [10]. The first QD-LEDs based on photoluminescence and the integration of QDs with a commercial LED chip were demonstrated in this program, exceeding the performance of the best EL-based QD-LEDs.

[♦] Keithley Instruments, Inc., Cleveland, OH 44139

5.3.4 Summary

The first light sources based on monodisperse CdS quantum dots were produced with promising luminous efficiencies (5.5 lm/W for blue, and 3.5 lm/W for white). As mentioned above, the emission color of the QDs was varied by changing the surface chemistry. This accomplishment illustrates the potential of QDs for use in SSL.

We have demonstrated a new technique for the evaluation of quantum efficiency and quantum yield of both liquid and solid luminescent materials. This technique is simple to use, requires minimal sample and sample preparation, and accounts for: (1) the spectral energy distribution of the emitted light; (2) detector responsivity; (3) lamp power fluctuations; (4) scattered light; (5) stray light; (6) leakage of the excitation light through the emission filter. This diffuse light method enables accurate measurements with as little as 1% of the incident light absorbed. With this technique we are able to reproduce the established QY for quinine sulfate to good accuracy and precision. The QE of conventional phosphors can be measured accurately in powder form and in optically clear silicone films. The QE/QYs of CdS and CdSe quantum dots are comparable to or better than those of ZnS:Cu,Al and ZnO:Zn conventional phosphors, as measured in this system under identical excitation conditions. The high QY of blue-emitting CdS (71%) in tetrahydrofuran solvent was maintained in an epoxy matrix, indicating that good dispersion and stability is achievable with encapsulated QDs.

This program demonstrated that semiconductor QDs are viable alternatives to conventional phosphors for solid state lighting.

5.3.5 References

1. G. O. Mueller and R. Mueller-Mach in *Physics and Chemistry of Luminescent Materials*, C. R. Ronda, L. E. Shea, and A. M. Srivastava, Editors, PV99-40, p. 91, *The Electrochemical Society Proceedings Series*, Pennington, NJ (2000).
2. A. M. Srivastava and H. A. Comanzo, U. S. Patent 6501100 (2002).
3. L. S. Rohwer, B. L. Abrams, and J. E. Martin, "Measuring the absolute quantum efficiency of luminescent materials," submitted to *Journal of Luminescence*, 2004.
4. W. H. Melhuish, "Quantum efficiencies of fluorescence of organic substances: Effect of solvent and concentration of the fluorescent solute," 65, 229-235 (1961).
5. S. Nad and H. Pal, "Photophysical properties of Coumarin-500 (C500): Unusual behavior in nonpolar solvents," *J. Phys. Chem. A.*, 107, 501-507 (2003).
6. M. Zachau, "Photocalorimetric measurement of the quantum efficiencies of phosphor," *J. Lumin.*, 72-74, 792-793 (1997).
7. T. Juestel, J. Krupa, and D. U. Wiechert, "VUV spectroscopy of luminescent materials for plasma display panels and Xe discharge lamps," *J. Lumin.*, 93, 179-189 (2001).
8. Y. R. Do and J. W. Bae, "Application of photoluminescence phosphors to a phosphor-liquid crystal display," *J. Appl. Phys.*, 88 [8], 4660-4665 (2000).
9. A. van Dijken, J. Makkinje, A. Meijerink, "The influence of particle size on the luminescent quantum efficiency of nanocrystalline ZnO particles," *J. Lumin.*, 92, 323-328 (2001).
10. S. Coe, W-K. Woo, M. Bawendi, and V. Bulovic, "Electroluminescence from single monolayers of nanocrystals in molecular organic devices," *Nature*, 420 [6917], 800-803 (2002).

5.3.6 Acknowledgments

Thanks are given to Jess Wilcoxon of Sandia Labs for providing quantum dot samples for these measurements, and Gerry Negley of Cree, Inc., for providing LED samples.

5.4 Encapsulants of Nanoparticles (SG Thoma, BL Abrams, LS Rohwer, A Sanchez, JP Wilcoxon, SM Woessner)

5.4.1 MOTIVATION

To identify and develop encapsulation strategies that enable incorporation of high concentrations of semiconducting nanoparticles into conventional, industrially relevant encapsulants (e.g. epoxies and silicones) without loss of quantum efficiency.

5.4.2 ABSTRACT

Solid state lighting devices that utilize semiconducting nanoparticles (quantum dots) as the sole source of visible light emission have recently been fabricated. The quantum dots in these devices have been demonstrated to have quantum efficiencies similar to those of conventional phosphors. The dispersion and concentration of the nanoparticles within a suitable polymeric matrix was found to be critical to device performance. Yet achieving suitable concentrations and adequate dispersion implies chemical compatibility between the nanoparticles and the matrix, which must be achieved without detrimental effect on either the physical/optical properties of the matrix or the stability/surface state of the quantum dots. A number of encapsulation strategies have been identified and are discussed with regard to their effect on nanoparticle dispersion and concentration within silicone and epoxy matrices.

5.4.3 INTRODUCTION

Semiconducting nanoparticles or ‘quantum dots’ are the subject of a great deal of research owing to their emissive properties and hence their potential use in solid state lighting devices. One approach to creating a solid state lighting device using quantum dots is to ‘suspend’ the nanoparticles in an optically clear matrix above a UV-emitting chip; the UV wavelength light is absorbed by the nanoparticles and re-emitted in the visible range. Recently Sandia National Laboratories has fabricated solid state lighting devices using UV emitting GaN chips and semiconducting nanoparticles¹. A polymeric dome containing quantum dots was formed over a standard commercial (Cree) fixtured GaN chip. This configuration enabled the fabrication of a lighting device with an output of 5.5 lumens/watt; similar efficiency to commercial blue LEDs. One of these devices emitted a very broad ‘white’ spectrum that more closely resembles the visible solar spectrum than ‘white’ light emitted from color-blended LEDs. The polymeric encapsulants used to form the dome were commercially available epoxy or silicone. While epoxy is currently the most industrially relevant optical encapsulant, optical grade silicones have the advantage of higher temperature stability making them candidates to replace the epoxy as an encapsulant for solid state lighting applications².

The body of research dealing specifically with incorporating quantum dots into polymeric matrices has grown considerably in recent years, however little of this research has focused on hydrophobic polymers, specifically epoxies and silicones. A common misconception is that the organically stabilized quantum dots, having an exterior surface that is hydrophobic in nature, would be entirely miscible with the hydrophobic polymers and hence high concentration dispersions of the quantum dots can be readily obtained. This, however, is only partly true. While the quantum dots are generally miscible with the encapsulating polymers in their (initial, pre-cured) liquid state, during curing Chemically Induced Phase Separation (CIPS) occurs, forcing the quantum dots into domains, thereby limiting quantum dot concentration and dispersion in the cured polymer. Furthermore, the suitability of an encapsulant toward metal sulfide or selenide nanoparticles can be limited by detrimental chemical interaction between the nanoparticles and the encapsulant. For instance, addition cure silicones that rely on a noble metal catalyst to effect the crosslinking reaction can be poisoned by the sulfur or selenium nanoparticles. Alternately, silicones using organic peroxides to cure the polymer are destructive to the nanoparticles. UV cure

¹ (a) <http://www.sandia.gov/news-center/news-releases/2003/elect-semi-sensors/quantum.html> ; (b) <http://lighting.sandia.gov>.

² OIDA (Optoelectronics Industry Development Association) roadmap, <http://www.oida.org>

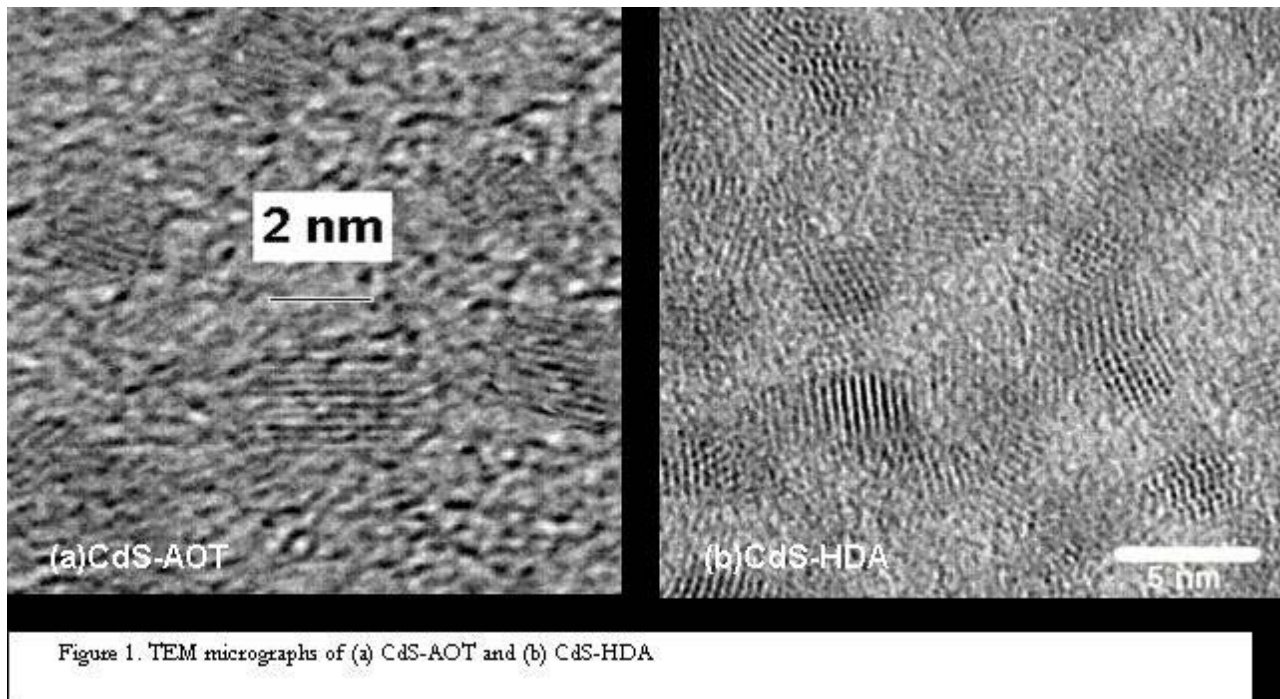


Figure 1. TEM micrographs of (a) CdS-AOT and (b) CdS-HDA.

systems that contain acrylate functionality can be similarly destructive to the nanoparticles. Hence, the commercially available encapsulants used in this work are an epoxy and a thermally activated 2-part amino-siloxane/epoxide system, as amine and epoxide groups are generally chemically benign to metal sulfide and selenide nanoparticles.

Many factors affect the photoluminescent spectrum and quantum yield (QY) of semiconducting nanoparticles, including particle size, chemistry, stoichiometry, the chemical nature of the stabilizing organic, as well as factors such as dispersion and concentration. Traditional thinking about obtaining white light from quantum dots is based on conventional phosphors whereby different materials with varied emission colors are blended to obtain a broad (white) spectrum. It was believed that this could be achieved in a facile fashion via blending different size nanoparticles. Unfortunately, this approach is impractical when using quantum dots due to competitive absorption; the larger, red emitting particles absorb the majority of the energy, making it difficult if not impossible to get an intense, broad spectrum emission. To avoid this pitfall, SNL fabricated their white light emitting device using extremely *monodisperse* (~ 2 nm diameter CdS) nanoparticles in which the absorption is at least partially decoupled from the photoluminescence (PL) and photoluminescence excitation (PLE)³. Furthermore, conventional wisdom also states that emission can be enhanced by passivation of the nanoparticle surface, i.e. elimination of surface trap states to maximize radiative recombination in the nanoparticle core. This is often achieved by the addition of a layer of wider band gap material to the surface of the nanoparticle core. On the other hand, for particle diameters less than approximately 3 nm, the vast majority of atoms are either on the surface or are next-nearest-neighbors to the surface, and are thus directly effected by adsorption of the stabilizing organic. We therefore chose to maximize emission by using the relatively abundant surface atoms as the emission source. The emission wavelength of the nanoparticle can be adjusted either to specific wavelengths or broadened (to white) by appropriate selection and application of the stabilizing organics³.

The ideal encapsulation system is therefore one that enables incorporation of high concentrations of nanoparticles without particle aggregation while maintaining or even enhancing luminescence via constructive chemical interaction between the nanoparticles and the encapsulant. Furthermore, the encapsulation system

³ "Optical Properties of II-VI Semiconductor Nanoclusters for use as Phosphors", Wilcoxon, J.P.; Newcomer, P.; Proceedings of SPIE 4808, 99-114, 2002.

needs to be highly manufacturable if it is going to find widespread application, implying facile, inexpensive, *bulk* processes. In this work, we demonstrate the effects of encapsulation on nanoparticle photoluminescence and discuss strategies to avoid emissive losses during the curing process as well use of the encapsulant as a participant in photoluminescence with an emphasis on manufacturable processes.

5.4.4 EXPERIMENTAL

Synthesis

CdS and CdSe quantum dots were synthesized by several different methods. The first method synthesizes quantum dots within surfactant inverse micelles at room temperature using simple metal salts as precursors^{4,5,6}. Surfactants used in these syntheses were Sodium Bis(2-ethylhexyl) sulfosuccinate (AOT) and dodecyltrimethylammonium chloride (DTAC) in octane yielding solutions .002-.005 M CdS. The surfactant concentration in these systems was 10 wt%. Trioctylphosphine selenide (TOP-Se) stabilized CdSe and alkylthiol stabilized CdS nanoparticles were synthesized in THF by a metathesis reaction³ yielding .005 M CdSe solutions. An equimolar amount of stabilizing alkylthiol was used. All of these nanoparticle solutions were used without further treatment. The third synthesis method is a high temperature ‘single-source’ precursor synthesis in hexadecylamine (HDA) that utilizes the decomposition of organometallic precursors to enable growth of the nanoparticles⁷. Nanoparticles synthesized by this method were repeatedly precipitated and redispersed in toluene and used in the final concentrations of approximately .10 M (CdS or CdSe). Quantum dots are hereafter identified by their chemistry and synthesis method as follows; CdS synthesized in AOT inverse micelles are referred to as CdS-AOT, etc.

Characterization

Thermal analysis was performed using a TA instruments SDT 2960 simultaneous Thermo Gravimetric Analyzer – Differential Thermal Analyzer (TGA-DTA). Samples were ‘dried’ under vacuum (625 mm Hg)

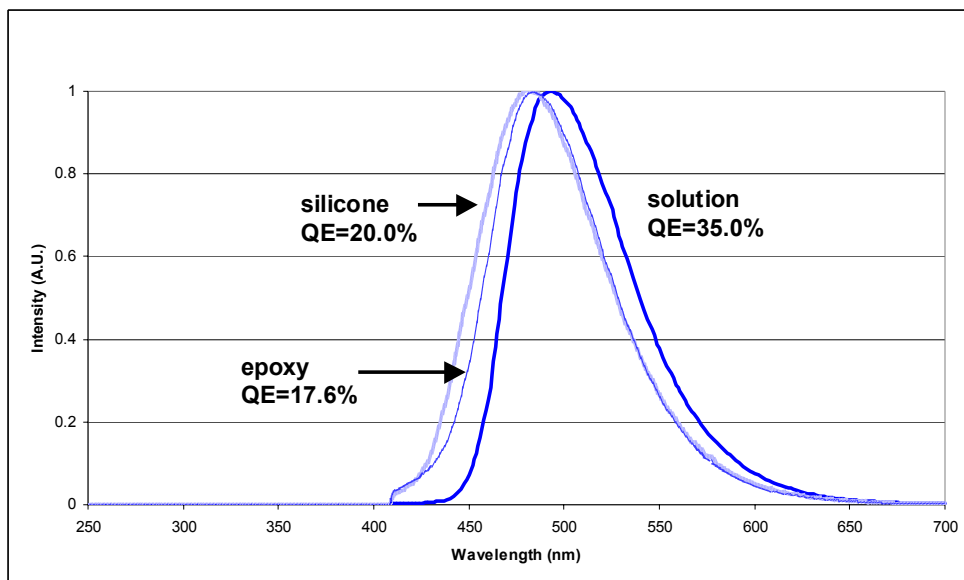


Figure 2. Photoluminescence spectra of CdS-DTAC in solution and encapsulated in epoxy and silicone at approximately .015 wt% CdS. Excitation wavelength = 390 nm.

⁴ “Small CdS Particles in Inverted Micelles”, Lianos, P.; Thomas, J.K.; J. Coll. Inter. Sci. **117**, 505-512, 1987.

⁵ “Formation of Metal Colloids in Inverse Micelles an Microemulsions”, Wilcoxon, J.P.;Williamson, R.L.; Macromolecular Liquids **177**, 269-274, 1990.

⁶ “Method for Preparation of Metal Colloids in Inverse Micelles and Product Preferred by the Method”, Wilcoxon, J.P.;US Patent #5,147,841, 1992.

⁷ “Inorganic Clusters as Single-Source Precursors for Preparation of CdSe, ZnSe, and CdSe/ZnS Nanomaterials”, Cumberland, S.L.; Hanif, K.M.; Javier, A.; Khitrov, G.A.; Strouse, G.F.; Woessner, S.M.; Yun, C.S.; Chem. Mater. **14**, 1576-1584, 2002.

yielding a thick gel or paste and then run under inert atmosphere. X-Ray powder diffraction (XRD) was performed solely for phase identification using a Bruker D8-Advance diffractometer in Bragg-Brentano geometry with Ni-filtered Cu-K α radiation. Transmission Electron Microscopy (TEM) samples were prepared by evaporating a small amount of dilute nanoparticle solution onto a holey carbon grid, wicking away the excess, and allowing to dry. The samples were examined by both low and high

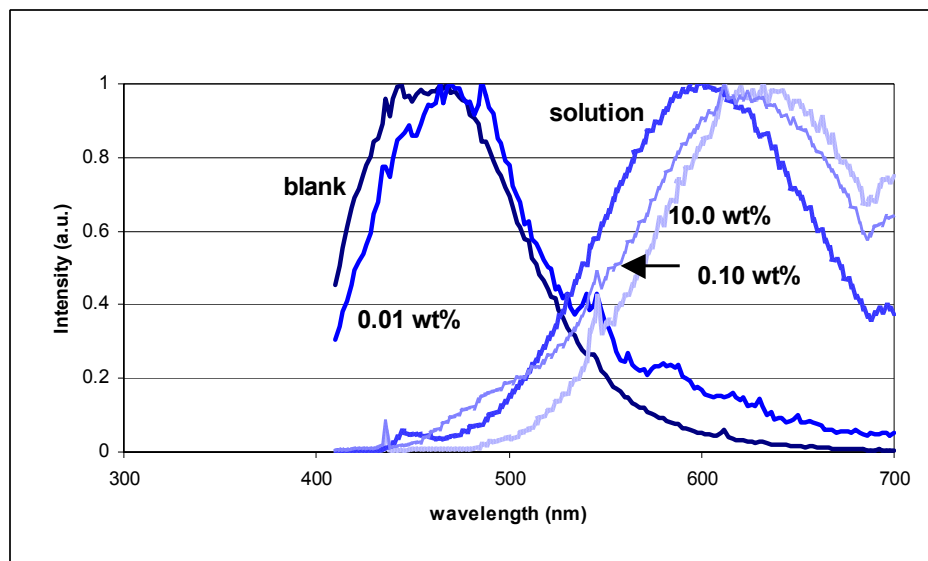


Figure 3. PL of CdS-HDA in liquid epoxy resin at various concentrations, blank epoxy resin, and CdS-HDA in (as-synthesized) solution. Excitation wavelength = 390 nm.

resolution TEM. PL and PLE measurements were made using a SPEX Fluorolog II double-double grating spectrometer with Xe arc lamp illumination and using a cooled S20-type PMT. Details on the methodology of the photoluminescent measurements can be found elsewhere³. Quantum yield (QY) values denote photons emitted / photons absorbed; quantum efficiency (QE) refers to emitted photon power/absorbed photon power, details of QY/QE measurements are also reported elsewhere⁸. PLE spectra have been omitted for clarity. For comparisons sake, PL spectral intensities have been normalized to peak intensity.

Encapsulation

The epoxy and silicone encapsulants were all commercially available products and used without modification. The epoxy systems used were Hysol OS4000 and Pacific Polytech PT5-42. Both of these are two part systems, and a 1:1 (wt) mixture was cured at 125 oC for 1 hour. The silicone used in this study was Dow Corning 2-8040 / 7-3109 system. One drop of 7-3109 cross-linker was mixed with one gram of 2-8040 polymer and cured at 150 oC for 1 hour, yielding an optically clear product. In all cases the pre-cured encapsulant mixture was outgassed at 625 mm Hg vacuum. The nanoparticle solution was then mixed into the encapsulant and outgassed again to remove solvents. All mixing was performed by hand and curing under static conditions in normal atmosphere. The nanoparticle content of the encapsulated samples are expressed as a weight percent, which refers to the weight percent inorganic only, not the weight percent inorganic-stabilizing organic composite.

5.4.5 RESULTS & DISCUSSION

Synthesis

Room temperature inverse micelle synthesis yields highly monodisperse nanoparticles, generally more so than high temperature synthesis (lyothermal) methods. While elevated temperature reflux at the close of lyothermal synthesis enables some increase in size homogeneity and defect elimination, it typically does not approach the results possible via room temperature synthesis. Size selective precipitation is frequently used to increase the monodispersity of lyothermally produced nanoparticles, but this process gradually removes the stabilizing organics which can diminish yield. Yields from room temperature (low energy) inverse micelle synthesis

⁸ "Thermal Quenching of Quantum Dots for Solid State Lighting Applications", Abrams, B.L.; Rohwer, L.S.; Wilcoxon, J.P.; Thoma, S.G.; to be submitted to Journal of Luminescence 2003.

CdS-HDA QY=4.4%)	(as-synthesized)	0.01 wt%	0.10 wt%	1.00 wt%	10.0 wt%
Liquid Epoxy	QY(%)	2.4	8.3	4.8	2.7
Cured Epoxy	QY(%)	3.5	7.0	5.5	6.4

Table 1. QY values of CdS-HDA in liquid and cured epoxy as a function of concentration.

approach 100%, the synthesis is highly scalable, utilizes inexpensive metal salts as precursors, creates little waste, routinely and reproducibly yields high efficiency nanoparticles, and the as-synthesized materials require no further processing; making this

an attractive synthesis method from a manufacturing standpoint. Typical TEM images of CdS-AOT and CdS-HDA nanoparticles are shown in Figure 1a³ and 1b, respectively.

The HDA lyothermal synthesis was chosen for use because of its ease, reproducibility, high yields (relative to other lyothermal methods). This synthesis method is very convenient because it enables the synthesis of high concentration solutions of nanoparticles, though the product is of relatively low QY. A sample of CdSe-HDA was vacuum ‘dried’ under the same conditions that the pre-cure encapsulant-nanoparticle samples were outgassed, and were therefore likely similar in composition to the materials dispersed in the encapsulant prior to curing. TGA of this material indicated that the ‘dried’ HDA material is about 35 wt% inorganic and 65 wt% organic. Note that since this analysis was performed under inert atmosphere that the 35 wt% represents the *maximum* amount of CdSe; some portion of this is likely deposited carbon. If we assume that the average nanoparticle size is 3 nm, which is covered with a 1 nm ‘shell’ of HDA, the composite sphere is approximately 4 wt% organic; i.e. there is clearly an excess of organic in this system relative to the amount that is able to surface adsorb. The surfactant systems, as mentioned, are 10 wt% organic, also an excess. The metathesis synthesized nanoparticle solutions have the lowest overall organic content.

Encapsulation Observations

In general, encapsulation of nanoparticles results in a loss in emission intensity and may be accompanied by a shift in the emission spectrum. Figure 2 shows the change in photoluminescence of CdS-DTAC nanoparticles incorporated at approximately .015 wt% CdS as a result of encapsulation in silicone and epoxy. The QY of this sample decreased from 59.3% in the as-synthesized solution to 26.0% and 22.7% when encapsulated in either epoxy or silicone, respectively. Another sample, CdS-alkylthiol, showed similar changes, dropping from a solution QY of 28.3% to 13.8 and 20.8% in epoxy and silicone, respectively. It is not uncommon for materials with as-synthesized double-digit quantum yields to exhibit losses to single-digits or even a complete loss of QY when the as-synthesized materials are simply mixed into an encapsulant and cured. There are several possible reasons for such emissive losses. Loss of stabilizing organics (loss of steric barrier) or interweaving of the stabilizing organic tails between adjacent nanoparticles may allow the nanoparticles to aggregate, bringing the inorganic cores close enough to electronically couple. If enough stabilizing organic is lost, the inorganic cores may coalesce into one larger particle, with loss of the quantum size. Another possibility is oxidative degradation of the inorganic, which may also be due in part to the removal or diminished association with the stabilizing organics. In the systems discussed here, however, we did not observe a change in the absorbance spectrum concurrent with emissive loss, and so unless the scattering contribution from the aggregation has exactly offset the change in absorption due to (change in) particle size, the cause of these losses is not oxidation or coalescence.

A factor that can affect the extent of aggregation is the degree of nanoparticle phase separation during the mixing and curing process. Phase separation of non-reactive species during a polymerization reaction is described as Chemically Induced Phase Separation (CIPS)⁹. Briefly, this type of phase separation is driven by

⁹ “Macroporous Thermosets by Chemically Induced Phase Separation”, Keifer, J.; Hedrick, J.L.; Hilborn, J.G.; *Advances in Polymer Science* **147**, 161-247, 1999.

changes in the free energy of the system as the reactive polymer grows in size. CIPS has been described mainly for two-phase systems, either polymer-solvent or polymer-colloid¹⁰. Factors known to affect CIPS in reactive polymer systems such as epoxies^{11, 12} and silicones¹³ include (polymer and solvent/colloid) molecular size and shape, polarity, hydrogen bonding ability, concentration, temperature, rate of reaction, etc. The

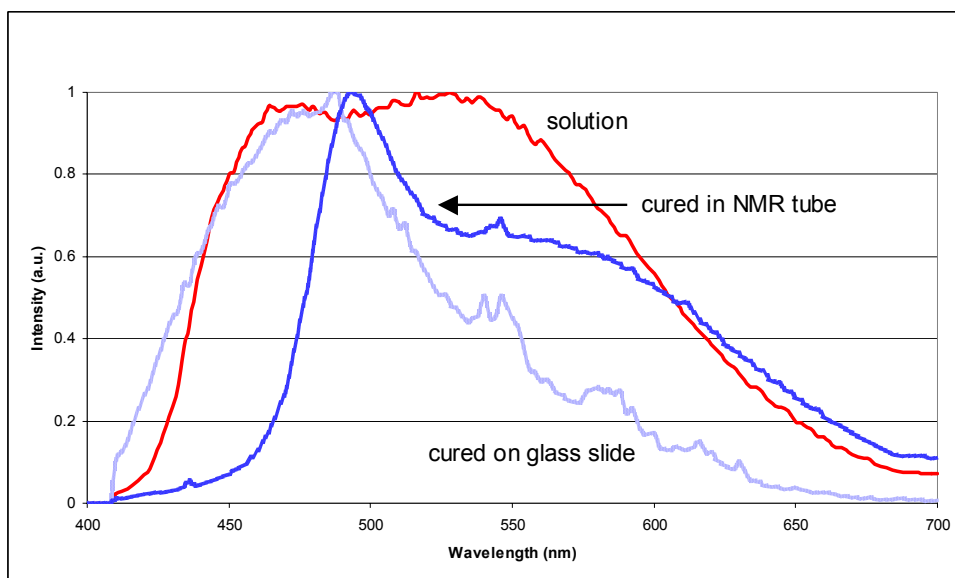


Figure 4. Effect of curing environment on PL of CdSe nanoparticles in silicone. Excitation wavelength = 390 nm.

encapsulant-nanoparticle systems used in this work are essentially a reactive polymer-colloid *and* solvent system; the ‘colloids’ are the inorganic nanoparticle/stabilizing-organic/residual solvent nanocomposite, and the ‘solvent’ is the excess (non-surface adsorbed) stabilizing organic. Initial Small Angle X-ray Studies (SAXS) indicate the curing process results in nanoparticle-rich domains, though it is unclear whether the excess stabilizing organic forms separate domains or remains dispersed in the encapsulant matrix. This has been observed in samples containing as little as 0.013 wt% CdS (CdS-AOT), corresponding to 3 wt% AOT; a lower content of non-reactive species than is generally associated with CIPS. Additional studies are needed to clarify this.

The maximum nanoparticle loading before overt (visible) phase separation took place, in either encapsulant, was approximately 1.0 wt% (inorganic) for CdS-alkylthiol; for the surfactant stabilized materials, and the HDA stabilized materials in silicone, the upper limit was closer to 0.1 wt%. However, the HDA stabilized materials can be incorporated up to tens of wt% in the epoxy. A precipitate forms upon mixing but redisperses as the solvent if the solvent is gradually removed. The QY values for of CdS-HDA as a function of concentration dispersed in a liquid epoxy resin and the same samples following curing are given in Table 1, and the PL of select liquid samples shown in Figure 3.

In Figure 3, the PL the 0.01 wt% sample is seen to be similar to the PL of the epoxy (blank). The PL of the 0.10, 1.00, and 10.0 wt% samples are nearly identical and show only emission from the CdS. This is simply an indication that below 0.01 wt% the excitation energy is absorbed primarily by the polymer, and at 1.0 wt% and above it is absorbed primarily by the nanoparticles; at high enough concentrations the energy is absorbed by the nanoparticles before it can be absorbed by the polymer. Based upon QY the optimum concentration is between 0.01 wt%, and in the liquid it the emission decreases with increasing wt%, possibly due to concentration-induced

¹⁰ “Depletion-induced Phase Separation in Colloid-Polymer Mixtures”, Tuinier, R.; Rieger, J.; de Kruif, C.G.; *Advances in Colloid and Interface Science* **103**, 1-31, 2003.

¹¹ “Predicting the Phase Behavior of Solvent-modified Epoxy Resins”, Plummer, C.J.G.; Kiefer, J.; *Colloid. Polym. Sci.* **278**, 736-745, 2000.

¹² “Kinetics and Mechanism of the Late Stage of Microphase Separation Induced by Curing”, Kuzub, L.I.; Irzhak, V.I.; *Colloid Journal* **63**, 86-91, 2001.

¹³ “Preparation of Polysiloxane Composite Films with Microphase-separated Silicone Oil by Photocrosslinking”, Yi, J.; Kim, J.; Kang, Y.; Kim, D.W.; Lee, C.; *Polymer-Korea* **27**, 3-8, 2003.

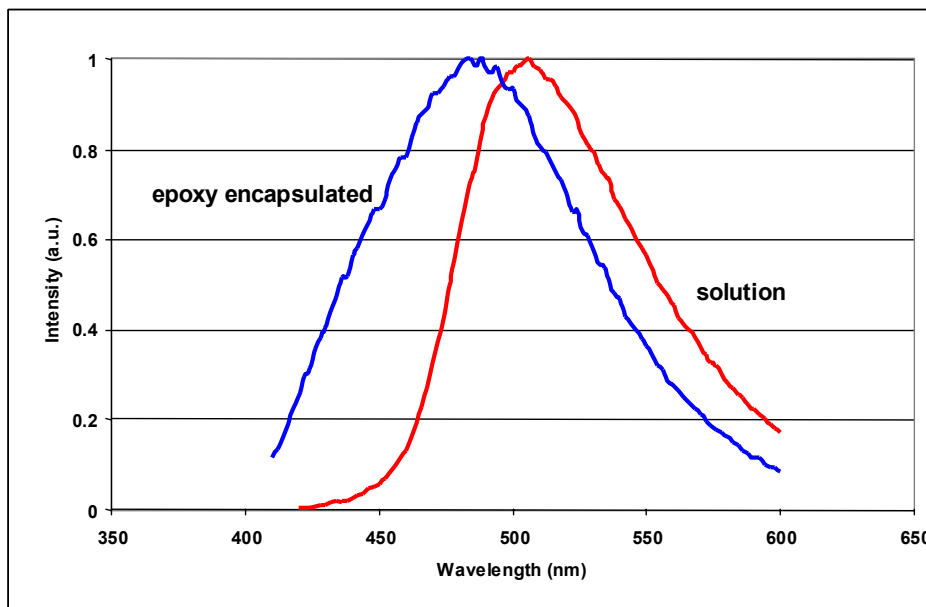


Figure 5. PL of solution and epoxy encapsulated difunctional molecule crosslinked CdSe-TOP-Se. Excitation wavelength = 400 nm.

aggregation. If indeed this is due to aggregation then it is reversible, because upon curing the QY *increases*, most notably in the 10 wt% sample. This behavior is in marked contrast to the surfactant, TOP-Se, or alkylthiol stabilized systems. Also note that there is a slight red shift from the as-synthesized solution, which is also in contrast to the other systems. This system however, although of low QY, stands to point out a possible relationship between miscibility and maintenance of QY from synthesis to encapsulant.

Another observation is that the photoluminescence spectrum can also be affected by the curing methodology. Figure 4 shows the PL of CdSe nanoparticles grown in silicone fluid and then cured in either an NMR tube or on a glass slide. The different curing environments yielded very different PL spectra. A relatively open versus closed curing environment may result in physical differences because of changes in the rate of evaporative loss of 'solvent' (e.g. volatile species from the reactive polymer system, residual organics, excess stabilizing organics) relative to the rate of crosslinking. The QY of the as-synthesized liquid and the NMR tube cured sample was 3.8 and 4.1%, respectively (the equipment used for QY determination will not accept samples on glass slides).

Encapsulation Strategies

In essence, virtually all synthesis and processing steps to create an encapsulated nanoparticle system may affect the PL and QY of the final product, many of which can be related (at least in part) to nanoparticle dispersion. There are, however, a number of strategies that may be employed to control the observed phenomena: (1) 'nano-encapsulate' the nanoparticles, i.e. form a shell around the individual nanoparticles-stabilizing organic composite, thereby both stabilizing the inorganic surface states and simultaneously creating an exterior surface that can be functionalized to suit any encapsulant; (2) 'controlled aggregation', i.e. use of multifunctional molecules as 'spacers' to limit the degree of aggregation of the nanoparticles; (3) 'polymeric stabilization', i.e. use of the polymeric encapsulant as an active participant in enhancing nanoparticle luminescence, via constructive interaction between the nanoparticle and the polymeric functional groups; (4) 'controlled phase separation', i.e. use the phase separation phenomenon to create domains of solvent containing nanoparticles.

With regard to 'nano-encapsulation', there are two main (published) routes to forming a shell around individual nanoparticles; formation of a silica shell^{14,15,16,17} and formation of a hydrocarbon shell¹⁸. Unfortunately,

¹⁴ "Preparation and Properties of Tailored Morphology Monodisperse Colloidal Silica-Cadmium Sulfide Nanocomposites", Chang, S-Y.; Liu, L.; Asher, S.A.; J. Am. Chem. Soc. **116**, 6739-6744, 1994.

¹⁵ "Enhancement of Photoluminescence in Manganese-doped ZnS Nanoparticles due to a Silica Shell", Ethiraj, A.S.; Hebalkar, N.; Kulkarni, S.K.; Pasricha, R.; Urban, J.; Dem, C.; Schmitt, M.; Kifer, W.; Weinhardt, L.; Joshi, S.; Fink, R.; Heske, C.; Kumpf, C.; Umbach, E.; Journal of Chemical Physics **118**, 8945, 2003.

¹⁶ "Synthesis and Properties of Biocompatible Water-Soluble Silica-Coated CdSe/ZnS Semiconductor Quantum Dots", Gerion, D.; Fabien, P.; Williams, S.C.; Parak, W.J.; Zanchet, D.; Weiss, S.; Alivisatos, A.P.; J. Phys. Chem. B **105**, 8861-8871, 2001.

the latter method offers little experimental detail. Of the former method, Wuister et al¹⁷ have presented a low-temperature synthesis method that combines the function of the stabilizing organic and the shell-forming material in one molecule. This methodology is critical to devising an industrially relevant synthesis process. A great deal more research on silica shell formation has been performed on metallic¹⁹ rather than semiconducting nanoparticles, and more work could be done toward optimizing the efficiency of silica ‘capped’ nanoparticles, perhaps via use of stabilizing/shell-forming

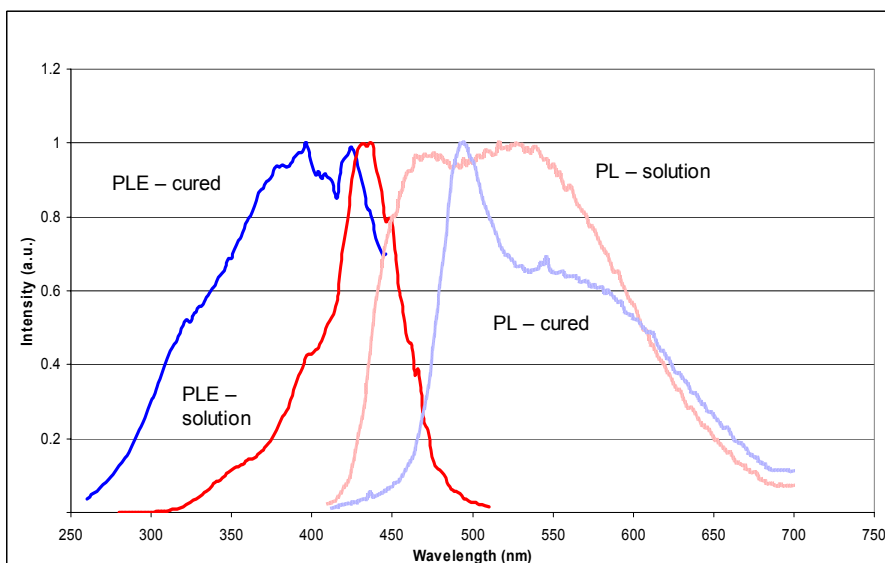


Figure 6. PL and PLE of CdSe grown in silicone, before and after curing. Excitation wavelength for PL = 390 nm.

molecules with different alkyl chain lengths and terminal functionality.

Controlled aggregation of nanoparticles via di- (or multi-) functional crosslinkers has been shown to be an effective method of controlling nanoparticle dispersion²⁰. The challenges in this area relate to developing a crosslinking molecule that not only provides physical stability but also a constructive chemical interaction with the nanoparticles, so that the QY is enhanced due to precipitation rather than diminished. Accomplishing this might also provide a route toward ‘fixing’ varied mid-gap states on the particle surface to yield a broad emission. There is also the challenge of precipitating the nanoparticles in small enough clusters (to avoid Rayleigh scattering) and using a crosslinking molecule that will enable controlled dispersion of these clusters in the encapsulant, either via direct chemical interaction with polymer functional groups or by improved miscibility. Figure 5 shows the PL of a ‘white’ emitting CdSe-TOP-Se sample precipitated using a difunctional crosslinker. Although the spectrum blue-shifted as a result of the encapsulation process, the QY decreased only from 32 to 31%, and it still maintained a (desired) broad emission.

The ideas and challenges associated with polymeric stabilization are very similar to those mentioned for controlled aggregation, except that the encapsulant also serves as the crosslinker, which has the added advantage of decreased processing steps. Enhancing interaction between nanoparticles and polymeric functional groups necessitates that the two species are able to come into sufficient proximity to enable chemical interaction; the very purpose of the stabilizing organics is to avoid this situation. However, if the nanoparticles are synthesized directly into the polymer, the polymer *is* the stabilizing organic and nanoparticle-polymer interaction is established *a priori*. Figure 6 shows the PL and PLE spectrum of CdSe grown directly into a silicone fluid, as-synthesized and then after cure (same sample as Figure 4, but presented separately for clarity sake). This sample

¹⁷ “Synthesis and Luminescence of CdS Quantum Dots Capped with a Silica Precursor”, Wuister, S.F.; Meijerink, A.; Journal of Luminescence **105**, 35-43, 2003.

¹⁸ “Functional Nanocomposites Prepared by Self-Assembly and Polymerization of Diacetylene Surfactants and Silicic Acid”, Yang, Y.; Ly, Y.; Lu, M.; Huang, J.; Haddad, R.; Xomeritakis, G.; Liu, N.; Malanoski, A.P.; Sturmayer, D.; Fan, H-Y.; Sasaki, D.Y.; Assink, R.A.; Shelnutt, J.A.; van Swol, F.; Lopez, G.P.; Burns, A.R.; Brinker, C.J.; J. Am. Chem. Soc. **125**, 1269-1277, 2003.

¹⁹ “The Assembly of Coated Nanocrystals”, Liz-Marzan, L.M.; Mulvaney, P.; J. Phys. Chem. B **107**, 7312-7326, 2003.

²⁰ “Structures and Properties of Nanoparticle Thin Films Formed via a One-Step Exchange Cross-Linking Precipitation Route”, Leibowitz, F.L.; Zheng, W.; Maye, M.W.; Zhong, C-J.; Anal. Chem. **71**, 5076-5083, 1999.

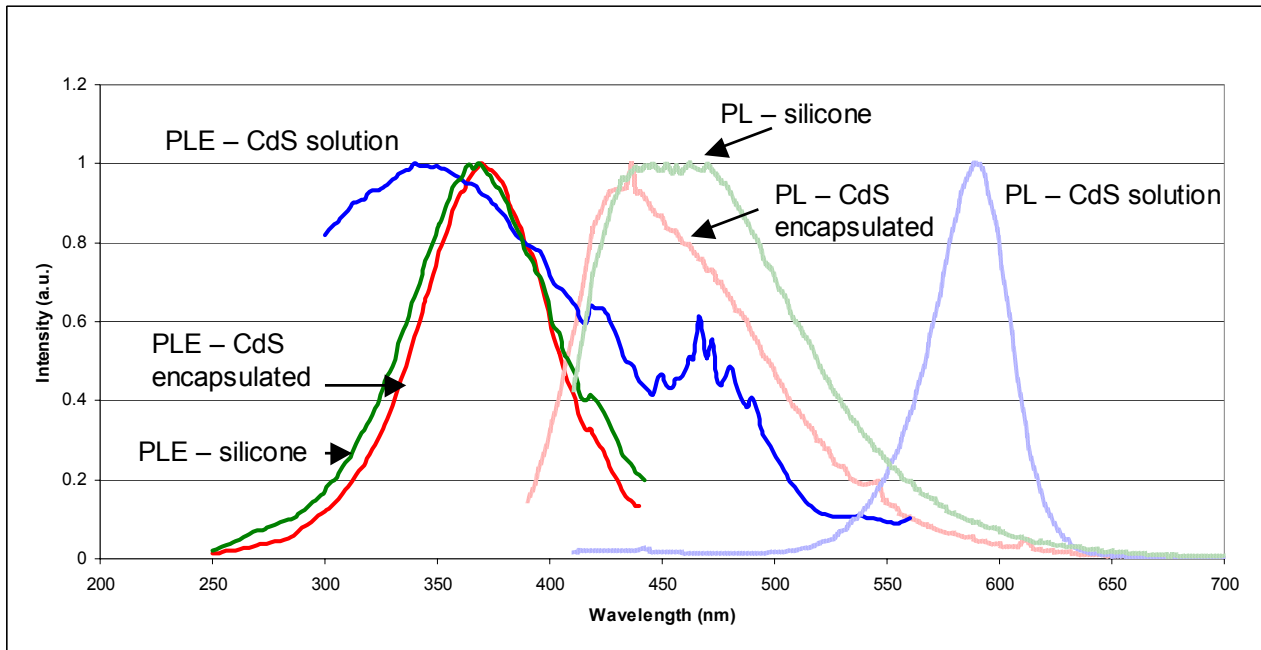


Figure 7. PL and PLE spectra of as-synthesized CdS-AOT, silicone encapsulated CdS-AOT, and blank silicone. Excitation wavelength for PL = 390 nm.

has a broad ‘white’ emission that is relatively unperturbed upon curing. Contrast this with the PL and PLE spectra shown in Figure 7, for a CdS-AOT material simply mixed into the encapsulant and cured. The originally broad emission is almost entirely lost from the encapsulation process. Although direct synthesis of nanoparticles in the polymeric encapsulant precursors can help maintain PL through the encapsulation process, it has yet to yield the high QY values as are achievable by room temperature inverse micelle synthesis.

‘Controlled phase separation’ is an attractive idea from the standpoint that it would enable the use of a (common) naturally occurring phenomena rather than working to avoid it, and would perhaps enable nanoparticle synthesized from a variety of methods to be encapsulated without emissive losses. It is also attractive from a manufacturing standpoint since it would allow as-synthesized nanoparticles to be incorporated into an encapsulant with a minimum of steps. It has the disadvantage that the ‘formula’ for creation of suitably small domains, reproducibly, will vary for every nanoparticle system as well as the encapsulant and curing conditions/environment. A great deal more work is necessary to understand phase separation behavior of organically stabilized nanoparticles in reactive polymers. Physical characterization of these systems remains a challenge.

5.4.6 Conclusions

Encapsulation of organically stabilized nanoparticles in silicones and epoxies can lead to phase separation and formation of domains of high nanoparticle concentration. Emissive losses in these systems seem to be related primarily to particle aggregation. The degree of aggregation and the associated emissive loss are affected by virtually all of the system variables, such as polymer and nanoparticle chemistry and concentration, as well as the curing procedure and conditions. Nanoencapsulation, controlled aggregation, polymeric stabilization, controlled phase separation, and combinations thereof may be effective strategies to mitigate the observed losses, and enable bulk manufacture of high- concentration encapsulated nanoparticle dispersions.

5.4.7 Results

We have succeeded in incorporating approximately 30 wt% (inorganic) semiconducting nanoparticles into a commercially available optical-grade epoxy, though this accomplishment was system-specific. Toward these ends we have also,

We have identified, and in some cases demonstrated, strategies to enable encapsulation of diverse (any) nanoparticle system into commercially available, optical grade, silicone or epoxies. This includes: Direct synthesis of semiconducting nanoparticles in silicone encapsulants.

6 TASK 6: STRATEGIC PLANNING AND BUSINESS DEVELOPMENT

6.1 Support for the National Lighting Initiative (JA Simmons)

Sandia was involved in promoting the idea of Solid State Lighting from the very beginning, starting with the 1999 white paper jointly authored by Hewlett-Packard scientists Roland Haitz and Fred Kish, and Sandia scientists Jeff Tsao and Jeff Nelson. During the course of the SSL GCLDRD, we continued: to outreach to potential industrial and university collaborators; and to give newspaper, trade journal, general interest magazine, and radio and television interviews. We regularly gave invited presentations at conferences devoted to LEDs and solid state lighting. Finally, we gave technical and background support to government agencies and offices with an interest in solid state lighting, including DOE's Office of Building Technologies, DOE's Office of Science, the National Academy of Science, and the Office of Senator Jeff Bingaman (D-NM). We continue to perform these types of activity to the present. This Section gives a brief synopsis of the most noteworthy of these actions.

Early on, starting slightly before the SSL GCLDRD received initial funding, Sandia was involved in planning the Solid State Lighting LED Technology Roadmapping Workshop, held in Albuquerque on Oct. 26-27, 2000. The Workshop was co-sponsored by the Optoelectronic Industry Development Association (OIDA), and DOE's Office of Building Technologies. Sandia's Eric Jones edited the final LED Technology Roadmap Report.

Around this time OIDA formed a group to try and support the development of legislation to start a national lighting initiative. This initiative, eventually named the Next Generation Lighting Initiative, had a targeted size of \$50M/year for 10 years, and was originally modeled after Sematech, a program put in place by Senator Bingaman. The OIDA-led group involved a core of ten companies with a major US presence – General Electric, Cree, 3M, Lumileds, Kodak, Osram, Phillips Lighting, Uniroyal Optoelectronics, Corning, and Dupont. Sandia occupied a special place as an associate, non-industrial member of the group, and was the only DOE National Lab to take on this role. Sandia PM Jerry Simmons attended multiple meetings of the group from 2000 through 2003, in which the structure and functioning of the NGLI was worked out, and legislative language proposed. At these meetings Sandia also helped to identify and prioritize the different technical areas in which R&D was needed. Finally, Sandia helped identify substantial contributions that the national labs could make, and urged closer coordination of planning with the DOE. In the past year or so, the National Electrical Manufacturer's Association (NEMA) took over the coordinating role from OIDA, in part because of a desire amongst the members to coordinate even more closely with DOE.

Authorization language for Next-Generation Lighting Initiative was contained in both the House (H.R.4) and Senate (S.1766) national energy policy bills that were passed, but never made it out of conference. The Senate version authorized \$480M over 10 years for NGL research in a "Sematech"-style government/industry partnership, and contained most of the language in the original bill (S.1166) introduced by Senators Bingaman and DeWine in 2001. Despite the fact that authorization for an NGLI never was passed, appropriations for solid state lighting began to flow to DOE/EERE, beginning with \$8M in FY03 and followed by \$12M in FY04. Finally, in November of 2003, an official NGLI program was kicked off in a DOE SSL workshop in Washington DC. At present, there are both industry and national-lab calls for proposals, with Sandia participating heavily.

Because of Sandia's special position as a non-industrial entity, we were also able to play roles that industry and OIDA could not. Thus we became a major contact and provider of technical background information to Senator Bingaman's office and elsewhere. We briefed Bingaman's staff on the technical potential of solid state lighting early on, and provided technical input to the writing of Bingaman's bill and associated Senate floor

speech. Sandia organized a tri-lab (SNL, LANL and LBL) visit to David Garman, Assistant Secretary of Energy for Energy Efficiency, to brief him on SSL and apprise him of the labs' support for a national initiative. Sandia also helped to organize a National Academy of Sciences/National Research Council workshop on SSL, and provided a presentation on SSL synergisms with National Security applications. Further, we performed a detailed analysis of a report from the Energy Information Agency on the R&D provisions in the major energy bills.

In the past year or so Sandia prepared, with the help of a market intelligence and technology intelligence consulting firm, Perspectives, a series of reports on economic activity, major companies, and government-sponsored initiatives in SSL in foreign countries, with a particular focus on Japan, Korea, China, and Taiwan. These reports were specifically requested by both DOE's Office of Building Technologies and by Senator Bingaman's office. In addition to the reports, we prepared viewgraphs summarizing foreign government investments, and provided them to DOE/OBT. This was to enable program managers in OBT to brief higher officers in DOE/EERE on foreign activity, so that they might better make informed decisions about the importance of a US initiative. Presently, Sandia has a contract with the Asian Technology Information Program (ATIP) for a more extensive report on activities in Asia, using their on-the-ground personnel in those countries for more in-depth intelligence.

Finally, Sandian Jerry Simmons accompanied Senator Jeff Bingaman and Senate Energy Committee staff on a weeklong Senate CODEL (Congressional Delegation) fact-finding trip to Japan and Taiwan in December of 2003. The CODEL visited numerous energy R&D installations, government bodies involved in setting energy policy, and industrial firms involved in solid state lighting. Jerry served to provide technical support and background to Bingaman's office during the trip. (Also accompanying was Jeff Nelson, a DARPA consultant at the time, who subsequently returned to Sandia.)

One of the most important and time-consuming activities in support of a national initiative, discussed further in Section 6.4, was our co-hosting of the second technology roadmapping workshop on LED lighting. (As mentioned earlier, Sandia also co-hosted the first workshop, in October 2000 in Albuquerque.) This meeting was held in Albuquerque on May 30, 2002, and featured ~80 attendees from leading SSL research efforts at industry, universities, and national labs. The purpose of the workshop was to assemble the experts in the community to identify the technical challenges and milestones for solid-state lighting to become competitive in general-purpose lighting markets. As with the first workshop, Sandia coordinated the compilation of information and input, and had overall responsibility for the final Roadmap Report. This final Report, prepared by Sandian Jeff Tsao and exceeding 100 pages in length, was a tour-de-force which is considered by the community as a kind of bible of Solid-State Lighting via inorganic LEDs. The document contains not only an enumeration of future decision points and recommendations for future R&D activities, but also provided a comprehensive tutorial on all the building blocks that must be assembled to produce an inorganic solid-state lighting system.

6.2 Public Relations and Community Outreach (JA Simmons, JM Gee)

Throughout the course of this GCLDRD project, the team strove to publicize the concept and potential energy savings of solid state lighting. Our purposes were manifold. A first purpose was to build awareness amongst the general public and, by extension, amongst energy-related policy stakeholders. A second purpose was to increase recognition of Sandia as a leading technical innovator in SSL. A third purpose was to ensure that our SSL GCLDRD was recognized by the LDRD office and our Sandia VP champions. Accompanied, of course, by solid technical breakthroughs, these purposes meld to become a virtuous and inspiring cycle of technical progress, internal and external recognition and program support, and impact on national energy policy.

In this Section, we summarize our public relations and community outreach activities, not including our website, which is covered separately in Section 6.5.

6.2.1 Print Media

Sandia's work on SSL was featured in numerous print articles. These included not only trade journals, but general interest magazines and newspapers. In addition, many trade journals published short notes announcing the existence of our SSL website, discussed below. Trade journals which printed articles on solid state lighting, and specifically mentioned Sandia, included EE Times, Electronic Materials Update, Electronics Weekly, Laser Focus World, Scientific American, Electronic Business News, Electronics Times, Design News, Compound Semiconductor News, and the Federal Technology Report. Particularly long feature articles appeared in the prestigious journals Business Week, The Economist, IEEE Spectrum, and MIT Technology Review. Sandia SSL personnel were also interviewed numerous times for private paid-subscription newsletters that wrote full technology profiles, such as Emerging Technology Currents.

We also received considerable newspaper coverage. Sandia personnel were interviewed multiple times by Barnaby Feder of the New York Times, and SNL was included in the draft article he wrote, but the Times editors ended up deleting the sections that discussed SNL's work in order to fit it into their allotted space. Nonetheless, the article gave a lengthy exposition of SSL. The Albuquerque Journal published a front page article, "Bingaman Thinks LEDs a Bright Idea," by John Fleck, on Nov. 10, 2003. The article gave prominent coverage to Sen. Bingaman's push for a national initiative on SSL, as well as to Sandia's Grand Challenge project. The article was also carried on the Associated Press newswire.

6.2.2 Radio and Broadcast Television

Sandia also received some television and radio coverage. The first of these was a piece by Cynthia Graber of Living-On-Earth, a 30 minute radio show on National Public Radio. The show entire show focused on SSL. The 7 minute piece by Graber focused on the energy savings potential of SSL, and featured voice clips from Sandian Jerry Simmons, Secretary of Energy Spencer Abraham, and Vice President of Color Kinetics, Kevin Dowling. The second piece, also 7 minutes and by Susan Shepard, focused on the use of LEDs integrated with solar photovoltaics to bring lighting to poor and remote areas of the world without electricity transmission lines, and interviewed Dave Irvine-Halliday of the Light-Up-the-World foundation.

Subsequently, ScienCentral, a video production company in New York, supported by the National Science Foundation which supplies pieces on science to NBC news and other video news outlets, sent a camera crew to Sandia to do a piece on SSL. This resulted in a 2 minute video clip on Sandia's program, hosted by Julia Schulhof, which was supplied to all NBC local news affiliates and aired throughout the country in the summer of 2003.

Shortly afterwards a camera crew and reporter arrived from Belos, a company which owns a large number of local television stations in the Midwest and Southwest, including, up until recently, Albuquerque's KASA. The Belos crew filmed a 4 minute segment on solid state lighting, with about half of it focused on Sandia's activities, which aired on the Texas Cable News Network.

Finally, Sandia also filmed an internal "Life at the Labs Clip" which aired for a brief time on the Sandia internal video network.

6.2.3 Summary of Media Coverage

Together, this media coverage was very important not only for Sandia's role in the solid state lighting community, but for promoting the concept of solid state lighting in general. Sandia continues to reap the benefit of these activities, and they have likely helped SSL secure its well-deserved role as a major tool in the toolbox for increasing the nation's and the world's energy efficiency and for protecting the environment.

A list of the most important media coverage is given here:

- Small Times, Jan 27, 2004, "Quantum Control Holds the key to a Shining LED Lighting Market," briefly covered Sandia's activities in quantum dot research, http://www.smalltimes.com/document_display.cfm?section_id=93&document_id=7305.

- "Sandia UV LEDs emit record power" 20 November 2003, Optics.org news, <http://optics.org/articles/news/9/11/14/1>.
- "Bingaman Thinks LEDs a Bright Idea", November 10, 2003, Albuquerque Journal, <http://www.abqjournal.com/paperboy/ia/scitech/108069science11-10-03.htm>.
- "A Billion Points of Light," EDN, September 2003, <http://www.reed-electronics.com/ednmag/contents/images/318734.pdf>.
- "A Laser in Your Lightbulb," Business Week, Oct 27, 2000, http://www.businessweek.com/bwdaily/dnflash/oct2000/nf20001027_054.htm.
- "Bringing home a brighter future," and associated video clip featuring Jerry Simmons and Mary Crawford, Dallas Morning News/Belo Interactive, August 4, 2003.
- "Light Switch," and associated video clip featuring Jerry Simmons, ScienCentral News, August 14, 2003.
- "LEDs vs. the Light Bulb," Technology Review, May 2003.
- "Revolutionary Lighting," Living On Earth (NPR) radio segment, November 1, 2002.
- "Let There Be Light," and "Government Funds Energize Solid-State Lighting," IEEE Spectrum, September 2002.

6.3 White Papers and Specialized Reports (JY Tsao, AE Miksovic, MA Monson, KW Boyack, N Rahal)

Sandia also engaged in a number of activities aimed at defining the high-level technical and economic issues associated with solid-state lighting. These include:

- The initial white paper catalyzing national interest in Solid State Lighting. This paper was first presented at a Washington, D.C. OIDA Forum in October, 1999, by R. Haitz, F. Kish, J.Y. Tsao and J. Nelson, "The Case for a National Research Program on Semiconductor Lighting," and is available from the Optoelectronics Industry Development Association (www.oida.org) and at <http://lighting.sandia.gov>.
- The Year 2000 Review of Japan's "Light for the 21st Century" Project, translated by K.V. Sereda and J.Y. Tsao, Mar 29, 2002, available from the Optoelectronics Industry Development Association (www.oida.org).
- Economic projections of technology progress for various levels of U.S. national investment in Solid-State Lighting R&D (J.Y. Tsao, unpublished).
- Database and map of U.S. SSL-related patents. The database was created using a keyword search, combined with a one-level citation expansion, followed by manual filtering, resulting in roughly 1000 patents. From that database, a visual map was also created, by Kevin Boyack and Jeff Tsao, using Sandia's VxInsight software along with lexical+manual similarity metrics for determining the sub-technology clusters. The result is shown in Figure 1, where each dot represents a patent, and the various mountains of dots have been identified with the various technical challenge areas developed in the 2002 SSL Roadmap.
- Invited overview articles and international conference overview presentations, including E. D. Jones, "LED Solid-state Lighting for Illumination: Status Report," SPIE Conference, 2001 SPIE Conference, January, 2001, San Jose, CA.; J. A. Simmons, "The Solid-State Lighting Initiative: Synergisms with Office of Science Materials Science Programs," Energy Materials Coordinating Committee, March, 2001, Washington, DC.; J. M. Gee, J. A. Simmons, T. E. Drennen, "Solid-State Lighting Initiative and Synergisms with National Security," Optical Society of America, 2001 Annual Meeting, October, 2001,

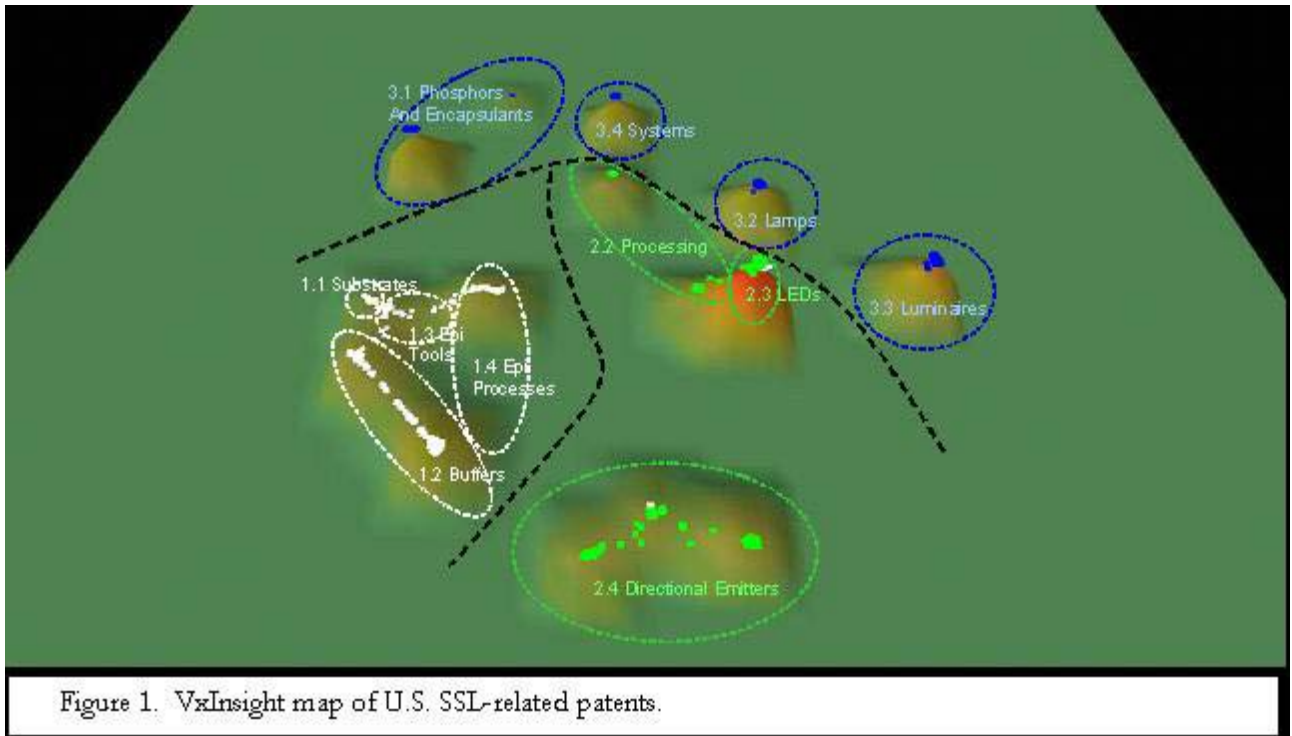


Figure 1. VxInsight map of U.S. SSL-related patents.

Long Beach, CA.; J. A. Simmons, "Fundamental Science Needs for Solid State Lighting," Basic Energy Sciences Forum on Basic Research Needs to Assure a Secure Energy Future, October, 2002, Gaithersburg, MD; J. M. Gee, J. Y. Tsao, J. A. Simmons, "Solid-State Lighting Research at Sandia National Laboratories," Workshop on Solid-state Lighting, Georgia Institute of Technology, February, 2003, Atlanta, GA; J. A. Simmons, "The Next Generation Lighting Initiative," Phosphor Global Summit 2003, March, 2003, Scottsdale, AZ; J. A. Simmons, "Solid State Lighting Research at Sandia National Laboratories," 203rd Electrochemical Society Meeting, April, 2003, Paris, France; J. M. Gee, J. Y. Tsao, J. A. Simmons, "The Role of GaN Semiconductors in the Solid-State Lighting Revolution and Synergisms with National Security," 2003 Military Sensing Symposium, Materials Specialty Group, February, 2003, Tucson, AZ; J. Y. Tsao, "The U.S. 'LEDs for General Illumination 2002' Roadmap," Laser Focus World, June, 2003; J. Y. Tsao, "The U. S. Solid-State Lighting Roadmap: Targets and Technical Challenges," 2003 International Conference on Compound Semiconductor Manufacturing Technology, May, 2003; J. M. Gee, J. Y. Tsao, J. A. Simmons, "Fundamental Science Initiatives to Enable the Solid-state Lighting Revolution," LED 2002 Conference, Intertech, October, 2003; J. Y. Tsao, "Materials Issues in Solid-State Lighting," AVS 50th International Symposium, November, 2003; J.Y. Tsao, "Solid-State Lighting: Lamps, Chips and Materials for Tomorrow" in IEEE Circuits and Devices (May/June 2004 Issue).

- Various technology focus reports commissioned by Sandia from Perspectives to help understand specific subtechnologies associated with Solid-State Lighting. These include reports on: OLEDs, use of phosphors in LEDs, gallium nitride initiatives and developments at various federal agencies, and LED quantum efficiencies and other key performance characteristics.
- Global context reports commissioned by Sandia from Perspectives to help understand Solid-State Lighting R&D levels in Japan, Korea, Taiwan, and other Pacific Rim countries, as well as Europe.
- Company profiles, some performed internally by M.A. Monson, and some commissioned by Sandia from Perspectives, to better understand partnering opportunities.

6.4 U.S. SSL Roadmaps (JY Tsao, ED Jones)

In response to the growing interest in a national-level program to accelerate technical progress in solid-state lighting, the U.S. Department of Energy Office of Building Technologies, through the Optoelectronics Industry Development Association, sponsored the creation of a series of U.S. SSL Roadmaps.

The objectives of these roadmaps were to:

- reach an industry consensus on the major commercial and military applications of solid-state lighting
- enumerate the technology milestones necessary to support these applications, and reasonable timescales, consistent with major national R&D investment, for achieving them
- identify the critical research and development challenges necessary to meet the technology milestones

The roadmaps drew on contributions from all resources in solid-state lighting: industry, academia and national laboratories. The first two roadmaps were completed in March, 2001. The first, “Light Emitting Diodes (LEDs) for General Illumination: An OIDA Technology Roadmap,” was compiled and edited by Eric Jones at Sandia National Laboratories. The second, “Organic Light Emitting Diodes (LEDs) for General Illumination: An OIDA Technology Roadmap,” was compiled and edited by Milan Stolka, an independent consultant to DOE. These two roadmaps summarized workshops held in Albuquerque, NM and Berkely, CA in October-December, 2000.

By 2002, the two roadmaps were in need of updating. The SSL-LED roadmap update was compiled and edited by Jeff Tsao at Sandia National Laboratories; the SSL-OLED update was compiled and edited by Milan Stolka. Because of the greater maturity and importance of SSL-LED technology, its roadmap was updated more comprehensively. The various stages in this updating process were:

- 2002 Feb. To initiate the Roadmap, OIDA (Arpad Bergh), in consultation with DOE (Jim Brodrick) and NEMA (Kyle Pitsor) identified a facilitator (Jeff Tsao, Sandia) and a technical steering committee (George Craford, LumiLeds, Michael Coltrin, Sandia, Steve DenBaars, UC Santa Barbara, and Jim George, Permlight). Then, OIDA, the facilitator and the steering committee identified the scope of the Roadmap update and the invited speakers for the workshop.
- 2002 Mar-May. Based on a number of primary references identified by OIDA, the facilitator, the steering committee and the invited speakers, the facilitator created a first-draft Roadmap, including introductory material and a comprehensive set of technical targets, challenges and possible approaches.
- 2002 May 30. A technical workshop was held in Albuquerque, NM. The workshop brought together experts from Universities, National Laboratories and Industry. These experts heard invited talks in various technical challenge areas; and in breakout sessions debated and fleshed out the targets, challenges, and possible approaches outlined in the first-draft Roadmap. They also binned the individual challenges by risk and reward, and identified reviewers for them.
- 2002 Jun-Jul. Based on comments and discussion at the May 30 workshop, the facilitator created a more-comprehensive second-draft Roadmap, including a revised set of technical targets, challenges and possible approaches. Explanatory background text was also added. This second-draft Roadmap was sent (in stages) to the steering committee and to the reviewers identified at the workshop.
- 2002 Jul-Aug. Based on final comments from the steering committee and from the individual challenge reviewers, the facilitator created a third-and-final-draft Roadmap. Figures and references were also added.
- 2002 Aug. Finally, the Roadmap was separated into, and released in, two parts: a Roadmap Update 2002, which summarizes the Targets, Decision Points, Challenges and Possible Approaches; and a Roadmap Tutorial, which provides more detail on the Targets, as well as introductory material to the various Challenge Areas.

- 2004 Jan. A complete version of the Roadmap, including the Update and the Tutorial, was released to the public.

6.5 SSL Website (JY Tsao, AE Miksovic, DC Meister, AO Pinson, MJ Pinzon)

6.5.1 Introduction

Sandia's Solid State Lighting website (<http://lighting.sandia.gov>) was launched in April 2002 to serve as a comprehensive information source on semiconductor LEDs. The information provided on the website is accessible to a wide audience -- from those with little technical background to experienced researchers in the field. The site's primary focus is on white LEDs and white LED lighting applications. The site also includes information on related materials, substrates, manufacturing techniques, packaging, legislation, and funding. The site is updated biweekly. The site was developed with the collaboration of Perspectives, a market intelligence and technology intelligence consulting firm. Perspectives maintains the website and develops most of the website content, in collaboration with the SNL SSL team.

6.5.2 Overview of the Sandia Solid-State Lighting Website

The website organization is designed to provide the user with both breadth and depth of information. Each section leads with non-technical information, but includes a large number of links to online publications, databases, and detailed technical information. This allows individuals new to solid-state lighting to understand the topic, while providing technical detail to specialists in the subject.

The data on the website have been drawn from regular searches of a wide range of data and information sources. These sources include patent databases, technical literature databases, online newsletters, news wires, company press releases, conference proceedings, review articles, federal and local funding databases, government solicitations, conference announcements, and discussions with industry experts. Additional sources of information include technical literature, presentations, and white papers developed by Sandia researchers and Solid-State Lighting team members. This information is reviewed regularly by researchers at Perspectives and Sandia for relevancy to the Solid-State Lighting Grand Challenge mission. The relevant information is then organized, categorized and posted on the web.

To facilitate navigation of the website, it is divided into 7 key sections, as illustrated in Figure 2:

- Overview
- National Initiatives and Programs
- Worldwide Links
- Science and Business News
- Patent database
- Calendar
- Solid-State Lighting at Sandia

Each of these sections is described below.

The **Overview** section discusses the vision behind the website and provides an overview of the benefits of switching to solid-state lighting from current lighting technologies. An overview of the challenges needed to be overcome if solid-state lighting is to be achieved is also given. Links are provided to selected recent review articles. In addition, an FAQ is provided that highlights the main issues and benefits of solid-state lighting.

The **National Initiatives and Programs** page provides an up-to-date overview of the US's **Next Generation Lighting Initiative (NGLI)**. NGLI seeks to accelerate the development of solid-state lighting

science and technology through a partnership of industry, university and national laboratories in order to more quickly attain the energy, environment and national security benefits of switching to solid-state lighting. This section provides a history of the initiatives and provides links to the full text of the legislation, speeches by Secretary of Energy Spencer Abrams, white papers authored by Sandia scientists and other groups, and links to organizations such as OIDA, NETL, and NEMA that have been active in drafting and lobbying for passage of this bill.

The National Initiatives and Programs page also provides a brief description, with links, to major publicly-funded solid-state lighting research initiatives at DARPA, the Office of Naval Research, Sandia National Laboratories, and Lawrence Berkeley National Laboratory. Finally, the section provides a brief overview of foreign solid-state lighting initiatives, such as Japan's Light for the 21st Century initiative, as well as information on European solid-state lighting initiatives.

A detailed list of links to organizations involved in solid-state lighting research can be found on the **Worldwide Links** page. This includes links to professional societies, magazines and online resources, non-profit organizations, and national and international laboratories and agencies.

The **Science and Business News** portion of the website provides late-breaking news about research breakthroughs, key industry developments, and commercialization of new lighting products. This part of the site contains a "Headline News" section that is updated biweekly by Perspectives. The Headline News provides quick access to information on the major developments in industry, academia, and government.

The Science and Business News section provides links to Science, Business and Technology tracking reports provided by Perspectives to the Sandia SSL team in support of their research and commercialization endeavors. These reports are published and added to the website bimonthly. The reports detail all the important developments in industry, academia, and government with respect to solid-state lighting. This includes not only developments relating specifically to white LEDs and white LED-based fixtures, but also advances in all areas of substrate manufacture and development, and packaging and reliability. Each report contains:



SOLID-STATE LIGHTING



Illumination through Semiconductor Science

Semiconductor light emitting devices, once limited to a narrow range of colors, now span nearly the entire visible spectrum. Someday, they may be bright, efficient and inexpensive enough to replace vacuum tubes for white lighting. Energy consumption and environmental pollution would be reduced, and the quality of the human visual experience would be enhanced, dramatically. Yet, enormous challenges lie ahead.

This web-site, which gathers together information and links relevant to Solid-State Lighting, is intended to help stimulate the development of the science and technology foundation, and the national initiatives, necessary to overcome these challenges.

Figure 2. Home page of SSL website, along with percentage of hits associated with website sub-pages.

- A detailed news section provides a complete listing of all news items relating to solid-state lighting during the period covered by the report. This supplements the Headline News section by providing additional information on the major events, as well as a large number of additional news stories relating to solid-state lighting. A typical news section might contain in excess of one hundred news stories.
- A scientific literature section, which provides a complete bibliography of solid-state lighting-related technical literature published during the period of the report. The bibliography includes links to journals and abstracts where these are publicly available online. A typical scientific literature section might contain 120 or more bibliographic references with links to additional information.
- A complete list of intellectual property claims published during the reporting period. This includes US Patents and US Patent Applications, European patents and patent applications, WIPO claims, INPADOC documents. Claims filed in various European and Asian nations, such as Japan, Germany, Australia, and New Zealand, are included as well. Typically, a patent section will include about 200

published claims. Towards the beginning of FY2004, these intellectual property listings were removed from the website, due to liability concerns.

The **Patent Database** section contains a list of US issued patents specifically related to white LED lighting. This patent list, along with analyses of the patents, was developed by Sandia in conjunction with Perspectives. Towards the end of FY2003, this part of the website was removed from the website, due to liability concerns.

The **Calendar** section of the website provides a list of upcoming conferences, symposia and workshop, organized by date, relating to solid-state lighting. Links are provided to details about the events, including overviews and agendas where available. The calendar is updated by Perspectives on a quarterly basis.

Finally, the **Solid-State Lighting at Sandia** portion of the website provides information on Sandia's contributions to solid-state lighting. This section:

- Summarizes Sandia's support for solid-state lighting as a whole, providing links to speeches by Sandia's former VP for Science and Technology Alton Romig, by Jerry Simmons, Jeff Tsao and other Sandia researchers involved in Solid-State lighting research and policy. Links to Sandia solid-state lighting related press releases are provided, as well as links to selected news stories about Sandia's solid-state lighting research that have appeared in the popular press.
- Details Sandia's Grand Challenge LDRD "[A Revolution in Lighting: Building the Science and Technology Base for Ultra-Efficient Solid-State Lighting.](#)" The summaries are supplemented with links to white papers and publications by Sandia researchers participating in the Grand Challenge in the areas of MOCVD science and technology, materials growth and physics, device fabrication and physics, and packaging and other issues. Links to bibliographies of scientific publications, intellectual property claims, presentations and other documents published by Sandia researchers in the area of solid-state lighting can be found in this section of the website.
- Provides an overview of Sandia's semiconductor materials and fabrication capabilities, providing links to Sandia's Center for Compound Semiconductor Science and Technology, the Microelectronics Development Laboratory, the Center for Integrated Nanotechnology, the Photovoltaics Systems Group, and the Microsystems and Engineering Science Applications Complex (MESA). Links to Sandia's Physical and Chemical Sciences, Microelectronics and Photonics, and Materials and Process Sciences divisions are also provided.
- The final portion of this section is an image database that provides access to a database of solid-state lighting related documents and publications available from Sandia. Free registration is required to access this portion of the site.

6.5.3 The Website has become an important public resource

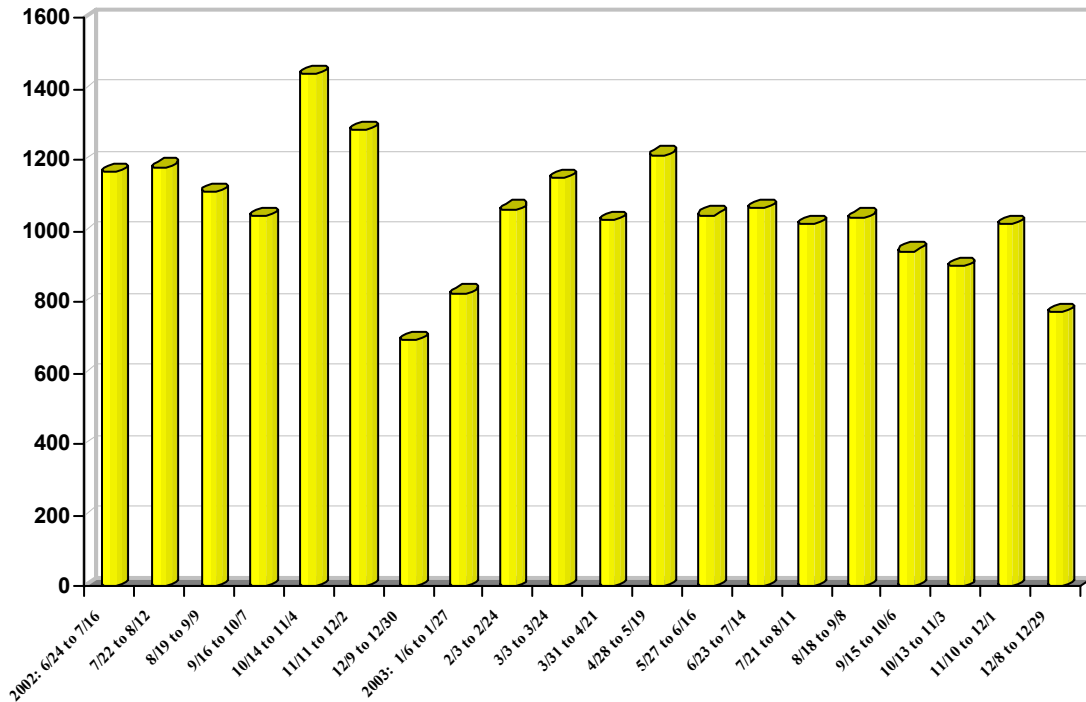
The website has become an important public resource. In an average month, the Solid-State Lighting website home page alone receives 1050 hits. Although there is some variation in this number, with the month of December being an annual low point for hits, the number of visits has been fairly constant over the life of the website, as shown in the graphic below.

In an average month, 387 unique visitors make a total of 690 visits to the website and view a total of 5,477 pages (averaging 8 pages viewed per visit and 14 pages viewed per unique visitor).

In an average week, the Science and Technology News portion of the website receives 96 hits with just over half of these hits (n=49) clicking through to the Headline News section. On average, in a given month approximately 400 hits are made on the Science and Technology News portion of the site, of which approximately 200 hits are on the Headline News section that is updated biweekly.

The public is not only very interested in what is going on in the SSL community at large, but also specifically in the work being conducted at Sandia. The "Solid State Lighting at Sandia" main page has an average of 87.5 hits per week (approximately 350 per month).

SSL Website: Homepage Hits Per Month (Average = 1050)



Other portions of the website also constitute an important community resource, as is shown by the hit rates for selected pages in the table below:

Page	Average weekly hits	Average monthly hits
Overview	146	584
FAQs	73	292
National Initiatives	44	176
WW Links	41	164
Calendar	38	152
Calendar Archive	47	188

6.5.4 Summary

The Sandia Solid-State Lighting website has fulfilled its goal of becoming and remaining an important resource for the solid-state lighting community. The website statistics show continued high rates of use of the site by community members. Site visitors are particularly interested in the Headline News, the Science and Technology Tracking Reports, and the information on Solid-State Lighting activities at Sandia, suggesting that these sections of the website in particular are of lasting interest and value to members of the Solid-State Lighting community as a whole.

With the Sandia Solid-State Lighting Grand Challenge LDRD in the latter part of its final year of funding, Sandia has sought outside support for the Solid-State Lighting website. Recently, the US Department of Energy's National Energy Technology Laboratory has agreed to fund continued development of the website through March 2005, including the production of the Science, Business and Technology tracking reports and the regular addition of headline news in the Science and Business News portion of the website.

6.6 Life after LDRD: SSL Follow-On Programs (JA Simmons, JM Gee)

From the outset, the Solid State Lighting Grand Challenge LDRD set as a major goal the development of follow-on programs which either directly continued our SSL research activities, or built upon them in a synergistic manner, such as using SSL-related GaN technology for deep-UV LEDs for chem.-bio detection or for high-power solid state amplifiers for micro-synthetic aperture radar. Of course, the biggest potential source of follow-on programs was considered to be the U.S. government-sponsored solid state lighting national initiative, or the Next Generation Lighting Initiative.

The SSL team had good success in developing such follow-on programs from the very beginning, with our first program starting roughly a year after the beginning of the GCLDRD. In FY02 and FY03 alone, the SSL team's external programs generated more than \$7 million in support – even more than the \$6.9M invested by Sandia during the project's three-year life as an LDRD Grand Challenge.

In this Section, we summarize those follow-on programs that are either active or proposed. We anticipate many other follow-on programs that build on the SSL GCLDRD capabilities, for which opportunities for formal proposals have not yet arisen.

6.6.1 DOE/OBT “Development of Key Technologies for White Lighting Based on Light-Emitting Diodes” (FY02-FY03)

Sandia Funding: FY02 - \$437K; FY03 - \$500K.

The proposal for this project was submitted barely three months after work on the GCLDRD had begun. It was submitted to a DOE Office of Building Technologies call for advanced lighting technologies, which specified that the project be industry-led, with no more than 50% of the funding going to a subcontractor. The proposal was joint between Sandia and Lumileds (a joint venture between Philips Lighting and Agilent Technologies), and requested 500K per year each for Sandia and Lumileds, for a duration of two years. The proposal focused on three thrust areas: (1) use of low dislocation density substrates created by Sandia's cantilever epitaxy process for higher efficiency blue and near UV LEDs; (2) development of in-situ monitoring techniques for wafer temperature and epitaxial film stress to enable better control over MOCVD-based LED growth techniques; and (3) investigation of the use of nanometer-sized nanocrystalline clusters of II-VI compound semiconductor materials for use as efficient replacements for conventional phosphor materials.

A slight wrinkle developed when our proposal was approved in December of 2001: while Lumileds received the full requested amount of \$500K per year, Sandia was only awarded \$250K per year. Both Sandia and Lumileds wrote letters to DOE over this development. Ultimately, we achieved an agreement whereby Lumileds and Sandia received 437K each during the first year, and then 500K each during the second year of the proposal. We note that Lumileds thus offered to have their requested funding amount reduced in order to supplement funds going to Sandia. As we will see below, this is something they chose to do again later, a strong indicator of the value they see in collaborating with Sandia. The work was covered by a non-funds-in CRADA with Lumileds.

This project was concluded in the fall of 2003, and overall was considered to have been very successful by Sandia, Lumileds, and DOE's Office of Building Technologies. Indeed, at the DOE workshop on SSL in Nov. of 2003, Lumileds' Mike Krames gave a talk in which he showed that the emissivity correcting pyrometry, developed by Sandia as an in-situ temperature monitoring technique, enabled Lumileds to reduce the wavelength-variation in their growth of LEDs by a factor of four.

6.6.2 DARPA “Semiconductor UV Optical Sources” (FY02-FY05)

Anticipated Sandia Funding (assuming the team can meet its performance goals): FY02 - \$400K; FY03 - \$1,000K; FY04 - \$1,200K; FY05 - \$800K.

In January of 2002, in response to a call for proposals from DARPA, Sandia submitted a proposal to develop bioagent detectors (focused particularly on anthrax) based on UV-induced fluorescence. Sandia's proposal had three thrusts, and two participants.

The first thrust was to develop UV LEDs, at the two target wavelengths of 340 nm and 280 nm, with a brightness as high as possible. (We note that at the time of the call, no LED had ever been demonstrated at wavelengths below about 340 nm, and the optical output powers were in the range of a few microwatts.) This thrust was to be carried out entirely by Sandia, and involved the same group that was working on solid state lighting. The work involved extending our efforts on (Al)(In)GaN LED growth to compounds containing higher amounts of aluminum and hence shorter wavelengths. The DARPA program manager, John Carrano, had been on Sandia's SSL EAC, and was aware of our capabilities.

The second thrust was to develop an optical testbed and a prototype detector system, in which the fluorescence of anthrax-simulants would be tested and detectivities measured. This thrust was also to be done entirely by Sandia, but it involved individuals who were not a part of the SSL group.

Finally, the third thrust was to transfer the UV-LED technology to industry, and develop manufacturable processes. This last thrust involved primarily Uniroyal Optoelectronics, an industrial firm in Florida, with a small amount of activity on the part of Sandia.

Initial Award. We were awarded the proposal in the spring of 2002, with a funding amount of \$4.5M over a little less than 4 years. About 35% of this was for the test-bed prototype development at Sandia, and about 15% was for tech transfer to Uniroyal, with the remaining 50% to go to UV LED research and development at SNL. Our first funding installment of 400K arrived in May of 2002.

Changes in Program Scope. However, within about 6 months there appeared some problems in the project, with which our DARPA program manager was quite unhappy. The testbed work was proceeding slowly, with the initial progress mainly being to reproduce fluorescence test results obtained in a similar, related project that had ended a year earlier. In addition, there were some discussion between DARPA and Uniroyal related to a separate, unrelated, proposal that Uniroyal had submitted. As a result of these two developments, DARPA instructed Sandia to cancel the test-bed development task, to cancel the tech transfer task, and to subsequently focus solely on the development of UV-LEDs. Our funding was correspondingly reduced to cover only this task, to about 50% of the original award.

To date, Sandia has received four funding installments on this project: the aforementioned amount of 400K, a second installment of 600K, and a third installment of 700K in the fall of 2003. Based on our excellent performance on the project during the past year, in which we broke previous world records for power output at wavelengths shorter than 300 nm, we received an additional plus-up in funding of 200K in the spring of 2004. Thus the total funding received to date through the DARPA SUVOS program is \$1.9M. The program is expected to continue for at least another year, and we anticipate that Sandia will receive additional funding of 700K or more in the coming year.

A short word is in order about our breakthroughs. In the past 8 months Sandia achieved 1.34 mW power output at 289 nm, and about 0.5 mw at 275 nm. These figures were nearly a factor of ten larger than what had been achieved previously. In addition, the spectral purity of the LED emission was considerably better than previous achievements by other groups. In addition, Sandia has supplied multiple packaged 290 nm LEDs to MIT-Lincoln Laboratory, which they have used in a non-line-of-sight communications demo, one of the sub-goals of the DARPA program. As a result of these achievements, Sandia was given two awards from DARPA at the SUVOS program review in November of 2003. Just recently, Asif Kahn's group at the Univ. of South Carolina has reported results that are about 50% better than Sandia's. We, of course, have something in the pipeline that we think may exceed this. And, so, the horserace continues!

6.6.3 DARPA "UV VCSEL Arrays" (FY03)

Sandia Funding: FY03 - \$350K.

A second opportunity with DARPA developed in the Fall of 2002. The DARPA SUVOS program manager John Carrano suggested we contact another DARPA program manager to discuss a GaN light emitter need.

Eventually, we ended up in conversations with DARPA's Doug Kirkpatrick, who was managing a program on the synthesis of DNA in large 2D arrays of fluidic synthesis cells for their "MicroBio" Program. To obtain programmatic control of the DNA in each cell, the program needed to be able to controllably illuminate each fluid cell independently with near-UV light, of wavelength near 365 nm. DARPA's program participants had been doing this with a single table-top laser and a micro-mirror array, but felt that the solution was bulky and inefficient. They requested that Sandia attempt to develop a 2D array of electrically injected VCSELs operating at 365 nm.

Sandia approached this project with considerable trepidation. At the time, the shortest wavelength VCSEL ever to have been demonstrated was a 383 nm VCSEL created by Sandia and Brown University in late 2000. Even that had only been optically pumped rather than electrically injected. To date (April 2004) no other group has succeeded in reproducing those results. Creation of a VCSEL at 365 nm would be substantially more difficult, since that wavelength corresponds to an energy higher than that associated with the bandgap of GaN. Achieving this energy thus entails adding Al to the quantum well material, which always renders the problem much more difficult. In addition, any MOCVD-grown distributed Bragg reflector (DBR) mirrors could not have any pure GaN layers, since they would absorb 365 nm light. Rather, any such mirrors would need to be composed of alternating layers of AlGaIn of two different Al compositions. If one adds to this the additional task of electrical injection, the demonstration of a single 365 nm VCSEL appears virtually Herculean. A project to demonstrate a 2D array of such devices, was, in our opinion, almost certain to fall far short of its goals. However, Sandia's attempts to negotiate a project on the technically less challenging goal of 385 nm VCSELs did not meet with success.

Despite the fact that we made this assessment quite clear to DARPA, they informed us that they wanted us to go ahead with the project. As a result, we submitted a proposal on "Development of a 2D Array of 365 nm VCSELs" in December of 2002, requesting \$2,000K in funding over two years. We made it quite clear in the proposal that we considered the project very high risk, and that we were prepared to finish early in the event that we did not achieve our first year milestones. The project was approved and we received our first funding installment of \$500K in March of 2003. We began work, and had a meeting with one of the other program participants who was primarily involved in the bio-aspects of the program, to better understand their needs. Work on active layers and on DBR growth was initiated.

Cancellation of DARPA's Program. Unfortunately, the entire DARPA MicroBio program was abruptly cancelled in September of 2003. This included not only Sandia's projects, but all other projects being performed by universities and other institutions. The cancellation occurred at a time when DARPA was under particular scrutiny by Congress, and was related to concerns about research into the general area of DNA synthesis, rather than to specific concerns about program performance. As a result, Sandia's project was cancelled after only about 350K of the total 2,000K award had been expended.

6.6.4 DOE/EESI "Photonic Crystal LEDs" (FY03-FY04)

Sandia Funding: FY03/04 - \$500K.

In the spring of 2002 Sandia and Lumileds submitted a joint proposal to the DOE's Office of Energy Efficiency and Renewable Energy, in response to their annual Energy Efficiency Science Initiative (EESI) call for proposals. Our proposal was on photonic crystal LEDs, a high-payoff high-risk topic about which both SNL and Lumileds were becoming increasingly excited, and in which we had already begun some preliminary work. Indeed, Sandia, Lumileds, and Stanford had already submitted a joint proposal on photonic crystal LEDs to the ATP program in October of 2001.

DOE's EESI program is focused on solving some fundamental science problems which would have a strong impact on EERE missions. The EESI program typically awards only one proposal each year, and covers all EERE areas, including solar photovoltaics, fossil fuels, building windows and insulations, and nuclear. Hence, the program is extremely competitive.

The internal DOE decision over whether to fund the Lumileds/Sandia/Stanford proposal was quite lengthy, and we did not receive any formal feedback concerning the proposal for two years. We finally received notice in

July of 2003 that the Lumileds/Sandia proposal would be funded. However, although Sandia and Lumileds had requested 500K per year each over a two year period, we were informed that we would only receive a total of 500K for the entire project, 1/4 of the requested amount. We were, however, told that we could spend it in as little as 12 months.

Faced with this situation, Lumileds opted to deliver their share of the funding to Sandia, so that Sandia could receive the full 500K. Sandia anticipates, however, continuing to collaborate on this important topic with Lumileds, with the likelihood of an eventual CRADA agreement. DOE agreed to this arrangement, and so all three parties have moved forward. Sandia chose to budget spending of its 500K over an 18 month period, and the project commenced with a kick-off meeting in January of 2004. At the time of the writing of this report, the project is continuing on track.

6.6.5 DOE/OBT “SSL Website” (FY04-FY05)

Anticipated Sandia Funding: FY04 - \$70K; FY05 - \$70K.

In addition to the above technical research projects, Sandia recently received funding to support its website on solid state lighting, <http://lighting.sandia.gov>. This website, described in detail in Section 6.5, is an effort to give a comprehensive overview of solid state lighting, and to serve the entire solid state lighting community with detailed information, links to online publications, and a breaking news section which describes news items of interest to the community, including product announcements, and science and technology breakthroughs. The website was launched in April of 2002 and was funded with SSL GCLDRD funds.

At a DOE-sponsored workshop on SSL in Nov. of 2003, it became apparent that the website had developed a strong following. Numerous university and industrial researchers made public endorsements of the utility of the website, and expressed a strong preference for having it continued. At this stage, it had become clear that Sandia only had funds available to continue the website until April of 2004, and we had solicited support from DOE to continue the site. Due to the endorsements of the site by the community, DOE agreed to fund us for one year beginning in April of 2004 and supplied us with 140K for this purpose. They also expressed to us their expectation that support of the site be transitioned over to the Next Generation Lighting Consortium of industrial firms over the next couple of years, with perhaps half the 140K operating costs being assumed by the Consortium in the second year, and all of the costs in the third year. The site is being revamped at present to better meet DOE needs and expectations, and continues to be heavily visited.

6.6.6 DOE/BES “Luminescence in Wide-Bandgap Semiconductors” (FY04-FY07)

Anticipated Sandia Funding: FY04 - 120K; FY05 - 440K; FY06 - 440K; FY07 - 440K.

In the spring of 2003, Sandia began to broach the idea to BES of a new-start project dealing with some of the fundamental science mysteries that were standing in the way of significant advances in solid state lighting. One topic in particular seemed very well suited to a BES-type project: compositional phase separation in InGaN quantum wells, and its effect on carrier transport and radiative and non-radiative recombination. This problem is believed to lie at the heart of the difficulty in making green LEDs. Pure GaN emits at a wavelength of about 380 nm, in the near UV, but these LEDs have quite low internal quantum efficiencies, on the order of a few percent. As In is added, the wavelength shifts out to longer wavelengths, moving into the violet and blue. Concomitantly, the internal quantum efficiency increases dramatically, reaching levels around 50% in the blue, at around 425 – 450 nm. This is believed to be due to In rich regions phase-segregating out of the quantum well, created localized potential wells where the electrons and holes are trapped, increasing their oscillator strength and hence the efficiency of radiative recombination. It is also believed that this helps keep excitons away from non-radiative defect centers associated with, for example, threading dislocations. However, conclusive evidence of this phenomenon does not exist and the explanation remains speculative.

Deepening the mystery is the fact that further increasing the In content, so that the wavelength moves to longer than 450 nm, results in a slow decrease in internal quantum efficiency, until it again reaches values of a 1 % or so near 550 nm. This is unfortunate, since 550 nm is at the peak of the eye response curve, and phosphide materials, typically used for red and yellow LEDs, also begin to fail in this region. If an LED of 50% internal

quantum efficiency could be made in the green, that would be a dramatic step in achieving the ultimate SSL goals of 200 lumens/Watt. The origin of the decrease in InGaN emission efficiency beyond 450 nm is believed to be due to an increasing role of polarization fields as the In segregates out.

After receiving encouraging comments from BES, Sandia submitted a new start proposal to systematically address the science issue of luminescence in these wide bandgap alloys based on InGaN. The proposal requested \$1M per year over three years, and was submitted on Oct. 1, 2003. In May, 2004, we received notice that the proposal was approved, though at a reduced budget level of \$440K per year beginning FY05. This is in addition to \$120K of preliminary seed funding we received from BES for the project in FY04.

6.6.7 DOE/OBT National Lighting Initiative (FY04-FY06)

As part of their ramp-up to full operation of the Next Generation Lighting Initiative, DOE issued two calls in March of 2004 for research and development activities in core technologies for SSL. One call targeted universities and small businesses, and one was restricted to DOE National Laboratories. The focus was more on fundamental science and technology investigations, rather than on technology demonstrations, and included topics relevant to both organic LEDs and inorganic LEDs. A total of \$6M was available in the National Lab call, to be spread over multiple years.

Sandia was included as a subcontractor on several calls submitted by universities and small businesses, including Rensselaer Polytechnic Institute, Superior Micropowders, and two from Arizona State University. (Subcontract amounts were limited to 10% of total requested funds.)

In addition, Sandia submitted 10 different proposals in response to the National Lab call. This was necessary, since the call instructions specified that no more than one technical approach could be included in each proposal. Given our wide variety of activities and capabilities in solid state lighting, multiple proposals were needed in order to represent our ideas properly. One proposal was joint with MIT/Lincoln Labs, and another was joint with LANL. These ten proposals and the funding requested (for Sandia only) for fiscal years FY04/FY05/FY06 were:

1. Non-Polar GaN materials for Improved LED Efficiency (joint w/MIT), 170K/170K/85K
2. Advanced p-GaN and p-InGaN Materials and Contact Design, 435K/450K/0K
3. High Efficiency Green Emitters for Solid State Lighting, 600K/600K/600K
4. Single- and Multicolor Light Emitting Devices Using New Architectures (joint w/ LANL), 200K/200K/200K
5. Improved InGaN Epitaxy Yield by Precise Temperature Measurement, 195K/155K/0K
6. Encapsulation Technology for High-Power Near-UV LEDs, 265K/265K/0K
7. Ultrahigh-Efficiency Microcavity Photonic-Crystal LEDs, 585K/615K/0K
8. Development of White LEDs Using Nanophosphor-Quantum Dot Blends, 416K/442K/0K
9. Molten-Salt-Based Growth of Bulk InN, 261K/261K/0K
10. Silicon and Germanium Based Nanophosphors for High-Efficiency SSL Devices, 400K/400K/0K

The total funding requests for SNL for these proposals is: FY04 - \$3,527K; FY05 - \$3,558K; FY06 - \$885K. Of course, since the total available in this call is only \$6M over multiple years, for all DOE National Laboratories, Sandia can only expect to have a few of these proposals approved. However, our strong past history and present capabilities and expertise in SSL give us a good chance of capturing a significant fraction of the available \$6M.

6.6.8 Attempted Follow-On Projects and CRADAs That Were Unsuccessful

The projects described above constitute those that were successful and actually started, or those proposals that are still pending and are considered to have a good chance of being approved and going forward.

In addition to these, of course, were many projects that never progressed beyond the proposal and/or discussion stage. Because the preparation of these proposals and negotiations of aborted CRADAs consumed significant amounts of the team's time and effort, a very brief enumeration of them seems appropriate here. This discussion can also serve to give future Grand Challenge LDRD teams an idea of the proportion of unsuccessful attempts that must be made in order to achieve the portfolio of successful follow-on projects portrayed above.

Advanced Technology Program

We submitted a proposal on photonic crystal LEDs to the NIST-administered ATP program in September of 2001. This predated our successful EESI proposal on the same topic. The proposal was joint between Lumileds and Sandia, with each institution requesting 500K per year for two years. Unfortunately, the proposal was rejected as too risky and too speculative.

DOE/Office of Building Technologies Industrial Program – Lumileds

We submitted our first proposal on dramatically increasing the efficiency of green LEDs in April of 2003. This proposal was also joint between Sandia and Lumileds, and was in response to a call to industry from DOE's Office of Building Technologies. (The call required an industry lead.) At this point in time we had been working with Lumileds for well over two years, and our joint project, also under DOE/BTS, had achieved many successes. BTS had often referred to us as a great success, and the DOE program managers often invited their management to attend the reviews of our program when they were held in DOE Forrestal offices.

When the call came out, Sandia and Lumileds each requested 800K for the first year, 1,200K for the second, and 1,600K for the third years of the proposal. However, this amount would have consumed BTS's entire appropriation for SSL for that year, and so they felt the amount was too large, and declined to fund us (rather than simply reducing the amount of funding). We note that in subsequent calls for proposals, BTS specified maximum funding amounts, and required separate proposals for each technical approach.

DOE/Office of Building Technologies Industrial Program – General Electric

We also submitted a joint proposal with General Electric on the development of new oxide-based nanophosphors for solid state lighting. This proposal was only for two years, and was considerably smaller, with only about 160K total going to Sandia. GE's expertise in phosphors is absolutely unparalleled, and this would have been an excellent collaboration, in our opinion. Unfortunately, this proposal too was rejected by BTS.

Funds-In CRADAs

Finally, we had discussions about funds-in CRADAs with numerous companies, including General Electric, Dow Corning, Fusion UV, and many others. Some of these discussions were quite extended, involving numerous meetings and site visits by both the company and Sandia. More than one of these discussions involved funds-in to Sandia of \$1M per year or more. Areas of research included cantilever epitaxy for reduced dislocation substrates, phosphors and encapsulants, and deep-UV LEDs. Unfortunately, none of these opportunities ever materialized. In addition to these serious discussions, Sandia was visited by many other companies which were simply doing reconnaissance, and who never progressed beyond the initial visit.

At this stage, there are a handful of other companies, some of which are global behemoths, which are still discussing possible partnerships with Sandia. The partnerships being discussed take the form of both funds-in CRADAs, and joint proposal writing to Federal agencies. We remain willing to partner with corporations in this manner.

Lockheed Martin Shared Vision

Finally, we note that Sandia is continuing to pursue a Shared Vision project with Lockheed Martin on deep-UV LEDs. We are enthusiastic about this possibility, since Lockheed Martin has been funding a Shared Vision project with General Electric on the same topic, with goals virtually identical to those Sandia is pursuing under the DARPA SUVOS program. Sandia, however, has achieved emission powers that are two orders of magnitude higher than those achieved by GE, and so we anticipate a good possibility of collaboration.

7 APPENDIX A: PUBLICATIONS, PRESENTATIONS, PATENTS, ETC

7.1 Publications

- C. I. H. Ashby, C. C. Mitchell, J. Han, N. A. Missert, P. P. Provencio, D. M. Follstaedt, G. M. Peake, and L. Griego, *Low-Dislocation-Density GaN from a Single Growth on a Textured Substrate*, Applied Physics Letters **77** (3233), 2000.
- H. Zhou, M. Diagne, E. Makarona, A.V. Nurmikko, J. Han, K.E Waldrip, J.J. Figiel, *Near Ultraviolet Optically Pumped Vertical Cavity Laser*, Electronics Letters **36** (1777), 2000.
- W. W. Chow, H. Amano and I Akasaki, *Filamentation and Fundamental Mode Operation in InGaN Quantum Well Lasers*, Applied Physics Letters **76** (1647-1649), 2000.
- A. F. Wright, *Interaction of Hydrogen with Nitrogen Interstitials in Wurtzite GaN*, Journal of Applied Physics **90** (6526), 2001.
- A.F. Wright, *Interaction of Hydrogen with Gallium Vacancies in Wurtzite GaN*, Journal of Applied Physics **90** (1164), 2001.
- W. R. Wampler, S. M. Myers, A. F. Wright, J. C. Barbour, C. H. Seager, and J. Han, *Lattice Location of Hydrogen in Mg Doped GaN*, Journal of Applied Physics **90** (108), 2001.
- S. M. Myers, A. F. Wright, G. A. Petersen, W. R. Wampler, C. H. Seager, M. H. Crawford, and J. Han, *Diffusion, Release, and Uptake of Hydrogen in Magnesium-Doped Gallium Nitride: Theory and Experiment*, Journal of Applied Physics **89** (3195), 2001.
- J. Han, K. E. Waldrip, S. R. Lee, J. J. Figiel, S. J. Hearne, G. A. Petersen, and S. M. Myers, *Control and Elimination of Cracking of AlGaIn using Low-Temperature AlGaIn Interlayers*, Applied Physics Letters **78** (67), 2001.
- H. C. Schneider, A. J. Fischer, W. W. Chow and J. Klem, *Temperature Dependence of Laser Threshold in an InGaAsN Vertical-Cavity Surface-Emitting Laser*, Applied Physics Letters **78** (3391-3), 2001.
- H. C. Schneider, W. W. Chow and S. W. Koch, *Many-Body Effects in the Gain Spectra of Highly Excited Quantum-Dot Lasers*, Phys. Rev. B. **64** (115315-21), 2001.
- A. F. Wright, K. Leung, M. van Schilfgaarde, *Effects of Biaxial Strain and Chemical Ordering on the Band Gap of InGaIn*, Applied Physics Letters **78** (189), 2001.
- C. H. Seager, S. M. Myers, B. L. Vaandrager, J. S. Nelson, *Isotope Effects on the Rate of Electron-Beam Dissociation of Mg-H Complexes in GaN*, Applied Physics Letters **80** (2693), 2002.
- S. M. Myers and A. F. Wright, *Theoretical Description of H Behavior in GaN p-n Junctions*, Journal of Applied Physics **90** (5612), 2001.
- L. Shi, C. D. Poweleit, F. A. Ponce, J. Menendez and W. W. Chow, *Anisotropic Diffusion and Drift of Photogenerated Carriers near Coreless Dislocations in InGaIn Quantum Wells*, Applied Physics Letters **79** (75-77), 2001.
- W. W. Chow and H. Amano, *Analysis of Lateral Mode Behavior in Broad-Area InGaIn Quantum Well Lasers*, IEEE Journal of Quantum Electronics **37** (265-73), 2001.
- H. C. Schnieder, W. W. Chow and H. Amano, *Filamentation and Fundamental Mode Operation in InGaIn Quantum-Well Lasers*, Proceedings of the SPIE International Symposium on Optoelectronics 2001, 1/20-26/01, San Jose, CA
- J. R. Creighton, *Vapor Pressures of the Adducts Formed During AlGaIn OMVPE*, Journal of Electronic Materials **31** (1337), 2002.

J. R. Creighton, W. G. Breiland, M. E. Coltrin, Sources of the Parasitic Chemical Reactions During AlGaInN, Proceedings of the State-of-the-Art Program on Compound Semiconductors XXXVI and Wide Bandgap Semiconductors for Photonic and Electronic Devices and Sensors II, the Electrochemical Society 2002-3 (28), 2002.

J. R. Creighton, W. G. Breiland, M. E. Coltrin, R. P. Pawlowski, Gas-Phase Nanoparticle Formation During AlGaInN MOVPE, Applied Physics Letters 81 (2626), 2002.

W.W. Chow, H.C. Schneider, A.J. Fischer and A.A. Allerman, Theoretical Investigation of Laser Gain in AlGaInN Quaternary Quantum Wells, Applied Physics Letters 80 (2451-2453), 2002.

H. C. Schneider, W. W. Chow and S. W. Koch, *Anomalous Carrier-Induced Dispersion in Quantum-Dot Active Media*, Phys. Rev. B. **66**, Rapid Communications 41310 (R), 2002.

H. C. Schneider, W. W. Chow, P. M. Smowton, E. J. Pearce and S. W. Koch, *Anomalous Carrier-Induced Dispersion in Semiconductor Quantum Dots*, Optics in 2002, Optics & Photonics News, Dec. 2002.

S. M. Myers, C. H. Seager, A. F. Wright, and B. L. Vaandrager, *Electron-Beam Dissociation of the MgH Complex in p-Type GaN*, Journal of Applied Physics **92** (6630), 2002.

C. H. Seager, S. M. Myers, A. F. Wright, D.D Koleske, and A. A. Allerman, *Drift, Diffusion, and Trapping of Hydrogen in p-Type GaN*, Journal of Applied Physics **92** (7246), 2003.

W. W. Chow and H. C. Schneider, *Theory of Laser Gain in InGaInN Quantum Dots*, Applied Physics Letters, to be published 2002.

A. F. Wright, *Substitutional and Interstitial Carbon in Wurtzite GaN*, Journal of Applied Physics **92** (2575), 2002.

J. P. Wilcoxon and P. P. Provencio, *Optical Properties of II-VI Semiconductor Nanoclusters for use as Phosphors*, Proceedings of the SPIE conference on "Optical Properties of Nanocrystals", **4808**, (99-115), 2002.

C. H. Seager, A. F. Wright, J. Yu, and W. Goetz, *The Role of Carbon in GaN*, Journal of Applied Physics, accepted.

S. M. Myers and A. F. Wright, *Trapping with Anisotropic Diffusion in an Applied Field: H⁺ in Mg-Doped GaN*, Journal of Applied Physics **93** (2608), 2003.

D. D. Koleske, R. L. Henry, M. E. Twigg, J. C. Culbertson, S. C. Binari, A. E. Wickenden, M. Fatemi, *The Influence of AlN Temperature on GaN Electronic Properties Grown on SiC*, Applied Physics Letters **80** (4372), 2002.

D. D. Koleske, A. J. Fischer, A. A. Allerman, C. C. Mitchell, K. C. Cross, S. R. Kurtz, J. J. Figiel, K. W. Fullmer, and W. G. Breiland, *Improved Brightness of 380 nm GaN Light Emitting Diodes through Intentional Delay of the Nucleation Island Coalescence*, Applied Physics Letters **81** (1940), 2002.

D. D. Koleske, A. E. Wickenden, R. L. Henry, M. E. Twigg, *Influence of MOVPE Growth Conditions on Carbon and Silicon Concentrations in GaN*, Journal of Crystal Growth **242** (55), 2002.

D.M. Follstaedt, P.P. Provencio, N.A. Missert, C.C. Mitchell, D. D. Koleske, A. A. Allerman, C.I.H. Ashby, *Minimizing Threading Dislocations by Redirection During Cantilever Epitaxial Growth of GaN*, Applied Physics Letters **81** (2758), 2002.

C. H. Seager, Comment on *Infrared Spectroscopy of Mg-H Local Vibrational Modes in GaN with Polarized Light*, Physical Review B, accepted.

P.P. Provencio, D.M. Follstaedt, N.A. Missert, D.D. Koleske, C.C. Mitchell, A.A. Allerman, C.I.H. Ashby, *Characterization of "Dark-Block" Defects in Cantilever Epitaxial GaN on Sapphire*, Fall 2002 MRS Symposium Proceedings, Vol. 743 (L3.15), 2003.

D.M. Follstaedt, P.P. Provencio, C.C. Mitchell, A.A. Allerman, N.A. Missert and C.I.H. Ashby, *Cantilever Epitaxy Of Gan On Sapphire: Further Reductions In Dislocation Density*, MRS Symposium Proceedings, Vol. 743 (L1.8), 2003.

D. M. Follstaedt, N. A. Missert, D. D. Koleske, C. C. Mitchell and K. C. Cross, *Plan-View Image Contrast Of Dislocations in GaN*, Applied Physics Letters **83** (4797), 2003.

J. R. Creighton, W. G. Breiland, M. E. Coltrin, R. P. Pawlowski, *Gas-Phase Nanoparticle Formation during AlGaInN MOVPE*, Applied Physics Letters **81** (2626), 2002.

H. C. Schneider, W. W. Chow, P. M. Snowton, E. J. Pearce, S. W. Koch, *Many-Body Effects in Quantum-Dot Lasers*, Proceedings of the Photonics West 2003 Conference, 1/25-31/03, San Jose, CA. (invited)

J. M. Gee, J. Y. Tsao, and T. E. Drennen, *Potential Impact of New Energy Efficiency Technologies on Global Climate Change: The Example of Solid-State Lighting*, submitted to Mitigation and Adaptation to Global Change, An International Journal Devoted to Scientific, Engineering, Socio-Economic and Policy Responses to Environmental Change (4/03).

J. Y. Tsao, *Solid-State Lighting: Lamp Targets and Implications for the Semiconductor Chip*, Proceedings of the 2003 International GaAs MANTECH Conference, 5/19-22/03, Scottsdale, AZ

A. F. Wright, C. H. Seager, S. M. Myers, D. D. Koleske, and A. A. Allerman, *Hydrogen Configurations, Formation Energies, and Migration Barriers in GaN*, Journal of Applied Physics, submitted.

J. J. Hader, V. Moloney, S. W. Koch, W. W. Chow, *Microscopic Modeling of Gain and Luminescence in Semiconductors*, IEEE Special Issue on Quantum Electronics, vol. 9, pp. 688, 2003. (invited review paper).

S. M. Myers, C. H. Seager, *Hydrogen Isotope Exchange and the Surface Barrier in P-Type Gallium Nitride*, Journal of Applied Physics, submitted.

W. R. Wampler, S. M. Myers, *Hydrogen Release from Magnesium-Doped GaN with Clean Ordered Surfaces*, Journal of Applied Physics, submitted.

C. H. Seager, S. M. Myers, A. F. Wright, D. D. Koleske, A. A. Allerman, *Drift, Diffusion and Trapping of Hydrogen in p-type GaN*, Journal of Applied Physics, submitted.

D. D. Koleske, M. E. Coltrin, A. A. Allerman, K. C. Cross, C. C. Mitchell, J. J. Figiel, *In-Situ Measurements of GaN Nucleation Layer Decomposition*, Applied Physics Letters **82** (1170), 2003.

J. Oila, K. Saarinen, A. Wickenden, D. D. Koleske, R. Henry, M. Twigg, *Ga Vacancies and Grain Boundaries in GaN*, Applied Physics Letters **82** (1021), 2003.

M. E. Coltrin, C. C. Mitchell, *Mass Transport and Kinetic Limitations in MOCVD Selective-Area Growth*, Journal of Crystal Growth **254** (35-45), 2003.

R. J. Shul, R. D. Briggs, K. H. A. Bogart, A. J. Fischer, D. D. Koleske, A. A. Allerman, S. Jones, C. C. Mitchell, C. Sanchez, *High-Density Plasma Etching of Wide-Bandgap Materials*, Vugraphs of Presentation to MRS Spring Meeting, 4/22-25/03, San Francisco, CA

H. C. Schneider, W. W. Chow, S. W. Koch, *Influence of Coupling between Localized and Continuum States in InGaN Quantum-Dot Systems*, physica status solidi B **238**, No. 3 (589-92), 2003.

C. Inoki, T. Kuan, C. Lee, R. Feenstra, D. D. Koleske, D. Diaz, P. Bohn, I. Adesida, *Growth of GaN on Porous SiC and GaN Substrates*, Journal of Electronic Materials, submitted.

L. S. Rohwer, A. M. Srivastava, *Development of Phosphors for LEDs*, The Electrochemical Society Interface, to be published summer 2003.

J. Y. Tsao, *The U.S. "LEDs for General Illumination 2002" Roadmap*, Laser Focus World, to be published 6/03.

W. W. Chow, H. C. Schneider, M. C. Phillips, *Theory of Quantum Coherence Phenomena in Semiconductor Quantum Dots*, Physical Review A **68** (053802), 2003.

A.G. Salinger, R.P. Pawlowski, J.N. Shadid, and B. van Bloemen Waanders, *Computational Analysis and Optimization of a Chemical Vapor Deposition Reactor with Large-Scale Computing*, I&EC Research, 2003, in press.

C. Eichler, D. Hofstetter, W. W. Chow, S. Miller, A. Weimar, A. Lell, V. Harle, *Microsecond Timescale Lateral Mode Dynamics in a Narrow Stripe InGaN-Laser*, Applied Physics Letters, accepted.

J. R. Creighton, G. T. Wang, W. G. Breiland, M. E. Coltrin, *Nature of the Parasitic Chemistry during AlGaInN OMVPE*, Journal of Crystal Growth **261** (204), 2004.

W. G. Breiland, S. R. Lee, and D. D. Koleske, *Effect of diffraction and film-thickness gradients on wafer-curvature measurements of thin-film stress*, J. Appl. Phys. **95** (3453) 2004.

7.2 Presentations

W. W. Chow, Quantum-Confined Stark Effect and Many-Body Interactions in Group-III Nitride Quantum Well Lasers, March American Physical Society Meeting, 3/20-24/00, Minneapolis, MN (invited).

W. W. Chow, H. Amano, I. Akasaki, Filamentation in InGaN Quantum Well Lasers, CLEO '00 Conference on Lasers and Electro-Optics, 5/7-12/00, San Francisco, CA..

W. W. Chow, H. Amano and I. Akasaki, On the Feasibility of Fundamental-Mode Operation in Unstable Resonator InGaN Lasers, International workshop on Nitride Semiconductors, 9/24-27/00, Nagoya, Japan..

C.I. Ashby, Cantilever Epitaxy: A Simple Lateral Growth Technique for Reducing Dislocation Densities in GaN and other Nitrides, 198th Meeting of the Electrochemical Society, Oct 2000 (invited).

M.E. Coltrin, C.C. Willan, M.E. Bartram, Crystal Growth Kinetics and Transport in GaN Epitaxial Overgrowth, 47th Annual Meeting of the American Vacuum Society, Oct 2000, Boston, MA.

C.C. Willan, M.E. Coltrin, J. Han, Mass Transport Processes in the Epitaxial Lateral Overgrowth of Gallium Nitride, Fall 2000 Meeting of the Material Research Society, Nov 2000, Boston, MA.

S. M. Myers, A. F. Wright, G. A. Petersen, W. R. Wampler, C. H. Seager, M. H. Crawford, and J. Han, Reversible Hydrogen Release and Dopant Activation in Gallium Nitride: Experiment and Theory, Fall 2000 Meeting of the Material Research Society, Nov. 2000, Boston, MA.

M.E. Coltrin, C.C. Willan, M.E. Bartram, GaN Epitaxial Lateral Overgrowth Kinetics, American Institute of Chemical Engineers, Nov 2000, Los Angeles, CA.

E. D. Jones, LED Solid-state Lighting for Illumination: Status Report, SPIE Conference, 2001 SPIE Conference, Jan 2001, San Jose, CA.

H. C. Schnieder, W. W. Chow, H. Amano, Filamentation and Fundamental Mode Operation in InGaN Quantum-Well Lasers, SPIE International Symposium on Optoelectronics 2001, 1/20-26/01, San Jose, CA.

H. C. Schnieder, W. W. Chow, S. W. Koch, Theory of Population Dynamics in Quantum-Dot Lasers, SPIE International Symposium on Optoelectronics 2001, 1/20-26/01, San Jose, CA.

E. D. Jones, National White Lighting Initiative: What's it all about?, 31st Winter Colloquium on Physics of Quantum Electronics Conference, Jan 2001, Snowbird, UT.

G. M. Peake, A.J. Fischer, J. Han, J.J. Figiel, C.C. Mitchell, R.M. Biefeld, UV LEDs with AlInGaN/InGaN and AlGaIn/InGaIn Active Regions Grown by OMVPE, Tenth Biennial Workshop on Organometallic Vapor Phase Epitaxy, 3/11-15/01, San Diego, CA.

J. Han, K.E. Waldrip, J.J. Figiel, MOCVD Growth and Characterization of AlGaIn/GaN/GaInN Vertical Cavity Surface Emitting Laser, 10th Biennial Workshop on MOVPE, Mar 2001, San Diego, CA.

J. A. Simmons, The Solid-State Lighting Initiative: Synergisms with Office of Science Materials Science Programs, Energy Materials Coordinating Committee, Mar 2001, Washington, DC.

W. G. Breiland, L. A. Bruskas, A. A. Allerman, and T. W. Hargett, Emissivity-Correcting Pyrometry for OMVPE Applications, Tenth Biennial Workshop on Organometallic Vapor Phase Epitaxy 3/11-15/01, San Diego, CA.

A. F. Wright, Theoretical Investigation of Hydrogen in Wurtzite GaN, March APS Meeting, 3/12-16/01, Seattle, WA (invited).

M.E. Coltrin, C.C. Mitchell, J. Han, Kinetics and Transport in Gallium Nitride Epitaxial Lateral Overgrowth, 199th Meeting of the Electrochemical Society, Mar 2001, Washington, DC.

J.R. Creighton, Low Temperature Nitride Precursor Reactions, Tenth Biennial Workshop on Organometallic Vapor Phase Epitaxy, 3/11-15/01, San Diego, CA.

A.F. Wright, S. M. Myers, Jr., Modelling of Hydrogen Behavior in Wurtzite GaN, New Mexico American Vacuum Society Meeting, 5/23-24/01, Albuquerque, NM.

C.I. Ashby, et al., Cantilever Epitaxy and its Potential for GaN Substrates with Whole-wafer Dislocation Densities Below 10^7 cm⁻², 43rd Electronic Materials Conference, June 2001, South Bend, IN.

J. M. Gee, National Security Implications of Solid-State Lighting, OIDA Workshop on Solid-State Lighting, CS-MAX Conference, 7/9-11/01, Boston, MA.

S. M. Myers, A. F. Wright, Theoretical Consideration of Hydrogen-Related Atomic Processes in Gallium Nitride, 4th International Conference on Nitride Semiconductors, 7/16-20/01, Denver, CO.

C. C. Mitchell, C. I.H. Ashby, D. M. Follstaedt, P. P. Provencio, N. A. Missert, A. A. Allerman, Cantilever Epitaxy and its Development to Produce GaN Substrates with Reduced Threading Dislocation Densities, American Conference on Crystal Growth and Epitaxy, 8/12-16/01, Burlington, VT.

A. J. Fischer, K. E. Waldrip, G. M. Peake, J. J. Figiel, A. A. Allerman, GaN/AlGa_N Epitaxial DBRs for Use in Blue and UV Light Emitters, 2001 OSA Annual Meeting/ILS XVII, 10/12-18/01, Long Beach, CA.

W.W. Chow, H. C. Schneider and H. Amano, Analysis of Fundamental Mode Operation in an Antiguide InGa_N Quantum Well Laser, 2001 Optical Society of America Annual Meeting and International Laser Science XVII, . 10/14-18/01, Long Beach, CA.

H. C. Schneider, W. W. Chow, Excitation Dependence of Lateral Beam Width in a Quantum-Dot Lasers, Proc. 14th Annual Meeting of the IEEE Lasers & Electro-Optics Society (LEOS), 11/11-15/01, La Jolla, CA .

J. R. Creighton, M. E. Coltrin, R. P. Pawlowski, W. G. Breiland, Search for the Missing Group-III Flux during AlGa_N OMVPE, AVS 48th International Symposium, Oct. 29-Nov. 2, 2001, San Francisco, CA.

J. Han, K.E. Waldrip, J.J. Figiel, Growth and Characterization of AlGa_N/Ga_N DBR Mirrors for UV Surface-Emitting Devices, Fall 2000 Meeting of the Material Research Society, Nov 2001, Boston, MA.

K.E. Waldrip, J. Han, S.J. Hearne, J.J. Figiel, G. Peterson, S.M. Myers, Control and Elimination of Cracking of AlGa_N Films Using Low-temperature AlGa_N Interlayers, Fall 2000 Meeting of the Material Research Society, Nov 2001, Boston, MA.

A. G. Baca, R. D. Briggs, C. Monier, J. R. Wendt, R. J. Shul, S. R. Kurtz, A. A. Allerman, D. D. Koleske, C. C. Mitchell, C. I. Ashby, M. G. Armendariz, C. Sandoval, Issues for Ga_N HEMTS Grown on MOCVD, ONR Workshop on Physical Effect and Device/Circuit Interactions in Solid State Devices, 9/1-13/01, Bar Harbor, ME.

J. M. Gee, J. A. Simmons, T. E. Drennen, Solid-State Lighting Initiative and Synergisms with National Security, Optical Society of America, 2001 Annual Meeting, Oct 2001, Long Beach, CA.

D.M. Follstaedt, P.P. Provencio, J.A. Floro and S.J. Hearne, Identification Of Misfit Dislocations Producing Relaxation Of AlGa_N/Ga_N Heterostructures, 2001 Fall MRS Meeting, 11/26-30/01, Boston, MA.

N. Missert, C. H. Seager, S. M. Myers, R. G. Copeland, B. Vaandrager, Scanning Cathodoluminescence Studies of H-Bonding in Ga_N:Mg Thin Films, , 2001 MRS Fall Meeting, 11/26-30/01, Boston, MA.

K.E. Waldrip, J.A. Floro, D.M. Follstaedt, S.R. Lee, J.A. Hunter, S.J. Hearne, D.D. Koleske, A.A. Allerman, J.J. Figiel and T.M. Kerley, Mechanism Of Catastrophic Stress Relief In AlGa_N/Ga_N, 2001 Fall MRS Meeting, 11/26-30/01, Boston, MA.

A. F. Wright, Interaction of Hydrogen with Gallium Vacancies and Nitrogen Interstitials in Wurtzite Gallium Nitride, 2001 Fall MRS Meeting, 11/26-30/2001, Boston, MA.

R. P. Pawlowski, R. J. Creighton, M. E. Coltrin, Gas-Phase Studies of the MOVPE of Al_N from Trimethylaluminum and Ammonia, National Meeting of the AIChE, Nov 2001, Reno, NV.

W. W. Chow, Gain and Carrier-Induced Refractive Index Change in Group-III Nitride Quantum Wells, Novel In-Plane Semiconductor Lasers, SPIE Photonics West, 1/19-25/02, San Jose, CA. (invited).

A.A. Allerman, D.D. Koleske, C.C. Mitchell, A.J. Fischer, D.M. Follstaedt, P.P. Provencio, N.A. Missert, and C.I.H. Ashby, Facet Controlled Growth In Cantilever Epitaxy For Low Dislocation Density Ga_N, 7th Wide Bandgap III-Nitride Workshop, 3/10-14/02, Richmond, VA.

J.A. Floro, D.M. Follstaedt, P.P. Provencio, S.J. Hearne and K.E. Waldrip, Brittle/Ductile Stress Relaxation During MOCVD Growth Of AlGa_N/Ga_N Heterostructures, March Meeting of the American Physical Society, 3/18-22/02, Indianapolis, IN.

D. D. Koleske, MOCVD Growth of Ga_N Based UV Light Emitters, Dept. of Materials Science & Engineering-Arizona State University, 3/29/02, Tempe, AZ.

J. R. Creighton, W. G. Breiland, M. E. Coltrin, Sources of the Parasitic Chemical Reactions during AlGa_N OMVPE, 201st Meeting of the Electrochemical Society, May 2002, Philadelphia, PA (invited).

W. W. Chow, Physics of Optical Response in Group-III Nitride Active Structures, OIDA LED Solid State Lighting Workshop, 5/30/02, Albuquerque, NM (invited).

P.P. Provencio, D.M. Follstaedt, C.C. Mitchell, D.D. Koleske, N.A. Missert, A.A. Allerman and C.I.H. Ashby, Significantly Reduced Threading Dislocations in GaN Grown by Cantilever Epitaxy, 38th Annual Symposium, New Mexico Chapter of the American Vacuum Society, 5/14-15/02, Albuquerque, NM.

L. S. Rohwer, Phosphor Synthesis Techniques of the Last Century, Centennial Meeting of the Electrochemical Society, 5/12-17/02, Philadelphia, PA.

L. S. Rohwer, Synthesis and Characterization of Cathodoluminescent Phosphors, GE Global Research Center, 5/17/02, Niskayuna, NY (invited).

M. E. Twigg, D. D. Koleske, R. L. Henry, A.E. Wickenden, Dislocation Density and Electrical Compensation in GaN Films, 44th Meeting of the EMC, 6/16-26/02, Santa Barbara, CA.

D.M. Follstaedt, P.P. Provencio, C.C. Mitchell, N.A. Missert, C.I.H. Ashby, D.D. Koleske and A.A. Allerman, Reducing Threading Dislocation in Laterally Grown GaN: Further Approaches, Electronic Materials Conference, 6/26-28/02, Santa Barbara, CA.

A.A. Allerman, D.D. Koleske, C.C. Mitchell, A.J. Fischer, D.M. Follstaedt, P.P. Provencio, N.A. Missert and C.I.H. Ashby, Facet Controlled Growth in Cantilever Epitaxy for Improved LED Performance, Electronic Materials Conference, 6/26-28/02, Santa Barbara, CA.

E. R. Glaser, J.A. Freitas, Jr., W.E. Carlos, B.V. Shanabrook, A.E. Wickenden, D.D. Koleske, R.L. Henry, M.W. Bayerl and M.S. Brandt, Defects Observed in Semi-Insulating GaN and SiC Through Optically-Detected Magnetic Resonance, ONR Workshop on Challenges in Semi-Insulating Nitrides and SiC, 7/14-18/02, Laugarvatn, Iceland.

C.C. Mitchell, D.D. Koleske, A.A. Allerman, A.J. Fischer, D.M. Follstaedt, P.P. Provencio, N.A. Missert, C.I.H. Ashby, Cantilever Epitaxy with Facet Controlled Growth for Low Dislocation Density GaN, 14th American Conference on Crystal Growth Epitaxy, 8/4-9/02, Seattle, WA.

J. A. Simmons, Research at Sandia in Solid State Lighting Technologies, Seminar at General Electric Corporate Research and Development, 9/25/02, Schenectady, NY (invited).

Chow, W. W., H. C. Schneider, E. J. Pearce, P. M. Snowton, Absence of Filamentation in Quantum-Dot Lasers: Theory and Experiment, 18th IEEE International Semiconductor Laser Conference, 9/29-10/3/02, Garmisch-Partenkirchen, Germany..

W. Götz, T. Mihopoulos, J. Yu, C. H. Seager, and A. F. Wright, Role of Carbon in Silicon-doped GaN Grown by Metalorganic Chemical Vapor Deposition, 4th Symposium on Non-Stoichiometric III-V Semiconductors, 10/2-4/02, Monterey, CA.

J. Y. Tsao, The U.S. Solid-State Lighting Roadmap: Targets and Technical Challenges, University of Michigan, 10/11/02, Ann Arbor, MI (invited).

A. F. Wright and S. M. Myers, Aspects of Hydrogen Behavior in GaN: Mg-Acceptor Passivation/Compensation and Interaction with Point Defects, Wake Forest University, 11/29/02, Winston-Salem, NC (invited).

A. F. Wright and C. H. Seager, Substitutional and Interstitial Carbon in Wurtzite GaN, 2002 Fall MRS Meeting, 12/2-6/02, Boston, MA (invited).

C. H. Seager, S. M. Myers, A. F. Wright, D. D. Koleske, and A. A. Allerman, Measurements and Modeling of H Diffusion in p-type GaN, 2002 Fall MRS Meeting, 12/2-6/02, Boston, MA.

D. D. Koleske, A. J. Fischer, M. E. Coltrin, A. A. Allerman, C. C. Mitchell, S. R. Kurtz, J. J. Figiel, K. W. Fullmer, W. G. Breiland, Optical Reflectance Measurements of the 3D to 2D Delayed Recovery of GaN on Sapphire with Correlation to Improved 380 nm LED Brightness, Symposium L: GaN and Related Alloys, 2002 Fall MRS Meeting, 12/2-6/2002, Boston, MA.

D. D. Koleske, M. E. Coltrin, S. R. Lee, K. C. Cross, C. C. Mitchell, A. A. Allerman, and J. J. Figiel, Toward Quantification and Control of GaN Film Evolution on Sapphire, Symposium W: Morphological and Compositional Evolution of Thin Films, 2002 Fall MRS Meeting, 12/2-6/02, Boston, MA.

A. N. Westmeyer, S. Mahajan, D. D. Koleske, A. A. Allerman and R. M. Biefeld, Vertical Composition Modulations in AlGa_N Epitaxial Layers, Symposium L: GaN and Related Alloys, 2002 Fall MRS Meeting, 12/2-6/02, Boston, MA.

D. Matlock, M.E. Zvanut, J. R. DiMaio, R. F. Davis, J.E. Van Nostrand, R. L. Henry, D. D. Koleske and A. E. Wickenden, Activation and Passivation of Mg Acceptor in GaN:Mg, Symposium L: GaN and Related Alloys, 2002 Fall MRS Meeting, 12/2-6/02, Boston, MA.

Z. -Q. Fang, B. B. Clafin, D. C. Look, T. H. Myers, D. D. Koleske, A. E. Wickenden, R. L. Henry, High Temperature Illumination-Induced Metastability in Undoped Semi-Insulating GaN Growth by Metalorganic Vapor Phase Epitaxy, Symposium L: GaN and Related Alloys, 2002 Fall MRS Meeting, 12/2-6/02, Boston, MA.

A. J. Fischer, D. D. Koleske, A. A. Allerman, C. C. Mitchell, K. H. A. Bogart, R. J. Shul, J. J. Figiel, K. W. Fullmer, InGa_N/Ga_N Multiple Quantum Well LEDs Grown by MOCVD using Cantilever Epitaxy, 2002 Fall MRS Meeting, 12/2-6/02, Boston, MA.

P.P. Provencio, D.M. Follstaedt, N.A. Missert, D.D. Koleske, C.C. Mitchell, A.A. Allerman and C.I.H. Ashby Comparisons of Lateral Defects in Cantilever Epitaxial GaN on Sapphire. 2002 MRS Fall Meeting, 12/2-6/02, Boston, MA.

R. M. Biefeld, D. M. Follstaedt, P. P. Provencio, N. A. Missert, C. C. Mitchell, D. D. Koleske, A. A. Allerman, A. J. Fischer, C. I. H. Ashby, Cantilever Epitaxial Ga_N : An Alternate Substrate, Workshop on Selective, Patterned and Self-Assembled Growth of Nano-Structures, 01/6-8/03, Hong Kong, China.

D. D. Koleske, A. J. Fischer, A. A. Allerman, C. C. Mitchell, K. H. A. Bogart, R. J. Shul, J. J. Figiel, K. W. Fullmer, K. C. Cross, Low Defect Density Epitaxy as a Substrate for 390 nm InGa_N/Ga_N Multiple Quantum Well LEDs, SPIE Photonics West, 1/25-31/03, San Jose, CA.

W. W. Chow, Wide-Bandgap Group-III Nitride Semiconductor Lasers, OSEP Optics Seminar, University of Colorado, 10/21/02, Boulder, CO (invited).

J. A. Simmons, Fundamental Science Needs for Solid State Lighting, Basic Energy Sciences on "Basic Research Needs to Assure a Secure Energy Future", 10/22/02, Gaithersburg, MD (invited).

J. R. Creighton, W. G. Breiland, M. E. Coltrin, Parasitic Reactions and Particulate Formation during AlGa_N MOCVD, National Meeting of American Institute of Chemical Engineers, 11/3-8/02, Indianapolis, IN.

J. R. Creighton, W. G. Breiland, M. E. Coltrin, Gas-Phase Nanoparticle Formation During AlGa_N MOCVD, AVS 49th Intl., Symposium, 11/4-8/02, Denver, CO.

A. F. Wright, Using Density Functional Theory to Help Understand the Behavior of Defects in Wurtzite Ga_N, Texas Tech University, 11/7/02, (invited).

K. H. A. Bogart, D. D. Koleske, A. A. Allerman, A. J. Fischer, K. W. Fullmer, K. Cross, C. C. Mitchell, Effects of LED Processing Steps on the Surface of Ga_N Epilayers, AVS Intl. Symposium, 11/4-8/02, Denver, CO.

J. Y. Tsao, The U. S. Solid-State Lighting Roadmap: Targets and Technical Challenges, 2002 OIDA Annual Forum, 11/20/02, Washington, DC (invited).

M. E. Coltrin, C. C. Mitchell, Mass Transport and Kinetic Limitations in Ga_N Epitaxial Lateral Overgrowth, 2002 Fall MRS Meeting, 12/2-6/02, Boston, MA.

D. M. Follstaedt, P. P. Provencio, D. D. Koleske, N. A. Missert, C. C. Mitchell, C. I. Ashby, A. A. Allerman, Cantilever Epitaxy of Ga_N on Sapphire: Further Reductions in Dislocation Density, 2002 Fall MRS, 12/2-6/02, Boston, MA.

A. A. Allerman, A. Fischer, D. D. Koleske, K. H. A. Bogart, R. Shul, S. Kurtz, MOCVD Growth of AlGa_N Alloys for 300 nm LEDs, 2002 Fall MRS, 12/2-6/02, Boston, MA.

S. M. Myers, W. R. Wampler, C. H. Seager, B. L. Vaandrager, D. D. Koleske, A. A. Allerman, Influence of Ambient on Surface-Inhibited H Release from P-Ga_N, 2002 Fall Meeting of the MRS, 12/2-6/02, Boston, MA.

D. D. Koleske, M. E. Coltrin, S. R. Lee, K. C. Cross, C. C. Mitchell, A. A. Allerman, J. J. Figiel, Toward Quantification of GaN Film Evolution of Sapphire, 2002 Fall MRS Meeting, 12/2-6/02, Boston, MA.

L. S. Rohwer, J. P. Wilcoxon, Characterization of II-VI Semiconductor Nanocrystals for Solid State Lighting Applications, Nanomaterials for Aerospace Symposium, January 2003, Corpus Christi, TX (invited).

A. A. Allerman, A. Fischer, D. Koleske, K. H. A. Bogart, R. Shul, S. Kurtz, J. Figiel, K. Cross, K. Fullmer, MOCVD Growth and Performance of Light Emitting Diodes for 300 nm Emission, Photonics West, 1/25-31/03, San Jose, CA.

J. Y. Tsao, Science and Technology Challenges in Solid-State Lighting, Workshop on Selective, Patterned and Self-Assembled Growth in Nanostructures, 1/6-8/03, Hong Kong, China (invited).

H. C. Schneider, W. W. Chow, P. M. Snowton, E. J. Pearce and S. W. Koch, Many-Body Effects in Quantum-Dot Lasers, Photonics West 2003, 1/25-31/03, San Jose, CA. (invited).

J. M. Gee, J. Y. Tsao, J. A. Simmons, Solid-State Lighting Research at Sandia National Laboratories, Workshop on Solid-state Lighting, Georgia Institute of Technology, 2/9-20/03, Atlanta, GA.

J. M. Gee, J. Y. Tsao, J. A. Simmons, The Role of GaN Semiconductors in the Solid-State Lighting Revolution and Synergisms with National Security, 2003 Military Sensing Symposium, Materials Specialty Group, 2/24-28/03, Tucson, AZ.

H. C. Schneider, W. W. Chow, S. W. Koch, Influence of Coupling between Localized and Continuum States in Quantum-Dot Systems, Nonlinear Optics and Excitation Kinetics in Semiconductors (NOEKS), 2/24-28/03, Karlsruhe, Germany.

S. R. Lee, W. G. Breiland, D. D. Koleske, The Effect of Film-Thickness Nonuniformity on In-Situ Wafer-Curvature Measurements of Thin-Film Stress, 2003 APS March Meeting, 3/3-7/03, Austin, TX.

J. A. Simmons, The Next Generation Lighting Initiative, Phosphor Global Summit 2003, 3/19-21/03, Scottsdale, AZ (invited).

J. M. Gee, What the PV Specialists Might Like to Know About Solid-State Lighting, National Center for Photovoltaics and DOE Solar Program Review Meeting, 3/24-26/03, Denver, CO.

J. R. Creighton, W. G. Breiland, M. E. Coltrin, Sources of the Parasitic Chemical Reactions during AlGaIn OMVPE, LumiLeds Lighting, 3/26/03, San Jose, CA.

M. H. Crawford, A. A. Allerman, A. J. Fischer, K. H. A. Bogart, D. D. Koleske, W. W. Chow, S. R. Kurtz, S. R. Lee, Progress and Challenges in the Development of AlGaIn-Based Deep-UV Light Emitters, Impurity Based Electroluminescence in Wide Bandgap Semiconductors Workshop, 4/13-16/03, Santa Fe, NM (invited).

J. A. Simmons, Solid State Lighting Research at Sandia National Laboratories, 203rd Electrochemical Society Meeting, 4/27-5/2/03, Paris, France (invited).

L. S. Rohwer, J. P. Wilcoxon, B. L. Abrams, S. M. Woessner, S. G. Thoma, Semiconductor Quantum Dots for White Light Generation, 203rd Meeting of the Electrochemical Society, April 2003, Paris, France.

J. P. Wilcoxon, L. S. Rohwer, P. Provencio, Optical Properties of II-VI and IV Semiconductor Nanoclusters for Use as Phosphors, 203rd Meeting of the Electrochemical Society, April 2003, Paris, France (invited) .

A. F. Wright, C. H. Seager, S. M. Myers, D. D. Koleske, A. A. Allerman, Hydrogen Drift, Diffusion and Trapping in p-type GaN, 2003 Spring MRS Meeting, 4/21-25/03, San Francisco, CA.

C. H. Seager, D. R. Tallant, A. F. Wright, J. Yu, W. Götz, Luminescence Behavior of GaN Co-doped with Si and C, 2003 Spring MRS Meeting, 4/21 – 4/25/03, San Francisco, CA.

R. J. Shul, R. D. Briggs, K. H. A. Bogart, A. J. Fischer, D. D. Koleske, A. A. Allerman, C. C. Mitchell, High-Density Plasma Etching of Wide-Bandgap Materials, 2003 Spring MRS Meeting, 4/21-25/03, San Francisco, CA.

D. D. Koleske, M. E. Coltrin, A. J. Fischer, A. A. Allerman, K. C. Cross, C. C. Mitchell, J. J. Figiel, and M. J. Russell, Using Optical Reflectance to Monitor and Control MOCVD Growth of GaN on Sapphire, New Mexico Chapter of the AVS Science and Technology Society, 4/29-30/03, Albuquerque, NM.

D. M. Follstaedt, N. A. Missert, C. C. Mitchell, K. C. Cross, D. D. Koleske, Counting Dislocations in GaN: Contrast in TEM, AFM and CL, NM Chapter of AVS 39th Symposium, 4/28-30/03, Albuquerque, NM.

M. E. Coltrin, C. C. Mitchell, D. D. Koleske, Gallium Nitride Crystal Facet Evolution and Kinetics, 39th Symposium of the NM Chapter of the AVS, 4/29-30/03, Albuquerque, NM.

A. F. Wright, C. H. Seager, S. M. Myers, D. D. Koleske, A. A. Allerman, Hydrogen Drift, Diffusion and Trapping in p-type GaN, 39th Symposium of the NM Chapter of the AVS, 4/29-30/03, Albuquerque, NM.

G. T. Wang, J. R. Creighton, Adduct Formation Chemistry between Magnescene (MgCp₂) and NH₃: Origin of the “Memory Effect”, 39th Symposium of the NM Chapter of the AVS, 4/29-30/03, Albuquerque, NM.

C. C. Mitchell, D. D. Koleske, D. M. Follstaedt, N. A. Missert, K. H. A. Bogart, K. C. Cross, M. E. Coltrin, A. A. Allerman, Defect Reduction in Gallium Nitride Using Cantilever Epitaxy, 39th Symposium of the NM Chapter of the AVS, 4/29-30/03, Albuquerque, NM.

Chow, W. W., Influences of Localized and Continuum State Coupling in Quantum-Dot Structures, Seminar at Physics Department, Texas A&M University, 5/13/03, College Station, TX (invited) .

J. Y. Tsao, The U. S. Solid-State Lighting Roadmap: Targets and Technical Challenges, 2003 International Conference on Compound Semiconductor Manufacturing Technology, 5/19-22/03, Scottsdale, AZ (invited).

C. Eichler, D. Hofstetter, W. W. Chow, Microsecond Timescale Lateral Mode Dynamics in a Narrow Stripe InGa_N-Laser, CLEO 2003, 6/1-6/03, Baltimore, MD.

D. M. Follstaedt, D. D. Koleske, C. C. Mitchell, N. A. Missert, A. A. Allerman, P. P. Provencio, Developing Cantilever Epitaxy of GaN for Advanced Devices, 2003 EMC, 6/25/03, Salt Lake City, UT.

A. M. West, S. R. Lee, A. A. Allerman, D. D. Koleske, S. R. Kurtz, K. E. Waldrip, J. J. Figiel, C. Abernathy, Correlation Between Threading Dislocation Density and Mobility of GaN Based HEMTs, 2003 EMC, 6/25-27/03, Salt Lake City, UT.

R. J. Kaplar, S. R. Kurtz, D. D. Koleske, A. J. Fischer, Electoreflectance Studies of Stark-Shifts and Polarization-Induced Electric Fields in InGa_N Quantum Wells, 2003 EMC, 6/25-27/03, Salt Lake City, UT.

G. T. Wang, J. R. Creighton, Identification of the Adducts Formed between Magnescene (MgCp₂) and NH₃: Origin of the “Memory Effect”, 2003 TMS Electronic Materials Conference, 6/25-27/03, Salt Lake City, UT.

C. C. Mitchell, D. D. Koleske, D. M. Follstaedt, N. Missert, P. Provencio, A. A. Allerman, M. E. Coltrin, Understanding GaN Growth Evolution in Cantilever Epitaxy Yields Improved Material, 15th American Conference on Crystal Growth and Epitaxy, 7/20-24/03, Keystone, CO.

D. D. Koleske, M. E. Coltrin, K. C. Cross, C. C. Mitchell, A. A. Allerman, J. J. Figiel, GaN Nucleation Layer Evolution on Sapphire before High Temperature Growth, 15th American Conference on Crystal Growth and Epitaxy, 7/20-24/03, Keystone, CO.

J. R. Creighton, G. T. Wang, M. E. Coltrin, W. G. Breiland, Nature of the Parasitic Chemical Reactions Occuring during AlGaInN OMVPE, 15th American Conference on Crystal Growth & Epitaxy, 7/20-23/03, Keystone, CO.

G. T. Wang, J. R. Creighton, Adduct Formation Chemistry between Magnescene (MgCp₂) and NH₃: Origin of the “Memory Effect”, 15th American Conference on Crystal Growth and Epitaxy, 7/20-24/03, Keystone, CO.

A. A. Allerman, A. J. Fischer, M. H. Crawford, K. H. A. Bogart, R. J. Shul, D. D. Koleske, S. R. Lee, S. R. Kurtz, Growth and Characterization of AlGa_N Alloys for 290-300nm Light Emitting Diodes, 11th Biennial Workshop on OMVPE, 7/20-24/03, Keystone, CO.

K. H. A. Bogart, M. H. Crawford, A. J. Fischer, D. D. Koleske, K. Fullmer, F. Jalali, R. J. Shul, S. Jones, Plasma Processing Induced Contact Defects in High % n-type AlGa_N for UVLEDS, Tri-Services DARPA Workshop, 8/17-21/03, Grants Pass, OR.

W. W. Chow and H. C. Schneider, Coherent Effects in Semiconductor Quantum Dots, OSA Annual Meeting, 10/5-9/03, Tucson, AZ (invited).

J. M. Gee, J. Y. Tsao, J. A. Simmons, Fundamental Science Initiatives to Enable the Solid-state Lighting Revolution, LED 2002 Conference, Intertech, 10/21-23/03, San Diego, CA.

J. M. Gee, Shawn-Yu Lin, James G. Fleming, James B. Moreno, Energy Applications of Photonic Crystals, Photonic and Electromagnetic Crystals-IV (PECS-IV), UCLA, 10/29-31/03, Los Angeles, CA.

D. D. Koleske, M. E. Coltrin, A. A. Allerman, K. C. Cross, C. C. Mitchell, J. J. Figiel, M. J. Russell, GaN Nucleation Evolution on Sapphire, 50th International Symposium of the AVS Science and Technology Society, 11/2-7/03, Baltimore, MD.

J. Y. Tsao, Materials Issues in Solid-State Lighting, AVS 50th International Symposium, 11/2-7/03, Baltimore, MD (invited).

K. H. A. Bogart, M. H. Crawford, A. J. Fischer, D. D. Koleske, K. W. Fullmer, F. Jalali, R. J. Shul, S. Jones, I. Adesida, D. Selvanathan, Investigations of Plasma Etching and Contact Processing on AlGaIn Alloys containing 0 to 50% Al, 50th AVS International Symposium, 11/3-7/03, Baltimore, MD.

K. C. Cross, K. H. A. Bogart, C. C. Mitchell, and R. D. Briggs, Plasma Etching of Cantilever Epitaxy Sapphire Substrates, 50th AVS International Symposium, 11/3-7/03, Baltimore, MD.

G. T. Wang, J. R. Creighton, Complex Formation between Magnesocene ($MgCp_2$) and NH_3 : Origin of the "Memory Effect", 50th AVS International Symposium, 11/3-7/03, Baltimore, MD.

7.3 Book Chapters and Reviews

H. X. Jiang, J. Y. Lin, and W. W. Chow, Time-resolved photoluminescence studies of III-nitrides, Chapter 1 in "Optical Properties of III-Nitrides" for the book series entitled "Optoelectronic Properties of Semiconductors and Superlattices," Volume I, edited by H. X. Jiang and M. O. Manasreh, to be published by Gordon & Breach Science Publisher (March, 2002).

L. E. Shea Rohwer and R. J. Walko, Synthesis and Characterization of Phosphors, in Handbook of Luminescence and Displays Materials and Devices, edited, H. S. Nalwa, American Scientific Publishers, Stevenson Ranch, CA. (to be published 2002).

J. Y. Tsao, "Introduction to Solid-State Lighting" (for MRS Bulletin) by Arturas Zukauskas, Michael S. Shur, and Remis Gaska, John Wiley and Sons, New York, 2002.

7.4 Reports and Websites

E. D. Jones, Solid-state Light-emitting Diodes for General Illumination: An OIDA Workshop Preliminary Report, Washington, DC. LED solid-state lighting roadmapping workshop that was jointly held with OIDA and sponsored by DOE.

K.V. Sereda and J.Y. Tsao, (translators), Year 2000 Report of Results for Light for the 21st Century Japan National Project, 3/02.

J.Y. Tsao, ed., Light Emitting Diodes for General Illumination Update 2002 (Optoelectronics Industry Development Association), 8/02.

A. A. Allerman, R. M. Biefeld, D. Follstaedt, D. Koleske, C. Mitchell, N. Missert, P. Provencio, L. Rohwer Development of Key Technologies for White Lighting on Light-Emitting Diodes (LEDs) – Quarterly Technical Report-Q3Y1

A. A. Allerman, R. Biefeld, W. Breiland, R. Briggs, M. Coltrin, R. Creighton, K. Cross, J. Figiel, D. Follstaedt, D. Koleske, N. Missert, C. Mitchell, A. Ongstad, P. Provencio, L. Rohwer, K. Waldrip, Development of Key Technologies for White Lighting Based on Light-Emitting Diodes (LEDs)-Quarterly Technical Report, - Q4Y1

R. M. Biefeld, A. A. Allerman, K. H. A. Bogart, J. R. Creighton, J. Emerson, D. Follstaedt, D. Koleske, C. Mitchell, N. Missert, P. Provencio, L. Rohwer, S. Thoma, G. Wang, J. Wilcoxon, Development of Key Technologies for White Lighting Based on Light-Emitting Diodes (LEDs) Technical Report – Budget Period 1, Technical Report (Lumileds)

C. C. Mitchell, Defect Reduction in Gallium Nitride using Cantilever Epitaxy, Thesis, UNM Electrical Engineering Department, 4/4/03, Albuquerque, NM

J.Y. Tsao, D.C. Meister, A.E. Miksovic, Solid-State Lighting Website -- <http://lighting.sandia.gov>, 3/02.

J.Y. Tsao, D.C. Meister, A.E. Miksovic, Solid-State Lighting Website 2003 Update -- <http://lighting.sandia.gov>, 3/03.

7.5 Patents Issued

C. I. Ashby, D. M. Follstaedt, C. C. Mitchell, J. Han, Cantilever Epitaxial Process, U.S. Patent No. 6,599,362, issued July 29, 2003.

7.6 Patent Applications

D. D. Koleske et al , Algorithm for Delayed Recovery of Gallium Nitride on Sapphire, SD 7301, U.S. Patent Application Number 10/670,880, filed on 9/24/03.

Jung Han, Stress Engineering in AlGaIn/GaN Distributed Bragg Reflectors for Ultraviolet Vertical Cavity Surface Emitting Devices, SD 6914, 5/21/01, U.S. Patent Application Number 09/998,114, filed on 11/29/2001.

W. G. Breiland and H. K. Moffat, Chamber for a Rotating Disk Chemical Vapor Deposition Reactor, SD 7056, 10/24/01, U.S. Patent Application Number 10/315,399, filed on 12/9/2002.

D. D. Koleske, A. J. Fischer, A. A. Allerman, C. C. Mitchell, K. C. Cross, S. R. Kurtz, J. J. Figiel, K. W. Fullmer, W. G. Breiland, Improved Brightness of 380 nm GaN Light Emitting Diodes through Intentional Delay of the Nucleation Island Coalescence, SD-7301/S100358 (10/02), U.S. Patent Application Number 10/670,880, filed on 9/24/2003.

7.7 Patent Disclosures

J. Han, Porous gallium nitride on porous silicon as stress relief layer for growing gallium nitride-based compound semiconductor device, SD 6827, 1/22/01.

S. A Kemme, Micro-emitter Array with Integrated Optics for High-Efficacy Light-emitting Diodes, SD 6878, 3/26/01.

J. R. Creighton, Radiation Pyrometry of Wide-Bandgap Semiconductors, SD 6954, 7/11/01.

W. G. Breiland, Emissivity-Correcting Pyrometer for Nitride Growth on Sapphire Wafers, SD 7055, 10/24/01.

S.G. Thoma, P.J. Cole, J.A. Emerson, Dispersion and Encapsulation of Nano-Scale Materials in a Polymeric Matrix, SD 7287, 9/02.

S.G. Thoma, P.J. Cole, J.A. Emerson, Spatially Controlled Synthesis of Nano-Scale Materials in Polymeric Fluids, SD 7288, 9/02.

A. A. Allerman, D. D. Koleske, Thermal Annealing of Sapphire for GaN Epitaxy, SD-7226/S99851.

D. D. Koleske, A. A. Allerman, A. J. Fischer, M. H. Crawford, K. H. Bogart, S. R. Kurtz, Development of Group IIIA/Group IIIB Nitride Quantum Wells for Brighter 550-590 nm Light Emitting Diodes, SD-7459/S-102,188 (5/03).

K. H. A. Bogart, C. C. Mitchell, K. C. Cross, R. D. Briggs, C. I. H. Ashby, Plasma Etching of Sapphire, SD 7496, 5/03.

W. W. Chow, M. H. Crawford, A. J. Fischer, A. A. Allerman, S. M. Wiczorek, S. R. Lee, Bandstructure Engineering for Mitigating Internal Field Effects in III-N Quantum-Well Light Emitters, SD-7717/S104,409, 3/04.

8 APPENDIX B: EXTERNAL ADVISORY COMMITTEE AND REVIEWS

8.1 Members

Dr. Charles Becker
Manager, LED Project
General Electric Corporation
Schenectady, NY

Arpad Bergh
OIDA
2010 Massachusetts Avenue, NW
Washington, DC 20036-1023
Ph.: 202-785-4426 Fx.: 202-785-4428
Email: aboida@osa.org

Jim Brodrick
DOE
1000 Independence Avenue, SW
Washington, DC 20585-0121
Ph: 202-586-8423 Fax: 202-586-5557
Email: james.brodrick@hq.doe.gov

LTC John Carrano, Ph.D.
Program Manager, MTO
DARPA
Arlington, VA

(CHAIR) M. George Craford
Chief Technology Officer
LumiLeds Lighting
370 W. Trimble Road, MS 91UK
San Jose, CA 95131
Ph.: 408-435-6561 Fx.: 408-435-5902
Email: george.craford@lumileds.com

Russell Dupuis
Microelectronics Research Center
PRC/MER1
606D/R9900
The University of Texas at Austin
Austin, TX 78712-1100
Ph: 512-471-0537 Fx: 512-471-0957
Email: dupuis@mail.utexas.edu

Steve Johnson
Lawrence Berkeley National Lab
1 Cyclotron Road, MS 90-3111

Berkeley, CA 94720
Ph: 510-486-4274 Fx: 510-486-4089
Email: sgjohnson@lbl.gov

Robert Karlicek
GELcore
4401 Rockside Road
Independence, OH 44131-2146
Ph.: 216-606-6590 Fx.: 216-606-6556
Email: bob.karlicek@gelcore.com

Jeffrey Nelson
Uniroyal Optoelectronics
3401 Cragmont Drive
Tampa, FL 33619
Ph.: 813-612-4416 Fx.: 813-612-4412
Email: jeff.nelson@uniroyalopto.com

Arto Nurmikko
Division of Engineering
Brown University
Box D
Providence, RI 02912
Ph: 401-863-2869 Fx: 401-863-1387
Email: arto_nurmikko@brown.edu

Edward Petrow
DOE
341 Lincoln Road
Sudbury, MA 01776
Ph: 978-443-5659
Fx: 202-586-5557 or 978-443-1336
Email: edward.petrow@ee.doe.gov

James Speck
Materials Department
University of California
Santa Barbara, CA 93106
Ph: 805-893-8005 Fx.: 805-893-8486
Email: speck@surface.ucsb.edu

Dr. John Zolper
Program Manager, MTO
DARPA

Arlington, VA

8.2 February 2, 2001 Review (ET Southwell)

This report is presented to the SSL Grand Challenge LDRD project team of Sandia National Laboratories (SNL) by its Program Review Committee (PRC), following the meeting of February 2, 2001.

Committee Present:

George Craford (Chair)	LumiLeds
Arpad Bergh	OIDA
Jim Brodrick	DOE
Russ Dupuis	Microelectronics Research Center, UT Austin
Steve Johnson	Lawrence Berkeley National Lab
Bob Karlicek	GELcore
Jeff Nelson	Uniroyal Optoelectronics
Arto Nurmikko	Division of Engineering, Brown University
Jim Speck	Materials Department, UC Santa Barbara

Following the welcome by Sandia VP Bob Eagan, Jerry Simmons presented the LDRD program concept and gave a brief overview of the SSL program. James Gee covered the structure and the objectives of the SSL Grand Challenge LDRD and we were then given presentations in the following specific areas of the program.

Task I: Fundamental Limits

- defect studies in nitrides
- Strained barriers for double-HET phosphide emitters
- Light extraction improvements for LEDs

Task II: Growth Chemistry

- Nitride growth issues
- Cantilever epitaxy

Task III: In-Situ Monitoring and Reactor Design

- Instability criterion
- In-situ monitoring

Task IV: Advanced Light Emitting Devices

- VCSELs
- Nanocrystals & phosphors

The presentations and questions lasted until around 2:30, at which time we adjourned and the committee caucused for an hour. The day ended with our committee giving a 30-minute verbal, preliminary summary to the team.

Your challenges to us were to answer the following questions.

1. Are the program goals focused on important and compelling achievements?
2. Given the time frame, do we have the right resources on task?

3. Have we identified and prioritized the right major hurdles to success?
4. Given our goals and resources, which other organizations should we talking with?

First, we'd like to suggest a re-statement of your Primary Goal to read: "To 'contribute' to the fundamental science and technology base that will be required for solid state, 'inorganic' lighting to be realized."

8.2.1 Summary Feedback

Now to address the important questions of whether your program goals are important and compelling and whether you've focused on the right major hurdles. In summary, "Yes," your program goals are very important and appropriate to your (Sandia National Labs') inherent strengths. Your breadth of expertise within the Labs allows you to bring together the many different disciplines that are needed to address the complex issues that need to be solved. You have a very strong team working on this LDRD. However, we feel that you need increased resources to accomplish your Tasks' objectives. (Another alternative is to reduce your Tasks.) We also recommend that you create a better integration of focus among the varying Tasks. The paragraphs that follow will provide more detail in these areas and give our advice within the specific Tasks of the program.

8.2.2 Resources

We are concerned that your resources are spread too thin. Your Primary and individual task goals are very ambitious for the amount of dollars (\$1 million this year) that you have budgeted. Although we were told that the program is leveraging off many other efforts within Sandia, it's difficult for us to understand how all the "0.1 FTEs" we saw assigned to the varying Tasks will give you enough resources. We fear that you may be overly optimistic here.

8.2.3 Integration of Focus

We initially discussed whether we'd recommend that you have an overall, device-performance, quantitative goal for the SSL program. This, we felt, would give more focus and help integrate the team with a common objective. Also, the achievement would cause the world to sit up and take notice. Upon further discussion, however, we feel that this single, device-performance metric of success would be inappropriate. There are a number of reasons.

1. Industry is certainly focused on this.
2. Your program Tasks are broad and include research goals in areas that show long-term promise, areas that should not be – at this stage – held to a performance metric (e.g., VCSELs).
3. The emphasis you have in basic science is the right focus for a National Laboratory and basic science work doesn't lend itself well to finite goals.

This isn't to say that performance metrics –possibly in VCSEL device performance – should not be considered appropriate success measurements in year two or year three of the project. (The work and achievements in VCSELs optimally could be transferred to LEDs at some point.)

We did feel, however, that program integration could be improved by a re-ordering of the tasks. The following are our suggestions.

- Cancel the work within Task 1 called "Strained layers for confinement in phosphides" (Our reasons are given in the next section)
- Move the work in cantilevered epitaxy presently within Task 2 into Task 1. This might require Task 1 to be renamed something like "Nitride efficiency improvement", which may be a good idea anyway.
- Combine Tasks 2 and 3, re-naming this to "III-Nitride Growth and Reactor Design."
- Under Task 2, group together the subtasks "Reactor experiments and modeling" with "In-situ experiments."

- “Stress engineering using MOSS” currently listed under Task 2, would seem a better fit under the current Task 4. And just as an observation – To us, this seems like a tool that is already a fait accompli and not a sub-task in any case.

8.2.4 Importance and Relevance of Task Objectives

We recommend that you consider dropping the “Strained layers for confinement in phosphides” work that is being done under Task 1 for three reasons: 1), your approach is plausible but arguable, 2), you need to better concentrate your resources, and 3) pushing the phosphides to higher energy is interesting and important but not nearly as critical to SSL as the Nitride issues.

We feel that your work in Nitride defect studies is important and are impressed with the quality of work going on here. The focus on point defects is good, but at the end of the day, its efficiency that counts. So we’d recommend that the work here be communicated more in terms of potential gains in efficiency.

Also of high importance within Task 1 is your work in photonic lattices. We recommend that you couple with John Joannopoulos at MIT in this area. A good connection can be made through Sandia’s Shawn Lin.

The work and success you have demonstrated so far in cantilever epitaxy growth is very exciting and looks as if this could be a significant breakthrough. As you are aware, industry is continuing to make linear improvements in nitride growth but, as we said, your work here is outstanding.

The work in reactor experiments and modeling of growth rate vs. flow and spin rates; and the work in in-situ experimentation with particulate formation is also very important. Additionally, the research approaches are well thought out and the early results fruitful. These comments go for all the work that was presented to us regarding your Tasks 2 and 3. This work fits well with your skill set. With reactor design, defining the boundary conditions for industry is exactly the right approach. But perhaps the work could be more fruitful if not limited within the scope of one reactor geometry. More input from industry could be helpful here. And again, the relevance of the work can be best communicated by coupling the design issues to potential performance merits.

The tools that you have and are developing for studying growth issues are already a success story.

Even realizing the long-term commitment and the risk, the research you are doing in VCSELs is very intriguing and, we feel, of potential high importance. This should be part of the LDRD but be cautious about putting it in the National Lighting Initiative. It appears to us that if you plan on making some breakthroughs in this critical area you will certainly need to put more resources on this task. We would also recommend an intermediate goal in this area -- An edge-emitting GaN laser, while less ambitious than a VCSEL, is still a challenge and is a good indicator of material quality.

While your work in UV and blue LEDs shows promise, we feel that you should do a thorough benchmarking ASAP against the best reported, and best commercially available, results to verify that you are focusing in appropriate areas and that you have goals that will still be important if you achieve them. Industry is moving very fast in this area particularly in the blue and near UV. This might be a good area to consider working closely with one or more industrial partners.

The work in phosphor nanostructures shown to us under your current Task 4 is good; however, you need to check your resource commitments here. Focus on the clusters and drop the inorganic phosphor work once you benchmark. While your theoretical phosphor mix may be optimized for performance, there are significant environmental issues to prevent widespread adoption.

8.3 November 2, 2001 Review (ET Southwell)

This report is presented to the SSL Grand Challenge LDRD project team of Sandia National Laboratories by its Program Review Committee (PRC), following the meeting of November 2, 2001.

Committee Present:

George Craford (Chair)	LumiLeds
Jim Brodrick	DOE
John Carrano	DARPA
Russ Dupuis	Microelectronics Research Center, UT Austin
Steve Johnson	Lawrence Berkeley National Lab
Ed Petrow	DOE
Jeff Nelson	Uniroyal Optoelectronics

Jerry Simmons presented a re-cap of the Grand Challenge goals, summarized the team's responses to the suggestions of the 1st PRC meeting and report, and presented the budget and resource allocation for this fiscal year. Jerry also covered the project's partnership accomplishments and a concept for a SSL website, one that would include Perspectives' Tracking Reports as well as industry and government information, a patent section, etc. James Gee related the task group objectives and milestones to the overall project goals, and covered some of the major accomplishments in each task area. We were then given presentations in the following specific areas of the program.

Task I: Nitride Materials Science and Substrate Optimization

- Hydrogen effects on p-type doping in GaN (Myers)
- Nitride material growth, cantilever epitaxy (Allerman)

Task II: Growth Chemistry & Reactor Design

- Kinetics and transport limitations in GaN crystal growth on patterned substrate (Coltrin)
- Reactor design, in-situ measurement, and process control (Brieland)
- Growth chemistry (Creighton)

Task III: Advance Light Emitting Devices

- Photonic lattices in LEDs (Hadley)
- LED benchmarking, microemitter arrays, and photonic lattices (Fischer)
- Strain effects on emission efficiency in AlInGaN (Chow)
- Nanocrystals and phosphors (Rohwer/Tallant)

Task IV: System and Packaging

- Packaging R&D needs and UV-resistant encapsulants (Emerson)

The presentations and questions lasted until around 2:20, at which time we adjourned and the full committee caucused for about 40 minutes. After a departure to the airport by three of the committee, we resumed our caucus for another 45 minutes. The day ended with our committee giving a 30-minute verbal, preliminary summary to the team.

Your challenges to us were to answer the following questions.

1. Goals: Are our long-term program goals still focused on important and compelling achievements?
2. Progress: Is the recent progress we've made in each of the task areas reasonable? What advice do you have to speed progress?
3. Smart Luminaire Task: As you know, a "smart luminaire" thrust was slated for FY02. we currently do not have sufficient resources for this task. Given additional future funding sources, what is a reasonable scope and associated goal here?

4. Partnering and Community Outreach: What advice do you have for future [partnering] efforts here? Will the website be of value to the SSL community?

8.3.1 Summary Feedback

First, we were gratified to learn that your budget for FY02 has been substantially increased. This was needed. We can summarize our impressions at this program review with just three statements.

5. Your program goals are still important, compelling and relevant.
6. You have made excellent progress since our first meeting in February.
7. You have a talented and passionate group of folks working on this project.

You are doing a great job. We recognize significant achievement one year into the program and are looking forward to hearing about your future progress. Keep the valve turned on high!

8.3.2 Observations and Advice

Goals

We discussed the disconnect between your UV-focused goals and the challenge the lighting industry faces – Color, particularly high-brightness green, LEDs. In light of the bigger Sandia mission of national security however, UV makes sense. And, most of the technology developments you are moving towards will readily translate to industry's challenges. We do advise that, in light of recent success, it is now time to incorporate a goal of reaching state-of-the-art performance levels of devices at the epi level. This additional goal will assist in giving a consolidating, application focus to the team's technology challenges and developments.

Nitride Materials and Substrate Optimization

You are ahead of the curve in your theoretical understanding of the fundamentals of how hydrogen moves around in a crystal. You are well positioned to move ahead. Now is the time, as you've planned, to coordinate the work with crystal growers and processing people on practical application issues, such as p-type doping (higher hole concentrations) and using actual growth and annealing conditions (temperature, atmosphere, RTA, etc).

It is good that you are continuing on into AlGaIn.

Recognizing that you have had reactor difficulties, your continued incremental improvements and results in the cantilever epitaxy work are roundly applauded. The cantilever work has looked promising for a long time now. We are hopeful that you will soon be able to demonstrate the full potential of cantilever epitaxy and how it compares to LEO and other techniques. The ability to complete the growth in a single step is desirable but performance is the ultimate criteria. Continue to push here.

Growth Chemistry and Reactor Design

You have core strengths in reactor modeling and growth chemistry and showed us some exciting results here, as well as continued promising research paths for each area. Make sure you file IP around your reactor design modeling.

Your kinetics work should really be beneficial to reaching your program goals. However, we didn't see the expected synergy – or even connections – with the experimental sub-group. It's wasn't clear to us that the modeling and experimental guys are benefiting that much from each other's work.

Advanced Devices

Congratulations on your LED performance breakthroughs here. Now you can reasonably set some state-of-the-art epi performance goals.

We heard about a wide array of possible devices here, but some committee members felt you should also consider such things as tunnel junction devices, and alternative active region design (i.e., quantum dots). However, there is obviously a lot on your plate currently. Please consider the input and decide whether a change in priorities is warranted.

You should also consider pushing quaternaries harder. The issue of indium concentration and localization is a key performance consideration

We question whether there is a practical way to push the photonic lattices to the needed wavelengths, but this is good exploratory research so continue onward.

The nanocrystals work appears to be making good progress. We are happy to see that you've brought in the LANL connection. (Make sure that you protect this nanocrystals work with filing of IP.)

UV-pumped blue-green phosphors is, in general, a reasonable area to work on. There is a technology need here. It seems that you now have the needed critical mass and resources here to begin to make some progress.

System and Packaging

We are excited about your commitment of capable resources here and are looking forward to seeing progress as your efforts get underway. This is a promising area and could even have some nice overlap benefit w/OLEDs.

Smart Luminaire

Keep work on the smart luminaire on the shelf for now.

Website

Two thumbs up! Very good idea! The Perspectives' *Information Tracking Report* that we were shown looked extremely useful and we'd want to see these available on the site as well.

Partnering

You've done a good job in partnering with industry so far. In the reactor design you might consider bringing in Applied Epi, Inc., to accelerate and diversify what you're doing with Emcore.

Future Goals

Some of us did not get a clear, succinct picture of your project goals for the next six to twelve months. Consider sending us a one-pager with goal statements. For example,

- Demonstrate 50% improvement in output power based on ...
- Demonstrate consistent $<10^8$ dislocation density in Cantilever EPI materials
- Develop understanding of package related reliability issues ...
- Demonstrate initial flow test for new epi reactor design using Al materials ...

Next Program Review Meeting

We'd like to meet again in summer, assuming we can arrange schedules. June or July might work best. You might want to make the meeting a day and a half, beginning the meeting in the afternoon of the first day. This last meeting was almost too fast-paced.

8.4 September 18-19, 2002 Review (ET Southwell)

This report is presented to the SSL Grand Challenge LDRD project team of Sandia National Laboratories by its External Advisory Committee (EAC), following the meeting of September 18 – 19, 2002.

8.4.1 Summary Observations and Advice

This Sandia project and team is a vital resource in inorganic solid-state lighting. You have established unique, core competencies that address a large number of scientific problems, which would otherwise slow our nation's progress in this important area. Stay the course; your goals and work are on target.

8.4.2 Critical Successes and Challenges

We saw significant progress in each of the areas reviewed in this meeting. Saying that, there are several areas in which we would view your work as outstanding successes.

- Understanding and characterization of the role of Hydrogen in Gallium Nitride.
- Understanding and characterization of buffered layer and overgrowth science, including cantilevered epitaxy, a Sandia team discovery.
- Elucidation of unexpected reactor physics and fundamental understanding of growth chemistry.
- The blazing of new territory in luminescent materials.
- The contribution of valuable public sector services like the SSL Website and your technical Road mapping support.

While the body of our report contains several specific suggestions, our Committee sees two critical challenges for the team over the next six months.

- Establish and demonstrate your own stable (reproducible) LED process so that you have a platform and basis for demonstrating and measuring technology improvements.
- Demonstrate the viability and advantages of organometallic quantum dots and for the new phosphors technology.

8.4.3 Funding Path Opportunities

Substantial funding from Next Generation Lighting Initiative (NGLI) may be targeted for your project, but the future of this important Congressional action remains unclear at this time. In addition, look for discrete funding possibilities within DOE (Building Technologies and Basic Energy Sciences), and possibly DARPA. It is imperative also for Sandia senior management to sustain this effort by providing bridge support (a 4th year funding of this Grand Challenge) until new funding opportunities – particularly NGLI, can be realized and leveraged. We support your near-term plans for on-site briefings to the other major LED players in the US. In addition to industry, consider also the numerous universities who are committing resources to solid-state lighting initiatives, including: UCSB, RPI, Georgia Tech and Texas. Even a visit to LBL would be beneficial.

8.4.4 Next Meeting

We would like the opportunity to meet again in April 2003. This will coincide with the timing of the above challenges as well as understanding the funding opportunities with NGLI.

8.4.5 Committee Present

George Craford (Chair)	CTO, LumiLeds
Chuck Becker	Manager LED Project, GE Global Research
Arpad Bergh	Executive, Director, OIDA
Russ Dupuis	Microelectronics Research Center, UT Austin
Steve Johnson	Lawrence Berkeley National Lab
Jeff Nelson	Uniroyal Optoelectronics
Arto Nurmikko	Brown University
Ed Petrow	Consultant to DOE
Jim Speck	UC Santa Barbara
John Zolper	DARPA MTO

The meeting agenda is attached. Specific observations and advice follow.

8.4.6 Specific Area Observations and Advice

1. Quantum Dots and Phosphors

The work at LANL with the quantum dots shows an impressive, tight distribution of particle sizes. While this work is still in the early stages and you are feeling your way in the right direction, we'd like to see specific goals laid out for this contribution.

Overall, the quantum dot work is very impressive. This is high-risk, high-payoff, outside-the-box, good research. You seem to have the right issues addressed and the right people on the various tasks. However, we feel that you would now benefit from more of an integrated approach. You need a systems perspective to drive this particular research pathway as well as a number of other technical efforts.

It is important to recognize the vastly different constraints placed on QDs for the contrasting application directions of fluorescent labeling of biomolecules, for example, and for solid state lighting. The latter significantly raises the bar for the performance of the QDs in several ways. We were satisfied to see that you have plans to soon begin measuring performance with real material and doing this at the right power densities and temperatures (by the way, 80 – 120C is a good operating range). Of course, you will need to encapsulate the QDs with a robust material, and this might have a negative – or even positive -- effect on output. You realize that it may not be fundamentally possible to pack these materials together and make them robust or efficient enough to compete with conventional phosphors. You will need to begin to set some close-to-practice, quantifiable goals. We suggest that you identify a “go” “no-go” milestone here and present your conclusions at our April meeting.

The conventional phosphor work looks promising, with the work with the micropowders a potentially big breakthrough. You'll also need to set some goals and demonstrate improved performance here soon as well. (We'd like to hear about this in April also.)

Keep going with the QD research on InGaN emission mechanisms. What you've done looks good, but we're sure you recognize that there are a lot of people working this problem. Like all your work, try to couple this research directly into LEDs at the right time.

2. Carbon Doping and Hydrogen Diffusion

The work here is first-rate and a solid tie-in with hydrogen and LED materials. You've made some real fundamental contributions here toward understanding. We'd like to see some additional emphasis now on learning more about how to reduce the surface barrier for hydrogen – this would be of real use to the community. Studying hydrogen in devices and at higher temperatures is important as well. A more active application of your techniques to treat issues in AlGaN, as well as connection to light emitter devices in general, would be welcome.

The role of Carbon is a “gap area” of fundamental knowledge that may be attractive to support by BES. It is the least understood of the three common impurities and could be ripe for a discrete funding pitch to BES next year.

We concur with your plan to de-emphasize LEEBI.

3. Buffer Nucleation and Defect Reduction

Your progress in this area has been outstanding. This body of work is intrinsically tied to getting much better MOCVD material. Now, you're getting into details that have been resolved in the planar growth area, but you need to keep going and continue to build your core competency here.

The work in cantilever epitaxy (CE) is beautiful. It's good that you are giving LED manufacturers some CE material (although additional relationships with manufacturers other than LL could increase the potential to get this technology to market). Their well-controlled processes will enable a better understanding of the role of GaN defects in higher brightness LEDs for the different wavelengths. You might find yourself questioning the hypothesis that continued reductions in dislocation density is efficacious, especially for systems that produce visible spectra. There is no compelling data that lower than 10⁹ defects have an effect on visible and near-UV

devices. This needs to be demonstrated with device results at different wavelengths. We'd like to see 380 nm LED device results and recommendations by our next meeting this coming April.

4. Device Structures

You've made some nice progress here. Your current output is reasonable. However, it's now important that you develop an easy-to-make device structure that gives you reproducible results. When you accomplish this, freeze the device structure as an R&D-test-bed-device-only, and maintain this as a baseline technology. (As we've said before, it's not important that you have the brightest LEDs around.) We'd like to see you hit this device goal by April, then focus on the science.

In the short-term, you might consider (if you're not already) obtaining some 380 – 400nm die from your industry and university contacts. These could be used immediately with the phosphor work, for instance.

We didn't hear about your current work in advanced light emitters and alternative structures at this meeting. Given the needs to get your base stable LED process in line, perhaps you should prioritize among these advanced emitters and present to us in April how and which of these might be continued in year 4.

5. MOSS

This is good research that is shedding light on growth kinetics and should be continued. As you realize, this will take some more time and effort to get into place. The capability would be useful in complex development processes. There is the concern that it will not be compatible with any commercial reactor design presently available because of the aperture requirement. Can MOSS be made compatible with commercial reactors, and scalable as reactor sizes continue to increase?

6. Reactor Design

We've said this before – what you are doing here is very exciting and shows wonderful promise. Your work is fundamentally world class and can hopefully integrate effectively to the material and device science goals sooner rather than later. At the right time, you will need to consider modeling at the larger scale and now is the time to develop the concepts on how to do this. You need to nurture your relationships with the reactor manufacturers, even given the fact that they are really hurting economically at present.

While the particle formation theory presented sounds on target, we caution you to be careful in the particle sampling technique you select. As you know, you can easily change the chemistry just by sampling. (We'd like to see the viability of the approach demonstrated during our April meeting.)

Just as an aside, your work here on the chemistry may have significance in GaAs and other materials growth.

7. Specific Feedback on the SSL Website

This website is very valuable and useful. At issue is how to continue to expand and fund it. Your resources on this LDRD are precious and this is something that could potentially be funded through DOE as a reimbursable item. Ed Petrow has offered to investigate how this might be facilitated. The Committee recognizes the value and expertise of the current team (particularly Jeff Tsao) that puts this site together and encourages that this be maintained. Finally, you should consider renaming the site the "White Light LED" website, in order to make room for an OLED website.

8.5 May 15-16, 2004 Review (E'T Southwell)

This report is presented to the SSL Grand Challenge LDRD project team of Sandia National Laboratories by its External Advisory Committee (EAC), following the meeting of May 15 & 16, 2003.

8.5.1 Summary Observations and Advice

This team is more knowledgeable and energized each time we meet. You have a critical mass hitting on all cylinders. As your advisory board, we are very concerned about the extreme cutbacks in funding planned for this project in FY '04. You have established a center of excellence, which exceeds critical mass and has a lot of

momentum. Your science is excellent. The aggregate is world class. Your investment in fundamental work has been directed where it needs to be and is critical to improved efficiency across all wavelengths.

Industry has reached a plateau in terms of efficiency improvements of LEDs and needs your efforts in the fundamental science. This team is putting defect impurity physics theory on firm ground with singular experimental work. Your work on growth chemistry and reactor diagnostics technology is also excellent and will contribute to the advance of nitride technology.

We heartily endorse your planned investment in a new reactor – it's good to see that you are applying significant capital resources to compliment a strength area for Sandia.

Your list of publications and papers is substantial. Assuming that your patents are seminal (we didn't have time to read and analyze these), you have generated a very good number relative to total project cost. Industry average is about one good patent per million dollars of investment, and you have possibly doubled that. Congratulations.

Your technology transfer to industry has been commendable so far, but this needs to continue for Sandia and industry to realize the potential opportunity. There is also good evidence that your work is relevant and useful to national security applications.

This team has done terrific service to the inorganic solid state lighting community with the Sandia SSL website, roadmapping workshops and white papers all serving as a central resource. Your internal funding of the website and this work is much appreciated.

8.5.2 Critical Successes of the SSL Project

- Our top-of-mind reflections on the outstanding successes of this project are:
- Your website, workshops and white papers for the SSL community
- The in-situ reactor diagnostics
- The increased understanding of reactor chemistry
- The entire body of work on defects physics, including the cantilever epitaxy discoveries
- Substantial progress in the area of quantum dots and understanding the issues relevant to their utilization as phosphors for solid state lighting

Additional important successes are covered area by area below.

8.5.3 Successes, Challenges & Investment Advice by Area

1. Phosphors, Encapsulants

You've done what we challenged you to do in this area and you've made great initial strides and excellent progress, particularly in the developments with encapsulants. However, you recognize that there are still enormous problems lurking in the near future, primarily stability issues, that must be overcome before you can count on your efforts having a direct impact on solid state lighting. This is high risk, high payoff research. If this SSL Grand Challenge is indeed forced to dramatically reduce spending in '04, we recommend that this effort stand on its own, seeking separate funding for this very promising work. Your focus and expertise in this area is unique and we hope that your research continues. (By the way, we think that the impressive encapsulants developments you have made would be valuable in other application areas as well, and you should explore this opportunity.)

2. Semiconductor Devices

For FY '04, our overall advice for the work captured under "Semiconductor Devices" is to focus your resources on nucleation studies and transition efforts from other tasks in this area to work on novel devices of your determination, like RC-LEDs, photonic lattices or VCSELs. The issue of extraction efficiency is one of the critical issues in solid state lighting and Sandia has the skill set to address this issue effectively. Use your judgment to target your resources in this area. More specific comments follow by task area.

- a) Nucleation Studies. This is very sound, fundamental science. You are gaining an improved understanding in this difficult area which will have important benefit for the community.
- b) Cantilever Epitaxy. Your work in cantilever epitaxy has been very innovative. Your work suggests that CE may make its biggest impact in high current density reliability (very useful because industry now is pushing chips as hard as they can), and in short wave lengths. CE benefits are yet to be quantified in comparison to other low dislocation density approaches, some of which are now commercially available. This is an area that could benefit from further definitive study, but with reduced resources in FY '04, we suggest that you go forward with industry collaborations as far as you can in this FY '03, then transfer to industry.
- c) Flip Chip Designs. While you haven't plowed new ground in flip chip design, you've met the challenge we gave you in this area and developed a core competency. We recommend you now pay more attention to the thermal properties of the chip and package combination.

3. Reactor Design

While we didn't see presentations at this meeting directed toward reactor design, past meetings have communicated terrific results in this area. Barring further information, and recognizing the severe budget constraints of '04, we feel it is time for the team to declare victory and move on, allocating resources to other areas of promise. Our recommendation is to concentrate on developing industry partnerships to transfer the technology developed, so that industry can realize the benefits of your work.

4. Growth Chemistry and In-Situ Monitoring

We saw excellent science presented in growth chemistries. There is still a need to relate the promising magnesium work you are doing to real-world growth, incorporating this into application with the Emcore reactor. The MOSS work we consider a strong opportunity for successful tech transfer – congratulations.

Your other developments in in-situ monitoring we also consider to be some of the most impressive results of your program. To the degree possible, this body of work is prime for industry collaboration and transfer.

5. Fundamental Material Physics

This team is putting defect impurity physics theory on firm ground with singular experimental work. You are uniquely set up and qualified to do this.

While you are just getting started with Indium alloys and perturbation studies, we are very enthusiastic about the results shown. Some of the biggest fundamental problems in solid state lighting are related to this work. Using your comprehensive approach, we encourage the team to keep going full ahead on this.

We feel that quite a bit of your material physics work, particularly the hydrogen studies, could find a receptive funding environment within Material Sciences at BES.

6. Website, Strategic Planning and Economic Modeling

The Advisory Committee feels that the visibility of Sandia in the SSL community does not reflect to the full quality and impact of your science. Your website is the vehicle that makes Sandia visible. In addition, of course, we recognize its value as an important resource. Having said that, we are reluctant to recommend any cutbacks here for FY '04. We think that the broad benefits of the website are such that Sandia management should fund this outside of, and in addition to, the project's LDRD funding for the coming year.

We continue to be impressed with the strategic planning and economic modeling contributions of Sandia. Please continue this compelling work and consider publication and / or website posting of the analysis presented by Jeff Tsao at our meeting.

8.5.4 Further Comments

If the funding of this project does not exceed the \$800k level you presented as probable for FY '04, then we feel that we could not contribute actionable advice with another Advisory Committee meeting. However, we hope that Sandia management sees the value of increased funding for next year, and that we will see you again.

We are very appreciative of the opportunity you have given us to be advisors on this project and wish to thank every member of the project team for their work, and for making us feel our advice was useful.

8.5.5 Committee Present

George Craford (Chair)	CTO, LumiLeds
Chuck Becker	Manager LED Project, GE Global Research
Arpad Bergh	Executive, Director, OIDA
Steve Johnson	Lawrence Berkeley National Lab
Jeff Nelson	Uniroyal Optoelectronics
Ed Petrow	Consultant to DOE
Jim Brodrick	DOE, BTS
Jim Speck	UC Santa Barbara

8.5.6 Agenda

Solid State Lighting Grand Challenge LDRD Project
External Advisory Committee Meeting, 15-16 May
LOCATION: Bldg. 897, Room 4056

Thursday, 15 May

- 1:00 Airport and Hotel Pickup
- 1:30 Badging
- 1:40 Refreshments
- 2:00 Jerry Simmons, Welcome and Overview
- 2:20 Jess Wilcoxon, "Optical Properties of II-VI Nanoparticles for use as Phosphors"
- 2:40 Lauren Rohwer, "Quantum Dot Characterization Update"
- 3:00 Steve Thoma, "Encapsulation of Quantum Dots for Solid State Lighting"
- 3:20 Dave Tallant, "Update on Conventional Phosphors"
- 3:30 BREAK
- 3:50 Steve Lee, "Perturbation-Induced Compositional Instability in InGaN, AlGaN, and InAlN Epitaxial Films"
- 4:10 George Wang, "Adduct Formation Chemistry between Magnesocene (MgCp₂) and NH₃: Origin of the 'Memory Effect'"
- 4:30 Randy Creighton, "III-Nitride MOCVD Chemistries and In-Situ Process Control"
- 5:00 Dan Koleske, "GaN Nucleation Layer Evolution on Sapphire"
- 5:20 EAC Caucus
- 6:15 Depart for Dinner (La Piazza Restaurant, Fashion Square Mall, corner of San Mateo and Lomas) EAC members and all Sandia SSL Team Members

Friday, 16 May

- 7:30 Hotel pickup
- 7:40 Continental Breakfast
- 8:00 Carl Seager, "Influence of ambient on the activation of H-passivated p-GaN(Mg)"
- 8:30 Alan Wright, "Configurations, energies, and thermodynamics of the neutral Mg-H complex in GaN"
- 8:50 Christine Mitchell, "Improvements in Cantilever Epitaxy of GaN"
- 9:10 Dave Follstaedt, "Characterization of Defects Using CL, AFM, and TEM"

9:30 BREAK
9:50 Kate Bogart, "Flip-chip LED Process and Reflective P-Metallization"
10:10 Art Fischer, "Near UV LEDs for Solid State Lighting"
10:30 Mary Crawford, "Deep-UV LEDs"
10:50 Jeff Tsao, "Website and Patent Database Update"
11:00 James Gee, Project Summary and A Look Ahead
11:30 Jerry Simmons, Summary of Meeting, Charge to EAC
11:40 LUNCH & Caucus
1:40 EAC feedback
2:20 Adjourn

DISTRIBUTION

- 1 James Gee
9125 San Diego NE
Albuquerque, NM 87122
- 1 Charles A. Becker
Manager, LED Project
General Electric Global Research
1 Research Circle
Niskayuna, NY 12309
- 1 Arpad Bergh
OIDA
1133 Connecticut Ave, NW, Suite 600
Washington, DC 20036
- 1 Jim Brodrick
DOE
1000 Independence Avenue, SW
Washington, DC 20585-0121
- 1 LTC John C. Carrano, PhD
Program Manager
DARPA, MTO
3701 N. Fairfax Dr.
Arlington, VA 22203-1714
- 1 M. George Craford
Chief Technology Officer
LumiLeds Lighting
370 W. Trimble Road, MS 91UK
San Jose, CA 95131
- 1 Russell Dupuis
Microelectronics Research Center
PRC/MER1 - 606D/R9900
The University of Texas at Austin
Austin, TX 78712-1100
- 1 Steve Johnson
Lawrence Berkeley National Lab
1 Cyclotron Road, MS 90-3111
Berkeley, CA 94720
- 1 Arto Nurmikko
Division of Engineering

Brown University
Box D
Providence, RI 02912

1 Edward Petrow
DOE
341 Lincoln Road
Sudbury, MA 01776

1 James Speck
Materials Department
University of California
Santa Barbara, CA 93106

1 John Zolper
Program Manager
DARPA, MTO
3701 N. Fairfax Dr.
Arlington, VA 22203-1714

1 Edwin T Southwell
22 West Plumage
Sedona, AZ 86336

1 Ann Miksovic
3213 Indiana NE
Albuquerque, NM 87110

1 Ariane Pinson, PhD
1817 32nd St SE
Rio Rancho, NM 87124

1 Marcia Pinzon
1012 Wade Circle NE
Albuquerque, NM 87112

1 Mike Krames, Manager
Advanced Laboratories
Lumileds Lighting
MS 91-UE
370 West Trimble Road
San Jose, CA 95131

1 Jonathan Epstein
703 Hart Senate Office Bldg.
United States Senate
Washington, DC 20510

1 MS 0114 B. A. Burdick

1 MS 0114 N. M. Rahal

1	MS 0161	R. Elliot
1	MS 0188	LDRD Office, 1030
1	MS 0310	K. W. Boyack
1	MS 0316	R. P. Pawlowski
1	MS 0323	M. L. Garcia
1	MS 0511	C. E. Meyers
1	MS 0513	J. P. Vandevender
10	MS 0601	J. A. Simmons, 1123
10	MS 0601	J. Y. Tsao, 1123
1	MS 0601	S. R. Kurtz, 1123
1	MS 0601	T. M. Bauer, 1123
1	MS 0601	R. J. Kaplar, 1123
1	MS 0601	W. W. Chow, 1123
1	MS 0601	E. D. Jones, 1123
1	MS 0601	K. E. Waldrip, 1123
1	MS 0601	S. R. Lee, 1123
1	MS 0601	A. J. Fischer, 1123
1	MS 0601	M. H. Crawford, 1123
1	MS 0601	K. W. Fullmer, 1123
1	MS 0601	R. M. Biefeld, 1126
1	MS 0601	D. D. Koleske, 1126
1	MS 0601	A. A. Allerman, 1126
1	MS 0601	J. J. Figiel, 1126
1	MS 0601	R. J. Creighton, 1126
1	MS 0601	M. E. Coltrin, 1126
1	MS 0601	K. C. Cross, 1126
1	MS 0601	C. C. Mitchell, 1126
1	MS 0601	T. M. Kerley, 1126
1	MS 0601	G. T. Wang, 1126
1	MS 0601	K. H. A. Bogart, 1126
1	MS 0603	G. R. Hadley
1	MS 0603	R. J. Shul
1	MS 0603	J. R. Wendt
1	MS 0703	J. S. Nelson
1	MS 0741	M. L. Tatro
1	MS 0748	M. Allen
1	MS 0834	H. K. Moffat
1	MS 0892	L. E. S. Rohwer
1	MS 0958	P. J. Cole
1	MS 0958	J. A. Emerson
1	MS 0960	R. M. Gonzales
1	MS 1008	M. A. Monson
1	MS 1056	D. M. Follstaedt
1	MS 1056	M. P. Moran
1	MS 1056	A. K. Norman
1	MS 1056	S. M. Myers
1	MS 1111	A. G. Salinger
1	MS 1231	A. D. Romig
1	MS 1411	R.L. Simpson
1	MS 1411	D. R. Tallant
1	MS 1413	C. H. Seager

1	MS 1413	J. M. Campbell
1	MS 1415	A. F. Wright
1	MS 1415	N. A. Missert
1	MS 1415	R. G. Copeland
1	MS 1421	B. L. Abrams, 1123
1	MS 1421	P. P. Provencio
1	MS 1421	S. G. Thoma
1	MS 1421	J. P. Wilcoxon
1	MS 1427	J. M. Phillips, 1100
1	MS 9018	Central Technical Files, 8945-1
2	MS 0899	Technical Library, 9616
1	MS 0612	Review & Approval Desk, 09612
1	MS 0161	Patent and Licensing Office, 1150
1	MS 0161	C. I. H. Ashby